IntechOpen

Zeolites and Their Applications

Edited by M.Nageeb Rashed and P.N. Palanisamy

ZEOLITES AND THEIR APPLICATIONS

Edited by **M.Nageeb Rashed**
and **P.N. Palanisamy**

Zeolites and Their Applications
http://dx.doi.org/10.5772/intechopen.70980
Edited by M.Nageeb Rashed and P.N. Palanisamy

Contributors

Habiba Shehu, Edidiong Okon, Ifeyinwa Orakwe, Edward Gobina, Arambiy Paranuk, Miguel Angel Hernández, Vitalii Petranovskii, Karla Quiroz, Andrey E. Krauklis, Amira Abdelrasoul, Mahboobeh Maghami, Xiaoyu Wang, Anh Nguyen, Mohamed Abatal, Iván Ayoseth Chulines Domínguez, Youness Abdellaoui, Jorge Bañuelos-Prieto, Leire Gartzia-Rivero, Iñigo Lopez-Arbeloa, Kepa Bizkarra, Urko Izquierdo, Victoria Laura Barrio, Jose Francisco Cambra, Mohamed Nageeb Rashed

© **The Editor(s) and the Author(s) 2018**
The rights of the editor(s) and the author(s) have been asserted in accordance with the Copyright, Designs and Patents Act 1988. All rights to the book as a whole are reserved by INTECHOPEN LIMITED. The book as a whole (compilation) cannot be reproduced, distributed or used for commercial or non-commercial purposes without INTECHOPEN LIMITED's written permission. Enquiries concerning the use of the book should be directed to INTECHOPEN LIMITED rights and permissions department (permissions@intechopen.com).
Violations are liable to prosecution under the governing Copyright Law.

Individual chapters of this publication are distributed under the terms of the Creative Commons Attribution 3.0 Unported License which permits commercial use, distribution and reproduction of the individual chapters, provided the original author(s) and source publication are appropriately acknowledged. If so indicated, certain images may not be included under the Creative Commons license. In such cases users will need to obtain permission from the license holder to reproduce the material. More details and guidelines concerning content reuse and adaptation can be foundat http://www.intechopen.com/copyright-policy.html.

Notice

Statements and opinions expressed in the chapters are these of the individual contributors and not necessarily those of the editors or publisher. No responsibility is accepted for the accuracy of information contained in the published chapters. The publisher assumes no responsibility for any damage or injury to persons or property arising out of the use of any materials, instructions, methods or ideas contained in the book.

First published in London, United Kingdom, 2018 by IntechOpen
eBook (PDF) Published by IntechOpen, 2019
IntechOpen is the global imprint of INTECHOPEN LIMITED, registered in England and Wales, registration number: 11086078, The Shard, 25th floor, 32 London Bridge Street
London, SE19SG – United Kingdom
Printed in Croatia

British Library Cataloguing-in-Publication Data
A catalogue record for this book is available from the British Library

Additional hard and PDF copies can be obtained from orders@intechopen.com

Zeolites and Their Applications
Edited by M.Nageeb Rashed and P.N. Palanisamy

p. cm.

Print ISBN 978-1-78923-342-1

Online ISBN 978-1-78923-343-8

eBook (PDF) ISBN 978-1-83881-505-9

We are IntechOpen, the world's leading publisher of Open Access books

Built by scientists, for scientists

3,550+
Open access books available

112,000+
International authors and editors

115M+
Downloads

151
Countries delivered to

Our authors are among the
Top 1%
most cited scientists

12.2%
Contributors from top 500 universities

CLARIVATE ANALYTICS
BOOK CITATION INDEX
INDEXED

WEB OF SCIENCE™

Selection of our books indexed in the Book Citation Index in Web of Science™ Core Collection (BKCI)

Interested in publishing with us?
Contact book.department@intechopen.com

Numbers displayed above are based on latest data collected.
For more information visit www.intechopen.com

Meet the editors

Prof. Mohamed Nageeb Rashed is a Professor of Analytical and Environmental Chemistry and the previous Vice-dean for Environmental Affairs, Faculty of Science, Aswan University, Egypt. His research interests have been analytical and environmental chemistry with special emphasis on water pollution monitoring, control and treatment; bioindicators for water pollution monitoring; wastewater impact and advanced oxidation treatment; photocatalysis, nanocatalyst, nanocomposite and adsorption techniques in water and wastewater treatment. Prof. Rashed supervised several MSc and PhD degree thesis in the fields of pollution, analytical and environmental chemistry. Ninety scientific papers were published in international journals and international conferences. He participated as an invited speaker in 20 conferences around the world. Prof. Rashed acts as an editor-in-chief and an editorial board member in several international journals in the fields of chemistry and environment. His society membership includes several national and international societies. Prof. Rashed was awarded the Egyptian National Award for Environmental Researches for the year 2001.

Dr. P. N. Palanisamy is a Professor and the Head of the Department of Chemistry, Kongu Engineering College, Perundurai, Erode. He has more than 21 years of research and teaching experience. His field of specialization includes catalysis, wastewater treatment by adsorption, electrocoagulation and photocatalysis. He successfully guided nine PhD degree students and is presently guiding another nine PhD degree students in the field of water and wastewater treatment. He holds 98 research publications on the national and international level reputed journals in the area focused on catalysis and textile industrial dye removal efficiency. Dr. P. N. Palanisamy organized a number of sponsored national and international seminars, workshops and conferences. He presented and participated in more than 120 national and international conferences. He is a lifetime member of the Indian Council of Chemists and a reviewer/editorial board member of many journals. He authored three text books entitled *Applied Chemistry, Engineering Chemistry* and *Environmental Science*, for the benefit of budding engineers. Dr. P. N. Palanisamy has completed two R&D projects as Principal Investigator funded by UGC and DST and has one ongoing project funded by UGC. He received Best Performing Researcher Award (R&D projects) for the year 2014 from Kongu Engineering College, Outstanding Scientist Award for the year 2015 from Venus International Foundation, Shri P. K. Das Memorial Best Faculty of Chemistry (Senior Category) Award for the year 2016 by Nehru College of Educational and Charitable Trust and Best Scientist Award by SIAA (South Indian Association of Scientists, Developers and Faculties Award) in 2017 .

Contents

Preface

Zeolites are natural volcanic minerals and are hydrated aluminosilicate minerals made from interlinked tetrahedra of alumina (AlO_4) and silica (SiO_4). They are in solid state with a relatively open, three-dimensional crystal structure built from the elements silicon, aluminum, oxygen and alkali or alkaline-earth metals plus water molecules trapped in the gaps between them. Zeolites form with many different crystalline structures, with large open pores in a very regular arrangement and roughly the same size as small molecules.

About 40 naturally occurring zeolites were found, forming in both volcanic and sedimentary rocks. According to the US Geological Survey, the most commonly mined forms of zeolites include clinoptilolite, chabazite and mordenite. More artificial and synthetic zeolites (around 200) have been designed for specific purposes, the best known of which are zeolite A, the petroleum catalyst ZSM-5 (a branded name for pentasil zeolite) and zeolites X and Y (two different types of faujasites) used for catalytic cracking.

The structure of zeolites makes them useful in all sorts of ways. One of the main uses of zeolites is in water softeners and water filters. Other applications include litter to animal food, industrial catalyst and nanocatalyst, composite and nanocomposite, adsorbents for pollutants, solar thermal collectors, catalysts in the pharmaceutical drug production and petrochemical industry, they help balance the body's pH levels and remove heavy metals from the body.

This book *Zeolites and Their Applications* deals with several aspects of zeolite morphology and applications. The book is divided into three sections and structured into nine chapters. The first section, "Introduction", includes the introductory chapter. The second section "Zeolite Morphology and Synthesis" explains mineralogy, morphology, and synthesis of zeolites and presents four chapters in detail: (1) "Linde Type L Zeolite: A Privileged Porous Support to Develop Photoactive and Catalytic Nanomaterials", (2) "Design and Evaluation of Gas Transport through a Zeolite Membrane on an Alumina Support", (3) "Separation of Binary Solutions on Zeolites" and (4) "Estimation of Nanoporosity of ZSM-5 Zeolites as Hierarchical Materials". The third section "Zeolite Applications" contains four chapters: (1) "Use of Synthetic and Natural Zeolites Tailored for As(V) Sorption", (2) "Zeolites-Mixed Matrix Membranes (Zeolites-MMMs) for Sustainable Engineering", (3) "Characterizations and Industrial Applications for Cement and Concrete Incorporated Natural Zeolite" and (4) "Potential Desalination of Coal Seam Gas Coproduced Water Using Zeolite.".

So, in this book, the readers will obtain updated information on mineralogy, morphology, synthesis and applications of zeolites. Scientists from different scientific fields reported in this book their findings.

The book *Zeolites and Their Applications* offers important information sources for researchers and professionals working in zeolite preparations and applications.

We would like to express our sincere thanks to Dr. A. Geetha, Assistant Professor, Department of Chemistry, Kongu Engineering College, Tamilnadu, India and Prof. Kamal A. Magd, Department of Geology, Faculty of Science, Aswan University, Egypt, for their contribution in the scientific revision of the book chapters. Also, we would like to extend our many thanks to Ms. Lada Bozic, Author Service Manager, IntechOpen, for her kind follow-ups and assistance.

M. Nageeb Rashed
Faculty of Science
Aswan University, Egypt

P. N. Palanisamy
Department of Chemistry
Kongu Engineering College
Perundurai, Erode, 638 060, Tamilnadu, India

Section 1

Introduction

Chapter 1

Introductory Chapter: Adsorption and Ion Exchange Properties of Zeolites for Treatment of Polluted Water

Mohamed Nageeb Rashed and
Pachagoundanpalayam Nachimuthugounder Palanisamy

Additional information is available at the end of the chapter

http://dx.doi.org/10.5772/intechopen.77190

1. Introduction

1.1. Water pollution

Over the last few decades, the world has become increasingly sensitive toward the protection of the ecosystem and its environment. As a result of the rapid increase in population and economic development; large quantities of waste were generated lead to severe environmental degradation and thereby resulting in pollution. One of the major environmental pollutions is water pollution. Waste water as one of the most reasons for water pollution may come from the domestic, agricultural, and industries.

Adsorption and ion exchange techniques for wastewater treatment have become more popular in recent years owing to their efficiency in the removal of pollutants. The most common adsorbent materials are alumina, calais, silica, zeolites, metal hydroxides, and activated carbon.

1.2. Zeolite minerals

Zeolites form a unique class of oxides, consisting of microporous, crystalline aluminosilicates that can be found in nature, or synthesized artificially. The zeolite framework is very open and contains channels and cages, where cations, water, and adsorbed molecules may reside and react. The specific adsorption and ion exchange properties of zeolites are used in industries, color removal, detergents, toothpaste, and desiccants, whereas their acidity makes them attractive catalysts [1].

IntechOpen

© 2018 The Author(s). Licensee IntechOpen. This chapter is distributed under the terms of the Creative Commons Attribution License (http://creativecommons.org/licenses/by/3.0), which permits unrestricted use, distribution, and reproduction in any medium, provided the original work is properly cited.

Zeolites are classified into two classes, one is natural zeolites, and the other is synthetic zeolites. Natural zeolites are hydrated aluminosilicates compounds with a characteristic three-dimensional structure of tetrahedrons as TO_4 (T = Si, Al, B, Ge, Fe, P, and Co) joined by oxygen atoms, with large pore apertures and pore system that allow the relatively easy exchange of cations between aqueous solutions and intracrystalline sites [2, 3]. Zeolites have in its internal structure cavities and channels interconnected of molecular dimensions, where compensation cations allowing the ion exchange [4, 5]. New functional groups may introduce to zeolites through several processes of modification that improve its activity and selectivity on the removal several substances [6–8]. Several authors studied the use of modified natural zeolite on environmental applications, mainly anions uptake from effluents by adsorption processes [9–11]. Due to the excellent ion exchange ability and high surface area, natural zeolites [12, 13], and synthetic zeolites [14–16].

Nearly 600 known zeolites were discovered. International Union of Pure and Applied Chemistry (IUPAC) endorsed a general classification of zeolites structures, that is, FAU for faujasites, mordenite framework inverted (MFI) for ZSM-5, and mordenite zeolite (MOR) for mordenite.

2. Adsorption and ion exchange phenomena

Adsorption and ion exchange, take advantage of many common features in regard to application in batch and fixed-bed processes for a unified treatment. These processes involve the transfer and distribution of solutes between a fluid phase and particles.

Adsorbents are natural or synthetic materials of the amorphous or microcrystalline structure. Those used on a large scale are activated carbon, molecular sieves, silica gel, and activated alumina.

Ion exchange occurs throughout a polymeric solid, which dissolves some fluid-phase solvent. In ion exchange, ions of positive charge in some cases (cations) and negative charge in others (anions) from the fluid, replace dissimilar ions of the same charge initially in the solid. The ion exchanger exhibits permanently bound functional groups of different charge. In ion exchanger, cation exchange resins generally contain bound sulfonic acid groups; less commonly, these groups are carboxylic, phosphonic, phosphinic, and so on. Anionic resins involve quaternary ammonium groups (strongly basic) or other amino groups (weakly basic) [17].

2.1. Adsorption phenomena in zeolites

Adsorption involves, in general, the accumulation (or depletion) of solute molecules at an interface (including gas–liquid interfaces, as in foam fractionation, and liquid–liquid interfaces, as in detergency).

The most adsorption processes are of gas–solid and liquid–solid interfaces, with solute distributed selectively between the fluid and solid phases. The accumulation per unit surface area is small; thus, highly porous solids with very large internal area per unit volume are preferred. Two classes of adsorption are identified, physical adsorption and chemical adsorption. Physical adsorption or physisorption involves van der Waals forces (as in vapor condensation), and retard chemical

adsorption or chemisorption, which involves chemical bonding. The former is well suited for a regenerable process, while the latter generally destroys the capacity of the adsorbent [18].

Adsorption techniques have gained favor recently due to their efficiency in the removal of pollutants. Also, adsorption process provides an attractive alternative treatment, especially if the adsorbent is inexpensive and readily available. The advantage of the adsorption process is its sludge free, clean operation, and complete removal of pollutants even from dilute solution. Therefore, adsorption considered as one of a low cost and powerful treatment processes for the removal of pollutants from waste water [19].

Zeolites are the most important inorganic cation exchangers and adsorptive materials. It shows higher cation exchange selectivities, good resistance to temperature and ionizing radiations, and excellent compatibility with the environment. Therefore, zeolites are widely used in modern technologies as selective adsorbents, molecular sieves, and particularly as catalysts. Ion exchange property is employed also as a tool for tailoring the structure in order to obtain specific performances, and so, it competes with cation exchange resins in water processing and in the purification of wastewater and sewage.

Zeolites have two main properties: adsorption and ion exchange. These two properties are due to reactive surfaces, due to the presence of Al^{3+} on adsorption sites with a Si^{4+} ion resides, and the micropores crystalline system. These properties allow the zeolite for several applications. Zeolites are essentially nontoxic and pose no environmental risk. Zeolite is also applied in toothpaste to bind calcium [20].

Because of their favorable ion exchange selectivity for certain cations, zeolite minerals, particular clinoptilolite, are of interest for use in the treatment of nuclear waste waters [21], municipal and industrial waste waters [22], acid mine drainage waters [23] and other construction materials.

2.2. Ion exchange phenomena in zeolites

Ion exchange is a function of solid and aqueous phase composition and aqueous solution concentration.

Ion exchange equilibria occur between two or more phases, one of which is liquid which exchanges two or more ions (cations or anions), more or less strongly bound to each phase. Ions exchangeable quantity by a solid exchanger depending on its structural features and is called the ion exchange capacity, usually expressed in meq/g. Ion transfer from one phase to the other is subject to the observance of electroneutrality and regulated by the ion concentration in both phases. This parameter is a function of both the energy of ion lattice interaction and the hydration energy (ion solution interaction).

A cation exchange reaction may be written as.

$$nM(m_s) + - \} - mN''(z+) + \sim - nM\ (m_z) + + mN''(s+) \tag{1}$$

where, m and n are the valences of exchanging cations.

M and N and subscripts s and z denote solution and zeolite phase, respectively.

Ion exchange property in zeolites resulted from the presence of extra cations, located on channels and cages of it [24]. In the zeolite structures, there are various cation sites, which differ from each other in framework position and therefore, in bond energy. When the zeolite contact with an electrolytic solution, its cations escape from their sites and replaced by other cations from the solution [25]. Cation sieving may be due to the inability of the negative charge distribution on the zeolite structure to accommodate a given cation [24] (**Table 1**).

2.3. Cations and acidity in zeolites

In the tetrahedral crystal, when Al^{3+} replaces Si^{4+} ions the units have a net charge of–1, and so the cation with a positive charges, such as Na^{+}, is neutralizing the negative charge. The number of cations presents within in a zeolite structure equals the number of alumina tetrahedral. A zeolite in its sodium compensated form is presented as Na-ZSM-5, Na-X, and so if Na^{+} ions are replaced by H^{+} (yielding H-ZSM-5, H-X,) the zeolite becomes a gigantic poly acid. The structure of an acid site with H^{+} on a Si–O–Al bridge is illustrated in **Figure 1**. As zeolite being a proton donor, the site is called a Brønsted acid, and its strength depends on the number of other aluminum ions in the environment and the local environment of the proton [20].

Zeolite	Representative unit-cell formula	Void volume (%)	Channel dimensions (Å)	Thermal stability (relative)	Cation Exchange Capacity[b] (meq/100g)
Analcime	$Na_2 (Al_{16}Si_{32} O_{96}) . 16H_2O$	18	2.6	High	4.54
Chabazite	$(Na_2 ,Ca)_6 (Al_{12}Si_{24} O_{72}) . 40H_2O$	47	3.7 x 4.2	High	3.84
Clinoptilolite	$(Na_3 K_3) (Al_6Si_{30} O_{72}) . 24H_2O$	34	3.9 x 5.4	High	2.16
Erionite	$(Na,Ca_{0.5}K) (Al_9Si_{27} O_{72}) . 27H_2O$	35	3.6 x 5.2	High	3.12
Faujasite	$Na_{58} (Al_{58}Si_{132} O_{384}) . 240H_2O$	47	7.4	High	3.39
Ferrierite	$(Na_2 Mg_2) (Al_6Si_{30} O_{72}) . 18H_2O$	28	4.3 x 5.5 3.4 x 4.8	High	2.33
Heulandite	$Ca_4 (Al_8Si_{28} O_{72}) . 24H_2O$	39	4.0 x 5.5 4.4 x 7.2	Low	2.91
Laumontite	$Ca_4 (Al_8Si_{16} O_{48}) . 16H_2O$	34	4.6 x 6.3	Low	4.25
Mordenite	$Na_8 (Al_8Si_{40} O_{96}) . 24H_2O$	28	2.9 x 5.7 6.7 x 7.0	High	2.29
Phillipsite	$(Na ,K)_5 (Al_5Si_{11} O_{32}) . 20H_2O$	31	4.2 x 4.4 2.8 x 4.8 3.3	Medium	3.31
Synthetic	Zeolites				
Linde A	$Na_{12} (Al_{12}Si_{12} O_{48}) . 27H_2O$	27	4.2	High	5.48
Linde X	$Na_{86} (Al_{86}Si_{106} O_{384}) . 264H_2O$	50	7.4	High	4.73

[b]Calculated from the unit-cell formula.

Table 1. Representative formulae, chemical composition, and selected physical properties of important zeolites [25, 26].

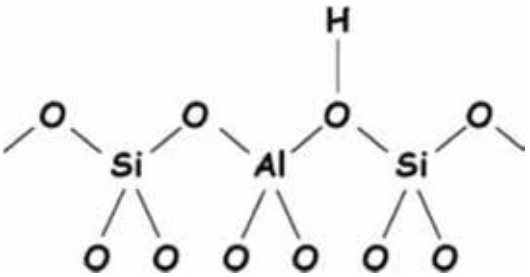

Figure 1. Example of a solid acid.

Author details

Mohamed Nageeb Rashed[1]* and Pachagoundanpalayam Nachimuthugounder Palanisamy[2]

*Address all correspondence to: mnrashed@hotmail.com

1 Department of Chemistry, Faculty of Science, Aswan University, Egypt

2 Department of Chemistry, Kongu Engineering College, Tamil Nadu, India

References

[1] Thomas JM, Bell RG, Catlow CRA. In: Ertl G, Knzinger H, Weitkamp J, editors. Handbook of Heterogeneous Catalysis, Vol. 1. Weinheim: VCH; 1997. p. 206

[2] Da Luz BA. Zeólitas: Propriedades e usos industriais. Rio de Janeiro: Centro de Tecnologia Mineral; 1997. p. 68

[3] Inglezakis LV, Grigoropoulou H. Effects of operating conditions on the removal of heavy metals by zeolite in fixed bed reactors. Journal of Hazardous Materials. 2004;**B112**:37-43

[4] Kesraoui-Ouki S, Cheeseman RC, Perry R. Natural zeolite utilization in pollution controls: A review of applications to metals effluents. Journal of Chemical Technology and Biotechnology. 1994;**59**(2):121-126

[5] Luna JF. Modificação de Zeólitas para Uso em Catálise. Química Nova. 2001;**24**(6):885-892

[6] Curkovic L, Cerjan-Stefanovic S, Filipan T. Metal ion exchange by natural and modified zeolites. Water Research. 1996;**31**(6):1379-1382

[7] Dentel KS, Jamrah IA, Sparks LD. Sorption and cosorption of 1,2,3-trichlorobenzene and tannic acid by organo-clays. Water Research. 1998;**32**(12):3689-3697

[8] Milosevic S, Tomasevic-Canovic, M. Modification of the surface of minerals for development the materials-adsorbents. In: 36th International October Conference on Mining and Metallurgy; 2004 Sep 2, October, Bor, Serbia and Montenegro; 2004

[9] Stocker K, Ellersdorfer M, Lehner M, Raith JG. Characterization and utilization of natural zeolites in technical applications. BHM. 2017;**162**(4):142-147

[10] Kędziora K, Piasek J, Szerement J, Ambrożewicz-Nita A. Use of modified zeolite in environmental engineering. A review. 2014;**781**(C):61-66

[11] Apreutesei RE, Catrinescu C, Teodosiu C. Surfactant-modified natural zeolites for environmental applications in water purification. Environmental Engineering and Management Journal. 2008;**7**(2):149-161

[12] Rožić ŠC-S, Kurajica S, Vančina V, Hodžić E. Ammoniacal nitrogen removal from water by treatment with clays and zeolites. Water Research. 2000;**34**(14):3675-3681

[13] Jung J-Y, Chung Y-C, Shin H-S, Son D-H. Enhanced ammonia nitrogen removal using consistent biological regeneration and ammonium exchange of zeolite in modified SBR process. Water Research. 2004;**38**(2):347-354

[14] Takami N, Murayama K, Ogawa HY, Shibata J. Water purification property of zeolite synthesized from coal fly ash. Shigen-to-Sozai. 2000;**116**(9):789-794

[15] Zhang M, Zhang H, Xu D, et al. Removal of ammonium from aqueous solutions using zeolite synthesized from fly ash by a fusion method. Desalination. 2011;**271**(1-3):111-121

[16] Yusof AM, Keat LK, Ibrahim Z, Majid ZA, Nizam NA. Kinetic and equilibrium studies of the removal of ammonium ions from aqueous solution by rice husk ash-synthesized zeolite Y and powdered and granulated forms of mordenite. Journal of Hazardous Materials. 2010;**174**(1-3):380-385

[17] Douglas LeVan M, Carta G, Yon CM. Adsorption and Ion Exchange. New York: McGraw Hill Comp Inc.; 1999

[18] Ruthven DM. Principal of Adsorption and Desorption Processes. New York: John Wiley and Sons; 1984

[19] Evans GM, Furlong JC. Environmental Biotechnology: Theory and Application I. K. International Pvt Ltd; 2003. 285 pp

[20] Chorkendorff I, Niemantsverdriet JW. Concepts of Modern Catalysis and Kinetics. Weinheim: Wiley-VCH Verlag GmbH & Co. KGaA; 2003

[21] Pansini M. Natural zeolites as cation exchangers for environmental protection. Mineralium Deposita. 1996;**3**(1):563-575

[22] Kallo D. Wastewater purification in Hungary using natural zeolites. In Ming DW, Mumpton FA, editors. Natural Zeolites '93: Occurrence, Properties, Use; International Committee on Natural Zeolites; Brockport, New York; 1995. pp. 341-350

[23] Zamzow MJ, Schultze LE. Treatment of acid mine drainage using natural zeolites. In: Ming DW, Mumpton FA, editors. Natural Zeolites '93: Occurrence, Properties, Use. International Committee on Natural Zeolites, Brockport, New York; 1995. p. 405413

[24] Dyer A. An Introduction to Zeolite Molecular Sieves. Chichester: John Wiley; 1988. 49 pp

[25] Colella C. Ion exchange equilibria in zeolite minerals. Mineralium Deposita. 1996;**31**:554-562

[26] Mumpton FA. Natural zeolites. In: Pond WG, Mumpton FA, editors. Zeo-Agriculture: Use of Natural Zeolites in Agriculture and Aquaculture. Colorado: Westview Press; 1983. pp. 33-43

Section 2

Zeolites Morphology and Synthesis

Chapter 2

Linde Type L Zeolite: A Privileged Porous Support to Develop Photoactive and Catalytic Nanomaterials

Leire Gartzia Rivero, Jorge Bañuelos, Kepa Bizkarra,
Urko Izquierdo, Victoria Laura Barrio,
Jose Francisco Cambra and Iñigo López Arbeloa

Additional information is available at the end of the chapter

http://dx.doi.org/10.5772/intechopen.73135

Abstract

Among the wide assortment of zeolites based on aluminosilicates, Linde Type L (LTL) zeolite outstands as a support host owing to its porous framework and high adsorption surfaces. Thus, the incorporation of suitable guest molecules (fluorophores or metals) allows the development of photoactive and catalytic nanomaterials. In this chapter, we describe the design of materials based on LTL zeolite to achieve artificial antennae, inspired in the natural photosynthesis, and ecofriendly materials for the catalytic reforming of biogas. First, we describe the microwave-assisted synthesis of LTL zeolite with tunable size and morphology. Afterward, we test the energy transfer probability between the guest fluorophores into the LTL zeolite pores as the key process enabling the antenna behavior of this hybrid material with broadband absorption and tunable emission or predominant red fluorescence. Finally, we also test the behavior of LTL zeolite as a support material for the catalytic reforming of biogas. To this aim, suitable metals were impregnated onto LTL zeolite featuring different shapes and alkaline metal exchange. Activity tests indicated that disk- and cylinder-shaped hosts were the most active ones, especially when bimetallic (Rh-Ni) catalysts were prepared. However, the alkaline metal exchange was ineffective to increase the hydrogen yield.

Keywords: LTL zeolite, hydrothermal synthesis, nanomaterials, energy transfer, catalytic support, hydrogen

1. Introduction

Zeolites are crystalline silicates and aluminosilicates linked through oxygen atoms, producing well-defined three-dimensional structures with cavities and channels where water, cations,

IntechOpen

© 2018 The Author(s). Licensee IntechOpen. This chapter is distributed under the terms of the Creative Commons Attribution License (http://creativecommons.org/licenses/by/3.0), which permits unrestricted use, distribution, and reproduction in any medium, provided the original work is properly cited.

and/or small molecules can allocate [1–5]. The term "zeolite" has its origin in the two Greek words *zeo* and *lithos*, literally meaning "boiling stone." The mineralogist Fredrik Cronstedt who observed that the heating of the material produced large amounts of steam water previously adsorbed by the pores coined this term in 1756 [6]. The zeolites are also known as molecular sieves and, albeit many of them occur naturally as minerals, most of these materials have been synthesized by the scientific community for different purposes in fundamental chemistry and technological fields. Nowadays, there are 191 types of zeolite frameworks registered and over 40 natural zeolite frameworks are known [7].

Likely, zeolites are the most widely used catalysts in the industry for oil refining, petrochemistry, and organic synthesis due to their high surface area and adsorption capacity, as well as their controllable adsorption properties [8]. Moreover, the possibility of designing frameworks *a la carte* with tunable porosity and chemical properties make them strong candidates for hosting different types of guests (such as ions, metals, and organic molecules) and for mass transport and/or occlusion [9].

Among the high diversity of natural and synthetic zeolites, Linde Type L (LTL) zeolite stands out owing to its appealing physicochemical and structural properties and high versatility [10]. LTL zeolite is a crystalline aluminosilicate of well-defined three-dimensional framework and a hexagonal symmetry (**Figure 1**). It is formed by corner sharing TO_4 tetrahedra (T being aluminum or silicon) leading to the arrangement of cancrinite cages and the final three-dimensional network. The presence of the trivalent aluminum infers an anionic character to the framework and charge-compensating cations are required to balance the charge of the tetrahedra. This is why the stoichiometry of LTL zeolite with monovalent charge compensating cations M^+ is $M_9[Al_9Si_{27}O_{72}]\cdot nH_2O$, where the number of water molecules n per unit cell equals 21 in fully hydrated materials and is about 16 at 20% relative air humidity. Its framework is characterized by uni-dimensional channels running along the c-axis of the crystal with a pore diameter suitable to host for many molecules of interest (7.1 Å), and hence, ideal to allocate organic fluorophores.

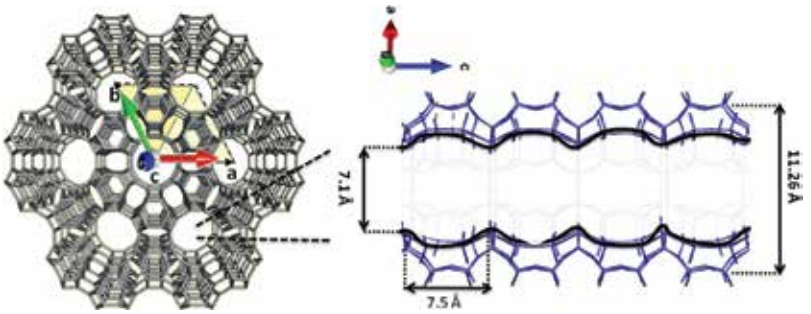

Figure 1. Top view of LTL zeolite framework, illustrating the hexagonal structure and the uni-dimensional pores. Side view of a channel that consist of 7.5 Å long unit cells with a van der Waals opening of 7.1 Å at the smallest and 11.26 Å at the widest place.

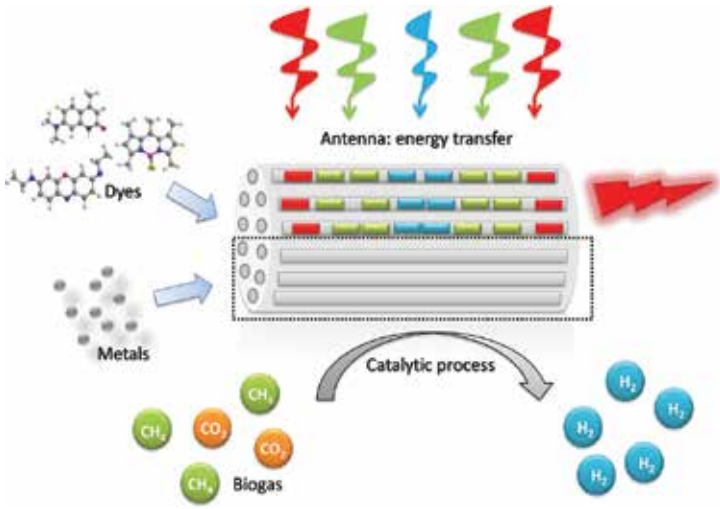

Figure 2. Schematic representation of the photoactive antenna and catalytic nanomaterials. Top: sequential insertion of three different dyes (absorbing and emitting in different ranges of the electromagnetic spectrum and undergoing energy transfer) into the LTL zeolite channels. Bottom: adsorption of metals onto the zeolitic surface to generate hydrogen from biogas by catalyzed reforming processes.

Over recent years, LTL zeolite has been successfully applied in a broad range of fields, including ion exchange and separation [11], catalytic processes [12], artificial antenna materials [13], photosensitizers in solar cells or light emitting diodes [14], luminescent solar concentrators [15], color changing media [16], microlasers [17], and in biomedicine [18].

In order to achieve competitive applications in advanced nanodevices is essential to provide high quality LTL zeolite crystals, which means, defined morphology, high crystallinity, and homogeneous size distribution of the particles. LTL zeolite is usually synthesized under hydrothermal conditions using conventional ovens. The crystal size and morphology are straightforwardly controlled by adjusting the starting gel composition (water content, alkalinity, or oxide proportion) as well as the heating conditions (heating rate and/or temperature). LTL zeolites with sizes ranging from nanometers to micrometers and disc-shaped or barrel-like morphologies have already been reported [19, 20].

Herein, we present a novel synthetic approach relied on the use of microwave-assisted heating for the production of high quality LTL zeolite crystals with tunable size and morphology. These inorganic crystals will then act as scaffolds for antenna systems (inspired in biosynthetic organisms), as well as environmentally friendly catalytic supports for energetic applications (metal-catalyzed hydrogen production from biogas reforming) (**Figure 2**). Indeed, the pore diameter of the host fits well to allocate organic fluorophores inside, whereas the constrained environment of the channel arranges hierarchically the chromophores, boosting the energy transfer, and hence, the antenna effect. Besides, the high adsorption capability of this support material, owing to its large available surface area, enables the efficient absorption of high amount of metals, thereby, enhancing the catalytic activity.

2. LTL zeolite: microwave-assisted hydrothermal synthesis

Microwave heating is an emerging technique in modern organic synthesis and in the production of nanoparticles and nanostructures. It usually affords an improvement in the yield and reproducibility of the synthetic processes, reducing the energetic costs, and favoring a friendlier environmental methodology [21, 22]. The main characteristics of microwave-assisted heating rely on the accurate control of the temperature, which ensures homogeneous distribution of the heat, preventing temperature gradients within the oven and samples. Therefore, the heating process is more efficient, side reactions are avoided in great extent, and as a consequence, reaction times are reduced notably.

This section is focused on describing the hydrothermal synthesis of LTL zeolite by extrapolating the optimal conditions referred in previous reports for conventional ovens and applied them to microwave heating [19]. One of the main aims is to improve the quality of the crystals and decrease reaction times, which otherwise takes several days and implies higher energetic costs. In this regard, we have studied the effect of reaction conditions (heating rate, time, temperature, and static/dynamic conditions) on the size, morphology and chemical properties of the resulting crystals. Thus, LTL zeolite crystals with size ranging from nanometers (15 nm) to micrometers (3 μm), and shape varying from disc or coin to barrel have been synthesized by tuning the gel composition and the aforementioned reaction conditions.

The herein used hydrothermal synthetic procedure is described in **Figure 3**. The general protocol consists on mixing two aqueous suspensions, one containing the silica source and the other composed by the aluminum source, in a basic environment, leading to a milky gel phase. Afterward, the gel is heated (at reaction temperatures usually higher than 100°C) in a sealed high-pressure polytetrafluoroethylene (PTFE) vessel for a certain time period (optimal for each kind of zeolite). The size and morphology of the crystals can be modulated by changing the source of reactants, composition of the gel (alkalinity, water content, SiO_2/Al_2O_3, among others) reaction time, temperature, and aging time of the gel [23]. To this aim and, starting from a fixed gel composition optimized for each kind of zeolite, we focused on modifying the reaction conditions and gel pre-treatment for a fine-tuning of the size and morphology of the crystals. For all types of zeolites the microwave-assisted heating reduced the synthesis times up to 90% (days to hours) compared to the one afforded by conventional ovens [19, 23]. Moreover, the precise control of the temperature and the homogeneous heating during the nucleation process in the microwave oven are reflected in a narrower size distribution of the particles and higher degree of crystallinity. Therefore, LTL zeolite crystals of different sizes and morphologies, and improved quality, can be attained in few hours, with the consequent time and energetic savings. The properties of these zeolites were further studied and classified to best fit different kind of applications.

2.1. LTL zeolite nanocrystals

The small size of these zeolites (15–50 nm) is suitable to allocate guests deep inside the pores thanks to the favored diffusion within the pores [23]. Furthermore, its large external surface makes them optimal supports for adsorption processes, e.g., adsorption of metal particles for catalytic processes [12].

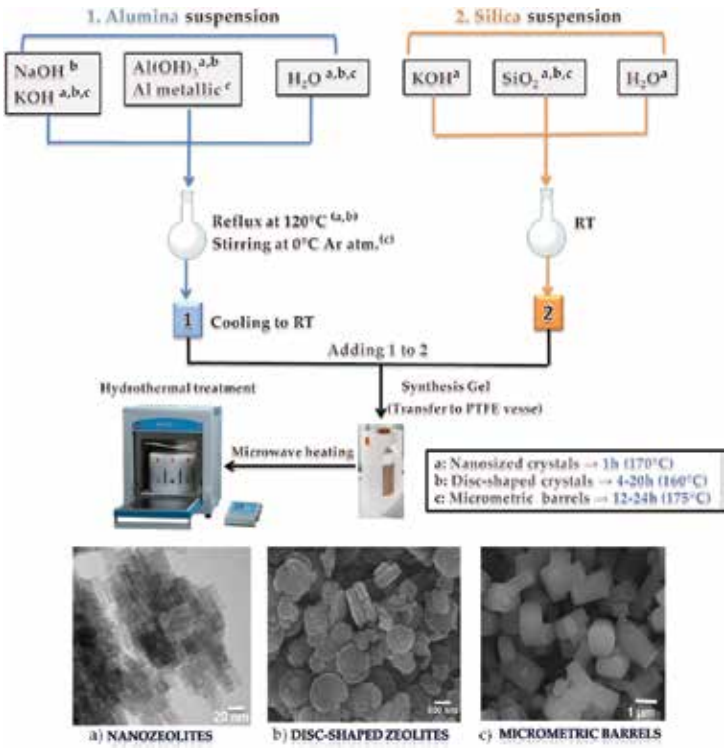

Figure 3. Scheme of the hydrothermal synthesis route for (a) nanosized, (b) disk-shaped, and (c) micrometric barrel-shaped LTL crystals and its respective morphologies analyzed by (a) transmission electron microscopy (TEM) and (b) and (c) scanning electron images (SEM) micrographs.

The synthesis procedure is described in **Figure 3** (route a) and the oxide molar ratio in the gel was fixed at 9.34 K_2O:1.00 Al_2O_3:20.20 SiO_2:412.84 H_2O. After heating the gel at 170°C under pressure for 1 h nanocrystals sizes were successfully obtained, where the size can be tuned from 15 to 50 nm by adjusting the synthesis conditions (gel ripening, static/dynamic conditions, or different silica sources). These nanosized LTL zeolites were subsequently used in energetic and photonic applications, such as catalytic supports for biogas reforming and fabrication of artificial antenna systems, respectively.

2.2. Disk-shaped LTL zeolite crystals

Disk-shaped crystals, characterized for having a low aspect ratio (length/diameter), were also synthesized in which their thickness and diameters were modified in a controlled way. This morphology is desirable to ease their coupling with external devices (e.g., to produce uniform and well-organized monolayers or membranes [10]), and to afford high number of uni-dimensional pores with short diffusion path lengths (around 100,000 channels in a crystal with diameter of 600 nm [24]).

The synthetic procedure is presented in the route b of **Figure 3**, starting in all cases from a fixed gel composition of 5.40 K_2O:5.50 Na_2O:1.00 Al_2O_3:30.00 SiO_2:416.08 H_2O oxides molar ratio and heating at 160°C. The variation of factors controlling the growing of the crystal, such

as the heating rate and the reaction time, allows the production of crystals with lengths ranging from 130 to 200 nm, and diameters spanning from 600 to 1200 nm.

2.3. Micrometric LTL zeolite barrels

The synthesis of large LTL zeolite crystals (from 1500 to 3000 nm length) with well-defined morphology and high aspect ratio (barrels-like microcrystals) has proven to be useful in the analysis of the distribution, orientation, and interaction of guest molecules by time- and space-resolved fluorescence measurements, such as fluorescence confocal microscopy at single-particle level [25].

The synthetic procedure is presented in the route c of **Figure 3**, starting in all cases from a fixed gel composition of 2.21 K_2O: 1.00 Al_2O_3:9.00 SiO_2:164.60 H_2O oxides molar ratio in the mixture and heating at 175°C.

To avoid undesirable process (mainly with organic dyes) owing to the high acidity of the channels, these synthesized zeolites were cation-exchanged with cesium or sodium.

3. Photoactive antenna materials

3.1. Dye-doped LTL zeolite

This section describes the development of photoactive nanomaterials based on the supramolecular organization of luminescent molecules into the channels of LTL zeolite. Taking inspiration from nature we will focus on one of the most sophisticated and vital processes in the earth, the photosynthesis, to develop a new generation of fluorescent nanomaterials. Using the *modus operandi* of the natural antenna systems present in photosynthetic organisms as a reference point, the main goal focused on the design and construction of artificial antenna systems able to mimic the functions and mechanism of these natural entities.

Many scientists all over the world are active participants in the challenge of developing artificial photoactive nanomaterials able to imitate the perfection and high efficiency of the mechanisms present in nature [26–28]. As a significant example, the photosynthetic organism present in plants appear as the most sophisticated solar energy storage systems in nature due to their unique ability to harvest solar radiation and transform it into chemical energy. The antenna systems, composed by few hundred of chlorophyll molecules are embedded in a protein environment (which keeps the photoactive moieties well arranged), are the responsible for absorbing the light and transfer the excitation energy to a specific reaction center [29]. Therefore, one of the main requirements for the proper operation of an artificial antenna system is the ability to harvest and transport the light to an acceptor moiety with the desired energy (**Figure 4**). The excitation energy transfer (EET) is a key factor ruling the effectiveness of the process. A careful understanding of the parameters controlling this phenomenon is mandatory, such as spectral overlap, ratio of donors and acceptors, interchromophoric distances, and relative orientations. The precise control of these variables enables the development of high-quality artificial antenna systems with potential applications in photonics,

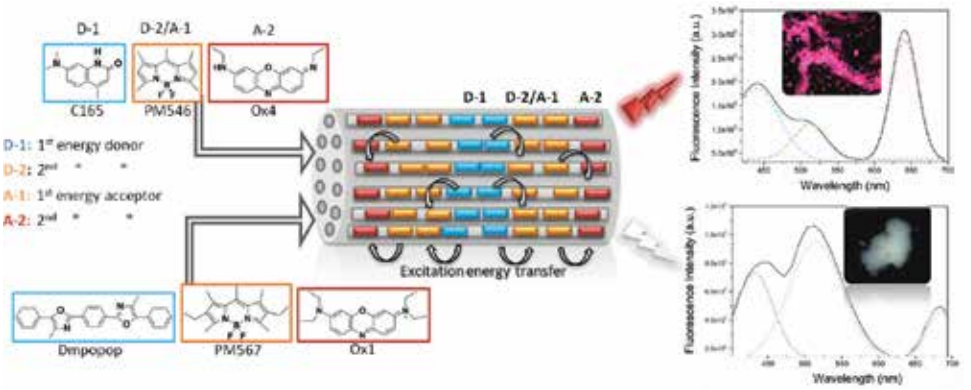

Figure 4. Schematic representation of the designed antenna material by means of the sequential insertion of three different dyes into LTL zeolite channels. The molecular structures of the two tested antenna systems using carbostyril (C165) and an oxazole (Dmpopop) as the blue-emitting energy donors, BODIPYs (PM546 and PM567) for the green-yellow region, and oxazines (Ox4 and Ox1) as red emitting final acceptors are also enclosed. The corresponding fluorescence spectra (upon selective excitation at the blue donor, 350 nm) and image (by fluorescence microscope) for each dye combination are also included. In all cases, the dye amount was the 10% of the available adsorption sites and the donor/acceptor ratio was 1:1:1.

optical coding, biosensing, catalysis, photosynthesis, logic devices, and theranostics, just to highlight some of them [30–32].

In our particular case, the strategy to develop competitive artificial antenna systems is based on the design of photoactive organic-inorganic hybrid materials. The protein matrix present in natural systems has been replaced by the LTL zeolitic host of nanometric dimensions, which apart from protecting the dyes, provides a constrained environment that induces a high degree of supramolecular organization. Furthermore, regarding the photoactive moiety, responsible for interacting with the light, the chlorophyll molecules have been replaced by small enough fluorescent molecules working in different regions of the electromagnetic spectrum (to ensure broadband absorption across the whole visible spectral region) and susceptible of promoting efficient EET processes. The energy transfer takes place via dipole-dipole coupling, better known as the through-space Förster mechanism (FRET), where one of the main requirements is the proper spectral overlap between the emission spectrum of the donor and the absorption spectrum of the acceptor. Therefore, by properly choosing the dyes to be encapsulated and controlling the spectral overlap of the combined dyes, the FRET efficiency can be finely tuned, and hence, the output emission light of the photoactive material will be modulated accordingly (**Figure 4**) [13, 33].

Here we present two antenna systems built by the sequential insertion of three different dyes into the pores of the LTL zeolite (**Figure 4**). As energy donors, oxazole (Dmpopop) and carbostyril (C165) dyes have been considered in the UV-blue region, whereas in the green-yellow part, BODIPYs (PM546 and P567) have been selected as first acceptors and succeeding energy donors. Finally, red-emitting oxazines (Ox1 and Ox4) where chosen as final energy acceptors. The UV-blue donors are placed in the center of the crystal, flanked by the green-yellow dyes, and with the red acceptors localized at the edges of the LTL zeolite crystal. In both antenna systems, the light is efficiently harvested over a broad spectral region and after selective excitation at the UV region, where only the first energy donors absorbs (C165 and Dmpopop,

respectively), its own emission is recorded but followed by that from the BODIPYs (PM546 and PM567) and the last energy acceptors (Ox4 and Ox1) (**Figure 4**).

However, there is a notorious difference in the energy output of each antenna system due to the different FRET process efficiency between the encapsulated dyes. The higher degree of spectral overlap in the antenna, composed by C165-PM546-Ox4 dyes, leaded to an efficient transformation of the harvested light into red emission (**Figure 4**). On the other hand, the less pronounced spectral overlap in the antenna, composed by Dmpopop-PM567-Ox1, decreased the FRET efficiency leading to the simultaneous detection of the emission from the three different chromophores with similar intensity. The sum of all these emissions covering the whole visible spectrum leads to white-light emission in which the energy output can be finely modulated over a broad region just using suitable filters (**Figure 4**). Therefore, by controlling the efficiency of the FRET hops, via the optimization of the magnitude of spectral overlap between the luminescent molecules inside de zeolitic channels, a fine modulation of the outcoming light energy can be reached, and hence either red-light or white-light emitting photoactive materials can be achieved.

3.2. External functionalization of LTL zeolite

In order to improve the degree of supramolecular organization, we tested a strategy based on the external functionalization of the channel entrances of LTL zeolite with tailor-made molecules (stopcock) via covalent linkage of such fluorophore (**Figure 5**) [13, 14]. These stopcock molecules grafted at the pores plug the channels to avoid the leakage of the guest molecules adsorbed inside and connect the inner space of the zeolite with the outside thanks to FRET processes, making the coupling of the material with other external devices straightforward.

The rational design of the stopcock molecule appears as key factor to ensure the suitable performance of it. On one hand, it needs to be small enough to diffuse into the pores and have the required functionalization to be covalently grafted at the channel entrances by reaction with free silanol groups (**Figure 5**). On the other hand, the emission should be placed at the red-edge of the visible spectral region to act as proper acceptor of the light harvested into the zeolitic channels. In this regard, we have designed a molecule made up of a label (triethoxysilane), a spacer and a head moiety (the fluorophore itself), taking BODIPY dyes as scaffold, owing to its excellent photophysical signatures and chemical versatility of its dipyrrin core subject to a plethora of organic reactions [34], and modified its backbone accordingly to fulfill the above mentioned perquisites. The next step consisted on the construction of the antenna system by its combination with a suitable energy donor; in this case, the above tested oxazole (Dmpopop), since it shows a broad absorption band in the UV-blue region and its emission overlaps well with the absorption band of the BODIPY-based stopcock. Therefore, the Dmpopop donor has been first inserted in the channels and right after the entrances were plugged with the silylated BODIPY. The selective excitation of the donor leads to a predominant red fluorescence from the stopcock centered at 610 nm (**Figure 5**), proving the ongoing FRET process from the inside to the outside of the crystal along the channel direction. Thus, the stopcock molecules enable the communication between the guest molecules encapsulated inside the pores with external materials or molecules outside. Besides, this closure molecule prevents small molecules like water or oxygen (fluorescence quenchers) from diffusing into the inner space of the crystals.

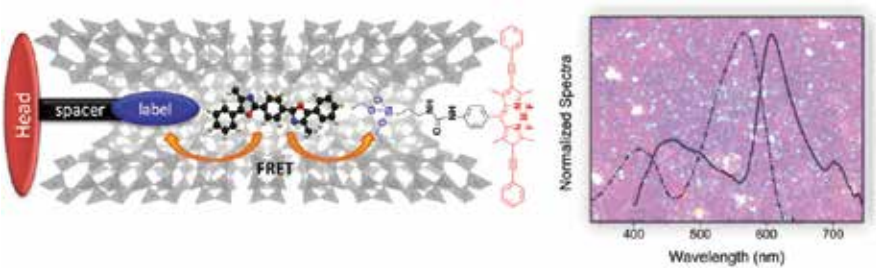

Figure 5. Schematic view of LTL zeolite channel doped with Dmpopop as energy donor (center), and the BODIPY-stopcock attached to the channel entrances as energy acceptor. The molecular structure of the stopcock and a scheme representing its three main components are shown in different colors. The corresponding normalized excitation (emission monitored at 600 nm, dashed line) and emission (excited at 350 nm, solid line) spectra, as well as the fluorescence microscopy image are also depicted.

4. LTL zeolite for hydrogen production through methane reforming processes

Catalyst supports play a key role in the process as it provides properties such as thermal stability, surface area, acidity, or the capacity of maintaining the metal dispersion during the reaction process. Those properties can be key factor for a catalyst to stand out from the existing ones [35]. For methane reforming processes, alumina supports are commonly used as they fit the mentioned properties [35–38]. Nevertheless, those properties are also present on zeolites. Accordingly, some zeolites were tested as support for methane reforming processes, in which, the influence of the nature of the zeolite support on the catalyst performance was analyzed [39, 40].

LTL zeolite has been used as catalyst support for methane reforming for hydrogen production, because hydrogen is considered the fuel of the future. For that purpose, LTL zeolite featuring different shapes (disc (DL), cylinders (CL), and nanocrystals (NL)), sizes (for the CL zeolites, between 1 and 3 μm and 30–60 nm) and alkaline metal (for the DL zeolites, with Cs, Na, or without them) exchange were used as catalyst support. Those supports were impregnated with nickel (13 wt.%) or co-impregnated with nickel and rhodium (13 and 1 wt.%, respectively) in order to prepare the corresponding monometallic or bimetallic catalysts, following the wet impregnation procedure [12, 23].

Nickel is a metal widely used for reforming processes because of its availability and relatively low price. On the other hand, although noble metals are more expensive than non-noble metals, it has been reported that the addition of small amounts of a noble metal to a non-noble metal catalyst increases the activity and dispersion of the non-noble metal due to the spill-over effect [41]. Therefore, a low amount of rhodium was incorporated to prepare bimetallic catalysts.

4.1. Chemical composition

The content of the metal incorporated into the zeolite supports was determined by Inductively Coupled Plasma-Atomic Emission Spectroscopy (ICP-AES) model 2000 DV (Perkin Elmer)

instrument. The composition, summarized in **Table 1**, indicates that the measured values were close to the nominal ones.

4.2. Textural properties

The textural properties of the LTL zeolite supported catalysts were determined by means of N_2 adsorption-desorption isotherms obtained at 77 K using an Autosorb-1C-TCD. The measured textural property values were not only affected by metal incorporation, but also by the calcination carried out on the catalyst preparation procedure.

The calcinations at 1073 K for 4 h before the metal impregnation produced an important decrease in the textural properties of the LTL zeolite, as shown in **Table 2**. As it could be expected, those values were further reduced when the metal impregnation and catalysts calcinations were carried out, as shown in **Tables 2** and **3**.

Due to the low amount of noble metal impregnated on the zeolites (1 wt.%), differences on the textural properties for monometallic and bimetallic catalysts (**Table 2**) were only observed for CL (30–60 nm) supported catalysts. The bimetallic catalyst presented a lower SSA value, in accordance to its higher pore volume and much higher PD, probably due to a higher coverage

Support	Rh	Ni	Catalyst	Rh	Ni
Ni/DL	—	11.1	Rh-Ni/DL	0.9	12.9
Rh-Ni/DL	0.9	12.4	Rh-Ni/DLCs	0.8	12.4
Ni/CL (1–3 μm)	—	12.7	Rh-Ni/DLNa	0.8	11.6
Rh-Ni/CL (1–3 μm)	1.0	14.0	Rh-Ni/NL	0.9	13.8
Ni/CL (30–60 nm)	—	11.9	Rh-Ni/NLCs	0.8	13.3
Rh-Ni/CL (30–60 nm)	1.1	13.2	Rh-Ni/NLNa	0.9	11.6

Table 1. Chemical compositions for catalysts prepared with LTL zeolite expressed as wt.% [12, 23].

Support	SSA (m^2/g)	PV (cm^3/g)	PD (Å)	Catalyst	SSA (m^2/g)	PV (cm^3/g)	PD (Å)
DL (F)	258	0.04	14	Ni/DL	40	0.10	54
DL (C)	134	0.06	17	Rh-Ni/DL	42	0.12	63
CL (1–3 μm) (F)	260	0.05	13	Ni/CL (1–3 μm)	23	0.05	55
CL (1–3 μm) (C)	152	0.04	13	Rh-Ni/CL (1–3 μm)	26	0.07	58
CL (30–60 nm) (F)	419	0.90	54	Ni/CL (30–60 nm)	95	0.45	96
CL (30–60 nm) (C)	335	0.93	67	Rh-Ni/CL (30–60 nm)	64	0.63	198

Table 2. Textural properties, specific surface area (SSA), average pore volume (PV) and average pore diameter (PD), of fresh (F) and calcined (C) LTL zeolite and their corresponding monometallic and bimetallic catalysts [12].

of the low size pores. Nevertheless, both CL (30–60 nm) supported catalysts presented the highest BET areas.

It is worth mentioning that in the cases of the metal impregnation on DLCs and DLNa catalysts, the measured BET area increased (**Table 3**). That happened due to the creation of new area with the metallic particles, as the original LTL zeolite surface area was low.

4.3. Temperature programmed reduction (TPR)

Catalysts reducibility was evaluated by temperature programmed reduction (TPR) using an Autosorb-1C-TCD device. The obtained reduction profiles are summarized in **Figure 6**. The profiles in the left side of **Figure 6** show that for bimetallic catalysts the reduction processes start at lower temperatures than their corresponding monometallic catalysts, probably due to the spill-over effect [12].

Support	SSA (m^2/g)	PV (cm^3/g)	PD (Å)	SSA (m^2/g)	PV (cm^3/g)	PD (Å)	SSA (m^2/g)
DL	59	0.07	30	Rh-Ni/DL	38	0.13	72
DLCs	13	0.08	122	Rh-Ni/DLCs	17	0.13	155
DLNa	1	<0.01	264	Rh-Ni/DLNa	3	<0.01	251
NL	210	0.79	79	Rh-Ni/NL	68	0.19	59
NLCs	96	0.65	136	Rh-Ni/NLCs	37	0.15	85
NLNa	144	0.74	106	Rh-Ni/NLNa	43	0.17	77

Table 3. Textural properties, specific surface area (SSA), average pore volume (PV) and average pore diameter (PD), of LTL zeolite and their corresponding bimetallic catalysts [12].

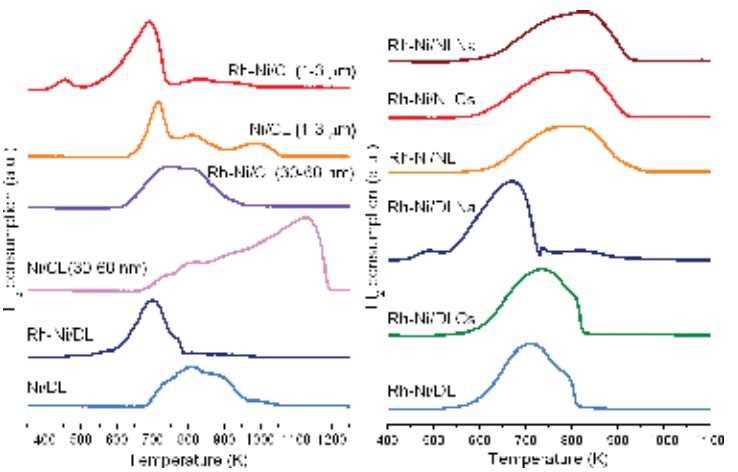

Figure 6. TPR profiles for zeolite L supported catalysts, modified from [12, 23].

Both, CL (1–3 μm) supported catalysts and Rh-Ni/DL catalyst, presented the main reduction peak around 700 K due to the reduction of NiO with low interaction with the support [42]. Ni/CL (1–3 μm) catalyst presented other two small peaks at 820 and 1000 K originated by the reduction of NiO particles with high interaction with support and Ni species located on the hexagonal prism, respectively [43]. Bimetallic CL (1–3 μm) and DL supported catalysts did not show those two reduction peaks, probably because they produced a more intense peak attributed to the NiO with low interaction with the surface. However, they presented a low peak and a shoulder at temperatures around 820 K, which could also be produced by the reduction NiO with high interaction with the surface. Similar profiles were produced for Rh-Ni/DL with and without alkali metal exchanged.

Ni/DL, Rh-Ni/CL (30–60 nm), and NL supported catalysts also presented similar profiles. On them, the hydrogen consumption peaks that took place around 700–750 K were produced by the reduction of NiO species [42, 44]. The reductions that took place at higher temperatures (~800 K) could be assigned to NiO particles with stronger interaction with support [43].

Among the studied catalysts, Ni/CL (30–60 nm) catalyst produced its main reduction peaks at the highest temperature (1150 K) because of the reduction of non-stoichiometric and stoichiometric Ni-spinels [45].

Rhodium reduction peaks were only detected for Rh-Ni/CL (1–3 μm) and Rh-Ni/DLNa catalysts at temperatures around 450 K [46]. Therefore, rhodium is probably stronger interacting with support in the other bimetallic catalysts, and thus, its reduction peak could be covered by more intense H_2 consumptions produced by Ni species.

4.4. X-ray diffraction (XRD)

Before activity tests, catalysts were also analyzed by X-ray diffraction (XRD) using a Philips X'PERT PRO automatic diffractometer operating at 40 kV and 40 mA, in theta-theta configuration, secondary monochromator with Cu Kα radiation (λ = 1.5418 Å) and a PIXcel solid state detector. Diffraction patterns are shown in **Figure 7**. In the left side of the figure, the XRD patterns of fresh calcined monometallic and bimetallic catalysts are shown, while on the right side the patterns of other reduced zeolite L with and without alkali modification supported catalysts are collected.

All the patterns of the LTL zeolite supported catalysts showed characteristic peaks of the LTL zeolite at 2 theta (θ) degrees from 10 to 42. Nevertheless, the intensity of the peaks is lower for the reduced catalysts. The loss of the intensity could be caused by the loss of the crystallinity happened during the reduction treatment. Accordingly, for some of the reduced catalysts, there is only a broad peak in the range in which LTL zeolite peaks should be placed, i.e., Rh-Ni/DLNa, Rh-Ni/NLCs, or Rh-Ni/NLNa catalysts.

Apart from the diffraction peaks attributed to the LTL zeolite structure, fresh calcined catalysts produced diffraction peaks attributed to NiO (Powder Diffraction File (PDF): 01-044-1159) at 43 and 63 2 theta degrees.

On the other hand, the XRD analyses for reduced LTL zeolite supported catalysts presented metallic nickel peaks at around 44 and 53 2 theta degrees (PDF: 01-087-0712). For these catalysts, peaks corresponding to nickel oxides were not observed.

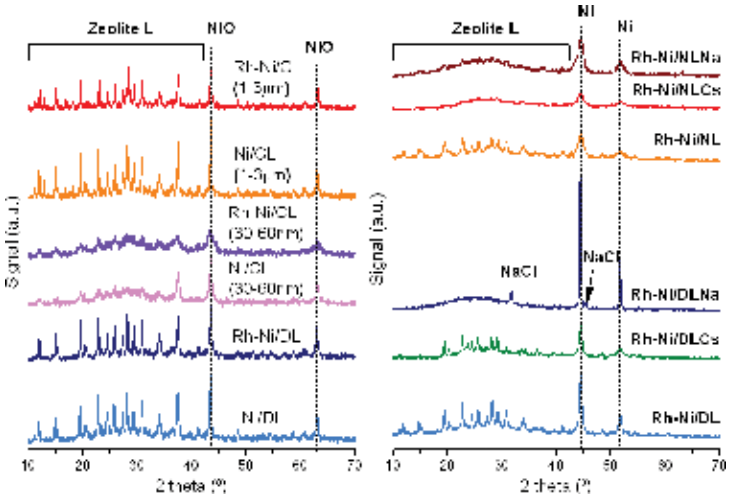

Figure 7. XRD patterns of zeolite L supported catalysts, modified from [12, 23].

The application of Scherrer equation on the most intense nickel diffraction peaks (2θ = 43 and 2θ = 44 for nickel oxide and metallic nickel, respectively) showed that, in general, bimetallic catalysts presented smaller NiO crystallite sizes (~30 nm) than their homologous monometallic catalysts (~60 nm), meaning that the active metal could be better dispersed in the bimetallic samples. The DL supported catalysts were the exception, as both monometallic and bimetallic catalyst containing NiO crystallites around 30 nm.

XRD analyses did not provide any diffraction peak attributed to rhodium (neither metallic nor oxide). Thus, rhodium particles smaller than the detection limit of the equipment (<4 nm) could be present on the catalysts, as the presence of rhodium on the catalysts was assured by ICP-AES.

For the LTL zeolite with and without alkali metal modification (Cs or Na) the estimated crystallite sizes were from 10 to 25 nm. In this case, Rh-Ni/DLNa catalyst was the exception and presented nickel crystals around 100 nm, as it can be observed in the TEM images (**Figure 8**) acquired on a Philips CM 200 transmission electron microscope at an acceleration voltage of 200 kV with a LaB_6 filament. The high crystallite size could be related with the low surface area and the consequent higher nickel agglomeration on the surface of the catalyst.

4.5. X-ray photoelectron spectroscopy (XPS)

The catalysts prepared with DL and NL with and without alkali modification were also reduced and analyzed by X-ray photoelectron spectroscopy (XPS) in order to compare surface (XPS) and bulk (ICP-AES) nickel and rhodium abundances. Results are summarized in **Table 4**. For that purpose, a VG Escalab 200R spectrometer equipped with a hemispherical electron analyzer and an Al Kα1 (hν = 1486.6 eV) 120 W X-ray source was used.

Both metals, Ni and Rh, were preferentially located on the external surface of the catalysts as indicated by the Ni/zeolite and Rh/zeolite ratios which were higher for the XPS than for

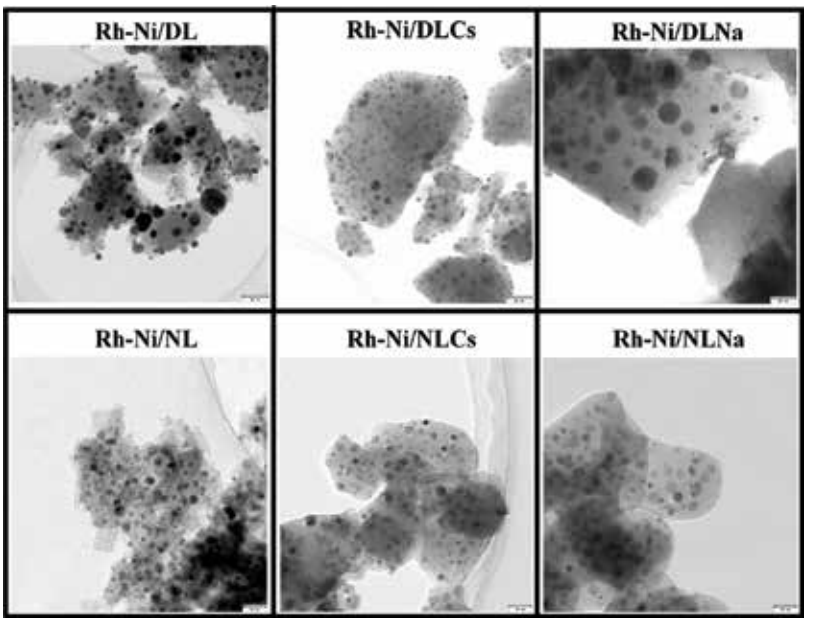

Figure 8. TEM images of the calcined catalysts. Scale size for DL and NL of 80 and 30 nm, respectively. Modified from [12].

Catalyst	Atomic ratios XPS/ICP	
	Ni/zeolite L	Rh/zeolite L
Rh-Ni/DL	3.10/0.22	0.89/0.01
Rh-Ni/DLCs	5.61/0.24	1.06/0.01
Rh-Ni/DLNa	5.17/0.25	–/0.01
Rh-Ni/NL	0.47/0.22	0.29/0.01
Rh-Ni/NLCs	2.02/0.26	0.44/0.01
Rh-Ni/NLNa	1.81/0.27	–/0.01

Modified from [23].

Table 4. Comparison of the surface atomic ratios measured by XPS and the bulk atomic ratios measured by ICP.

the ICP-AES. The difference between the high XPS and lower ICP-AES ratios were more significant for DL with and without Cs and Na modification supported catalysts, because they presented the lowest SSA values. On the other hand, for DL and NL supported catalysts, a similar trend was observed; the lowest metallic content on the external surface was measured to the unmodified support, while highest values were measured for the Cs containing catalysts. Therefore, the presence of Cs and Na hinders the metal incorporation into the pores [23].

4.6. Catalytic activity

The catalytic activities of the monometallic and bimetallic catalysts supported on DL, CL (30–60 nm) and CL (1–3 μm) were evaluated for 90 min at 1073 K and atmospheric pressure under different biogas reforming conditions, summarized in **Table 5**.

A ¼ inch 316 L stainless steel fixed bed reactor was used for the experiments. The catalytic bed was composed of 0.34 g of catalyst (0.42 < particle diameter (dP) < 0.50 mm) mixed with 1.53 g of inert CSi (0.50 < dP < 1.0 mm). The catalytic bed was placed in the middle of the length of the reactor and kept in place by filling the rest of the reactor with inert CSi (1.0 < dp < 3.0 mm).

The reactor was placed in a Microactivity Reference bench-scale plant (PID Eng&Tech) to perform the activity experiments. Biogas ($CH_4 + CO_2$), N_2 and O_2 were fed by electronic controllers, while deionized water was injected using an HPLC-Gilson water pump. Catalysts were reduced at 1073 K before the activity tests using 350 N mL min^{-1} of a 3:1 N_2:H_2 mixture for 4 h. The composition of the product gases was determined by an online connected micro GC equipped with thermal conductivity detector (TCD). The measured parameters were defined as:

$$\text{Methane conversion}: X_{CH4}\,(\%) = \left(V_{CH4}{}^{in} - V_{CH4}{}^{out}\right)/V_{CH4}{}^{in} \times 100 \tag{1}$$

$$\text{Carbon dioxide conversion}: X_{CO2}\,(\%) = \left(V_{CO2}{}^{in} - V_{CO2}{}^{out}\right)/V_{CO2}{}^{in} \times 100 \tag{2}$$

$$\text{Hydrogen yield}: H_2\text{ yield}\,(\%) = V_{H2}{}^{out}/\left(2 \times V_{CH4}{}^{in} + V_{H2O}{}^{in}\right) \times 100 \tag{3}$$

$$\left(H_2/CO\right)^{out}\text{ molar ratio}: \left(H_2/CO\right)^{out} = \left(V_{H2}/V_{CO}\right)^{out} \tag{4}$$

where V_i^{in} and V_i^{out} correspond to the inlet and outlet volumetric flow rate of reactant i (NmL/min), respectively.

Process	Feed ratios	WHSV (h^{-1})
Dry reforming (DR)	Biogas: CH_4/CO_2 = 1.5	75.0
Steam reforming (SR)	Biogas + water at S/C = 1.0	104.8
	Biogas + water at S/C = 2.0	134.6
Oxidative reforming (OR)	Biogas + air at O/C = 0.25	131.8
	Biogas + air at O/C = 0.50	188.6
Tri-reforming (TR)	Biogas + water + air at S/C = 1.0 and O/C = 0.25	161.5

Table 5. Summary of the processes and feed ratios for the tests for zeolite L supported catalysts.

The experimental results, summarized in **Figures 9** and **10**, showed that even if in some cases there were no important differences in the hydrogen yield produced by monometallic or bimetallic catalysts, the highest hydrogen yields were generally achieved by bimetallic catalysts.

During DR experiments (**Figure 9(a)**), high conversions and hydrogen yields were achieved. In those conditions, CL (1–3 μm) supported catalysts were the less active ones. On the contrary, Ni/DL catalyst achieved a CH_4 conversion (X CH_4) and consequently hydrogen yield, much higher than equilibrium values, probably caused by the presence of hot spots inside the reactor [12].

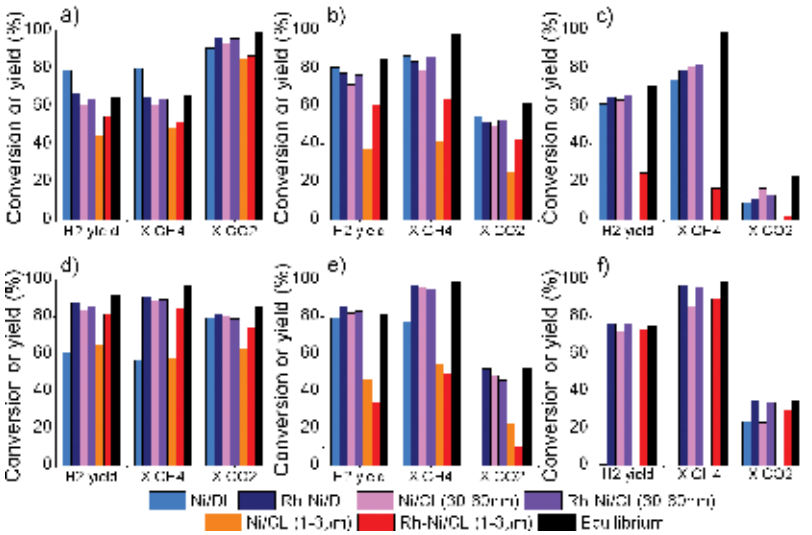

Figure 9. Activity results obtained for several biogas reforming processes carried out at 1073 K and atmospheric pressure at different feeding ratios: (a) DR, (b) SR at S/C = 1.0, (c) SR at S/C = 2.0, (d) OR at O/C = 0.25, (e) OR at O/C = 0.50, and (f) TR at S/C = 1.0 and O/C = 0.25. Figure modified from [12].

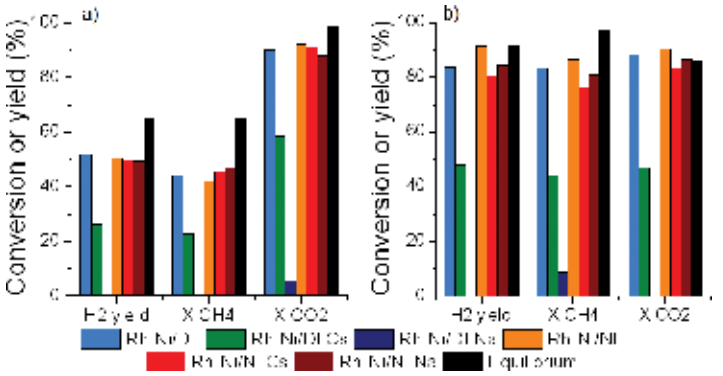

Figure 10. Activity results obtained for two biogas reforming processes at 1073 K and atmospheric pressure: (a) DR and (b) OR at O/C = 0.25. Figure modified from [23].

The addition of steam for SR produced an increase in the methane conversion, but a decrease in the CO_2 conversion (X CO_2) at S/C = 1.0 (**Figure 9(b)**) Thus, the hydrogen yields were higher than in DR conditions for most of the catalysts. However, when the S/C ratio was increased from 1.0 to 2.0 (**Figure 9(c)**) the methane conversion was not increased, but reduced in most of the cases, while the CO_2 conversion was even more reduced. Accordingly, hydrogen yields were also lower when an S/C ratio of 2.0 was used. In both SR experiments, the CL (1–3 μm) supported catalysts achieved again the lowest hydrogen yields because of their low methane conversions. At the S/C ratio of 2.0, the Ni/CL (1–3 μm) catalyst produced a negative CO_2 conversion, due to a higher selectivity to the water gas shift reaction. The rest of the catalysts achieved hydrogen yields, and methane and carbon dioxide conversion values, close to the ones predicted by the equilibrium calculations.

The setting of OR conditions produced some modifications on the activities. When an O/C ratio of 0.25 was used (**Figure 9(d)**), Ni/DL and Ni/CL (1–3 μm) catalysts were the less active ones converting CH_4. Accordingly, they were less active than the rest of the catalysts producing hydrogen. Surprisingly, the Rh-Ni/CL (1–3 μm) catalyst showed similar activities than Rh-Ni/DL, Ni/CL (30–60 nm) and Rh-Ni/CL (30–60 nm) catalysts, with a hydrogen yields, methane and carbon dioxide conversion values above 80%.

Nevertheless, the feeding of a higher amount of oxygen (air) to the reactor (**Figure 9(e)**), demonstrated again the poor activity of the CL (1–3 μm) supported monometallic and bimetallic catalysts in comparison with the rest of the catalysts. Ni/DL catalyst almost produced as much hydrogen as the three most active catalysts. The O/C increase produced an increase of the methane conversion, but a significant decrease in both equilibrium and experimental CO_2 conversion values. The higher CO_2 conversion values measured in OR at O/C = 0.25 than 0.50 could be originated by the lower amount of oxygen available to react with methane (assuming that all the oxygen fed reacts with methane), and therefore, a higher amount of methane is available to react with carbon dioxide by means of the DR reaction.

Finally, when oxygen (air) and steam were fed together with biogas in order to carry out TR experiments (**Figure 9(f)**), results similar to the ones achieved during OR at O/C ratio of 0.25 were obtained. Once again, Ni/DL and Ni/CL (1–3 μm) catalysts were the less active. Surprisingly, the Ni/DL catalyst produced negative CH_4 and CO_2 conversions, thus a methanation reaction was carried out [39]. Ni/CL (1–3 μm) catalyst also produced a negative CO_2 conversion.

Monometallic and bimetallic DL and CL (30–60 nm) supported catalysts achieved the highest methane conversions in most of the studied processes. For those catalysts, the rhodium incorporation improved the methane conversion by reaching values higher than 80%. The methane conversion measured for these two bimetallic catalysts was almost complete when they were tested under OR at O/C = 0.50 and TR conditions. Therefore, the bimetallic catalysts supported on DL and CL (30–60 nm) turned out to be the most appropriates ones for the studied reforming processes. The highest hydrogen yields for the most active catalysts were achieved under OR conditions at the O/C ratio of 0.25.

Due to the poor methane and carbon dioxide conversions reached by Ni and Rh-Ni/CL (1–3 μm) catalysts, their hydrogen production yield was lower than the rest of the catalysts.

For all the experiments, the synthesis gas ratio (H_2/CO molar ratio), was also measured. For liquid hydrocarbon production through Fischer-Tropsch for methanol synthesis, a syngas with a ratio close to 2 is desired. On the other hand, a synthesis gas with a ratio of 1 is necessary for oxo or hydroformylation reaction. According to equilibrium calculations, the SR process at S/C = 2.0 is the only process able to produce a syngas ratio higher than 2. The SR at S/C = 1.0 and TR processes can also produce syngas ratios with values close to 2. Therefore, those processes would require an additional step (apart from the purification) for reaching the desired syngas ratio. On the contrary, for obtaining a syngas ratio close to 1, the equilibrium calculations indicate that both OR processes (at O/C = 0.25 and 0.50) and DR process are more suitable. These equilibrium predicted values were, in general, in good agreement with experimental values for most of the catalysts.

According to the above summarized results, we decided to prepare bimetallic catalysts to study the effect of alkali metals modification. The processes selected to test the bimetallic catalysts were DR and OR (**Figure 10**). On the one hand, the DR process presents the harsher reaction conditions and therefore, it is appropriate to distinguish the activity of the catalysts. On the other hand, the OR process is the most favorable in terms of hydrogen production.

Similar catalytic activity was observed for both studied processes. First, the NL, NLCs, NLNa, and DL supported bimetallic catalysts achieved the highest CH_4 and CO_2 conversions and H_2 yield values, while Ni/DLCs catalyst produced intermediate results. Second, the less active catalyst was Rh-Ni/DLNa, which remained almost inactive in both biogas reforming processes. Therefore, there was a good agreement between the activity, the BET areas, the particle sizes estimated by XRD, and the ones observed by TEM, and the atomic Rh and Ni concentration. Thus, the most active catalysts presented the highest BET areas, the smaller metal particle sizes and the most equilibrated Rh and Ni surface concentrations.

5. Conclusions

The herein reported step-by-step strategy to develop dye- and metal-doped LTL zeolites is suitable to attain materials which can be applied in photonics and eco-friendly catalysis. To this aim, we started from the beginning, by the microwave-assisted synthesis of the LTL zeolite crystals. This kind of heat allows a fine control of the size (from tens of nm to few μm) and shape (from barrels to coins) of the zeolite, which can be tuned just fixing the hydrothermal synthesis conditions. Afterwards, the kind of guest adsorbed into the zeolitic support will rule the application field of the material. On one hand, the allocation of rationally selected fluorophores into the uni-dimensional zeolitic channels, or grafted to the pore entrances, provide a hierarchically ordered material able to harvest light over a broad spectral interval and provide predominant red fluorescence, or alternatively white-light emission, just adjusting the energy transfer efficiency. On the other hand, the deposition of suitable metals onto the zeolite guest boosts the catalysis efficiency in the biogas reforming. Among the different LTL zeolite morphologies used, DL and CL (30–60 nm) supports were the most active ones for the studied reforming processes, especially when Rh and Ni metals were incorporated in order to prepare bimetallic catalysts. High activities are attributed to the high metal dispersion and the strong interactions among NiO and the different supports. The metal exchange of Cs and Na carried out on DL and NL supports mainly affected the morphology, and consequently,

the activity of DL catalyst series. However, the modification of the zeolites with Cs or Na was unsuccessful for biogas reforming catalytic applications because the Rh-Ni/DL and Rh-Ni/NL catalysts showed higher reforming capacity.

Summing up, LTL zeolite arises as a suitable and versatile support to allocate small-enough chromophores into their channels. Such cage effect protects and aligns the fluorophores, whereas the encapsulation enhances the energy transfer efficiency even at low dye loadings, being ideal for antenna or microlaser devices. Besides, its high specific surface allows the incorporation of metals boosting their catalytic efficiency toward the desired reaction, in this case biogas reforming, a long seeking clean energy source as an alternative to polluting fuels.

Acknowledgements

Financial support from MICINN (MAT2014-51937-C3-3-P), MINECO (OIL2H2. ENE2011-23950), European Regional Development Fund (ERDF) and Gobierno Vasco (IT912-16 and IT993-16) is acknowledged. L. G.-R. and K. B. thanks Gobierno Vasco for a postdoctoral and predoctoral fellowship, respectively. Dr. Y. Xiao (from Dalian University in China) is gratefully thanked by the synthesis of the silylated-BODIPY stopcock.

Author details

Leire Gartzia Rivero[1], Jorge Bañuelos[1]*, Kepa Bizkarra[2], Urko Izquierdo[2], Victoria Laura Barrio[2], Jose Francisco Cambra[2] and Iñigo López Arbeloa[1]

*Address all correspondence to: jorge.banuelos@ehu.es

1 Department of Physical Chemistry, University of the Basque Country (UPV/EHU), Bilbao, Spain

2 Faculty of Engineering, University of the Basque Country (UPV/EHU), Bilbao, Spain

References

[1] Ogawa M, Kuroda K. Photofunctions of interaction compounds. Chemical Reviews. 1995;**95**:399-438. DOI: 10.1021/cr00034a005

[2] Cheetman AK, Férey G, Loiseau T. Open-framework inorganic materials. Angewandte Chemie, International Edition. 1999;**38**:3268-3292. DOI: 10.1002/(SICI)1521-3773(19991115)38:22<3268::AID-ANIE3268>3.0.CO;2-U

[3] Ramamurthy V. Controlling photochemical reactions via confinement: Zeolites. Journal of Photochemistry and Photobiology C. 2000;**1**:145-166. DOI: 10.1016/S1389-5567(00)00010-1

[4] Tao Y, Kanoh H, Abrams L, Kaneko K. Mesopore-modifed zeolites: Preparation, characterization and applications. Chemical Reviews. 2006;**106**:896-910. DOI: 10.1021/cr040204o

[5] Schulz-Ekloff G, Wöhrle D, van Duffel B, Schoonheydt RA. Chromophores in porous silicas and minerals: Preparation and optical properties. Microporous and Mesoporous Materials. 2002;**51**:91-138. DOI: 10.1016/S1387-1811(01)00455-3

[6] Cronsted AF. Akad. Hankl. Stockholm. 1756;**18**:120. Translation: Sumelius IrG. In: Occelli ML, Robson H. Molecular Sieves. New York: Van Nostrand Reinhold; 1992

[7] Baerlocher C, Meier WH, Olson DH. Atlas of Zeolite Framework Types. 6th ed. Elsevier; 2007. Available from: http://www.iza-structure.org/databases/

[8] Corma A. Inorganic solid acids and their use in acid-catalyzed hydrocarbon reactions. Chemical Reviews. 1995;**95**:559-614. DOI: 10.1021/cr00035a006

[9] Mech A, Monguzzi A, Meinardi F, Mezyk J, Macchi G, Tubino R. Sensitized NIR erbium(III) emission in confined geometries: A new strategy for light emitters in telecom applications. Journal of the American Chemical Society. 2010;**132**:4574-4576. DOI: 10.1021/ja907927s

[10] Devaux A, Calzaferri G, Belser P, Cao P, Brühwiler D, Kunzmann A. Efficient and robust host-guest antenna composite for light harvesting. Chemistry of Materials. 2014;**26**:6878-6885. DOI: 10.1021/cm503761q

[11] Lee TP, Saad B, Ng EP, Salleh B. Zeolite Linde Type L as micro-solid phase extraction sorbent for the high performance liquid chromatography determination of ochratoxin A in coffee and cereal. Journal of Chromatography. A. 2012;**1237**:46-54. DOI: 10.1016/j.chroma.2012.03.031

[12] Izquierdo U, Barrio VL, Bizkarra K, Gutierrez AM, Arraibi JR, Gartzia L, Bañuelos J, Lopez-Arbeloa I, Cambra JF. Ni and Rh-Ni catalysts supported on zeolites L for hydrogen and syngas production by biogas reforming processes. Chemical Engineering Journal. 2014;**238**:178-188. DOI: 10.1016/j.cej.2013.08.093

[13] Gartzia-Rivero L, Bañuelos J, López-Arbeloa I. Photoactive nanomaterials inspired by nature: LTL zeolite doped with laser dyes as artificial light harvesting systems. Materials. 2017;**10**:495. DOI: 10.3390/ma10050495

[14] Huber S, Calzaferri G. Energy transfer from dye-zeolite L antenna crystal to bulk silicon. Chemphyschem. 2004;**5**:239-242. DOI: 10.1002/cphc.200301002

[15] Suarez S, Devaux A, Bañuelos J, Bossart O, Kunzmann A, Calzaferri G. Transparent zeolite-polymer hybrid materials with adaptable properties. Advanced Functional Materials. 2007;**17**:2298-2306. DOI: 10.1002/adfm.200600925

[16] Vohra V, Calzaferri G, Destri S, Pasini M, Porzio W, Botta C. Toward white light emission through efficient two-step energy transfer in hybrid nanofibers. ACS Nano. 2010;**4**:1409-1416. DOI: 10.1021/nn9017922

[17] Vietze U, Kraub O, Laeri F, Ihlein G, Schüth F, Limburg B, Abraham M. Zeolite-dye microlasers. Physical Review Letters. 1998;**81**:4628-4631. DOI: 10.1103/PhysRevLett.81.4628

[18] Marega R, Prasetyanto EA, Michiels C, De Cola L, Bonifazi D. Fast targeting and cancer cell uptake of luminescent antibody-nanozeolite bioconjugates. Small. 2016;**12**:5431-5441. DOI: 10.1002/smll.201601447

[19] Zabala A, Brühwiler D, Ban T, Calzaferri G. Synthesis of zeolite L. Tuning size and morphology. Monatschefte für Chemie. 2005;**136**:77-89. DOI: 10.1007/s00706-004-0253-z

[20] Lupulescu AI, Kumar M, Rimer JD. A facile strategy to design zeolite L crystals with tunable morphology and surface architecture. Journal of the American Chemical Society. 2013;**135**:6608-6617. DOI: 10.1021/ja4015277

[21] Tompsett GA, Conner WC, Yngvesson KS. Microwave synthesis of nanoporous materials. Chemphyschem. 2006;**7**:296-319. DOI: 10.1002/cphc.200500449

[22] Bilecka I, Niederberger M. Microwave chemistry for inorganic nanomaterials synthesis. Nanoscale. 2010;**2**:1358-1374. DOI: 10.1039/B9NR00377K

[23] Gartzia-Rivero L, Bañuelos J, Izquierdo U, Barrio VL, Bizkarra K, Cambra JF, López-Arbeloa I. Microwave synthesis of LTL zeolites with tunable size and morphology: An optimal support for metal-catalyzed hydrogen production from biogas reforming processes. Particle and Particle Systems Characterization. 2014;**31**:110-120. DOI: 10.1002/ppsc.201300275

[24] Calzaferri G. Nanochannels: Hosts for the supramolecular organization of molecules and complexes. Langmuir. 2012;**28**:6216-6231. DOI: 10.1021/la3000872

[25] Martínez-Martínez V, García R, Sola-Llano R, Gómez-Hortigüela L, Sola-Lano R, Pérez-Pariente J, López-Arbeloa I. Highly luminescent and optically switchable hybrid material by one-pot encapsulation of dyes into MgAPO-11 unidirectional nanopores. ACS Photonics. 2014;**1**:205-211. DOI: 10.1021/ph4000604

[26] Benniston AC, Harriman A. Artificial photosynthesis. Materials Today. 2008;**11**:26-34. DOI: 10.1016/S1369-7021(08)70250-5

[27] El-Khouly M, El-Mohsnawy E, Fukuzumi S. Solar energy conversion: From natural to artificial photosynthesis. Journal of Photochemistry and Photobiology C. 2017;**31**:36-83. DOI: 10.1016/j.jphotochemrev.2017.02.001

[28] Zan G, Wu Q. Biomimetic and bioinspired synthesis of nanomaterials/nanostructures. Advanced Materials. 2016;**28**:2099-2147. DOI: 10.1002/adma.201503215

[29] Scholes GD, Fleming GR, Olaya-Castro A, van Grondelle R. Lessons from nature about solar light harvesting. Nature Chemistry. 2011;**3**:763-774. DOI: 10.1038/nchem.1145

[30] Hötzer B, Medintz IL, Hildebrandt N. Fluorescence in nanobiotechnology: Sophisticated fluorophores for novel applications. Small. 2012;**8**:2297-2326. DOI: 10.1002/smll.201200109

[31] Claassens NJ, Volpers M, Santos V, van der Oost J, de Vos WM. Potential of proton-pumping rhodopsins: Engineering photosystems into microorganisms. Trends in Biotechnology. 2013;**31**:633-642. DOI: 10.1016/j.tibtech.2013.08.006

[32] Feng X, Ding X, Chen L, Wu Y, Liu L, Addicoat M, Irle S, Dong Y, Jiang D. Two-dimensional artificial light-harvesting antennae with predesigned high-order structure and robust photosensitizing activity. Scientific Reports. 2016;**6**:32944. DOI: 10.1038/srep32944

[33] Insuwan W, Rangsriwatananon K, Meeprasert J, Namuangruk S, Surakhot Y, Kungwan N, Jungsuttiwong S. Combined experimental and theoretical investigation on fluorescence

resonance energy transfer of dye loaded on LTL zeolite. Microporous and Mesoporous Materials. 2017;**241**:372-382. DOI: 10.1016/j.micromeso.2016.12.020

[34] Loudet A, Burgess K. BODIPY dyes and their derivatives: Syntheses and spectroscopic properties. Chemical Reviews. 2007;**107**:4891-4932. DOI: 10.1021/cr078381n

[35] Frontera P, Macario A, Aloise A, Crea F, Antonucci PL, Nagy JB, Frsusteri F, Giordano G. Catalytic dry-reforming on Ni–zeolite supported catalyst. Catalysis Today. 2012;**179**: 52-60. DOI: 10.1016/j.cattod.2011.07.039

[36] Bereketidou OA, Goula MA. Biogas reforming for syngas production over nickel supported on ceria-alumina catalysts. Catalysis Today. 2012;**195**:93-100. DOI: 10.1016/j.cattod.2012.07.006

[37] Damyanova S, Pawelec B, Arishtirova K, Fierro JLG. Biogas reforming over bimetallic PdNi catalysts supported on phosphorus-modified alumina. International Journal of Hydrogen Energy. 2011;**36**:10635-10647. DOI: 10.1016/j.ijhydene.2011.05.098

[38] Xu J, Zhou W, Li Z, Wang J, Ma J. Biogas reforming for hydrogen production over a Ni-Co bimetallic catalyst: Effect of operating conditions. International Journal of Hydrogen Energy. 2010;**35**:13013-13020. DOI: 10.1016/j.ijhydene.2010.04.075

[39] Kaengsilalai A, Luengnaruemitchai A, Jitkarnka S, Wongkasemjit S. Potential of Ni supported on KH zeolite catalysts for carbon dioxide reforming of methane. Journal of Power Sources. 2007;**165**:347-352. DOI: 10.1016/j.jpowsour.2006.12.005

[40] Nimwattanakul W, Luengnaruemitchai A, Jitkarnka S. Potential of Ni supported on clinoptilolite catalysts for carbon dioxide reforming of methane. International Journal of Hydrogen Energy. 2006;**31**:93-100. DOI: 10.1016/j.ijhydene.2005.02.005

[41] San-José-Alonso D, Juan-Juan J, Illán-Gómez MJ, Román-Martínez MC. Ni, Co and bimetallic Ni–Co catalysts for the dry reforming of methane. Applied Catalysis A: General. 2009;**371**:54-59. DOI: 10.1016/j.apcata.2009.09.026

[42] Diskin AM, Cunningham RH, Ormerod RM. The oxidative chemistry of methane over supported nickel catalysts. Catalysis Today. 1998;**46**:147-154

[43] Luengnaruemitchai A, Kaengsilalai A. Activity of different zeolite-supported Ni catalysts for methane reforming with carbon dioxide. Chemical Engineering Journal. 2008; **144**:96-102. DOI: 10.1016/j.cej.2008.05.023

[44] Garrido Pedrosa AM, Souza MJB, Silva AOS, Melo DMA, Araujo AS. Synthesis, characterization and catalytic properties of the cobalt and nickel supported on HZSM-12 zeolite. Catalysis Communications. 2006;**7**:791-796. DOI: 10.1016/j.catcom. 2006.02.012

[45] El Doukkali M, Iriondo A, Cambra JF, Jalowiecki-Duhamel L, Mamede AS, Dumeignil F, Arias PL. Pt monometallic and bimetallic catalysts prepared by acid sol–gel method for liquid phase reforming of bioglycerol. Journal of Molecular Catalysis A: Chemical. 2013;**368-369**:125-136. DOI: 10.1016/j.molcata.2012.12.006

[46] Ocsachoque M, Pompeo F, Gonzalez G. Rh-Ni/CeO_2-Al_2O_3 catalysts for methane dry reforming. Catalysis Today. 2011;**172**:226-231. DOI: 10.1016/j.cattod.2011.02.057

Chapter 3

Design and Evaluation of Gas Transport through a Zeolite Membrane on an Alumina Support

Habiba Shehu, Edidiong Okon,
Ifeyinwa Orakwe and Edward Gobina

Additional information is available at the end of the chapter

http://dx.doi.org/10.5772/intechopen.75545

Abstract

This chapter details the synthesis and applications of zeolite membranes (gas separation and zeolite membrane reactors). Gas separation is still not carried out at industrial level for zeolite membranes. Related areas, such as the possibility of incorporating a zeolite membrane in a reactor for possible catalytic action of the zeolite particles and scale-up issues are also discussed. The basic concept of mass transport through the zeolite layer has been presented. Zeolites can enhance the selectivity of methane more which can lead to the reduction of greenhouse gases in the atmosphere.

Keywords: zeolite membranes, greenhouse gases, catalytic membrane reactor and gas separations

1. Introduction

Volatile organic compounds vapourises easily to the atmosphere due to their high vapour pressure. Light hydrocarbons like methane, ethane and propane are considered as VOCs [1]. As stated previously, methane has a global warming potential (GWP) 21 times greater than CO_2. **Table 1** shows the GWP for methane, carbon dioxide and several hydrocarbon gases, while **Figure 1(a)** shows the percentage of the GHGs emitted.

Worldwide emissions of GHG can be presented according to the economic activities that lead to their production, as indicated in **Figure 1(b)** [2]. These include,

IntechOpen

© 2018 The Author(s). Licensee IntechOpen. This chapter is distributed under the terms of the Creative Commons Attribution License (http://creativecommons.org/licenses/by/3.0), which permits unrestricted use, distribution, and reproduction in any medium, provided the original work is properly cited.

Components	GWP
Methane	21
Ethane	5.5
Propane	3.3
Butane	4
Carbon dioxide	1

Table 1. Global warming potentials for several VOC components [1].

- Electricity and heat production: This sector accounts for the highest percentage of GHG emissions at 25% (in 2010), as reported by the United States Environmental Protection Agency (EPA). Hence, the burning of fossil fuels (*i.e.* coal, natural gas and oil) for electricity and heat generation are the main activities that contribute to the global increase of GHG.
- Industry: GHG emissions from industry primarily involve onsite burning of fossil fuels for energy. This area incorporates emissions from mineral transformation processes which are not as a result of energy consumption, chemical, metallurgical and emissions from activities of waste management. This sector accounts for 21% of GHG (**Figure 1(b)**).
- Agriculture, forestry and other land uses: GHG emissions from this sector originate primarily from deforestation and planting of trees. This value does not include carbon dioxide removed from the atmosphere by dead organic matter, carbon sequestering in biomass and soils, which reduces about 20% of emissions from this sector.

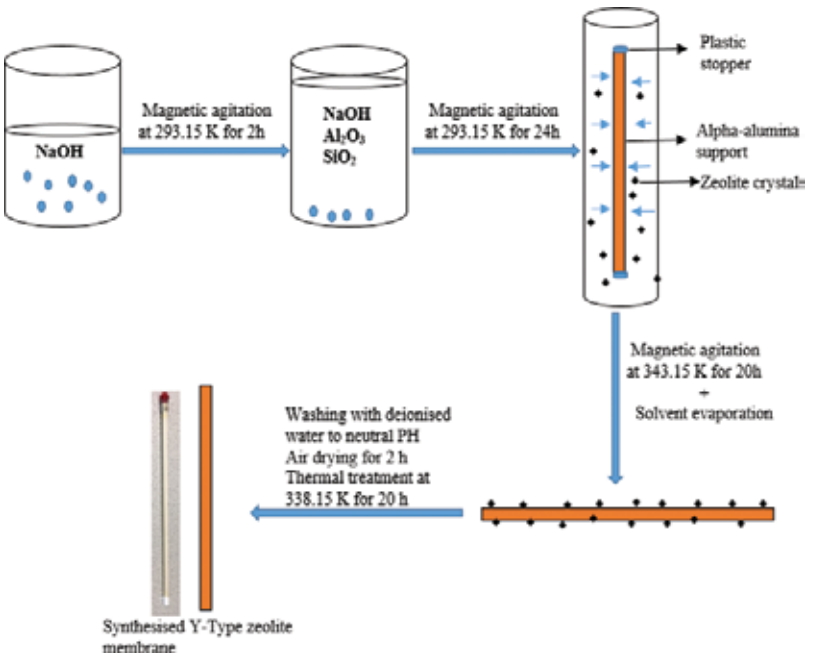

Figure 1. Schematic of the solid-state crystallisation route for y-type zeolite synthesis.

- Transportation: GHG emissions from transportation include the use of fossil fuels that are burned for rail, road, water and air transportation. Petroleum-based fuels account for about 96% of global transportation energy; this is mainly from diesel and gasoline.
- Buildings: This area accounts for the smallest GHG emissions (6%) and the emissions mainly arise from onsite energy generation and burning fuels for heat in buildings or cooking in homes.
- Other Energy: Other sources of GHG emissions come from the Energy sector which are not directly associated with electricity or heat production. For example, oil and gas extraction, refining, processing, and transportation.

The work carried out in this research considers the economic sector of GHG emissions namely, transportation and storage of crude oil as well as natural gas processes. A technology to separate the major GHGs methane and carbon dioxide and further utilise them in valuable feed stock has been explored using a y-type zeolite membrane.

Zeolites are natural or synthetic compounds that are composed of hydrated alumina-silica structures of alkaline and alkaline-earth metals. They have attracted increased interest because of their similar pore size on the molecular scale, which enables the separation of liquid and gaseous mixtures in a continuous way [3]. Zeolites have good chemical and thermal stability. As such, they can be used for high temperature processes and for processes that employ organic solvents. In addition, zeolite materials exhibit intrinsic catalytic property, which promotes the use of zeolite membranes as catalytic membrane reactors (CMRs).

In the previous two decades, enormous progress has been made on zeolite membrane synthesis. However, only 20 out of approximately 170 zeolite structures are used for the preparation of a membrane [4]. The high cost and poor reproducibility of the synthesis hinders the application of the zeolite membranes on a large industrial scale [5, 6]. Zeolite frameworks are made of silicon oxides and aluminium oxides. Moreover, the silicon and aluminium atom centres have a tetrahedral shape, which are linked to each other by bridging oxygen atoms. The strong acidity and uniformity of the micropores (less than 2 nm in diameter), together with a unique crystal structure ensures that zeolites have a high selectivity for separation based on the shape or chemical configuration of molecules in different chemical reactions. For example, alkylation, aromatisation, cracking, pyrolysis, and hydrodesulphurisation.

In comparison to natural zeolites, synthetic zeolites (*i.e.* X, Y and A) are often more applicable in membrane technology due to their uniform particle size and high purity. In addition, they can be designed to separate hydrocarbons. Van Bekkum et al. [7] have previously prepared an MFI-type zeolite membrane on a porous stainless steel disk. These exhibited a high permselectivity for *n*-butane (n-C_4H_{10}) over *i*-butane (i-C_4H_{10}) at room temperature. Jia et al. [8] reported on a zeolite membrane that showed a n-C_4H_{10}/i-C_4H_{10} selectivity of approximately 50 at 20°C. However, the authors reported no data at elevated temperatures. Yan et al. [9] previously prepared an MF membrane on an alumina porous disk. The authors reported a n-C_4H_{10}/i-C_4H_{10} permselectivity of 6.2 at 108°C and 9.4 at 185°C. Vroon et al. [10] reported the formation of an MFI-type membrane on an alumina support. This was shown to exhibit a n-C_4H_{10}/i-C_4H_{10} permselectivity of 90 at 25°C and 11 at 200°C. Thus, reproducibility in the membrane formation process is one of the vital factors for the application of zeolite membranes.

In addition, the effect of the supporting substrate on permeation properties of zeolite membranes is critical. Yan et al. [9] reported that the membrane morphology changed for the same porous substrate, under different synthetic conditions. Kusakabe et al. [11] produced an MFI-type zeolite membrane on the exterior surfaces of a porous alumina support tube using a hydrothermal reaction. The authors found no direct relationship between film morphology and permselectivity. The authors also synthesised a Y-type zeolite membrane on a porous α-alumina support tube and carried out single gas permeation test on CO_2, N_2, CH_4, C_2H_6 and SF_6. The authors found that the selectivity of CO_2/CH_4 through the membrane was higher at permeation temperatures that are lower, and tends to decrease with increases in temperature.

1.1. Mass transfer through a zeolite membrane

The process of mass transport through a zeolite layer arises via the five steps listed below [12, 13]:

1. Adsorption of the substance on the outer surface of the membrane.
2. Mass transport from the outer surface into the zeolite pore.
3. Diffusion of intra-crystalline zeolite.
4. Mass transport out of the zeolite pores to the external surface.
5. Desorption from the outer surface to the bulk.

Adsorption and desorption of species from the outer surface of a zeolite layer depends on the permeation conditions (*i.e.* temperature and pressure), type of crystalline material and the nature of the chemical species. Steps 2, 3 and 4 are usually activated processes [14].

Intra-crystalline permeation through a zeolite membrane can be described using several approaches [15]. The Fickian approach considers the concentration gradient as the driving force in a zeolite membrane. Alternatively, the gradient of the thermodynamic potential is the driving force in the Maxwell-Stefan (MS) approach. The MS approach allows for the approximation of the flux through the membrane for multicomponent gas mixtures by using information about single gas permeations [16]. The Fickian approach can be applied for permeation of single gas components through a zeolite membrane at a wide range of temperatures. Moreover, it can be assumed that the total flux N is the combination of the surface flux N_s, which takes place at low to medium temperatures, and the activated gaseous flux N_g, which is prevalent at high temperatures [13–15]. This is given by Eq. (1):

$$N = N_s + N_g \tag{1}$$

Fick's diffusivity D_s is given by Eq. 32:

$$D_s = D_o \Gamma \tag{2}$$

where D_o is the intrinsic or corrected diffusivity and Γ is the thermodynamic correction factor, which is expressed as:

$$\Gamma = \frac{dln\, p_i}{dln\, c_i} \tag{3}$$

where P_i and c_i are the pressure and concentration of component i.

The transport diffusivity is dependent on the temperature. This is more apparent at higher temperature. The assumption of an Arrhenius type dependence on temperature can be assumed [16], giving by:

$$D_o = \frac{D_g}{RT}\left(\frac{dp}{dz}\right) \tag{4}$$

The dependence on temperature will be affected by the adsorption of the component on the zeolite as well as the operating conditions. Moreover, the adsorption phenomena can be negligible at elevated temperatures. Under these conditions molecules can be considered to be in a quasi-gaseous state in the zeolite framework. This is referred to as activated Knudsen diffusion or gas translational diffusion. When this occurs, the flux is expressed as:

$$N_g = -\frac{D_g\, dp}{RTdz} \tag{5}$$

where dp/dz is the pressure gradient and also the permeance driving force. The diffusion coefficient that is dependent on the gas molecular velocity is given by:

$$D_g = d_p\, u_m\, e^{-E_J/RT} \tag{6}$$

where d_p is the pore diameter and u_m is the average velocity.

For ideal gases, kinetic theory can be used to calculate the molecular velocity given by Eq. (7):

$$u_m = \sqrt{\frac{8RT}{\pi M}} \tag{7}$$

From the equations above, it is clear that gas transport through a zeolite membrane is dependent on the adsorptive interaction between the permeating gas molecule and the zeolite. Moreover, the permeating flux is meant to increase with an increase in temperature. This is true for a defect free zeolite membrane. However, Knudsen and viscous flow can contribute to the overall flux and will strongly influence the expected temperature dependence when defects are present [16].

The ramification of predicting the mass transport and separation through synthesised zeolite membranes, where defects of inter-crystalline nature also need to be considered, is evident even though a simple approach has been used. High selectivity separations can be achieved by using nearly perfect zeolite membranes. In addition to high permselectivity, zeolite membranes should exhibit a high permeation flux in order to be suitable for industrial scale

applications. This can be achieved with minimal membrane thickness. Regrettably, decreasing the membrane thickness results in negative effect of inter-crystalline defects on permselectivity can be limiting. The thickness of a zeolite layer is dependent on the synthesis routes, conditions and on the number of depositions. For example, White et al. [15] obtained a ZSM-5 membrane by direct *in situ* crystallisation with a two-step deposition and showed a thickness between 30 and 40 μm. At laboratory level, zeolite membranes with a thickness of a few microns can be obtained with sufficient quality. Currently there are ongoing investigations to find a way to avoid, reduce or eliminate the presence of inter-crystalline defects, which, aside from poor synthesis reproducibility, are the main obstacle to the widespread industrial application of zeolite membrane. Moreover, if mixtures of gas and vapour having high molecular masses, or liquid mixtures of two species with different volatility and surface tension, are considered, the separation factors and permeation fluxes can be very interesting. However, these separations cannot be extrapolated from the permeances of the pure gases.

1.2. Membrane transport mechanism

In order to understand the fundamentals of membrane gas separation, a brief introduction to some laws and processes commonly employed is required.

1.2.1. Graham's law (Thomas Graham in 1848)

Graham's law states that the rate of diffusion of a gas is inversely proportional to the square root of its molecular weight. This can be written as,

$$\frac{Rate_a}{Rate_b} = (M_b/M_a)^{1/2} \tag{8}$$

where $Rate_a$ is the rate of diffusion of the first gas (volume or number of moles per unit time), $Rate_b$ is the rate of diffusion for the second gas, and M_a and M_b are the molar masses of gases a and b in g mol^{-1}.

1.2.2. Fick's first law

Fick's first law relates the diffusive flux to the concentration under the assumption of steady state. It postulates that the flux goes from regions of high concentration to regions of low concentration. The law fundamentally describes diffusion of species and was enunciated by Adolph E. Fick in 1855, who noted a similarity between diffusion of solutes and Fourier's law describing the flow of heat in solids. Fick's law was theoretically deduced in 1860 by James C. Maxwell from the kinetic theory of gases. The derivation of Fick's law includes the following assumptions: (1) statistical laws apply, (2) the average duration of a collision is short compared to the average time between collisions, a condition pertaining to dilute solutions, (3) particles move independently, (4) classical mechanics can be used to describe molecular collisions, (5) energy, momentum and mass are conserved in every collision, and (6) the diffusing solute particles are much larger than the solvent molecules of the liquid.

The separation of gases in membranes is possible due to the difference in the movement of the different species through the membrane. For membranes having large pore sizes of 0.1–10 μm,

the gases permeate via convective flow and there is no separation of the gases observed. For mesoporous membranes, separation is based on the collision amongst the molecule and hence molecular diffusion is dominant and the mean free path (which is the average distance travelled by a gas molecule between collisions with another gas molecule) of the gas molecules is greater than the pore size. The diffusion here is governed by Knudsen mechanism and it follows from the kinetic theory of gases that the rate of transport of any gas is inversely proportional to the square root of its molecular weight, which coincides with Graham's law of diffusion [16]. However, for a microporous membrane with pore size less than 2 nm, separation of gases is based mostly on molecular sieving. The transport mechanism in these type of membranes is often rather complex and involves surface diffusion that occurs when the permeating species exhibit a strong affinity for the membrane surface, thus adsorbing on the walls of the pores [16].

The permeation of gases through a membrane is dependent on both the diffusion and the concentration gradient of the species along the membrane. The selective transport of a gas molecule through a membrane is often associated with the pressure, temperature, electric potential and concentration gradient. The permeability and selectivity are some of the parameters that are used to determine the performance of a membrane. The permeance, P (mol m^{-2} s^{-1} Pa^{-1}), represents the proportionality coefficient with a flux at steady state for a gas passing through a membrane and is defined by Eq. 9:

$$P = \frac{Q}{A.\Delta p} \tag{9}$$

where Q is the gas molar gas flow through the membrane (mol s^{-1}), A is the membrane surface area (m) and Δp is the pressure difference across the membrane (Pa). The permeance is a measure of the quantity of a component that permeates through the membrane [16].

The ideal gas selectivity $\alpha_{i,j}$, is the ratio of the permeability coefficients of two different gases as they permeate independently through the membrane is given by Eq. (10):

$$\alpha_{ij} = \frac{P_i}{P_j} \tag{10}$$

where P_i and P_j are the permeance of the single gases through the membrane respectively. The selectivity is the measure of the ability of a membrane to separate two gases and is used to determine the purity of the permeate gas, as well as determine the quantity of product that is lost. The permeability coefficient is related to the diffusivity coefficient, D (m^2 s^{-1}), and the solubility coefficient, S (mol m^3 Pa), for a component, i, [16] and is given by:

$$P_i = D_i.S_i \tag{11}$$

Combining Eqs. (4) and (5), the selectivity of a membrane can be expressed as:

$$\alpha_{ij} = \frac{D_i}{D_j}\frac{S_i}{S_j} \tag{12}$$

For a binary mixture of gases with components i and j, the separation factor SF is given by:

$$SF_{ij} = \frac{(Y_i/Y_j)}{(X_i/X_j)} \tag{13}$$

where Y and X are the percentage concentrations in the permeate and feed end of the membrane. During experiments, the concentration of the gases (X_i and X_j) are fixed while at the permeate side Y_i and Y_j are determined using gas chromatography (GC).

1.3. Knudsen diffusion

Knudsen diffusion arises from differences in the molecular weights of components to be separated. This proceeds at a speed that is inversely proportional to the square root of the molecular weight of the component. Separation by Knudsen diffusion requires that the pore diameter of the membrane to be smaller than the mean free path of the components. Generally, diffusion of gases through porous membranes is dependent on the type of collisions that occur. At low concentrations, where there is predominantly molecule-pore wall collisions then the flow is Knudsen flow. Knudsen flow can be achieved with membranes whose pore size is greater than 4 nm. However, for it to dominate the pore size should be less than 50 nm [17]. In addition, the separation factor for a mixture of binary gases can be estimated from the square root of the ratio of the molecular weights of the gases. This is because gas permeation by Knudsen diffusion varies inversely with the square root of the molecular weights of the gases. Hence an ideal Knudsen separation for a mixture of binary gases is equal to the inverse of the square root of their molecular mass ratio [18]. The transportation equation for Knudsen and viscous flow is given by Eq. (8):

$$J = A\bar{P} + B \tag{14}$$

where $\bar{P}$ is the average pressure across a porous membrane, and A and B are constants relative to the membrane structure, molecular weight and size. According to Eq. (8), A is the constant representing Knudsen flow, while B is the constant representing viscous flow.

1.4. Molecular sieving

The molecular sieving effect in gas separations occurs when the pores of a membrane decrease to the 5 to 10×10^{-10} nm range. If the gases to be separated have different kinetic diameters then the smaller molecules will permeate through the membrane while the larger molecules will be retained. Very high separation can be achieved using this effect [18]. The kinetic diameter of a gas is defined as the intermolecular distance of closest approach for two molecules colliding with zero initial kinetic energy. This is dependent on the molecular shape, size and dipole–dipole interactions [19]. **Table 1** lists the kinetic diameters and molecular weights of several molecules found in natural gas or shuttle tanker exhaust off-gases.

Research in the production of membranes exhibiting these properties has accelerated. Zeolites and ceramic membranes can be modified to achieve these properties. None of the membranes

that have exhibited these properties are known to be commercially available. However, there have been reports indicating the separation of gases that differ in size by just 0.1×10^{-10} nm [17].

1.5. Surface diffusion

Surface diffusion and adsorption is a further mechanism that governs the permeation of gases through membranes that have small pore sizes. When the pore diameter of a membrane is in the range of 50–100 Å then adsorption on the walls of the membrane is observed. It is often noted that the amount of gas that is absorbed on the membrane pore walls is greater than the amount of gas that is not absorbed. The absorbed gas molecules then move by surface diffusion through the membrane with the flow rate obeying Fick's law [17].

1.6. Capillary condensation

Capillary condensation occurs when a porous membrane is in contact with a vapour and the saturation vapour pressure in the pores is different from the saturation vapour pressure of the components [20]. In addition, capillary condensation can occur with increasing gas pressures at temperatures below the critical temperature [21]. Therefore, condensed gas molecules are transported across the membrane pores.

For transport measurements, the molecular fluxes of the gases need to be determined from the uneven concentration profile, which can be used to determine the diffusion coefficient [21].

2. Synthesis of zeolite membrane

Zeolite membranes are normally synthesised on porous alumina supports or stainless steel, because a self-standing zeolite layer is very fragile. The commonly employed procedures used for zeolite membrane synthesis include:

(a) vapour-phase transport.

(b) direct *in situ* crystallisation.

(c) secondary growth.

The structured pores of zeolites, and the ability of zeolites to withstand high temperatures and pressures have made them a unique material for designing membranes. Significant high-profile research is currently being undertaken to develop the synthesis of zeolite membranes. Several of the developed methods for the synthesis of zeolite membranes are reviewed in this section.

2.1. Zeolite films that are free-standing

For molecular sieving applications, this method of preparation is most commonly employed. Teflon and cellulose supports are used as temporary supports for the synthesis [22]. This preparation method has been discontinued because of the fragility of the self-supported membrane.

2.2. Supported zeolite membrane

This is the most commonly synthesised zeolite membrane. An *in-situ* hydrothermal synthesis process is used in the preparation. This method is direct and can produce good membranes. In this process a thin layer of zeolite is crystallised on the pores of the porous support. Various forms of porous inorganic materials can be used as supports. These include titania, alumina, dense glass, carbon and stainless steel. Crystal growth on the support involves the pre-treatment of the support, preparation of zeolite seeds and the seeding. Seeding can be achieved by employing several methods including, rub-coating, dip-coating, vacuum seeding, spin coating and filtration seeding [25].

2.3. Polymeric-zeolite filled membranes

This method involves embedding zeolite crystals in to a polymer matrix [23]. The space between the zeolite crystals is sealed with a gas-tight polymeric structure. A major concern with this preparation method has been pore sizes that are different across the matrix and poor thermal stability.

3. Zeolite membrane characterisation

The morphological of zeolite membranes can be determined using several techniques. In this work, the thickness and morphology of the zeolite membrane have been determined using the SEM. The outer surface and cross-sectional view shows the thickness of the zeolite layer on the support and a top view shows the size and shape of the crystals. EDAX has been used to determine the Si/Al ratio as well as the elemental compositions of zeolite membranes.

Fluorescence confocal optical microscopy is a good instrument for the non-destructive analysis of zeolite membranes. The defects of the membrane and the grain boundary network of the zeolite can be observed along the thickness of the membranes and defects may be clearly visualised [24]. N_2 physisorption experiments are typically used to determine the pore volume and porosity of the zeolite powders and membranes. However, this method is difficult to use for supported zeolite membranes, because the supports generally do not fit inside the sample tubes within commercial equipment.

Therefore, in this work, a witness sample of the supported zeolite was used for all characterisation measurements alongside a mortar and pestle that was used to further grind the samples. An alternative method for the determination of porosity in thin films is the porosimetry, which allows analysis of the contribution of micropores and defects to the overall flux through the membrane.

4. Zeolite membrane reactors

Zeolite membrane reactor concept has been developed for equilibrium-limited reactions, products removal and increased reactant conversion rates. They have been used for the in-situ removal of

hydrogen in dehydrogenation reactions. Zeolite membranes having an MFI structure have been used for the conversion of alkanes to olefins. Also, isobutane dehydrogenation has been studied in a membrane reactor combining a platinum/zeolite catalyst and a supported MFI membrane with a tubular configuration [25]. The results provide proof that isobutene yield was found to be about four times greater than the values observed when using a normal reactor. Another study of the dehydrogenation of isobutane revealed that the H_2/isobutane mixture separation factor was close to one at a temperature of about 23°C and increased to 70 at 500°C [22]. These results can be related to the fact that, at reduced temperature, permeation is controlled by adsorption and the permeate is enriched in butane. Diffusion becomes the dominant mechanism when the temperature is increased, this is because the butane is adsorbed less. Furthermore, for the various conditions that were considered experimentally, the membrane reactor showed increased isobutane conversion with respect to the conversion obtained using a normal reactor.

Qi et al. [17] prepared MFI zeolite membranes that contain partial modification of the zeolite channels are able to obtain a high selectivity and permeance during hydrogen separation following a water gas shift reaction at an elevated temperature. Gu et al. [18] have previously modified a zeolite membrane by *in-situ* catalytic cracking of methyl diethoxysilane. The synthesised zeolite membrane showed a H_2/CO_2 permselectivity of 68.3 with a hydrogen permeance of 2.94×10^{-7} mol m^{-2} s^{-1} Pa^{-1}. The membrane also presented a high stability in the temperature range 400–550°C. Moreover, the membrane reactor achieved a carbon monoxide conversion of 81.7% at 550°C. This is higher than that obtained using a PBR.

Fischer–Tropsch synthesis (FTS) allows for the synthesis of liquid hydrocarbons from various feedstocks, including coal and natural gas. The removal of water from this synthetic process is important for the following reasons:

- To increase reactor productivity.
- To reduce deactivation of the catalysts.
- To increase the conversion of CO_2 to long-chain hydrocarbons by shifting the equilibrium of the water gas shift reaction [19].

Different hydrophilic zeolite membranes have been used for the selective removal of water from mixtures of H_2 and CO. For example, ZSM-5 and mordenite membranes have been used for the water removal under normal FTS conditions [20]. Mordenite membranes have exhibited increased H_2O fluxes and high permselectivities. An A-type (NaA) zeolite membrane was used to study the permeation of single components of H_2O vapour, CO, H_2, CH_4 and their binary mixtures [21]. The permeance of water vapour in the binary mixture is almost close to the value found in the single gases. However, the permeance of each gas component went down with increasing water content. The results obtained can be used to explain how the adsorbed water molecules in the membrane block the other gas molecules. On raising the temperature, the amount of water adsorbed in the membrane goes slightly lower and the selectivity for water in the binary mixture reduces.

Zeolite membranes act also as distributors to regulate the number of reactants added to a catalyst and thus limit side reactions. The use of membrane reactors is also highly relevant for carrying out oxidative dehydrogenation of alkanes to control the oxygen feed, in order

to limit total combustion that is highly exothermic [23]. Zeolite membranes have also been found to be active for the partial oxidation of propane at 550°C. Another possible application of these membranes is to use them as an active contactor, which is catalytically active but not necessarily permselective [24]. Bernado et al. [24] showed how a catalytic zeolite membrane, with catalytically active particles dispersed in to a thin zeolite layer ensures ultimate contact between reactants and the active site of the catalyst. This reduces by-pass problems that occur in PBR and reduces the pressure drop. The same authors have also studied carbon monoxide selective oxidation (Selox) from hydrogen-rich gas streams using catalytic zeolite membranes.

5. Materials and method

The chemicals, materials and gases used for the experimental work carried out in this chapter are listed as follows:

1. 0.1 M sodium hydroxide (NaOH) supplied by Sigma-Aldrich, UK.
2. Aluminium oxide (Al_2O_3) supplied by Sigma-Aldrich, UK.
3. Deionised Water by Purelab Flex, Elga.
4. Gases (Oxygen, Propane, Methane, Nitrogen, Helium, and Carbon dioxide) supplied by BOC, UK.
5. Silicon dioxide (SiO_2) supplied by Sigma-Aldrich, UK.
6. Y-type Zeolite powder supplied by Sigma-Aldrich, UK

5.1. Zeolite synthesis

A y-type zeolite membrane was synthesised by mixing NaOH, Al_2O_3, SiO_2 and deionised H_2O with a molar ratio of $1SiO_2$:$10Al_2O_3$:14NaOH:$798H_2O$. The NaOH and Al_2O_3 were first dissolved in H_2O. This was followed by the addition of SiO_2 and the mixture was agitated with a magnetic stirrer for 24 h at 293.15 K. 2 g of NaX powder was then added. The γ-alumina support, which consists of 77% alumina and 23% TiO_2 and has a permeable length of 348 mm and an internal and external diameter of 7 and 10 mm respectively was subsequently dipped in the resulting sol and kept under magnetic agitation at 343.15 K for 20 h making sure that it was kept central to the measuring cylinder and also vertical. This allowed the solvent to evaporate and resulted in the deposition of y-type zeolite crystals on the support matrix. The resulting membrane was then washed with deionised H_2O until the pH of the wash water was neutral. The membrane was then air dried for 2 h, using a motor powered rotatory drier at room temperature. It was then subjected to thermally treatment at 338.15 K in an oven for 20 h. The α-alumina support was weighed before and after zeolite deposition to determine the amount of zeolite loaded on the support. A schematic of the crystallisation process is shown in **Figure 1**.

6. Results and discussion

6.1. SEM and EDAX observation of solid-state crystallisation deposition on the alumina support

SEM and EDAX have been carried out for different synthesis conditions to reveal the solid-state crystallisation of the zeolite on the support. Zeolite nanoparticles have been found to have an average size of 0.18–3.72 nm (**Figure 2a** and **b**). **Figure 2c** shows the SEM of a fresh support. Following crystallising in a mixture of sodium, aluminium and silicone oxides for 24 h the membrane revealed zeolite nanoparticles embedded in the matrix of the support (**Figure 2d**). These nanoparticles began aggregating in several locations that had unclear boundaries. Moreover, the nanoparticles have a spherical shape and a uniform particle size. The high magnification SEM image (**Figure 2b**) revealed that the nanoparticles could be mesoporous. This has been attributed to the assembly of many nanoparticles of 0.35 to 0.37 nm.

Figure 3 shows an EDAX spectrum for zeolite powder. The EDAX spectrum provides details about the elemental composition of the sample. The results confirm the molecular formula of zeolite to be TO_4, where T is either silicon or/and aluminium. Therefore, the elemental composition indicates that the zeolite powder is made up of tetrahedral units of AlO_4 and SiO_4. The percentage weights of O, Al and Si are 138.04, 34.27 and 37.05 respectively. The percentage weight of Oxygen present is approximately four times that of aluminium and silicon.

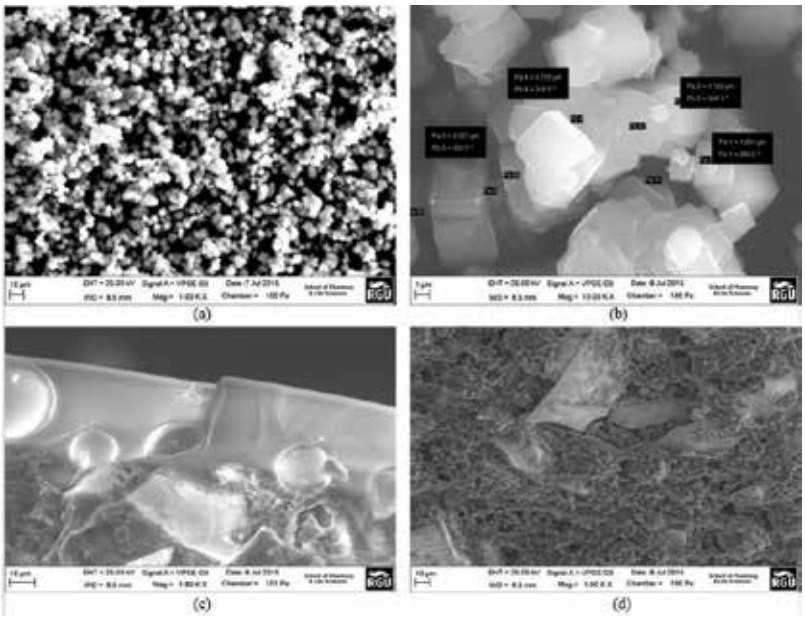

Figure 2. SEM of the zeolite particle samples at (a) before deposition (b) higher magnification before deposition (c) alumina support (d) 24 h crystallisation.

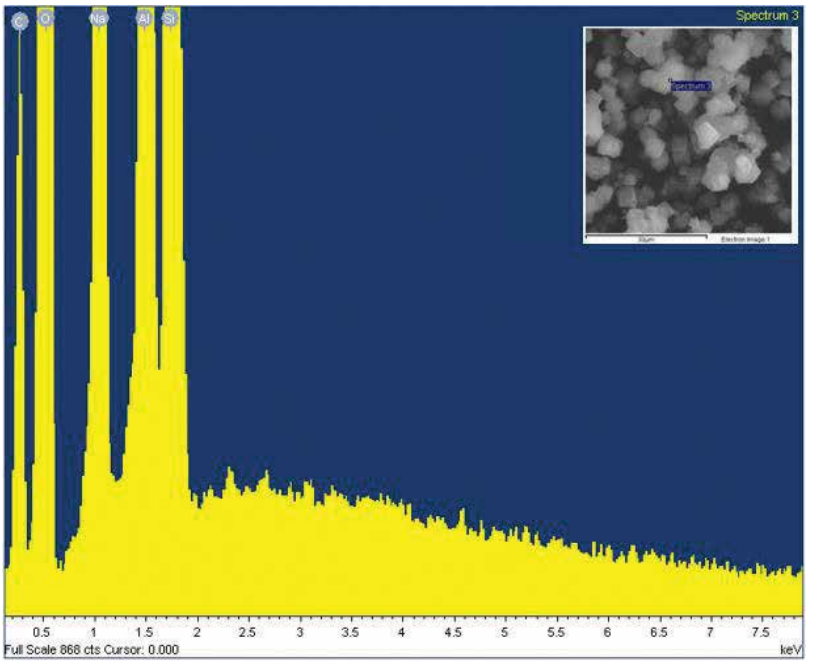

Figure 3. EDAX spectrum of zeolite powder before deposition on alumina support.

In addition, an elemental composition analysis of the y-type zeolite membrane has been determined using EDAX. This is presented in **Figure 4**. The associated data is provided in **Table 2**.

6.2. Nitrogen physisorption measurements

Nitrogen adsorption isotherms of the membrane are shown in **Figure 5**. A summary of the adsorption/desorption data is provided **Table 3**. The pore diameters have been calculated using the Barret-Joyner–Halenda (BJH) model. The BET surface areas for the support and zeolite membranes were found to be 10.69 and 0.106 m^2/g. Zeolites are believed to have large surface areas, however, the synthetic Y-type zeolite has a lower surface area than the support.

6.3. Gas permeation

6.3.1. Effects of temperature on single gas permeation

The single gas permeances for CO_2, N_2, O_2, CH_4 and C_3H_8 have been determined using the gas permeation setup. The permeate stream has been measured at standard temperature and pressure. The flux of the permeate gas has been measured using a volumetric digital flow meter (L min^{-1}). Gas phase conditions have been employed exclusively in the feed and the permeate sides. Subsequently, single gases were fed into the membrane reactor at a pressure range of 0.1 to 1 $\times 10^5$ Pa and at temperatures of 293, 373, 473 and 573 K. Data indicating the change in the flux of the gases through the zeolite membrane, as a function of temperature, are

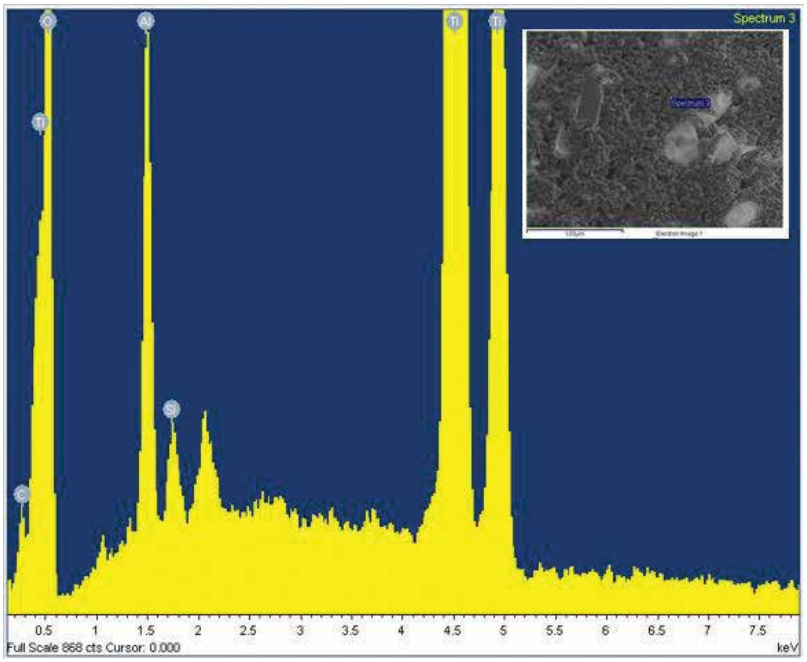

Figure 4. EDAX spectrum of y-type zeolite membrane 24 h after deposition.

presented in **Figures 6** and **7**. The flux is shown to be different for each gas. On increasing the temperature from 273 to 373 K, propane showed an increase of 146% in its flux, whereas there was only a 17% increase for methane. The extent of the effect of temperature is determined by the adsorption of the component on the zeolite. As observed from **Figure 8**, zeolite has a higher affinity towards methane compared to propane. Moreover, the influence of adsorption

Gas	Kinetic diameter ($\times 10^{-10}$ *nm*)	Molecular weight ($g\ mol^{-1}$)
CO_2	3.30	44.01
CH_4	3.80	16.04
N_2	3.64	28.01
CO	3.76	28.01
Ar	3.40	39.95
O_2	3.46	32.00
SO_2	3.60	64.07
NO_2	3.30	46.01
He	2.60	4.00
H_2	2.89	2.02

Table 2. Kinetic diameter and molecular mass of various molecules found in off-gases [19].

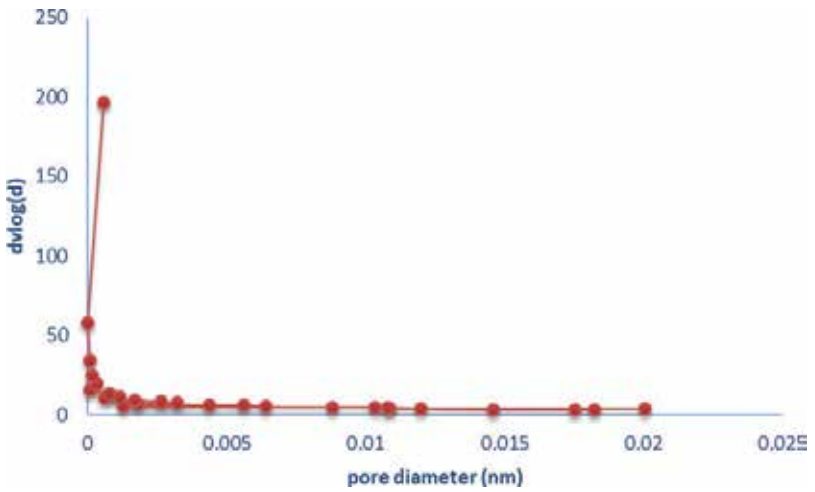

Figure 5. Pore size distribution of zeolite membrane measured by N_2 adsorption/desorption (**Table 4**).

Element	Zeolite powder weight (%)	Synthesised y-type zeolite membrane weight (%)
C	53.72	3.82
Al	34.27	3.11
O	138.04	53.19
Si	37.05	0.50
Ti	—	60.63
Na	30.46	—

Table 3. Elemental composition of the zeolite powder and the synthesised y-type zeolite membrane.

is greater than that of temperature. At elevated temperatures, it is likely that adsorption is negligible and the molecules exist in a quasi-gaseous state in the zeolite framework. Diffusion in this state is referred to as activated Knudsen diffusion or gas translational diffusion.

Selectivity is a measure of the ability of a membrane to separate two gases. It is used to determine the purity of the permeate gas and to determine the quantity of product lost. **Figure 8** shows that C_3H_8/CH_4 selectivity increases from 0.3 at 293 K to 0.9 at 373 K. The higher temperature favours the separation of CH_4 over C_3H_8. However, changes in temperature did not show much significant difference in the separation factors for the CO_2/CH_4 and N_2/CH_4. Moreover, for O_2/CH_4, separation is found to be more favourable at lower temperature (293 K).

6.3.2. Mixed gas permeation using gas chromatograph mass spectrometer (GCMS)

The selectivity of mixed gases was determined by the measure of the concentration of feed and permeate gases through the GCMS using Eq. (7). Details of the GCMS column, carrier

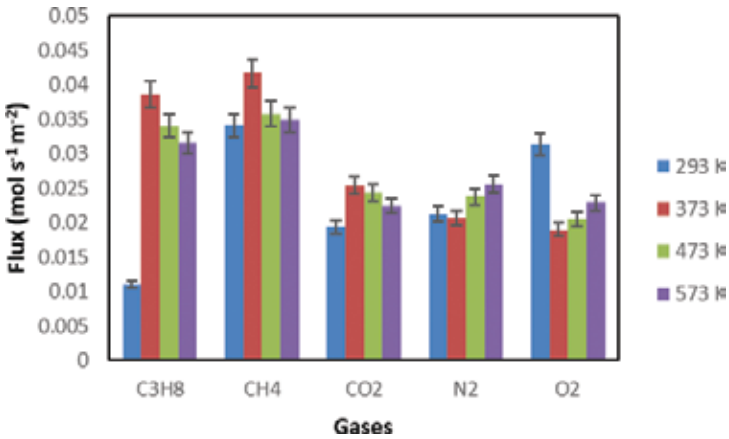

Figure 6. Flux of gases with increase in temperature at 1×10^4 pa.

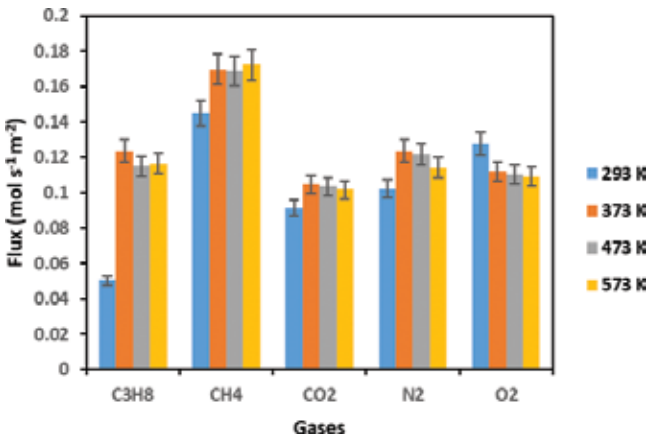

Figure 7. Flux of gases with increase in temperature at 1×10^5 Pa.

gas and operating conditions are given in Section 5.6.6. The values calculated for the different binary gas pairs are listed in **Table 5**.

6.3.3. Transport mechanism determination using gas permeation

It has been previously postulated that the linear proportionality of single gas permeance to the inverse of the square root of the molecular weight of the gases indicates that the mode of transport through the membrane is Knudsen diffusion [3]. **Figure 9** plots the relation between the molar gas flux and the inverse of the square root of the gas molecular weight at $1x10^4$ Pa and 293 K. Based on this plot it can be deduced that the gas molar flux is dependent on the molecular weight as previously reported.

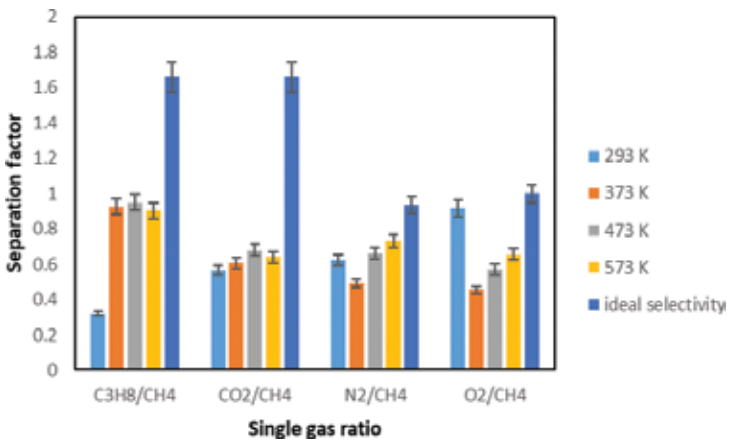

Figure 8. Separation factor of gases with increasing temperature.

Membrane	BET surface area (m^2/g)	Pore diameter (nm)	Pore volume (cm^3/g)
y-type zeolite membrane	0.106	3.139	0.025

Table 4. BET surface area, average pore diameter and pore volume of the membrane.

	CH_4/CO_2 (1.65)	CH_4/N_2 (1.32)	CH_4/C_3H_8 (1.65)
293 k (mixed gases)	1.3	1.8	2.5
293 k (single gases)	1.1	1.6	3.1

Table 5. Selectivity of methane through a zeolite membrane at 293 K.

The order of molecular weight is $CH_4 > O_2 > N_2 > CO_2 > C_3H_8$. However, the R^2 value of 0.807 suggests there is a deviation from Knudsen flow mechanism. CO_2 and C_3H_8 have a similar molecular weight of 44.01 g/mol but the molar flux of CO_2 is greater than that of C_3H_8, this could be explained by molecular sieving flow mechanism, as the kinetic diameter of CO_2 (0.38 nm) is lower than that of C_3H_8 (0.43 nm). **Figure 10** shows the relation between the molar flux and the kinetic diameter of the gases at $1x10^4$ Pa and 293 K. For gases to flow via a molecular sieving mechanism, the smaller molecules must move with a higher molar flux than the larger molecules. There was a deviation to this mechanism, as the order of kinetic diameter is $O_2 > N_2 > CH_4 > CO_2 > C_3H_8$. Moreover, CO_2 and C_3H_8 are observed to permeate through the membrane layer based on their size as C_3H_8 has higher size as compared to CO_2.

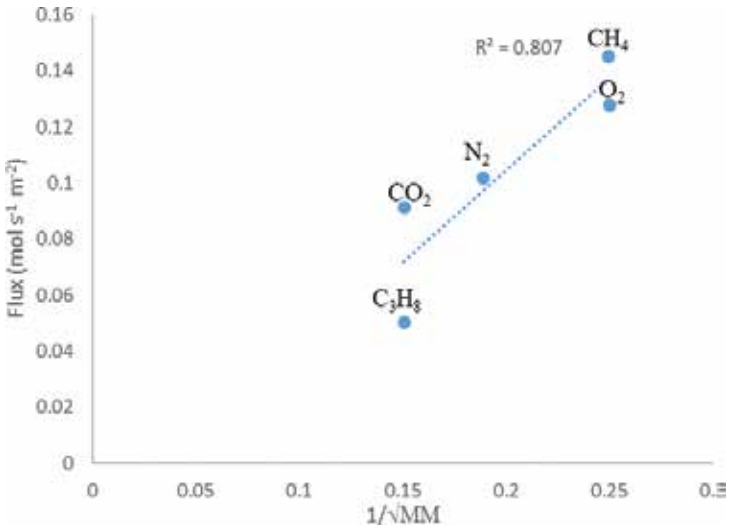

Figure 9. Gas molar flux against the inverse square root of molecular weight.

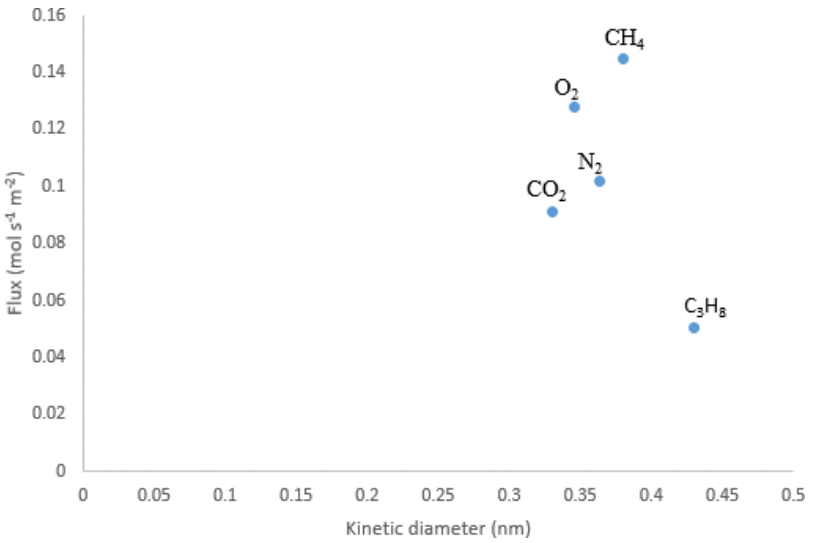

Figure 10. Gas molar flux against kinetic diameter of gases.

7. Conclusions

An evaluation of the performance of y-type zeolite/γ-alumina membrane for natural gas processing has been carried out for separation ability. The transport of gases through the membrane has been shown to be governed by Knudsen diffusion. However, CO_2 and C_3H_8 have been shown to exhibit a molecular sieving mechanism. N_2 adsorption/desorption showed that

at a lower surface area of 0.106 m^2/g, the membrane is more effective at the separation of methane compared to the support. The SEM images revealed asymmetric structure deposition of the zeolite layer. Further studies are planned to demonstrate membrane performance for separating the heavier components of natural gas mixtures that can arise during dew point adjustments, thermal problems during crude oil storage and transportation, and when expanding highly compressed natural gas components.

Author details

Habiba Shehu, Edidiong Okon, Ifeyinwa Orakwe and Edward Gobina*

*Address all correspondence to: e.gobina@rgu.ac.uk

Center for Process Integration and Membrane Technology, Robert Gordon University, Aberdeen, United Kingdom

References

[1] Tamaddoni M, Sotudeh-Gharebagh R, Nario S, Hajihosseinzadeh M, Mostoufi N. Experimental study of the VOC emitted from crude oil tankers. Process Safety and Environmental Protection. 2014;**92**(6):929-937

[2] Ürge-Vorsatz D, Herrero ST, Dubash NK, Lecocq F. Measuring the co-benefits of climate change mitigation. Annual Review of Environment and Resources. 2014;**39**:549-582

[3] Basile A. Handbook of Membrane Reactors: Fundamental Materials Science, Design and Optimisation. Elsevier; 2013

[4] Baerlocher C, McCusker LB, Olson DH. Atlas of Zeolite Framework Types. Elsevier; 2007

[5] McLeary E, Jansen J, Kapteijn F. Zeolite based films, membranes and membrane reactors: Progress and prospects. Microporous and Mesoporous Materials. 2006;**90**(1):198-220

[6] Caro J, Noack M, Kölsch P. Zeolite membranes: From the laboratory scale to technical applications. Adsorption. 2005;**11**(3):215-227

[7] Geus E, Jansen J, Van Bekkum H. Calcination of large MFI-type single crystals: Part 1. Evidence for the occurrence of consecutive growth forms and possible diffusion barriers arising thereof. Zeolites. 1994;**14**(2):82-88

[8] Jia M, Chen B, Noble RD, Falconer JL. Ceramic-zeolite composite membranes and their application for separation of vapor/gas mixtures. Journal of Membrane Science. 1994;**90**(1-2):1-10

[9] Yan Y, Davis ME, Gavalas GR. Preparation of zeolite ZSM-5 membranes by in-situ crystallization on porous. Alpha.-Al_2O_3. Industrial & Engineering Chemistry Research. 1995;**34**(5):1652-1661

[10] Vroon Z, Keizer K, Gilde M, Verweij H, Burggraaf A. Transport properties of alkanes through ceramic thin zeolite MFI membranes. Journal of Membrane Science. 1996;**113**(2):293-300

[11] Kusakabe K, Kuroda T, Murata A, Morooka S. Formation of a Y-type zeolite membrane on a porous α-alumina tube for gas separation. Industrial & Engineering Chemistry Research. 1997;**36**(3):649-655

[12] Burggraaf A. Single gas permeation of thin zeolite (MFI) membranes: Theory and analysis of experimental observations. Journal of Membrane Science. 1999;**155**(1):45-65

[13] Den Exter M, Jansen J, van de Graaf J, Kapteijn F, Moulijn J, Van Bekkum H. Zeolite-based membranes preparation, performance and prospects. Studies in Surface Science and Catalysis. 1996;**102**:413-454

[14] Barrer RM. Porous crystal membranes. Journal of the Chemical Society, Faraday Transactions. 1990;**86**(7):1123-1130

[15] Krishna R, Van Baten J. Describing binary mixture diffusion in carbon nanotubes with the Maxwell-Stefan equations. An investigation using molecular dynamics simulations. Industrial & Engineering Chemistry Research. 2006;**45**(6):2084-2093

[16] Van Dyk L, Miachon S, Lorenzen L, Torres M, Fiaty K, Dalmon J. Comparison of microporous MFI and dense Pd membrane performances in an extractor-type CMR. Catalysis Today. 2003;**82**(1):167-177

[17] Richard W. Baker. Membrane Technology and Applications. 3rd ed. United Kingdom: John Wiley and Sons Ltd; 2012

[18] Gu X, Tang Z, Dong J. On-stream modification of MFI zeolite membranes for enhancing hydrogen separation at high temperature. Microporous and Mesoporous Materials. 2008;**111**(1):441-448

[19] Breck D. Ion exchange reactions in zeolites. Zeolite Molecular Sieves: Structure Chemistry and Use. 1973:529-592

[20] Sidhu PS, Cussler E. Diffusion and capillary flow in track-etched membranes. Journal of Membrane Science. 2001;**182**(1):91-101

[21] Choi J, Do D, Do H. Surface diffusion of adsorbed molecules in porous media: Monolayer, multilayer, and capillary condensation regimes. Industrial & Engineering Chemistry Research. 2001;**40**(19):4005-4031

[22] Illgen U, Schäfer R, Noack M, Kölsch P, Kühnle A, Caro J. Membrane supported catalytic dehydrogenation of iso-butane using an MFI zeolite membrane reactor. Catalysis Communications. 2001;**2**(11):339-345

[23] Tavolaro A, Drioli E. Zeolite membranes. Advanced Materials. 1999;**11**(12):975-996

[24] Lai Z, Bonilla G, Diaz I, Nery JG, Sujaoti K, Amat MA, et al. Microstructural optimization of a zeolite membrane for organic vapor separation. Science (New York, NY). 2003;**300**(5618):456-460

[25] Miachon S, Ciavarella P, Van Dyk L, Kumakiri I, Fiaty K, Schuurman Y, et al. Nanocomposite MFI-alumina membranes via pore-plugging synthesis: Specific transport and separation properties. Journal of Membrane Science. 2007;**298**(1):71-79

Chapter 4

Separation of Binary Solutions on the Basis of Zeolites

Paranuk Arambiy, Saavedra Huayta Jose Angel and Khrisonidi Vitaly

Additional information is available at the end of the chapter

http://dx.doi.org/10.5772/intechopen.73513

Abstract

In this chapter, the author analyzed binary systems, ethanol + water, methanol + water and benzene + water, and an original mathematical model allowing the determination of the complete adsorption of binary systems on KaA, CaA, CaX, NaA and NaX zeolites using the Gibbs adsorption theory is proposed. The Gibbs equation and the Gibbs-Duhem equation have a number of limitations and do not take into account the properties of the investigated zeolites. Therefore, it is necessary to use the equations obtained by the author as a result of laboratory research, for the theoretical calculation and development of dehydration and concentration systems for alcohols.

Keywords: zeolites, binary solutions, molecular sieve properties, Van der Waals forces, surface tension of the solution

1. Introduction

The study of the processes occurring at the phase interface attracts many researchers from all over the world, and they have enormous practical and theoretical importance. A detailed description of the processes occurring at the phase interface is given in [1].

Considering these processes can be argued, the issues of adsorption of gas on adsorbents have been studied quite deeply and have an extensive theoretical and experimental basis.

But the behavior of the adsorbed liquid on the surface of solid zeolite adsorbent is very difficult to describe and the explanation is very simple - the internal structure of the liquid is much more complex than the internal structure of gases and crystals. Comparing gas and liquid, it can be asserted that the density of the liquid is many times greater than the density of the gas. Considering and comparing the molecular level, the distance between molecules in liquids is

IntechOpen

© 2018 The Author(s). Licensee IntechOpen. This chapter is distributed under the terms of the Creative Commons Attribution License (http://creativecommons.org/licenses/by/3.0), which permits unrestricted use, distribution, and reproduction in any medium, provided the original work is properly cited.

so small that the properties of the liquid are largely determined by the intrinsic volume of the molecules and by the mutual attraction between them, while in gases under ordinary conditions the influence of these factors is negligible and can be neglected. Small distances in fluid molecules impose certain limitations on the mathematical models being developed and also impose serious limitations that require taking into account the polar properties and geometric parameters of the molecules [2].

The properties of polar liquids depend on the interaction of the molecule with the molecule, but also on the interaction between individual parts of different molecules [2].

The first attempts to create a theory of fluid and to develop a mathematical model for analyzing the behavior of liquid molecules were based on a comparison of the liquid with mathematical models of the behavior of molecules in gas and did not yield any practical results, since they did not reflect the complexity of the interaction between molecules in the liquid [2].

The verification and application of new methods for analyzing the internal structure of liquids made it possible to establish the polarity of the molecules studied and the dielectric properties. And the use of nuclear magnetic resonance has led to the development of models for describing the behavior of molecules in a liquid [2].

It is established that the molecules of the liquid have a polarity, in addition, the attraction between them, inherent to nonpolar molecules, which manifests itself in a weak interaction between different parts carrying an electric charge. The total effect of mutual attraction of molecules is often described as the internal pressure of a liquid. For liquids other than electrolytes or weak electrolytes, the internal pressure varies from 3000 to 6000 bar under standard conditions [2]. At strong electrolytes, it can reach 10,000 bar. A large internal pressure, which is inherent in electrolyte liquids, characterizes the rest of their properties, such as considerable absorption of heat during evaporation and low compressibility [2].

2. Drying of liquid media

The moisture content of organic liquids significantly changes the properties of the materials. In this regard, their dehydration is of great importance.

Dewatering freon refrigeration oils: The reliability and durability of airtight refrigeration machines largely depends on the purity of the refrigerants and lubricating oils. Up to 80% of the contaminants generated in freon refrigerating machines, which cause corrosion of the system, and ultimately, the combustion of the built-in electric motors is associated with the presence of moisture [3].

When drying oil with zeolites without a binder (NaA), the degree of drying, the time of the protective effect of the layer and the dynamic activity increase significantly [3].

Dehydration of transformer oil: Methods of dehydrating transformer oil with zeolites and oil degassing are developed on the basis of mass transfer processes. In the adsorption method, contacting the oil with zeolites is carried out at ordinary temperatures and, as a result, does

not cause oxidative processes that occur during heating. The adsorption process is widely used for the recovery of waste transformer oils, for decreasing the dielectric losses of fresh transformer oils, for drying oils with zeolites, in filters for continuous regeneration of transformer oil, and so on [3].

Removal of radionuclides from liquid wastes of nuclear power plants: Synthesis of ceramic matrices by the method of sorption of radionuclides on zeolites and their subsequent conversion to feldspar allows using radionuclides to remove radionuclides from liquid wastes using a simple process scheme [3]. This method is based on the ability of synthetic zeolites with high selectivity to react with respect to Sr and Cs. Zeolites are completely iso-chemical to feldspars; moreover, the ion-exchange sorption process makes it possible to obtain zeolites of a given composition, and this process is relatively easy to control. Ion exchange on zeolites is technologically well developed and is widely used in the industry for purification of liquid waste [3].

2.1. The mechanism of the penetration of atoms and molecules through the windows of molecular sieves

The mechanism of the passage of molecules through the windows connecting the cavities of zeolites is complex because here are faced with the peculiarities of the forces of attraction and repulsion between individual molecules and atoms, as well as the structure of molecules and the structure of zeolites [4].

Numerous studies have shown that molecular sieves with a small size of the connecting windows (e.g., 5 Å) adsorb paraffin hydrocarbons of normal structure, but they do not adsorb the isomers of these hydrocarbons, since they have a branched structure and cannot pass through these channels. **Figure 1** shows that isooctane cannot pass through a window of molecular sieves with a diameter of 4.9 Å, while normal octane passes freely [4].

Adsorption of molecules, whose size is close to the diameter of the entrance windows of the zeolite, proceeds with the expenditure of additional energy. The possibility of deforming molecules containing two or more atoms within a small range makes it possible to adsorb molecules even within a larger critical diameter, through the window size [4].

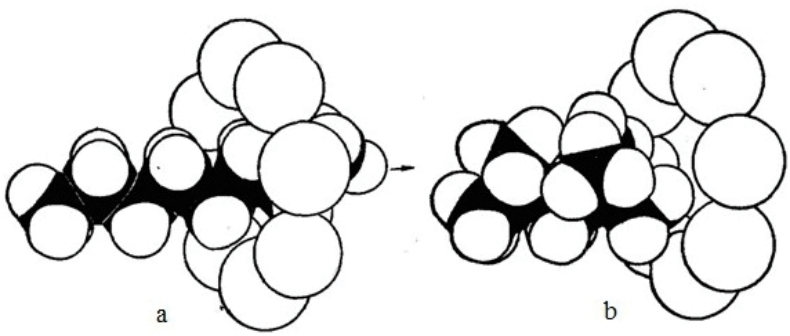

Figure 1. The separation of normal octane (a) and isooctane (b) into calcium containing zeolite.

For example, through the windows NaA penetrates into the internal structure of ethane molecules having a critical diameter of 4 Å; penetration facilitates the thermal pulsation of the crystallite lattice. However, at some temperature characteristic of the sorbed material, the kinetic energy reserve of the molecule becomes insufficient to overcome the energy barrier; below this temperature, the substance is not sorbed by the zeolite of this type [4].

In **Figure 2** (according to R. Barreru) are curves showing how the adsorption of some gases changes with NaA-type zeolites, but as the temperature decreases. At 0°C, oxygen is only slightly adsorbed by zeolites, but at a temperature of liquid nitrogen, that is, at −196° C, approximately 12 molecules of oxygen are adsorbed in each cavity. For 1 g of zeolite, this will be about 130 cm^3 of oxygen (when reduced to normal conditions). Thus, there is a process of adsorption of oxygen, on a zeolite accompanied by an increase in the adsorption capacity in oxygen with a decrease in temperature [4].

However, the adsorption of other gases (nitrogen and argon) occurs differently. As the temperature decreases, initially the adsorption of these gases increases, goes also as oxygen, but then, having reached a certain maximum, sharply decreases. The maximum adsorption of nitrogen is achieved at −120°C and argon at −150°C. At very low temperatures (−190°C and below), the adsorption of nitrogen and argon becomes quite insignificant compared to its maximum value [4].

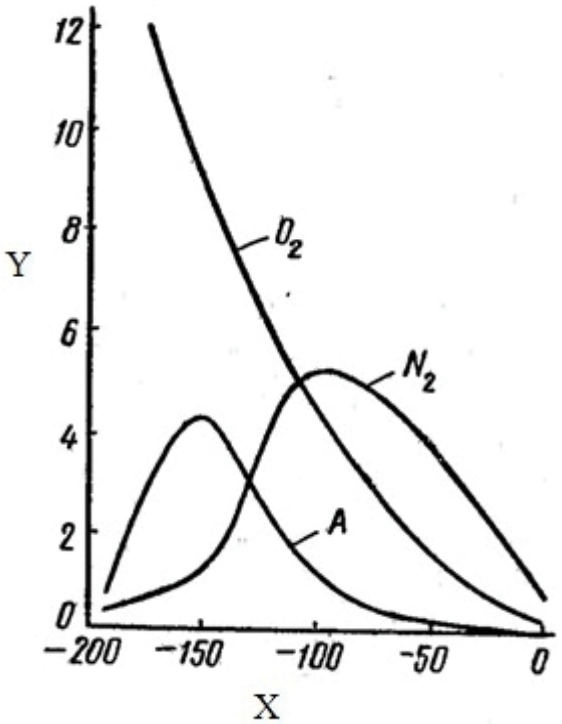

Figure 2. Adsorption of some gases by zeolites at low temperatures. (X)—number of molecules in each cavity; (Y)—temperature in degrees.

Even at a temperature of −196°C, the windows between the cavities do not contract so much that the oxygen molecules cannot shine through them. At the same time, larger molecules of nitrogen and argon do not pass through the windows at very low temperatures, as a result of a decrease in their cross section.

Studies have shown that even relatively small changes in the cross section of the windows connecting the surfaces lead to significant changes in the nature of the adsorption of the individual components. Both shabasite- and CaA-type screens adsorb normal hydrocarbons, but they do not adsorb isomers of hydrocarbons having a branched structure that cannot pass through the windows of these zeolites [4]. However, in crystals of both types, a certain difference in adsorption is observed, and shabasite adsorbs different normal hydrocarbons unequally [4]. The greater the molecular weight of the hydrocarbon, the slower it adsorbs the shabasite. For example, u-heptane is not adsorbed insignificantly [4]. At the same time, synthetic molecular sieves of the CaA type adsorb even a normal hydrocarbon such as tetradecane (n-$C_{14}H_{30}$), the hydrocarbon chain of which is twice as long as n-heptane [4].

Different types of natural and synthetic zeolites have windows of unequal dimensions [4]. The penetration of molecules through these windows depends on the properties of those ions that are located at the edges of the window. A cation that compensates for the charges of the Si—O or Al—O complex is often located at the edge of the inlet (window) and prevents the penetration of molecules whose dimensions exceed the critical diameter, that is, the diameter that allows the molecule to penetrate through the narrowed window due to the presence of the cation [4].

2.2. Effect of water on zeolites

The addition of water to the dehydrated zeolites results in a pronounced change in the electrical conductivity. With an increase in the water content at a temperature of 25°C, the electrical conductivity of zeolite X increases by a factor of 10^4. In the case of type A zeolite, the electrical conductivity increases nonlinearly, which indicates preferential hydration of cations of the same type.

In the case of type A zeolite, electrical conductivity increases with hydration until the water content is about five molecules per unit cell. This is equivalent to the hydration of four mobile sodium ions, in the vicinity of the eight-membered oxygen rings forming the entrance windows. Apparently, these sites have the highest adsorption energy. Complexes of water-sodium ions, localized in eight-membered rings, very effectively block the entrances and prevent the penetration of other molecules there.

Thus, it can be concluded that the circumstances confirm the results of the determination of physical adsorption, showing that in the presence of even traces of water adsorption of gases of the oxygen type does not occur.

Hydration of water molecules is accompanied by the formation of an unstable bond with sodium ions, and the localization of ions, and there is also an insignificant increase in the electrical conductivity of the sample. After the number of water molecules in each unit cell

exceeds 16, H^2O molecules occupy places with the lowest adsorption energy, forming hydrogen bonds with the anionic surface of the zeolite. As the crystals are saturated with water, the electrical conductivity of the zeolites increases; therefore, the system of channels is filled with water molecules. Some of the sodium ions remain sufficiently free to chaotically move through the channels of the zeolites. These conclusions are in agreement with the data of IR (adsorption of water) and NMR spectra.

2.3. Hypothetical properties of zeolites

The first works of prediction of skeletons were carried out in the 1960s of the past century [5]. Most of these pioneering studies were performed manually. The development of computer technology and new algorithms allowed the generation of millions of hypothetical structures of zeolites [6, 7]. At present, there are two main directions for forecasting zeolite frames. One of the directions is based on the creation of hypothetical zeolites with given structural features. These hypothetical scaffolds are of great importance for functionally oriented synthesis [8, 9]. Another way of predicting zeolite frames is to create as many hypothetical structures as possible and enumerate all possible three-dimensional grids under certain topological and geometric constraints [10, 11]. Thus, in [12, 13], in order to enumerate all possible four-connected grids with a given number of unique T-atoms for all spatial groups, generation of hypothetical structures was carried out, consisting of the following basic procedures:

- Crystallographically unique T-atoms were successively placed in different positions (private and general) of the unit cell and by means of symmetry operations were generated on the whole cell.
- Of all the possible distributions of T-atoms in the cell, those that allow tetrahedral coordination of atoms are selected.
- When the parameters of the unit cell were varied, optimization was performed to obtain acceptable values for the distances T–T and the angles T–T–T. At the last step, oxygen atoms were added between the bound T atoms, and the whole cell was optimized. As a result, several million hypothetical four-connected zeolite frameworks were obtained with a number of unique T-atoms ≤7, which are now presented in an online database [12, 13].

2.4. Zeolite Molecular Sieve

Zeolites are molecular sieves [4, 14]. Their wide application that they can be used for the separation of substances, not only on the basis of selectivity of adsorption, but also on the basis of the difference in size and shape of the molecules to be absorbed. In order to penetrate the adsorption cavity, the critical diameter of the adsorbate molecules must be smaller than the size of the entrance window [15].

The main factor determining the molecular sieve properties is the size of the entrance windows of zeolites, which depends on the location of the oxygen rings of the zeolite and on the number of oxygen atoms in the ring. The size of the input window is also affected by the size

of the cation entering the zeolite. Cations located close to the window block the entrance for molecules. For example, in cation exchange, in which two sodium cations are replaced by a single calcium cation, the input window expands; As a result, the Na zeolite has an inlet window size of 4Å, and the CaA zeolite has a size of 5Å [15]. A similar exchange in a zeolite of type X leads to a certain narrowing of the window. Considering the properties of the KA zeolite, it can be explained that, at ordinary temperatures, this kind of zeolite sorbs water very well. This property has prevented its use for the drying of unstable substances prone to polymerization reactions.

If we consider the property of NaA zeolite, which is capable of sorbing most of the components of industrial gases, the critical size of the following molecules does not exceed 4Å: hydrogen sulfide, carbon disulfide, carbon dioxide, ammonia, lower diene and acetylene hydrocarbons, ethane, ethylene, propylene, organic compounds with one methyl group in molecule, as well as methane, neon, argon, krypton, xenon, oxygen, nitrogen and carbon monoxide [15]. The latter group of substances is absorbed in considerable quantities only at low temperatures. Propane and organic compounds with more than three carbon atoms in the molecule are not adsorbed by the zeolite and thus do not suppress the adsorption of the above impurities during drying and purification.

CaA zeolites adsorb hydrocarbons and alcohols only of a normal structure, and therefore, it is widely used in the processes of separation of multicomponent organic substances on a molecular sieve basis. Moreover, zeolite CaA is absorbed by methyl and ethyl mercaptans, organic compounds with the number of carbon atoms in molecule 2 (ethyl alcohol, ethylamine), diborane, and so on. Among the general-purpose zeolites of CaA type is increased resistance in a weakly acid medium, and therefore, it is used in desulfurization processes and decarbonization of gases.

Zeolites of type X have rather wide entrance windows and adsorb the vast majority of the components of complex mixtures: all types of hydrocarbons are organic sulfur, nitrogen and oxygen compounds (mercaptans, thiophene, furan, quinoline, pyridine, dioxane, etc.), halogenated hydrocarbons (chloroform, carbon tetrachloride and freons), pentaborane and decaborane [15]. The use of zeolites of CaX and NaX is based on the selectivity of adsorption and not on molecular sieve properties. With the complete replacement of the sodium cation for calcium, the zeolite of CaX, unlike the NaX zeolite, does not adsorb aromatic hydrocarbons or their derivatives with branched radicals, e.g., 1, 3, 5β-triethylbenzene and metadichlorobenzene. This method is based on the method for identifying the zeolites of these two types and establishing the completeness of the ion exchange in the preparation of the zeolite of CaX.

In the case when the critical diameter of the molecule is close to the diameter of the input window, the adsorption process occurs with a high activation energy and the ad-molecule must have a certain kinetic energy reserve to overcome the energy barrier. The kinetic energy of molecules rises with increasing temperature [15]. At the same time, an increase in temperature leads to an increase in the thermal pulsation of the zeolite lattice, which facilitates the penetration of the molecule into the adsorption cavity. Thus, by changing the temperature regime, it is possible to reach a point at which the adsorbent molecules begin to be absorbed by the zeolite.

Localization of cations in the zeolite structure: The localization of cations in the structure depends on the degree of hydration of the zeolites. Dehydration promotes the migration of cations in its structure, and it is necessary to take into account the degree of hydration of the zeolite under given conditions. In addition, protons from 100°C also show increased mobility. The location of the cation is determined not only by the degree of hydration of the zeolite, but also by the nature of the reacting substances. Thus, it was shown that in zeolites of type Y a significant number of Ni^{2+} and Cu^{2+} ions again move from small cavities to large ones when the latter are filled with olefins, ammonia, pyridine or NO molecules [16].

In NaA zeolite, the possible sites for cation localization are four-, six- and eight-membered rings and large cavities. Cations in the eight-membered rings react to the pore size due to the partial blocking of the entrance windows of the cavities [16]. In the faujasite structure, the cations are localized apparently at the centers of hexagonal prisms and on six- and four-membered rings.

The catalytic properties of zeolites, which are studied using X-ray diffraction analysis, should be carefully considered; in fact, the localization of cautions largely depends on the conditions for pretreatment of the zeolite: the heating rate and the final temperature of the zeolite, the concentrations and the parameters for calcinations, the thickness of the layer and the possibility of reducing the cautions by hydrocarbons, and also from the possibility of separation from the vacuum lubricant used in installation.

As a rule, when analyzing the cation distribution in faujasite, the following factors are taken into account [16]:

1. the need for optimal coordination; in hexagonal prisms, cations are easily coordinated with six skeleton oxygen atoms, whereas in the sodalite cavities tetrahedral coordination with three skeleton oxygen atoms and one residual water molecule is possible;
2. the difficulty of local charge compensation with the help of multiply charged ions;
3. the need to minimize the electrostatic energy of the system (direct repulsion of the cation-cation should be excluded);
4. stabilization by a crystalline field or a field of ligands;
5. covalence and the existence of directed bonds.

2.5. Adsorption properties of zeolites

Considering the term adsorption can be understood this term as the ability of solids to absorb certain substances. This ability is closely related to the special properties of the surface of solids. Molecules of a gaseous or liquid substance are in contact with a solid, adsorbed by the surface of solids. The larger the surface of a solid, the more the amount of gas or liquid a given body can hold [4].

If the adsorbed substance is located for a long time on the surface of the adsorbent, the process of diffusion of adsorbed molecules inside [4] of the solid begins. Molecules of gaseous and

liquid substances adsorbed on the surface of a solid. They have a certain mobility, due to which they gradually penetrate into the solid body.

At low pressures, adsorption increases in proportion to the increase in pressure. However, as the pressure rises, the linear relationship is broken; the amount of adsorbed gas decreases, and then, at a certain pressure, saturation appears; with further increase, the pressure of adsorption of substances does not increase [4].

In a number of cases, the relationship between the gas pressure and the amount of gas absorbed by the adsorbent is more complex; after reaching a certain pressure, the amount of adsorbed gas begins to increase sharply. It was found that the nature of this dependence is related to the shape and size of the adsorbent pores [4].

In the adsorbent pores, at a certain relative pressure, the vapor becomes a liquid state and the entire internal structure begins to be filled with condensing vapor, as a result of which the amount of absorbed substance sharply increases. This phenomenon is called capillary condensation. In the fine pores of molecular sieves, capillary condensation does not occur; it can be noted only in relatively large pores formed by a binder during granulation—in a secondary porous structure [4].

Theories were advanced to explain the features of adsorption processes, and equations describing the dependence of the amount of adsorbed matter on pressure, temperature, and other conditions were derived.

The theory developed by Langmuir proceeds from the concept of the formation of a monomolecular layer of an adsorbed substance due to the action of active sites of the adsorbent.

In the potential theory advanced by Polanyi, it is assumed that the scope of the attractive forces during adsorption extends not only to the nanomolecular layer of matter.

Proceeding from all of the above, the main ways to regulate the selective adsorption capacity of zeolites are as follows.

1. Change in composition in the process of crystallization. From the same starting materials, it is possible to obtain aluminosilicate porous crystals having different properties. For example, type A zeolite is formed from mixtures rich in alkalis and poor in silica, and type Y zeolite crystallizes in the region with the lowest alkalinity of the medium and the highest concentration of silica [17].

2. Method of ion exchange. Ionic exchange can be regulated by molecular sieve properties, especially type A. Knowing the dimensions of the adsorbed molecules and zeolite windows, it is possible to select a particular cation exchange form of the zeolite to separate any mixture of gases or dissolved gases. For example, a zeolite, a spacecraft with a window size of about 3 Å, adsorbs water well, but water does not adsorb molecules of methanol, carbon dioxide, whose critical molecular diameter is greater than 3 </s>. Zeolite NaA in which the window size is 4 ÅA^0 adsorbs methanol and carbon dioxide and does not adsorb the molecules of propane, hexane and other molecules with a critical diameter greater than 4 </s>. On a CaX zeolite with a window size of 8 Å, 1,3,5-triethylbenzene molecules are not adsorbed, and on NaX zeolite (the size of windows 9 Å) they are well adsorbed [17].

Zeolites can manifest themselves as ions in many processes. For example, sodium in zeolite type X cannot be exchanged for alkyl ammonium cations because of the large size of the latter. Cation sieve effects in zeolites can also be caused by the fact that due to too large a size the cation cannot penetrate into small channels and cavities in the zeolite framework, or exchange cations during the synthesis of some zeolites are localized in inaccessible areas and therefore not are replaced [17].

Adsorption on the surface of zeolite of polar substances, around the entrance windows, prevents the diffusion of adsorbate molecules, and prevents their movement. Thus, for example, the pre-sorption of small amounts of water vapor on zeolite type A sharply reduces the adsorption of oxygen. Effective window diameters can be adjusted to form organometallic complexes. Thus, when pyridine is treated with a copper form of zeolite X, a very strong pyridine cation complex is formed. The adsorption of molecules of gases and vapors on such a zeolite indicates a significant decrease in pore sizes due to their blocking by organometallic complexes [17].

A special place among the cation-substituted zeolites is occupied by hydrogen, or decationized, forms of zeolites. Replacement of cations of zeolite with hydrogen is one of the ways of modifying porous crystals. The hydrogen form of zeolites, unlike other forms, cannot be obtained by simple treatment of the zeolite with acids, since the latter destroy the crystal lattice, especially low-silica zeolites. Therefore, in the beginning, sodium ions are replaced by ammonium ions, then the latter is thermally decomposed, ammonia is released and a proton is formed, which ensures the neutrality of the zeolite lattice [17].

One of the methods for modifying zeolites is dealumination. Treatment of zeolite with acids leads to the dissolution of tetrahedral aluminum in the lattice. As a result, the adsorption capacity of the zeolite increases. Dealumination can also be carried out by treating the zeolite with substances that form complex compounds with aluminum ions or by treating the zeolite layer with water vapor at elevated temperatures [18]. Dealumination allows, within certain limits, to vary the ratio of silicon and aluminum-oxygen tetrahedra in the zeolite without changing its crystal lattice.

Selective adsorption on zeolites is also possible when the molecules of all components of the mixture are sufficiently small and freely penetrate into the adsorption space. Other things being equal, the exchange cations are adsorption centers and determine the specificity of the interaction during adsorption on the zeolites of molecules of different structure and electronic structure [18]. By changing the nature and size of the exchange cation, it is possible to enhance or weaken the contribution of a specific interaction to the adsorption energy. In addition to interacting with the positive charge of cations, the adsorbate molecule undergoes strong dispersion effects from other atoms forming the walls of the zeolite channels. One of the important issues of adsorption interaction on zeolites is the elucidation of the nature of active centers [18].

2.6. A mathematical model for determining the total adsorption of solutions on zeolites

Considering the process of adsorption from solutions should be considered as a process of concentration on the surface of one of the two adsorbed components. Therefore, to determine

the adsorption energy of solutions, we use the data on the surface tension of the pure components and try to obtain the adsorption through Gibbs energy.

Considering the fundamental Gibbs law, we get

$$-d\sigma = G_1 d\mu_1 + G_2 d\mu_2 \tag{1}$$

where G_1 and G_2 are the values of the Gibbs adsorption of components; μ_1 and μ_2 are the chemical potential of the components in order to relate Gibbs adsorption to the concentration of the component; it is necessary to use the Gibbs-Duhem Eq. [19]

$$x_1 d\mu_1 + x_2 d\mu_2 = 0 \tag{2}$$

where x_1 and x_2 are the mole fraction of the components.

Then,

$$\mu_1 = -\frac{x_2}{x_1} d\mu_2 \tag{3}$$

We substitute it into the Gibbs Eq. (3) and obtain

$$-d\sigma = \left(G_2 - G_1 \frac{x_2}{x_1}\right) d\mu_2 \tag{4}$$

Surface properties of solutions are considered from the surface properties of pure liquids and strongly depend on the composition of the surface layer [20]. When a substance having a lower surface tension than a pure solvent dissolves, the surface tension of the solution decreases spontaneously, since the free energy of the system decreases. The concentration of solute in the surface layer as compared to its concentration in the solution volume increases [20]. Substances that increase the surface tension of the solution, on the contrary, are contained in the surface layer in a lower concentration than those in the volume [20].

Often substances that increase the surface tension of the solvent themselves have a higher surface tension in their pure form, while lowering substances have a lower surface tension than the solvent. A large surface tension means greater energy unsaturation of molecules on the surface [20]. Such molecules tend to leave the surface, since to reduce free surface energy it is more advantageous to have molecules with low energy unsaturation. Naturally, the complete separation of molecules is impeded by the loss of entropy of solution formation [20]. As a result of the action of these two factors, a composition change occurs on the surface of the solution as compared with the volume, that is, adsorption occurs [21]. For all liquid organic substances, the surface tension is less than the surface tension of water. Assuming that the total number of moles before and after adsorption remains unchanged, we find that when one component is adsorbed, the amount of the other is increased evenly. Then, $G_1 = G_2$, $x_2 + x_1 = 1$. From this, it turns out:

$$G_2 = (1 - x_2) \frac{d\sigma}{d\mu_2} \tag{5}$$

and replacing μ_2 by c_2, we obtain an equation similar to the Gibbs adsorption equation for dilute solutions

$$G_2 = (1 - x_2)\frac{c_2}{RT}\frac{d\sigma}{dc_2} \tag{6}$$

Thus, the most important feature of the Gibbs method is that it allows us to give some general characteristic of the region of inhomogeneity without knowing the true course of the concentration profile.

To solve Eq. (6), it is necessary to find the value of the surface tension for a binary solution.

Determination of the surface tension of a binary solution is

$$\sigma = \sigma_0 + 0.049 \cdot \left(1 - \frac{c_2}{c_1}\right) \tag{7}$$

where N/m is the surface tension of water; c_1 is the initial concentration of the solution, % vol.; c_2 is the final concentration of the solution, % vol.

Since Gibbs adsorption does not allow comparison of the results with the results of the experiment, it is necessary to use the equation to determine the total adsorption. Let us single out that to determine the total adsorption (absolute adsorption), it is necessary to relate Gibbs adsorption to the experimental results [21–24].

$$a = G_2 + W \cdot \rho \tag{8}$$

where W is the volume of the space in which adsorption occurs, cm³/g; a is the complete adsorption of g /g; ρ is the density of the equilibrium phase, g/cm³.

Then,

$$a = (1 - x_2)\frac{c_2}{RT}\frac{d\left[\sigma_0 + 0,049 \cdot \left(1 - \frac{c_2}{c_1}\right)\right]}{dc_2} + W \cdot \rho \tag{9}$$

Thus, Gibbs adsorption does not reflect the properties of zeolite adsorbents; therefore, it is necessary to combine the formulas (6)–(8) into a single equation for the theoretical calculation of the total adsorption of binary solutions on zeolites. With the application of the method of complete content, from the concept of the region of inhomogeneity at the interphase interface as a separate real phase of finite volume [22–24].

3. Experimental part

As a result of experimental research in the laboratory, the following hydrometer Hydrometer AHON-1 (measuring range 700–1840 kg/m³), laboratory scales Leki 5002, calipers digital 31C628 (error) and SORBTOMETR-M were used.

Adsorbent	Diameter of grain, mm	*a*, total adsorption, g/g	*W*, the volume of the space in which adsorption takes place, cm^3/g
Zeolite CaA	3	0.26	0.23
Zeolite CaA		0.191	0.17
Zeolite NaA		0.245	0.2
Zeolite NaX		0.304	0.292
Zeolite KaA		0.197	0.1912

Table 1. Characteristics of zeolite adsorbents of grades A, X [24, 25].

Name	c_1—initial concentration of water, % vol.	c_2—final concentration of water solution, % vol.	Density of the solution, g/m^3	x_2—mole fraction of components	Temperature *T*, K
C_2H_5OH (65%)	35	25	0.8795	0.58	293
CH_3OH (75%)	25	15	0.8616	0.38	293
C_6H_6 (60)	40	30	0.836	0.76	293

Table 2. Characteristics of the investigated organic substances.

The following characteristics of the investigated adsorbents are established (**Table 1**). The volume of the solution is 200 ml, and the mass of adsorbent for adsorption is 100 g.

To check the theoretical relationships and compare them with the experimental data, it is necessary to analyze a number of binary solutions, such as ethanol + water, methanol + water, and benzene + water; we distinguish that in **Table 2** the characteristics of the pure components of organic solutions for theoretical calculations are listed.

For a simplified calculation, let us set the condition that adsorption in the systems under consideration occurs only for one of the components; therefore, the concentration change will be monitored by the change in the percentage of water in the solutions in question. To do this,

Adsorbent	*a*—total adsorption, g/g		
	$C_2H_5OH + H_2O$	$CH_3OH + H_2O$	$C_6H_6+H_2O$
Zeolite CaA	0.202	0.198	0.192
Zeolite CaA	0.15	0.146	0.142
Zeolite NaA	0.176	0.172	0.167
Zeolite NaX	0.257	0.252	0.244
Zeolite KaA	0.169	0.165	0.16

Table 3. Calculated values of total adsorption.

when testing the mathematical model for calculating the total adsorption, we take the initial water concentration of the binary systems under consideration. The results of the calculation using formula (9) are given in **Table 3**.

4. Conclusion

The data presented show that the mathematical model developed by the author allows us to reliably estimate the total adsorption of various binary systems. When comparing theoretical values with experimental ones, it can be asserted that the values obtained fully satisfy the requirements of theoretical calculations and can be used in the design of drying apparatuses and concentrating alcoholic solutions. Let us emphasize that the accumulation of data on Gibbs adsorption will contribute to the refinement and verification of models taking into account bulk effects in adsorption solutions and will allow theoretical calculations to be carried out with high accuracy [26, 27].

Thus, the use of the approximate method of calculating absolute adsorption makes it possible to obtain more realistic information about the properties of adsorption solutions, which indicates significant structural changes in them, depending on the concentration.

Author details

Paranuk Arambiy[1]*, Saavedra Huayta Jose Angel[1] and Khrisonidi Vitaly[2]

*Address all correspondence to: rambi.paranuk@gmail.com

1 Kuban State Technological University, Krasnodar, Russia

2 Federal State Budget Education Establishment of Higher Professional Education, Maikop State Technological University, Maykop, Russia

References

[1] Workshop on physical chemistry NSU. Chemical thermodynamics and kinetics. Adsorption from solutions on a solid surface: Method, Manual/O.V. Netskina. Novosibirsk: Novosibirsk State University; 2015. 17 p

[2] Kireev VA. Course of physical chemistry. 3rd ed. recycled. and additional. M., "Chemistry". 1975. 776 p. 2. Adsorption at the solid-liquid interface. Tutorial M.: MITHT them. M.V. Lomonosov, 2005

[3] Paranuk AA, Khrisonidi VA. Industrial application of molecular sieves. Interactive Science. 2016;**5**:51-53

[4] Sokolov VA, Torocheshnikov NS, Keltsev NV. Molecular sieves and their application. Chemistry; 1964. 156 p

[5] Barrer RM, Villiger H. The crystal structure of the synthetic zeolite. Zeitschrift für Kristallographie. 1969;**128**(3-6):352-370

[6] Deem MW, Newsam JM. Determination of 4-connected framework crystal structures by simulated annealing. Nature. 1989;**342**(6247):260-262

[7] Earlab DJ, Deem MW. Parallel tempering: Theory, applications, and new perspectives. Physical Chemistry Chemical Physics. 2005;**7**(23):3910

[8] Boisen MB Jr, Gibbs GV, O'Keeffe M, Bartelmehs KL. A generation of framework structures for the tectosilicates using a molecular-based potential energy function and simulated annealing strategies. Microporous and Mesoporous Materials. 1999;**29**(3):219-266

[9] Draznieks CM, Newsam JM, Gorman AM, Freeman CM, Fйrey G. De novo prediction of inorganic structures developed through automated assembly of secondary building units (AASBU method). Angewandte Chemie, International Edition. 2000;**39**(13):2270-2275

[10] Foster MD, Treacy MMJ, Higgins JB, Rivin I, Balkovsky E, Randall KH. A systematic topological search for the framework of ZSM-10. Journal of Applied Crystallography. 2005;**38**:1028-1030

[11] Li Y, Jihong Y, Wang Z, Zhang J, Guo M, Ruren X. Design of chiral zeolite frameworks with specified channels through constrained assembly of atoms. Chemistry of Materials. 2005;**17**(17):4399-4405

[12] The database on prospective zeolite structures. URL: http://www.hypotheticalzeolites.net/

[13] Treacy MMJ, Rivin I, Balkovsky E, Randall KH, Foster MD. Enumeration of periodic tetrahedral frameworks. II. Polynodal graphs. Microporous and Mesoporous Materials. 2004;**74**(1-3):121-132

[14] Grubner O, Jiru P, Ralek M. Moleku larsiebe. Berlin: VEB Deutscher Verlag der Wissenschaften; 1968. 176 p

[15] Keltsev NV. Basics of adsorption techniques. 2nd ed., Revised. and additional. M., Chemistry; 1984. 592 p

[16] Benson G, Yun K. Interphase boundary gas-solid body. The World. 1970:172

[17] Considering the term adsorption can be understood this term as the ability of solids to absorb certain substances. This ability is closely related. Melnikov OK, Lobachev AN. Growth of crystals from high-temperature aqueous solutions. Science. 1977;5-11

[18] Neimark IE. Synthetic mineral adsorbents and catalyst carriers. Kiev: Science. Dumka. 1982. 216 p

[19] Sokolov VA, Torocheshnikov NS, Keltsev NV. Molecular sieves and their application. Chemistry. 1964

[20] Aivazov BV. Workshop on the chemistry of surface phenomena and adsorption. Textbook. Manual for Institutions. Higher School. 1973. 208 p

[21] Tolmachev AM, Godovikova MI, Egorova TS. // Zhurn.fizich.chemii, 2005. P. 79, № 1, p. 1

[22] Paranuk AA. A mathematical model for calculating the adsorbers for drying and concentration of methanol on zeolites. Chemical and Petroleum Engineering. 2017, P. 53, № 1-2, p. 41-43

[23] Zaitsev ID, Aseev GG. Physicochemical properties of binary and multicomponent solutions of inorganic substances. Ref. ed. -M: Chemistry, 1988. p. 416

[24] Paranuk AA, Krisonidi VA, Ponomareva GV. KACO zeolite adsorption of ethyl alcohol. Journal of Engineering and Applied Sciences. 2016, №11(13), p. 2876-2878

[25] Tolmachev AM, Stekli F, Trubnikov OI, Kuznetsova TA. The Journal of Physical Chemistry A. 1999;**73**(7):1267

[26] Paranuk AA, Krisonidi VA, Skhalyakho ZC, Shugalya AI. Technological scheme development of the azeotropic mix separation. Journal of Engineering and Applied Sciences. 2016, №11(13), p. 2878-2880

[27] Paranuk AA, Saavedra KH, Kinenez LK. Separation of multicomponent solutions by adsorption methods on zeolites. Exposition Oil Gas. 2015, №6(47), p. 66-67

Chapter 5

Estimation of Nanoporosity of ZSM-5 Zeolites as Hierarchical Materials

Miguel Angel Hernández, A. Abbaspourrad,
Vitalli Petranovskii, Fernando Rojas,
Roberto Portillo, Martha Alicia Salgado,
Gabriela Hernández, Maria de los Angeles Velazco,
Edgar Ayala and Karla Fabiola Quiroz

Additional information is available at the end of the chapter

http://dx.doi.org/10.5772/intechopen.73624

Abstract

The nanoporosity in zeolite ZSM-5 was analyzed as a function of SiO_2/Al_2O_3 molar ratio (MR). The internal pore structure was studied by high-resolution adsorption. Surface areas, microporous volume, characteristic energy of sorption, and pore-size distributions were calculated from N_2 sorption isotherms by the BET, Langmuir, *t*-method of de Boer, α_S-plot of Sing, direct comparative plots of Lee, Newnham, Dubinin-Astakhov, differential adsorption curves, and nonlocal density functional theory methods. The results indicated that MR dependence in these zeolites caused structural defects through micropore opening and widening as well as the emergence of further slit-like mesopores.

Keywords: ZSM-5 zeolite, sorption, nanopore measurements

1. Introduction

The nanoporous, ordered, and three-dimensional structure of zeolites makes them materials of great practical importance in the hierarchy. The broad use of microporous zeolites (pore diameter $w < 2$ nm) makes them very important in very specific areas, such as acid catalysts and adsorbents, as well as in refining processes and the basic petrochemical industry due to their unique properties both in activity and in selectivity [1]. The great majority of zeolites possess two types of porosity: primary and secondary. Primary porosity with a well-defined

IntechOpen

© 2018 The Author(s). Licensee IntechOpen. This chapter is distributed under the terms of the Creative Commons Attribution License (http://creativecommons.org/licenses/by/3.0), which permits unrestricted use, distribution, and reproduction in any medium, provided the original work is properly cited.

size is associated with the crystalline structure of the zeolite and fundamentally depends on its structure type. Imperfections, including defects occurring during the growth of zeolite crystals, as well as defects generated by various treatments, cause secondary porosity, that is, the presence of mesopores ($2 < w < 50$ nm) and macropores ($w > 50$ nm) [2]. The secondary porosity differs from the framework porosity, since it does not directly depend on the crystalline structure of the zeolite. Taken together, these comprise the texture of a sorbent. The primary porosity is characterized by a microporous volume (W_0) with pore size as seen in the zeolite structure; secondary—by the pore-size distribution (PSD) and the external surface area (A_E). These parameters are usually calculated from nitrogen sorption isotherms [3]. Many, but not all, catalysts are porous materials, in which most of the surface area is internal. Sometimes it is convenient to talk about the structure and texture of such materials. The structure is defined both by the distribution in space of atoms or ions in the material part of the catalyst and by the distribution on the surface. The texture is defined by the detailed geometry of the void space in the catalyst particles. Porosity is a concept related to texture and refers to the porous space in the material. However, with zeolites, most of the porosity is determined by the crystal structure. To accurately describe the texture of the porous catalyst, a very large number of parameters will be required. With respect to porous solids, the surface associated with the pores can be called the internal surface. Since the availability of pores can depend on the ratio of the dimensions of the channel and molecules, the extent of the accessible internal surface may depend on the size of the molecules contained in the mixture and may be different for various components of the mixture (molecular sieve effect) [4].

ZSM-5 and, its purely siliceous analog, silicalite (both have a structural code "MFI" in accordance with the IZA database) are among the most widely studied zeolites. MFI is one of the most versatile and commercially significant zeolites; it is widely used in the petroleum industry to convert methanol into complex hydrocarbons in methanol-to-gasoline processes, as well as in the alkylation of aromatic compounds and their subsequent separation [5]. The microporous network of this zeolite consists of intersecting straight and sinusoidal channels. The straight channels have pore openings defined by a cross-section of 10-member rings of 0.54–0.57 nm and sinusoidal channels by elliptic pores of 0.51–0.54 nm in cross-section. The intersections are cavities of 0.8 nm in diameter [6] (see **Figure 1**).

A detailed study on the different types of adsorption sites that constitute the structural skeleton of this zeolite was carried out by Cho et al. [7]. They classified the sorption sites into three types: (1) the S_S sites located in straight channels; (2) the S_Z sites located in zigzag (sinusoidal) channels; and, finally, (3) the S_I sites located at the intersections (**Figure 2**). One of the most important catalytic properties of ZSM-5 is its shape selectivity. This is a consequence of its primary microporous structure and is the basis for most of its successful applications [8].

Another important parameter that allows to adjust the zeolite properties is their chemical composition, that is, their SiO_2/Al_2O_3 molar ratio (MR). The amount of Al in the framework is proportional to the number of exchangeable cations, H^+ among others, which affects both Lewis and Brønsted acidity. The main interactions of the sorbate molecules in the pores of the zeolite are realized through the oxygen atoms of the lattice and extra-framework cations. Microporosity and secondary porosity in zeolites and similar materials can be determined from the low- and medium-pressure regions of the sorption isotherm using various approaches [3]. The shape-selective activity of MFI can be attributed to the presence of active

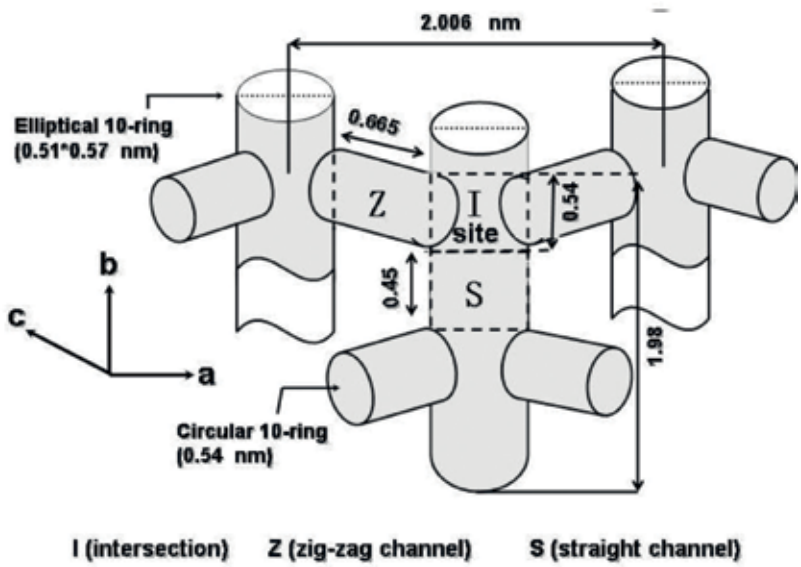

Figure 1. ZSM-5 zeolite structure. The dimensions of the pore channels are in nm. I, S, and Z are S_I, S_S, and S_Z sites, respectively.

sites in micropores. It was shown that the shape-selective properties of zeolites may be greatly reduced due to the presence of active sites in the secondary porosity with a wide distribution of the pore diameter and on the external surface of their crystallites, so zeolites with a large outer surface area are less selective than those with fewer imperfections.

The presence of molecules that blocks the pores of the zeolite or a partial destruction of its structure can drastically decrease its activity by reducing the microporous volume accessible for the reactants. The effect that the external surface area of ZSM-5 zeolite crystals used

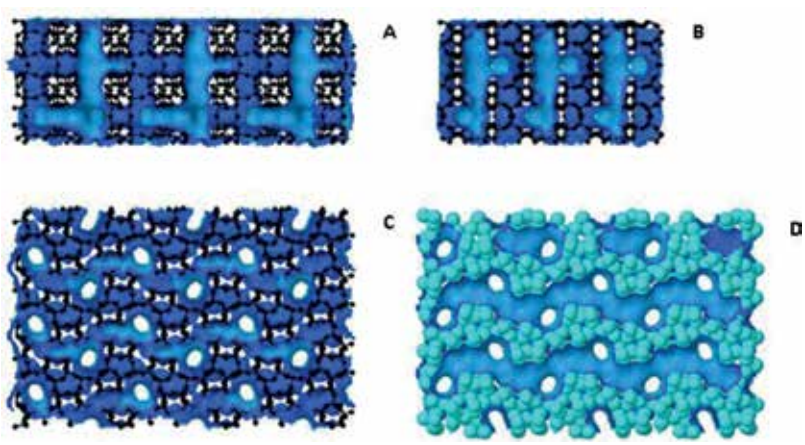

Figure 2. Front (A), right (B), and top (C) views of a "ball and stick" ZSM-5 (MFI) model; crosscutting of zigzag channels (D) of an "ionic radii" model; all from the IZA page: http://izasc.ethz.ch/fmi/xsl/IZA-SC/ftc_3d.php.

for shape-selective reactions causes, was reported previously [9]. Some authors in reported works have used the α_S-plot of Sing as alternative method to evaluate the external surface area and the true intra-crystalline capacity [10].

The aim of this study was to accurately describe the dependence of all the different types of ZSM-5 porosity on MR and to show which methods are best suited for measuring them in each range. This will allow us to develop an approach to the application of various existing methods of texture characterization for samples of zeolite with mixed porosity.

2. Methodology

A set of ZSM-5 zeolites in their sodium form (Na-ZSM-5) with a SiO_2/Al_2O_3 molar ratio (MR) varying from 30 to 120 was synthesized using a template of tetrapropylammonium bromide (TPABr) following the methodology reported by Ghiaci et al. [11]. Through the text and figures, these samples are called Z, followed by the MR value (30, 70, 95, or 120), for example, Z30 means an Na-ZSM-5 sample with an MR equal to 30. For comparison, a set of Na-ZSM-5 samples supplied by TOSOH Co., Japan, with MR 20, 23.3, and 30 were also studied. These TOSOH samples are called ZT, followed by MR value. A reference macroporous solid material required to estimate micropore volumes was obtained from the Tehuacan area in the state of Puebla, Mexico. This reference substrate was identified by X-ray powder diffraction (XRD) as α-SiO_2. X-ray powder diffraction of ZSM-5 samples was obtained in the 2θ ranges of 5–50 degrees using diffractometer Bruker D8, using nickel-filtered Cu Kα (λ = 0.154 nm) radiation. Scanning Electron Microscopy images were collected from a JEOL JSM-6610LV electron microscope with tungsten filament and an electron detector operated at 20 kV. N_2 adsorption isotherms were measured at the boiling point of liquid N_2 (76.4 K at the 2200 m altitude of Puebla City, México) in the interval of relative pressures, p/p^0 extending from 10^{-6} to 1 in an automatic volumetric adsorption system (Quantachrome AutoSorb-1C) in order to determine the textural parameters of ZSM-5 samples in addition to the evaluation of microporosity, which was analyzed through the determination of pore-size distributions calculated by the differential adsorption curves (DAC), Dubinin-Astakhov equation (D-A), and nonlocal density functional theory (NLDFT) approaches.

3. Results and discussion

3.1. X-ray analysis

The XRD patterns of all samples (**Figure 3**) are typical of ZSM-5 zeolites [12]. In general, all the samples showed reasonably sharp diffraction patterns, indicating good crystallinity. Please note that commercial TOSOH samples and those prepared in the laboratory are nearly identical. The main peaks appear at the following 2θ angles: 8.0°, 8.9°, 9.8°, 14.0°, 14.8°, 20.9°, 23.2°, 23.9°, 24.5°, 29.4°, and 30.0° (**Figure 3**). Most of these peaks are not resolved; usually, one peak is a superposition of several closely located reflections. For example, the [−101], [011], and

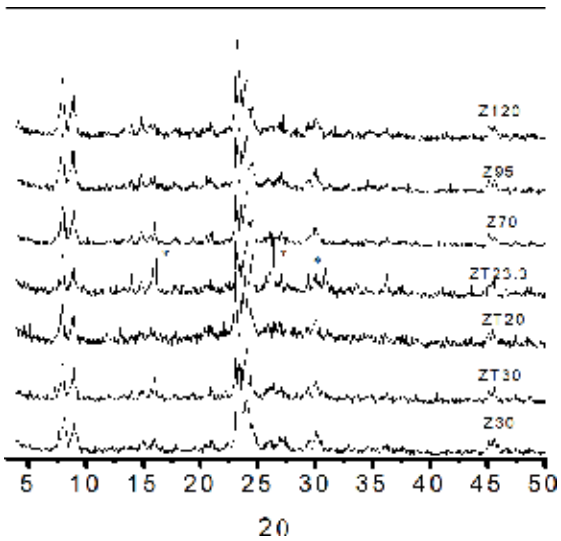

Figure 3. X-ray diffraction patterns.

[101] reflections positioned at 2θ = 7.92°, 7.93°, and 8.01°, respectively, gave rise to a total peak at ~8.0. The most important difference between the standard XRD pattern and the observed for both sets of samples is the relative intensity of the various peaks, but a detailed discussion of the changes in the structure of ZSM-5 due to MR variations and synthesis conditions is beyond the scope of the present work and will be discussed elsewhere. Three peaks that appear at 2θ = 16.0°, 26.4°, and 30.9° in the ZT23.3 sample (marked with asterisks) are most probably associated with an unidentified impurity.

3.2. Scanning electronic microscopy

In **Figure 4**, it can be seen that the effect of the templates used during the synthesis process affects the morphology of the zeolite crystals obtained. Thus, for example, in **Figure 4(a)** and **(b)** corresponding to zeolites ZT-20 and ZT-23.3, it can be seen that the crystals obtained have lath-like shapes. In the case of the ZT-30 and ZT-23.3 zeolites, clusters of spheroidal crystals are observed where the crystals of the zeolites coexist, as seen in **Figure 4(c)** and **(d)**. Finally, the SEM images of the zeolites ZT-30 and ZT-23.3 do not exhibit a predominant or defined geometry, as seen in **Figure 4(e)** and **(f)** [13].

3.3. High-resolution adsorption

N_2 sorption isotherms at 77 K for both sets of samples are shown in **Figure 5** as sorbed volume at standard temperature and pressure (STP) in cm^3 per gram of zeolite versus p/p^0. **Figure 5** shows the sorption isotherms using a logarithmic p/p^0 scale in the range of $10^5 \leq p/p^0 \leq 1$. The hysteresis loops shown by ZSM-5 zeolites are of the Type H3 or H4, characteristic of capillary condensation in the slit-like pores attributed to intercrystallite adsorption within aggregates. **Table 1** gives the values of some important parameters obtained from the analysis of isotherms.

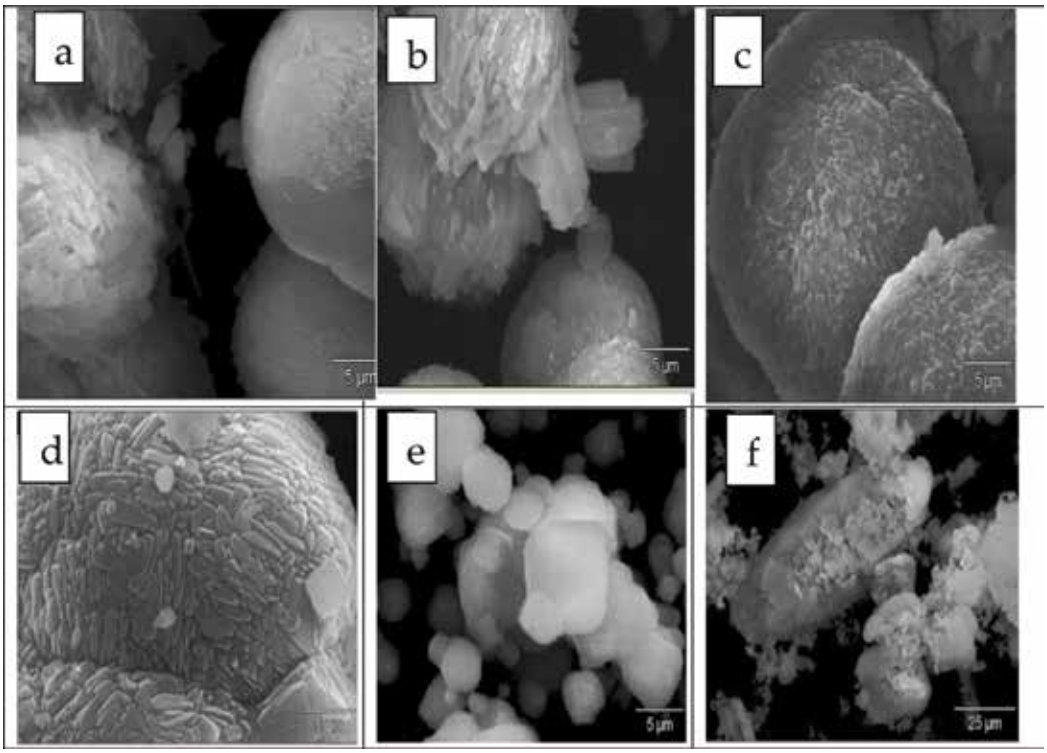

Figure 4. SEM images of ZSM-5 zeolite samples with different forms and crystal sizes: (a) ZT-20, (b) ZT-23.3, (c) ZT-30, (d) ZT23.3, (e) Z-30, and (f) Z-120.

All the N_2 isotherms are of Type I according to the IUPAC classification [14]. They indicate: (1) a high sorption at a very low relative pressure caused by the enhanced sorption potential of the ZSM-5 channel system and (2) formation of a monolayer at $0.1 \leq p/p^0 \leq 0.8$.

3.3.1. External surface area

To calculate the volume of the micropores from the sorption data, De Boer *t*-plots (thickness plots) and Harkins-Jura estimates are given in **Table 2**. An accurate estimate of these values can be influenced by the choice of the standard isotherm of a nonporous material selected to estimate the statistical thickness of the adsorbed layer (t) and the range of t values considered for the linear fitting [15] (**Figure 6**).

3.3.2. Microporosity

The total micropore volumes in $cm^3\ g^{-1}$ for all the samples are given in **Table 2**. These values were calculated from: (1) α_S-plots, (2) *t*-plots, and (3) the D-A equation (in this case, optimizing the values of the parameters n and E_0). The ratio of the micropore-filling capacity to the total sorption uptake, W_0/V_Σ, a parameter that somehow indicates the degree of crystallinity of the zeolite being analyzed, is also included in **Table 2** [16]. For the construction of the α_S and direct comparison plots, the adsorption volumes of the α-quartz without thermal processing

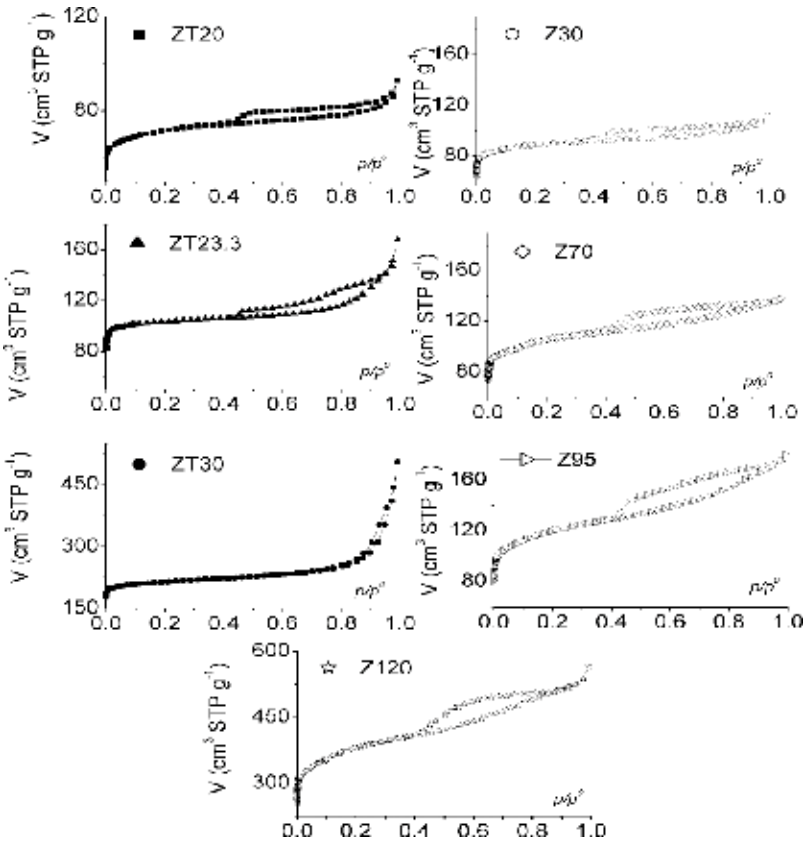

Figure 5. N_2 sorption isotherms at 77 K. For this figure and throughout, all samples supplied by TOSOH (ZT series) are designated by filled symbols, while samples synthesized for the present work (Z series) are designated by open symbols. The selection of symbols (circles, squares, etc.) is constant for all figures. Note that the ordinate scales are not always the same.

were used as reference values; α-quartz was chosen as a reference material, since adsorption on these substrata occurs similarly as on a flat surface; access to the underlying microporous structure is impeded by water molecules in the pore openings. The standard nitrogen

ZSM-5 zeolite	Si	Al	Na	O	Si/Al
Na-20	45.72	4.5	2.65	47.315	10.16
Na-23.3	47.313	3.61	2.58	46.496	13.10
Na-30	48.893	2.866	1.326	46.906	17.06
30	46.483	4.156	2.383	46.976	11.18
70	48.82	0.826	0.823	49.560	56.68
95	52.986	1.45	0.91	44.656	36.54
120	50.766	0.96	0.66	47.61	52.88

Table 1. ZSM-5 zeolite chemical composition (mass %, EDS).

Sample	A_{SL} (m² g⁻¹)	A_{SB} (m² g⁻¹)	A_E (m² g⁻¹)	V_Σ (cm³ g⁻¹)	BET p/p^0 range	C_B	dp (nm)	W_0/V_Σ
ZT20	287.6	224.5	13.39	0.217	0.09–0.27	−56	3.866	33.179
ZT23.3	459.5	375.4	33.32	0.390	0.05–0.17	−244	4.155	26.153
ZT30	399.4	313.9	91.27	0.812	0.05–0.19	−202	1.034	25.738
Z30	533.6	409.0	19.72	0.129	0.05–0.19	−343	1.261	68.992
Z70	491.2	349.2	47.12	0.162	0.05–0.24	−110	1.855	63.580
Z95	562.3	397.0	83.41	0.207	0.05–0.27	−107	2.085	54.106
Z120	1784	1314	279.30	0.812	0.05–0.21	−276	2.471	54.451

Table 2. Adsorption structural parameters of ZSM-5 zeolites.

isotherms [17] are very similar to the adsorption isotherms of α-quartz along the adsorption branch up to a relative pressure of about 0.8. Since the same material was used as a reference for the α_S direct comparison plots, similar microporous volumes were obtained from all of these methods. However, *t*-plots give slightly different results because the reference isotherm corresponds to de Boer equation.

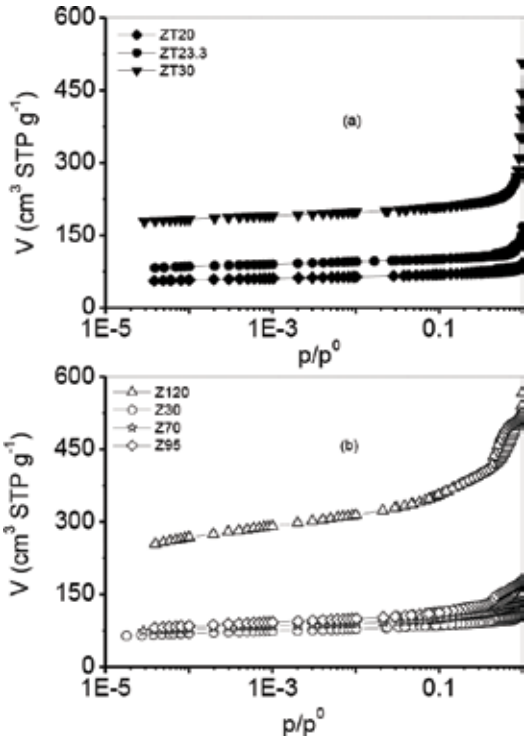

Figure 6. High-resolution N_2 sorption isotherms using a logarithmic p/p^0 scale. The graphs are divided in (a) and (b) parts with different scales due to the presence of higher values for most of the measured parameters for ZT30 and Z120 for this and the following figures.

A_{SL} is the Langmuir-specific surface area; A_{SB} is the BET-specific surface area; A_E is the external surface area; V_Σ is the volume sorbed at $p/p^0 = 0.95$; p/p^0 is the range used for the BET plot; C_B is the BET constant; *dp* is average particle diameter; and W_0/V_Σ is the degree of crystallinity.

3.3.2.1. High-resolution α_S-plots

The filling of macro, meso, and micropores can be proved by analyzing high-resolution α_S-plots starting at low relative pressures, that is, 10^{-5}; see **Figure 7**. There are some significant differences in the form of α_S-plots as a function of MR, mainly for Z120. A pronounced distortion of the isotherm shape is observed at a very low p/p^0, which can be explained by the enhancement of the sorbent-sorbate interaction in the pores of molecular dimensions, that is, the process of micropore filling [18]. This type of α_S-plot is characteristic of microporous adsorbents having a wide range of pore sizes and results in two or more separate stages of micropore filling. **Figure 7** shows three linear ranges. Region III, with $\alpha_S > 1.6$, corresponds to sorption in the mesopores and adsorption on the external surface of the zeolite. Extrapolation of the line to the ordinate at $p/p^0 = 0$ allows to estimate the total microporous volume W_0. Region II with $\alpha_S = 0.6$–1.6 can be a sorption in the porosity created by partial removal of the constituents of the zeolite matrix with the formation of structural defects. This type of porosity is typically developed by acid leaching. Region I, with $\alpha_S < 0.25$, is due to the stages of final filling of the volume of ultramicroporous elliptical sinusoidal channels (0.55 × 0.51 nm) and nearly circular straight channels (0.54 × 0.56 nm). This behavior is mainly due to the combined

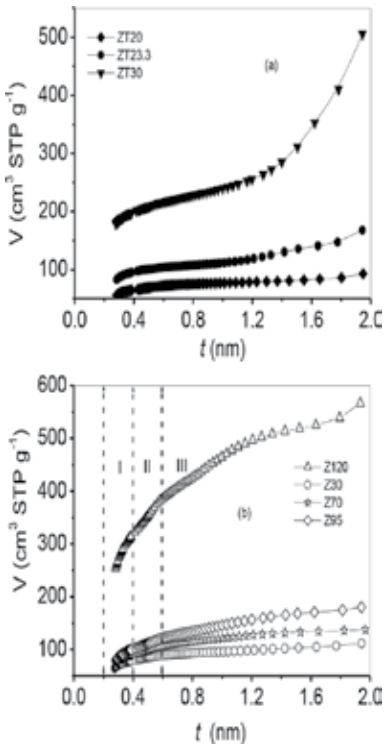

Figure 7. *t*-plots for the N_2 sorption isotherms.

filling of channels. However, this region is related to the filling of the ultramicropores corresponding to the narrowing and to the initial stages of channel filling. Zones of this α_S-plot for Z120 appear because the substratum has mesopores, supermicropores, and uniform micropores with elliptical and nearly circular free openings. The diameter of these channels corresponds to approximately 1–3 diameters of molecules. The micropore filling regions obtained through high-resolution plots for all samples are presented in **Table 2** (**Figures 8** and **9**).

3.3.3. Pore-size distributions calculated by the DAC, D-A, and NLDFT approaches

3.3.3.1. DAC method

Calculation of pore-size distributions from desorption branches of N_2 isotherms using the differential adsorption curves (DAC) [19] method yields bimodal distributions (**Figure 10**), with the thickness of the pore size of ca. 0.36 and 0.55 nm for all samples. The plots are unimodal with the pore ca. 0.36–0.40 nm. This approach correctly describes the essential qualitative features of N_2 sorption in the microporous zeolites, such as ZSM-5, that is, pores in the range of 0.3–0.6 nm. The results of these estimates are shown in **Table 3**.

3.3.3.2. D-A method

The pore-size distributions obtained by the D-A method [20] are shown in **Figure 11**. The average pore diameter, seen as a maxima on the curves by this method, varies according to

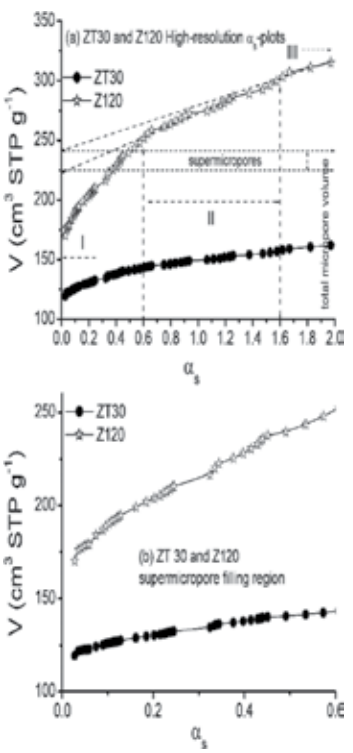

Figure 8. High resolution α_S-plot for N_2 sorption on ZT30 and Z120, showing (a) the ultramicropore and supermicropore volume regions and (b) the supermicropore linear region.

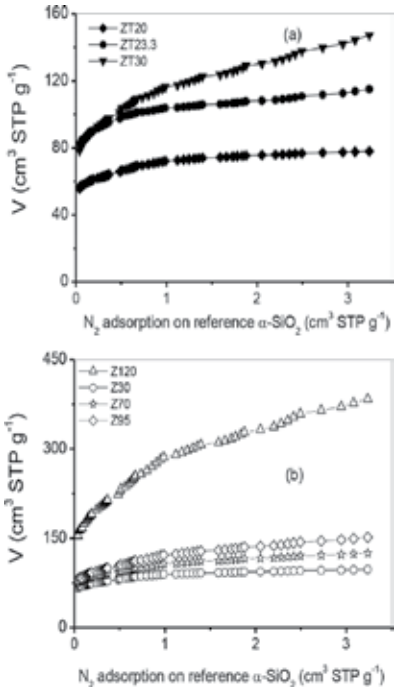

Figure 9. Comparative plots of the N_2 sorption isotherms versus adsorption using an α-SiO_2 reference.

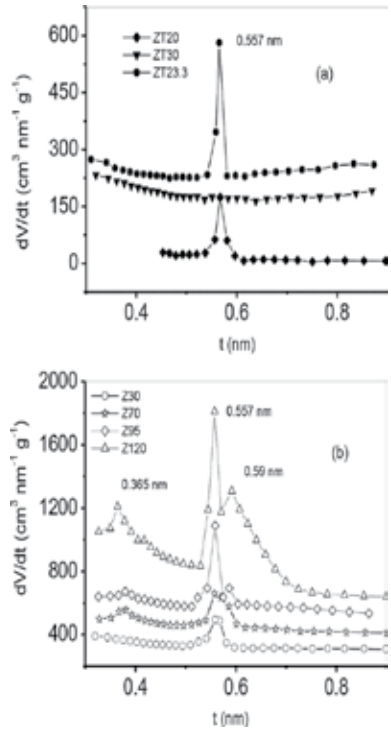

Figure 10. Micropore size distribution calculated from N_2 sorption isotherms using the DAC approach.

Sample	α_S	DAC	t	D-A	V_{meso}	E_0 (kJ mol^{-1})	n
ZT20	0.072	0.108	0.106	0.110	0.145	26.50	1
ZT23.3	0.102	0.131	0.147	0.165	0.288	20.50	1.3
ZT30	0.209	0.313	0.294	0.335	0.603	15.50	1.1
Z30	0.089	0.106	0.129	0.141	0.040	20.50	1.1
Z70	0.103	0.120	0.144	0.141	0.059	18.50	1
Z95	0.112	0.129	0.149	0.186	0.095	16	1
Z120	0.354	0.529	0.466	0.582	0.458	15.50	1

Table 3. Total micropore and mesopore volumes (W_0, V_{meso}, cm^3 g^{-1}) by various methods of analysis.

MR. **Table 3** lists the optimized W_0, n, and E_0 values using the D-A equation. The filling of elliptical channels of ZSM-5 with a length of 1.98 nm (width 0.51 × 0.57 nm) and connected through a zigzag path with a length of 0.665 nm (width 0.54) is the main contribution to the volume adsorbed. **Figure 11** shows ZSM-5 pore-size distributions obtained by the D-A method, assuming a cylindrical microporous channel; these plots provide average diameters very similar to the width of the porous cavities of the zeolites ZSM-5 (5th column of **Table 3**). The D-A results shown in **Table 2** suggest that MR in ZSM-5 zeolites promotes the opening and widening of their micropores. Nevertheless, the microporous volumes calculated from

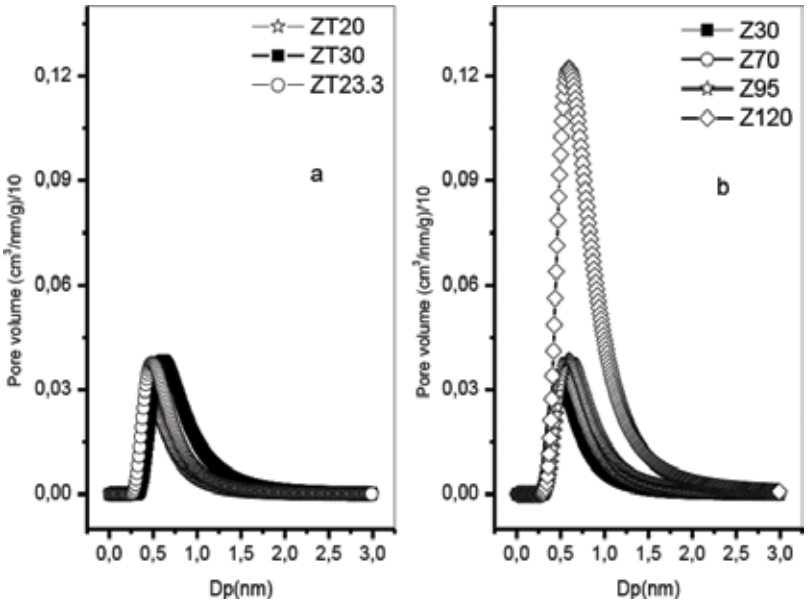

Figure 11. Micropore size distribution calculated from N_2 adsorption on the ZSM-5 zeolites through D-A approach.

the D-A equation are somewhat different from the microporous volumes calculated by the α_S and t methods. The fact that these D-A microporous volumes are always larger than the volumes calculated by the other methods suggests that the uptake at low relative pressures should be corrected for mesopore adsorption. This correction will result in a lower extrapolated value of the micropore volume from the D-A equation, and better agreement with other (α_S and t) methods will be reached. It can be seen there that the D-A treatment, while overestimating somehow the pore sizes, still provides an approximate estimate of the micropore volumes and their corresponding pore sizes. The E_0 values obtained by the D-A method decrease as MR increases: ZT20 > ZT23.3 > ZT30; Z30 > Z70 > Z95 > Z120 (**Table 2**). These values reflect

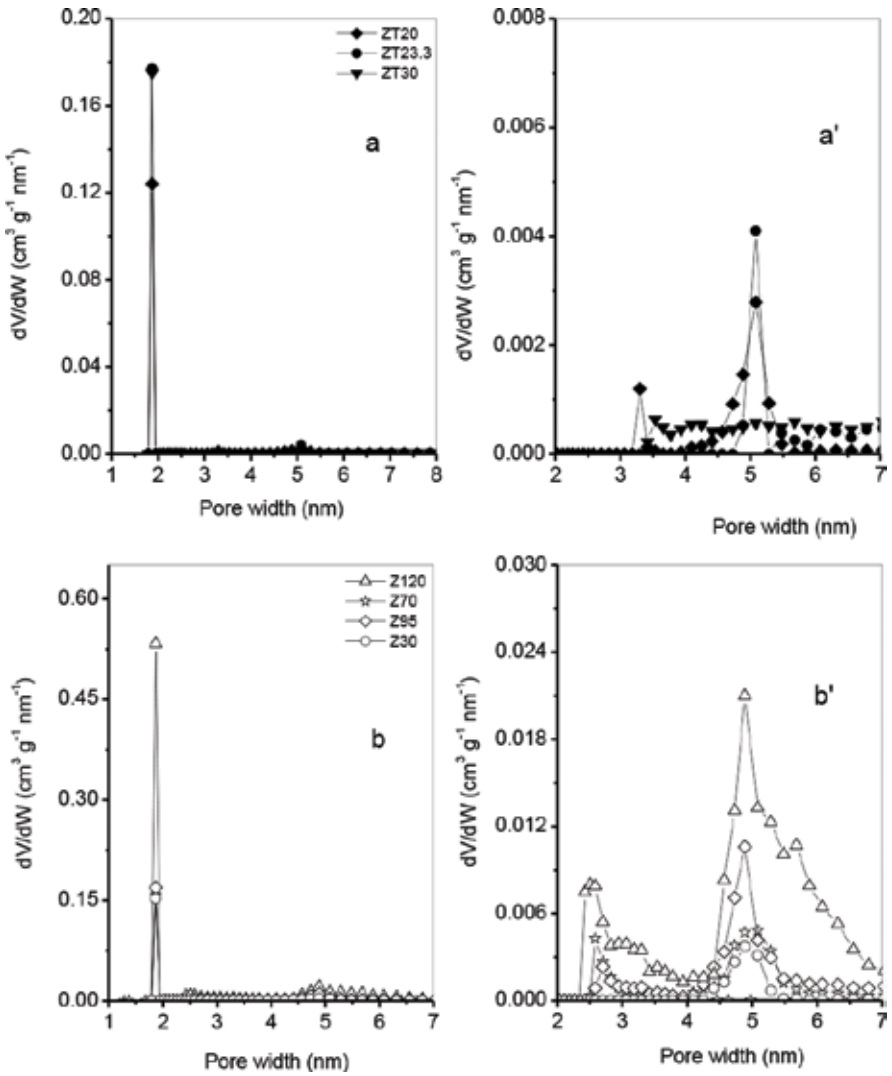

Figure 12. (a and b) NLDFT pore-size distribution showing the supermicropore region; (a′ and b′) close-up of the NLDFT pore-size distribution showing the supermicropore region on ZSM-5 zeolites.

Sample	DAC	D-A	NLDFT
ZT20	0.568	0.55	1.8/5.0
ZT23.3	—	0.57	1.8/5.0
ZT30	0.564	0.64	1.8
Z30	0.561	0.59	1.8/4.9
Z70	0.379/0.56	0.62	1.8/5.0
Z95	0.379/0.560	0.65	1.8/4.8
Z120	0.364/0.560/0.590	0.66	1.8/4.9

DAC is the differential curves of comparison plots method, D-A represents the Dubinin-Astakhov equation, and NLDFT is the nonlocal density functional approach.

Table 4. Pore diameter (nm) by different methods of analysis.

the dependence of this parameter on the SiO_2/Al_2O_3 ratio. Due to the crystalline nature of the zeolites, the force field created by the oxygen atoms in their structure must have symmetrical properties. Therefore, the E_0 values are affected by the aluminum content, which has changed some atoms of the zeolite framework in the channels to be displaced, as well as changing the sorption potential. From the comparison of the E_0 values obtained for these zeolites, this parameter is influenced not only by the pore sizes. Consequently, the Al content and the geometry of the pores have modified the electric field within the pores of the zeolites and thus have influenced the characteristic sorption energy.

3.3.3.3. Nonlocal density functional theory method

Nonlocal density functional theory (NLDFT) was developed to take into account pore sizes in voids of well-defined geometry [21]. With this approach, the molecules adsorbed in the pores tend to be packaged in accordance with the adhesion forces established with the substrate (i.e. attractive forces between adsorptive and adsorbent molecules) and interactions with the remaining fluid molecules. The molar density of the adsorbed phase varies as a function of pore size. The adsorption isotherm is calculated from a given pore shape (spherical, cylindrical, slit-like, etc.), and the experimental isotherm is given as the sum of a series of individual single-pore isotherms multiplied by their relative abundance over a range of pore sizes. In the present case, the microporous structure of ZSM-5 zeolite can be approximated as a bundle of parallel cylindrical pores and the nature of the adsorbent can be assumed as that of the silica. In this way, the distribution of supermicroporous zeolitic adsorbents can be calculated from high-resolution adsorption isotherms. The results of the analysis of the size of the supermicropores using the NLDFT method are shown in **Figure 12** and are listed in **Table 4**. The pore-size distributions obtained from the N_2 isotherms using the NLDFT cylindrical pore model yield bimodal distributions with pore size characteristics of 1.8 and 5.0 nm. It is observed from this figure

that the intensity of the distribution at 5.0 nm is poorly developed; however, it is represented in all distributions. A possible explanation is that the structures are not homogeneous and that it contains a significant amount of slit-like pores and pores of other irregular shapes. Based on the NLDFT method, one can get an idea about the actual widths and pore sizes of the supermicropore voids existing in ZSM-5 zeolites for which high-resolution N_2 isotherms are available.

α_S is Sing's α_S method, DAC is direct comparison plots, t is the t-plot employing the de Boer adsorption equation, D-A represents the Dubinin-Astakhov equation, V_{meso} is calculated by subtracting $W_{0\alpha S}$ from V_Σ (**Table 2**), E_0 is the characteristic energy of sorption, and n is the order of the sorption energy distribution from the Dubinin-Astakhov equation.

4. Conclusions

The obtained samples exhibit reasonable diffraction patterns, indicative of good crystallinity. The most important difference between the standard XRD pattern and those observed for both sets of samples is the relative intensity of the various peaks. The ZSM-5 samples synthesized are composed of crystals with different geometry in a range of sizes 5–10 μm. N_2 isotherms have been measured, starting at a relative pressure of 10^{-5} and up to 1. To evaluate the texture properties of ZSM-5 zeolites, BET, Langmuir, Ast, surface areas, and external surface area were used. A significant amount of micropores was found in all ZSM-5 zeolites. Such methods as α_S, t, and comparative plots (DAC) were used to estimate micropores in all zeolites. Nanopore size distributions (NSD) obtained from the N_2 adsorption at 77 K are in perfect agreement with the type of present pores for all the samples, that is, micropores, mesopores, and macropores. Thus, adsorption is probably the most sensitive tool for evaluating quality and structural properties of the microporous materials such as ZSM-5 zeolites. To characterize these nanomaterials, a combination of comparative methods based on reference isotherms on well-characterized ZSM-5 zeolites is recommended, as well as the results of DAC, D-A, and the NLDFT.

Acknowledgements

This work was partially supported by DGAPA-UNAM IN107817 Grant, VIEP, and the Academic Body "Investigación en zeolitas," CA-95 (PROMEP-SEP).

Conflicts of interest

The authors declare no conflict of interest.

Author details

Miguel Angel Hernández[1]*, A. Abbaspourrad[2], Vitalli Petranovskii[3], Fernando Rojas[4], Roberto Portillo[5], Martha Alicia Salgado[5], Gabriela Hernández[6], Maria de los Angeles Velazco[7], Edgar Ayala[7] and Karla Fabiola Quiroz[8]

*Address all correspondence to: vaga1957@gmail.com

1 Zeolites Research Department, Autonomous University of Puebla, Puebla, Mexico

2 Azad University of Shahryar-Shahre Ghods, Shahre Ghods, Tehran, Iran

3 Center for Nanoscience and Nanotechnology, National Autonomous University of Mexico, Ensenada, Mexico

4 Department of Chemistry, Autonomous Metropolitan University, Mexico City, Mexico

5 Faculty of Chemistry, Autonomous University of Puebla, Puebla, Mexico

6 Department of Chemical Engineering, Autonomous Metropolitan University, Mexico City, Mexico

7 Faculty of Chemical Engineering, Autonomous University of Puebla, Puebla, Mexico

8 Interdisciplinary Professional Unit of Biotechnology of the National Polytechnic Institute, Mexico City, Mexico

References

[1] MML RC, Russo PA, Carvalhal C, PJM C, Marques P, Lopes JM, Gener I, Guisnet M, Ribeiro FR. Adsorption of n-pentane and iso-octane for the evaluation of the porosity of dealuminated BEA zeolites. Microporous and Mesoporous Materials. 2005;**81**:259-267

[2] Kortunov P, Vasenkov S, Chmelik C, Karger J, Ruthven DM, Wloch J. Influence of defects on the external crystal surface on molecular uptake into MFI-type zeolites. Chemistry of Materials. 2004;**16**:3552-3558. DOI: 10.1021/cm0401645

[3] Remy MJ, Poncelet G. A new approach to the determination of the external surface and micropore volume of zeolites from the nitrogen adsorption isotherm at 77 K. The Journal of Physical Chemistry. 1995;**99**:773-779. DOI: 10.1021/j100002a047

[4] Rouquerol F, Rouquerol J, KSW S, Llewelyn P, Maurin G. Adsorption by Powders and Porous Solids. third ed. Amsterdam, The Netherlands: Academic Press; 2014. p. 495

[5] Matsumoto A, Zhao J, Tsutsumi K. Adsorption behavior of hydrocarbons on slit-shaped micropores. Langmuir. 1997;**1997**(13):496-501. DOI: 10.1021/10.1021/la950958l

[6] Sivasankar N, Vasudevan S. Adsorption of n-hexane in zeolite-5A: A temperature-programmed desorption and IR-spectroscopic study. The Journal of Physical Chemistry B. 2005;**109**:15417-15421. DOI: 10.1021/10.1021/jp0518714

[7] Cho HS, Miyasaka K, Kim H, Kubota Y, Takata M, Kitagawa S, Ryoo R, Terasaki O. Study of argon gas adsorption in ordered mesoporous MFI zeolite framework. Journal of Physical Chemistry C. 2012;**116**:25300-25308

[8] Ch B, Meier WM, Olson DH. Atlas of Zeolite Framework Types. 5th revised ed. Amsterdam, Netherlands: Elsevier; 2001. p. 213

[9] Sing KSW. The use of physisorption for pore structural characterization. In: Haynes JM, Rossi-Doria P, editors. Principles and Applications of Pore Structural Characterization. Bristol: Arrowsmith; 1985. pp. 1-11

[10] Lu X, Jaroniec M, Madey R. Use of adsorption isotherms of light normal alkanes for characterizing microporous activated carbons. Langmuir. 1991;**7**:173-177. DOI: 10.1021/acs.jced.6b01068

[11] Ghiaci M, Abbaspourad A, Arshadi M, Aghabarari B. Internal versus external surface active sites in ZSM-5 zeolite. Part 2: Toluene alkylation with methanol and 2-propanol catalyzed by modified and unmodified H_3PO_4/ZSM-5. Applied Catalysis A: General. 2006;**316**:32-46. DOI: 10.1016/j.apcata.2005.09.015

[12] Kawase R, Iida A, Kubota Y, Komura K, Sugi Y, Oyama K, Itoh H. Hydrothermal synthesis of calcium and boron containing MFI-type zeolites by using organic amine as structure directing agent. Industrial and Engineering Chemistry Research. 2007;**46**:1091-1098. DOI: 10.1021/ie060624z

[13] Sang S, Chang F, Liu Z, He C, He Y, Xu L. Difference of ZSM-5 zeolites synthesized with various templates. Catalysis Today. 2004;**93**:729-735. DOI: 10.1016/1.4943324

[14] Thommes M, Kaneko K, Neimark AV, Olivier JP, Rodriguez-Reinoso F, Rouquerol J, Sing KSW. Physisorption of gases, with special reference to the evaluation of surface area and pore size distribution (IUPAC technical report). Pure and Applied Chemistry. 2015;**87**:1051-1069. DOI: 10.1515/pac-2014-1117

[15] Hudec P, Smieskova P, Zidek Z, Schneider P, Solcova O. Determination of microporous structure of zeolites by t-plot method. State of the art. In: Aiello R, Giordano G, Testa F, editors. Studies in Surface Science and Catalysis. Vol. 142. Amsterdam, The Netherlands: Elsevier; 2002. pp. 1587-1602. DOI: 10.1021/la049817

[16] Hernández MA, Rojas F, Portillo R, Petranovskii V, Salgado MA. Influence of the Si/Al framework ratio on the microporosity of dealuminated mordenite as determined from N_2 adsorption. Separation Science and Technology. 2006;**41**:1907-1925. DOI: 10.1080/01496390600674901

[17] Sing KSW. Physisorption of nitrogen by porous materials. Journal of Porous Materials. 1995;**2**:5-8. DOI: 10.1007/BF00486564

[18] Sing KSW. Characterization of porous materials: Past, present and future. Colloids and Surfaces A: Physicochemical and Engineering Aspects. 2004;**241**:3-7. DOI: 10.1260/0144-5987.31.3.337

[19] Zhu HY, Lu GQ, Cool P, Vansant EF, Su BL, Gao X. Quantitative information on pore size distribution from the tangents of comparison plots. Langmuir. 2004;**20**:10115-10122. DOI: 10.1021/ja01145a126

[20] Stoeckli F, Lavanchy A, Hugi-Cleary D. Dubinin's theory: A versatile tool in adsorption science. In: Meunier FA, editor. Fundamentals of Adsorption VI. Amsterdam, The Netherlands: Elsevier; 1998. pp. 75-80. oai:doc.rero.ch:20080509175439-GP

[21] Astala R, Auerbach SM, Monson PA, Density Functional PA. Theory study of silica zeolite structures: Stabilities and mechanical properties of SOD, LTA, CHA, MOR, and MFI. The Journal of Physical Chemistry. B. 2004;**108**:9208-9215. DOI: 10.1021//jp0493733

Section 3

Zeolites Applications

Chapter 6

Use of Synthetic and Natural Zeolites Tailored for As(V) Sorption

Andrey E. Krauklis

Additional information is available at the end of the chapter

http://dx.doi.org/10.5772/intechopen.72614

Abstract

Arsenic in drinking water poses serious potential health risks in more than 30 countries with total affected population of around 100 million people. Natural and synthetic zeolites can be tailored in order to obtain improved sorption of As(V) making them a relatively cheap and efficient material for water remediation. The chapter is concentrated on the zeolitic materials for water remediation, and reports new findings regarding modification methods and comparison of such materials for the use in As(V) sorption applications. Methods of modification of zeolites are developed and explained. On the experimental and novel scale, using developed methods, 11 novel materials are synthesized and studied. Initial and modified materials are characterized by optical microscopy, SEM and EDX, as well as by metal content in those which are determined using dissolution in acids and FAAS.

Keywords: zeolites, water remediation, As(V), adsorption, sorbents, arsenic, environmental remediation, equilibrium, kinetics, heavy metals, metalloids

1. Introduction

Groundwater contamination with arsenic compounds is an everyday problem for millions of people as water resources are crucial for use as drinking water, as well as in food production and agriculture [1–3]. Accumulation of arsenic in the body poses significant health risks and may lead to arsenicosis [3]. USA Environmental Protection Agency (EPA) in 2006 has diminished acceptable maximum contaminant level (MCL) for arsenic in drinking water from 50 down to 10 μg/L, and stricter norms have been set in headquarters of Peoples Republic of China, United Nations Health Organization, and European Union [4–6]. Arsenic contamination is both natural and due to anthropogenic sources. Weathering of rocks and minerals is a typical example of a natural process, while pesticides, metal waste, fertilizers and fossil fuel combustion are due to industrial and agricultural activities [7–9].

IntechOpen

© 2018 The Author(s). Licensee IntechOpen. This chapter is distributed under the terms of the Creative Commons Attribution License (http://creativecommons.org/licenses/by/3.0), which permits unrestricted use, distribution, and reproduction in any medium, provided the original work is properly cited.

Sorption is considered as one of the most reasonable water remediation techniques because of its lower costs [10–13]. Zeolites are crystalline, microporous, hydrated aluminosilicate minerals containing alkali or alkaline cations. These materials are often praised for their efficient sorptive properties. Zeolite surface modification is a possible route for substantially improving oxyanion sorption [12]. Zeolites generally possess high values of specific surface area, which can be larger than 700 m^2/g [14]. This parameter is an extremely important one for adsorptive properties. Most of zeolitic water remediation technologies are based on cation exchange principles; however, there are cases when zeolites are used and useful for anion removal, such as cases of arsenate and arsenite sorption [15, 16]. Advantages of zeolitic sorbents are as follows: Generally, they are environmentally friendly, relatively cheap and can be treated for secondary use. Considering affinity of metalloids to interact with Fe and Mn-containing compounds [17], studies of As(V) sorption can be promoted in direction of using iron- and manganese-modified zeolites.

1.1. Clinoptilolite

Clinoptilolite is a high silicate content heulandite group mineral $(Na,K,Ca_{0.5},Sr_{0.5},Ba_{0.5},Mg_{0.5})_6$ $[Al_6Si_{30}O_{72}]$ $20H_2O$ – HEU, often main component of natural zeolites. Its effective pore diameter is in range from about 4.5 up to 6.0 Å. Such clinoptilolite's properties as chemical stability in basic environments, thermostability and high sorption rate make it a useful material in chemical research and industry [15].

1.2. Zeolite A

Zeolite A is one of the most widely used synthetic zeolites. It has a Linde Type A (LTA) structural type as defined by International Zeolite Association (IZA). Most commonly used in its sodium form (4A), its chemical formula in dehydrated form is $[Na_{12}Al_{12}Si_{12}O_{48}]_8$ [18]. Potassium (3A) and calcium (5A) forms are also widely used. These zeolite names roughly represent pore opening diameters in ångstrøms (Å). It is possible to convert one form into another one via ion exchange [18].

1.3. Zeolite X

Zeolites X contain 12 rings or pore openings with a diameter of 7.4 Å (8.1 Å when completely empty). Diameter of the central cavity is 13.7 Å [19].

1.4. Iron oxides

Iron oxides and hydroxides are known for their use in wastewater treatment [20]. Natural iron oxides (without using zeolites as the host material) have affinity for arsenic compounds but show low sorption efficiency of treating aqueous solutions contaminated with As compounds (0.02–0.4 mg/g) due to low specific surface area [5, 21–23]. Thus it is important to introduce a host material with high specific surface area, i.e. zeolite, which can be modified with iron compounds, such as FeOOH. Fe(III) ionic radius is 0.67 Å [24], small enough in order to use it for modification of zeolites.

1.5. Manganese oxides

As(V) is sorbed more easily onto solid surfaces than As(III), and thus oxidation of As(III) followed by adsorption is a potentially effective route for the removal of arsenic compounds [25, 26]. It has been reported that clinoptilolite modification with MnO_2 significantly enhances sorption capacity of As(V) and is believed to be independent of pH [27]. MnO_2 can oxidize As (III) to As(V) based on sources [24, 28], which is backed up with the following red-ox reactions, shown in Eqs. 1 and 2:

$$HAsO_2 + 2H_2O \leftrightarrow H_3AsO_4 + 2H^+ + 2e^- \quad \left(\varphi^\circ = -0.56\ \mathrm{e}\right) \tag{1}$$

$$MnO_2 + 4H^+ + 2e^- \leftrightarrow Mn^{2+} + 2H_2O \quad \left(\varphi^\circ = +1.23\ \mathrm{e}\right) \tag{2}$$

The summary red-ox reaction is represented by Eq. 3:

$$HAsO_2 + MnO_2 + 2H^+ \leftrightarrow H_3AsO_4 + Mn^{2+} \quad \left(\varphi^\circ = +0.67\ \mathrm{e}\right) \tag{3}$$

The value of standard potential (ϕ° = +0.67 e) is positive, which indicates that equilibrium is shifted towards right of Eq. 3, in direction of As(V) as a product [24].

Mn(II), Mn(IV) and Mn(VII) ionic radii are 0.80–0.91 Å, 0.50–0.52 Å and 0.46 Å, respectively [24]. Mn-O bond in a permanganate ion is 1.629 Å, and Mn is in the tetrahedron's centre [29]. This is small enough in order to use it for modification of zeolites.

1.6. Sorption models

Langmuir and Freundlich isotherms are the most popular models in describing sorption in water environments; however, other models are also known and widely used such as Dubinin–Radushkevich, Temkin and Redlich–Peterson models [18, 30].

1.7. Langmuir model

The model is based on assumption that each sorption active centre is equivalent, and it is energetically irrelevant whether adjacent sorption centres are empty or already occupied [20]. Langmuir sorption model [31]:

$$q_e = \frac{q_m K_L C_e}{1 + K_L C_e}, \tag{4}$$

where q_e [mg/g] is equilibrium concentration in adsorbent which corresponds to initial concentration in solution C_0 [mg/L]; q_m [mg/g] is maximum monolayer coverage capacity; C_e [mg/L] is equilibrium concentration in solution; K_L [L/mg] is Langmuir constant.

Linearized form of Eq. 4 is represented with Eq. 5:

$$\frac{C_e}{q_e} = \frac{1}{q_m} C_e + \frac{1}{q_m K_L} \tag{5}$$

In order to compare experimental data's fit with the model, linearized form is used, plotting data in coordinates $\frac{C_e}{q_e}$ – C_e and obtaining determination coefficient R^2 [30].

1.8. Freundlich model

Freundlich model is based on assumption that sorption occurs on nonequivalent sorption centres, which is due to repulsion between the sorbed particles. It is assumed there is an infinite number of sorption centres [20]. Freundlich sorption model [32]:

$$q_e = K_F C_e^{\frac{1}{n}}, \tag{6}$$

where K_F [$mg^{1-1/n} \cdot L^{1/n}/g$] is Freundlich coefficient; n [−] is Freundlich constant.

Linearized form of Eq. 6 is represented with Eq. 7 [30]:

$$\ln q_e = \ln K_F + \frac{1}{n} \ln C_e \tag{7}$$

In order to compare experimental data's fit with the model, linearized form is used, plotting data in coordinates $\ln q_e$ – $\ln C_e$ and obtaining determination coefficient R^2 [30].

1.9. Dubinin-Radushkevich model

Usually the model is used to differentiate between physisorption and chemisorption. Initially it was used to describe physisorption. Dubinin-Radushkevich sorption model [33]:

$$q_e = q_s e^{\left(-K_{DR}\varepsilon_{DR}^2\right)} \tag{8}$$

$$\varepsilon_{DR} = RTln\left(1 + \frac{1}{C_e}\right) \tag{9}$$

$$E = \frac{1}{\sqrt{2K_{DR}}}, \tag{10}$$

where ε_{DR} [kJ/mol] is Dubinin–Radushkevich isotherm variable; E [kJ/mol] is mean free energy of adsorption; q_s [mg/g] is theoretical Dubinin–Radushkevich saturation sorption capacity; K_{DR} [mol^2/kJ^2] is Dubinin–Radushkevich constant.

Linearized form of Eq. 8 is represented with Eq. 11 [30]:

$$\ln q_e = \ln q_s - K_{DR}\varepsilon_{DR}^2 \tag{11}$$

In order to compare experimental data's fit with the model, linearized form is used, plotting data in coordinates $\ln q_e$ – ε_{DR}^2 and obtaining determination coefficient R^2 [30].

1.10. Temkin model

The model is based on assumption that heat of adsorption (function of temperature) decreases linearly with increasing amount of sorbed particles. Temkin sorption model [33]:

$$q_e = \frac{RT}{b_T} \ln K_T C_e, \tag{12}$$

where R [8.314 J/(mol·K)] is universal gas constant; T [K] is temperature; K_T [mg/L] and $b_T \left[\frac{J \cdot g}{mol \cdot L}\right]$ are parameters describing adsorbate-adsorbent interactions.

Linearized form of Eq. 12 is represented with Eq. 13 [30]:

$$q_e = \frac{RT}{b_T} \ln K_T + \frac{RT}{b_T} \ln C_e \tag{13}$$

In order to compare experimental data's fit with the model, linearized form is used, plotting data in coordinates q_e – lnC_e and obtaining determination coefficient R^2 [30].

1.11. Redlich-Peterson model

The model is a hybrid between Langmuir and Freundlich models. When value of coefficient β_{RP} is equal to 1, the model becomes equivalent with Langmuir model. Often this three-parameter model is able to explain experimental data more precisely. Redlich–Peterson sorption model [34]:

$$q_e = \frac{K_{RP} C_e}{1 + \alpha_{RP} C_e^{\beta_{RP}}}, \tag{14}$$

where $\alpha_{RP} \left[\left(\frac{L}{mg}\right)^{\frac{1}{\beta_{RP}}}\right]$, β_{RP} [−] and K_{RP} [L/g] are Redlich–Peterson isotherm parameters.

Linearized form of Eq. 14 is represented with Eq. 15 [30, 34]:

$$\ln\left(K_{RP} \frac{C_e}{q_e} - 1\right) = \beta_{RP} \ln C_e + \ln \alpha_{RP} \tag{15}$$

K_{RP} is optimized by finding the closest fit to the model via the highest determination coefficient. In order to compare experimental data's fit with the model, linearized form is used, plotting data in coordinates $\ln\left(K_{RP} \frac{C_e}{q_e} - 1\right)$ – $\ln C_e$ and obtaining determination coefficient R^2 [30, 34].

1.12. Purpose and aim of this work

The purpose of this work is to present zeolites as potential sorbents for As(V) sorption for water remediation as well as to present novel modification methods and materials. The aim of the study is to provide and interpret results of As(V) sorption onto raw and modified zeolites.

2. Materials

2.1. Slovakian natural clinoptilolite (Slov)

Clinoptilolite natural zeolite from Slovakian deposit Nižný Hrabovec was used. Its specific weight is 2200–2440 kg/m^3; porosity 24–32%; clinoptilolitic content fluctuates in range from 86

to 94%; according to manufacturer, it also contains cristobalite, clay mica, plagioclase, rutile, quartz; Si:Al ratio is in range 4.80–5.40; fraction of 1–2.5 mm was used [35].

2.2. Ukrainian natural clinoptilolite (Ukr)

Clinoptilolite natural zeolite from Ukrainian Zakarpattian deposit Sokirnicke (ukr. Сокирницьке родовище). Specific weight 2370 kg/m^3; porosity 44%; clinoptilolitic content 77%; fraction 1–3 mm [36].

2.3. Russian natural clinoptilolite (Khol)

Clinoptilolite natural zeolite from Russian Zabaykalsky Krai deposit Kholinskoe (rus. Холинское месторождение). Specific weight 1900–2800 kg/m^3, bulk density 1.02–1.20 g/cm^3. Porosity is in range of 20–23% [37]. Zeolite was crushed and sieved using vibro sieve FRITSCH analysette 3 SPARTAN (Germany; International), collecting fraction from 0.8 up to 1.4 mm.

2.4. Synthetic zeolite A (4A)

SYLOSIV A 4 was used (purchased from Grace Davison, USA), zeolite 4A in fine powder form (particle size 6–9 μm). According to manufacturer, this material is chemically stable in basic, neutral and weak acidic environments; specific surface area 800 m^2/g; effective pore volume 0.25–0.30 cm^3/g; specific weight 1900–2300 kg/m^3 [38].

2.5. Synthetic zeolite X (13X)

Zeolite 13X was used (purchased from Hong Kong Chemical Corp.). Bulk density 0.601 g/cm^3; porosity 0.55%; fraction 4–5 mm.

2.6. Reagents

All compounds used were of analytical grade (≥ 98%) and were used without further purification. Sodium hydroxide, potassium chloride and 65% nitric acid were obtained from Sigma-Aldrich (Riedel-de Haën, Germany). Iron(III) chloride hexahydrate, calcium chloride dihydrate and 30% hydrogen peroxide were obtained from Enola (Riga, Latvia). Manganese(II) chloride tetrahydrate was obtained from Firma Chempur (Piekary Śląskie, Poland). All aqueous solutions were prepared using high purity deionized water (10–15 MΩ·cm), produced via water purification system Millipore Elix 3 (Billerica, USA). Arsenate stock solution was prepared using disodium hydrogenarsenate heptahydrate $Na_2HAsO_4{\cdot}7H_2O$ obtained from Alfa Aesar (Haverhill, USA).

3. Zeolite modification methods

Zeolites Ukr, Slov, Khol, 4A and 13X were modified using 6 different methods. Altogether, using these methods, 11 novel materials were synthesized and are described in this chapter. Additionally, FeOOH-modified zeolites A were obtained and described in the following source [17]. It should be also noted that another aluminosilicate, clay montmorillonite was modified using a similar approach and described in another work [39].

3.1. First method

First method is based on the method described in source [40]. The basis for FeOOH-modified sorbent synthesis is the iron oxohydroxide precipitation on the raw material. Description of modification is the following: 0.25 mol $FeCl_3 \cdot 6H_2O$ is dissolved in 250 mL DI water, adding 250 mL 3 M NaOH solution and aged for 3 h. Obtained $Fe(OH)_3$ precipitates are decanted. 100 g of raw material are mixed in the $Fe(OH)_3$ dispersion. The mixture is then carefully mixed and filtered under vacuum and washed with 250 mL DI water. The filtered and washed material is then dried in air atmosphere for 1 h at room temperature and then dried in the oven Gallenkamp Plus II (London, UK) for 4 h at 60°C.

Materials obtained using this method: Fe-Ukr(1); Fe-Slov.

3.2. Second method

Second method is based on the first method, modified based on the idea that the material is first soaked with a respective metal salt, followed by the reaction (FeOOH synthesis) inside the zeolite structure. The developed method is the following: 1 M $FeCl_3 \cdot 6H_2O$ solution is prepared and 100 g of zeolite are placed into it. The mixture is aged for 24 h. The mixture is then filtered, and without washing, 250 mL of 3 M NaOH solution are added to the soaked material and aged for 24 h. The mixture is filtered under vacuum and washed with 250 mL DI water. The filtered and washed material is dried in air atmosphere for 1 h at room temperature and subsequently dried in the oven Gallenkamp Plus II (London, UK) for 4 h at 60°C.

Materials obtained using this method: Fe-Ukr(2); Fe-13X; Fe-KHol.

3.3. Third method

Third method is based on the first method, adapted to be applicable for efficient modification of powders (as in case of Fe-4A and Fe-5A described in another work [17]). The idea is to conduct a reaction in the wet FeOOH mass, simplifying and accelerating modification process. The developed method is the following: 0.25 mol $FeCl_3 \cdot 6H_2O$ is dissolved in 250 mL DI water, 250 mL of 3 M NaOH is added and the mixture is aged for at least 3 h. Synthesized $Fe(OH)_3$ precipitates are decanted. The mass is filtered under vacuum, mixing in 100 g of raw material into the $Fe(OH)_3$ precipitates, while carefully mixing. Porridge-consistency mixture is washed with 250 mL DI water. The filtered and washed material is then dried in air atmosphere for 2 h at room temperature, and further dried in the oven Gallenkamp Plus II (London, UK) for 4 h at 110°C.

Materials obtained using this method: Fe-Ukr(3); in combination with other methods, FeMn-Slov with fourth method.

3.4. Fourth method

Fourth method is based on methods described in sources [27, 41] which are natural zeolite modification methods with manganese oxides. Concentrations used are the same as described in source [27]. 100 g of zeolite is weighted in the beaker and dried in air atmosphere from initial moisture in air atmosphere in the oven for 1 h at 70°C. 2.5 M $MnCl_2$ solution and 10 M NaOH solution are prepared. 100 mL of prepared 2.5 M $MnCl_2$ solution is added, while

mixing, to the zeolite in the beaker. 1 mL of prepared 10 M NaOH solution is added and mixed. Solution is aged for 24 h. Without filtering, the mixture is placed in the oven for 3 h at 150°C. The result is densified zeolite granule/pellet mass, covered with precipitates. This mass is then placed into the crucibles. Crucibles with the obtained mass are placed in the muffle furnace and are held there for 5 h in air atmosphere at 550°C. Crucibles are then taken out and cooled down in air at room temperature. After cooling, modified zeolite is washed with 300 mL of DI water. Material is dried in air for 1 h at room temperature, and further dried in the oven Gallenkamp Plus II (London, UK) for 4 h at 60°C.

Materials obtained using this method: Mn-Slov(1); in combination with other methods, FeMn-Slov with third method, CaMn-Slov with sixth method.

3.5. Fifth method

Fifth method is based on fourth method, but, while fourth method is rooted in Mn(II) oxidation at elevated temperature, this method is based on Mn(VII) reduction reaction using ethanol. The reaction as represented by Eq. 16 is conducted at room temperature [42]:

$$2KMnO_4 + 3C_2H_5OH \rightarrow 2MnO_2 + 3CH_3CHO + 2KOH + 2H_2O \tag{16}$$

This modification method is developed and chosen in order to perform modification of zeolites with MnO_2 in softer conditions at room temperature. Concentration and volume of potassium permanganate solution is chosen based on $KMnO_4$ solubility in water at room temperature (if limited by) and in order to introduce the same amount of Mn atoms as in fourth method (0.25 mol Mn). The amount of ethanol is chosen such so that C_2H_5OH and $KMnO_4$ are in molar ratio 1:1 (stoichiometrically). 100 g of zeolite is weighted in the beaker. Then, 1.5 L 0.17 M $KMnO_4$ solution is prepared and added into the beaker with the zeolite. The aging proceeds for 96 h in the solution. Then, 24.3 mL 60% C_2H_5OH is added to the mixture in order to reduce $KMnO_4$. Acetaldehyde is obtained and characteristic smell can be felt. Modified zeolite is filtered under vacuum and washed with 300 mL DI water. Material is then dried in air atmosphere at room temperature for 1 h, and further dried in the oven Gallenkamp Plus II (London, UK) for 4 h at 60°C.

Materials obtained using this method: Mn-Slov(2), Mn-4A.

3.6. Sixth method

The sixth method is a Ca^{2+} ion-exchange reaction used in combination with previously described methods. It is based on a principle that one can tailor the effective micropore diameter in zeolites by exchanging the cations. Divalent Ca^{2+} cations are used to increase the effective pore opening [18]. 20 g of zeolite are placed in 100 mL glass vessels. 4.5 M $CaCl_2$ solution is prepared and 50 mL is added to the material. The vessels are then placed on the orbital shaker Biosan Multi-functional Orbital Shaker PSU-20i (Riga Latvia), setting frequency to 150 rpm for 96 h. The mass is decanted and then washed with 100 mL DI water. Afterward, the material is dried for 2 h at room temperature in air atmosphere, and then subsequently dried at 110°C in the oven for 4 h.

Materials obtained using this method: in combination with other methods, CaMn-Slov with fourth method.

4. Material characterization

Modified and raw zeolites were characterized using optical microscopy, scanning electron microscopy (SEM), energy-dispersive X-ray spectroscopy (EDX, EDS), by analysis of Fe and Mn content, which was performed by dissolution in acids followed by flame atomic absorption spectrometry (FAAS). Bulk density of all sorbents was determined.

4.1. Optical microscopy

Optical microscopy allows to study the surface of the material and to evaluate homogeneity. Optical microscope Leica was used with a digital camera Leica DFC480, ocular Leica 10X/21B, which enables magnification from x7.1 up to x115. Additional lighting was used: Leica Fluorescent Ringlight and Leica CLS150X (Germany; International) [43]. Software used for obtaining images was Leica Application Suite v4.1.0. A square of 1 cm was cut out of millimetre paper, which was placed adjacent to the sample as a scale. In order to obtain qualitative images, 11 micrographs were used on average using focus stacking (pyramid) approach. Software used for stacking was Helicon Focus (Kharkiv, Ukraine).

4.2. SEM and EDX

Materials were covered with a thin layer of gold in order to prevent charging due to electron beam. Gold sputtering was performed using Quorum Technologies Emitech K550X (Laughton, UK). Methods were performed using Tescan Mira/LMU (Brno, Czech Republic) in backscattered electron regime with working voltage of 15 kV.

4.3. FAAS

Fe and Mn content was obtained using dissolution in acids followed by flame atomic absorption spectrometry (FAAS). 1 g of each material was weighed in a beaker, using analytical scales (± 0.1 mg). 25 mL 65% HNO_3 and 5 mL 35% H_2O_2 were then added in each beaker. Beakers were placed in a thermostat Biosan MyLab Thermo-Block TDB 400 (Riga, Latvia) and heated up to 160°C. When half of the solution had evaporated, 25 ml 65% HNO_3 was added while heating the sample. The solutions were allowed to cool down in air at room temperature, filtered into a graduated vessel and diluted with DI water to a total volume of 60 mL each. Furthermore, a blank sample was prepared for background correction. 10 mL of each solution were moved in test tubes, using pipettes. Prepared samples were analysed using PerkinElmer AAnalyst 200 (Waltham, USA) with flame atomization. Mn and Fe content measurements were performed using background correction in air–acetylene flame. Fe and Mn content in samples was calculated using Eqs. 17 and 18:

$$w_{Fe} = C_{Fe} \cdot \frac{V}{m} \tag{17}$$

$$w_{Mn} = C_{Mn} \cdot \frac{V}{m}, \tag{18}$$

where w_{Fe} and w_{Mn} are Fe and Mn mass fractions in materials, respectively [mas%]; C_{Fe} and C_{Mn} are Fe and Mn ion concentartions in solution, respectively [mg/L]; V is volume of the solution (0.060 L) [L]; m is mass of sorbent (1000 mg) [mg].

4.4. Determination of bulk density

The method of bulk density determination is based on a standard method, which is described in literature [44–46]. An empty 250 mL graduated cylinder was weighted, using analytical scales Kern ALJ 220–4 (± 0.1 mg). Approximately, 100 g of powder or granules/pellets were placed in the graduated cylinder, while determining the total mass of material and the cylinder. Deducing cylinder's mass from the total, the mass of the material was obtained. The cylinder was gently hit on the flat surface until the material became compacted and the change in volume was not observable. The volume of the material was determined using the closest mark on the graduated cylinder. The bulk density was determined as the ratio of obtained mass and volume.

5. Sorption experiments

Sorption experiments were conducted using batch system. $Na_2HAsO_4{\cdot}7H_2O$ was used for preparing arsenic stock solutions at various concentrations (300, 200, 100, 50, 25, 10 and 5 mg/L). 0.5000 ± 0.0001 g of each sorbent was weighed in every 100 mL glass vessel using analytical scales Kern ALJ 220–4 (Balingen, Germany). 30.00 ± 0.05 mL of an As(V) solution was then added to every vessel with the adsorbent. Vessels were then shaken for 24 h at room temperature (23 ± 1°C) at 150 rpm using orbital shaker Biosan Multi-functional Orbital Shaker PSU-20i (Riga, Latvia) to ensure sorption equilibrium was achieved. Suspensions were filtered into 50 mL test tubes, and concentration of As(V) in the filtrate was then analysed using PerkinElmer AAnalyst 200 with flame atomization. Absorption was measured using background correction in N_2O-C_2H_2 flame. A spectral line of 193.7 nm was used. FAAS spectrometer was calibrated with 1000 mg As/L standard solutions obtained from Scharlau (Barcelona, Spain) (As_2O_3 in 0.5 M HNO_3). Each measurement was performed 3 times. In order to ensure arsenic analysis quality control, experiments were performed systematically; accurate As(V) concentration of respective stock solutions was measured 3 times and standard deviation was determined, which then was taken into account when describing sorption capacity of the materials.

6. Experimental results

6.1. Homogeneity and bulk density

Homogeneity of materials was evaluated using optical microscope. All studied materials were homogeneous except Fe-Ukr(1), Fe-Ukr(2), Fe-Ukr(3) and Fe-Slov. Due to inhomogeneities, these materials were not further analysed with SEM and EDX. Obtained information about bulk density and homogeneity is summarized in **Table 1**.

6.2. Metal ion content

Fe and Mn content by weight in all materials is summarized in **Table 2** as an average of three repeated measurements with standard deviation. Material with highest Fe content is FeMn-Slov

Material	Bulk density ($\frac{g}{mL}$)	Form	Homogeneity
4A	0.46 ± 0.02	Powder	Homogeneous
Mn-4A	0.77 ± 0.03	Powder	Homogeneous
13X	0.75 ± 0.03	Granules/Pellets	Homogeneous
Fe-13X	0.74 ± 0.03	Granules/Pellets	Homogeneous
Ukr	1.04 ± 0.04	Granules/Pellets	Homogeneous
Fe-Ukr(1)	1.05 ± 0.04	Granules/Pellets	Non-homogeneous
Fe-Ukr(2)	1.01 ± 0.04	Granules/Pellets	Non-homogeneous
Fe-Ukr(3)	1.00 ± 0.04	Granules/Pellets	Non-homogeneous
Slov	0.91 ± 0.04	Granules/Pellets	Homogeneous
Fe-Slov	0.92 ± 0.04	Granules/Pellets	Non-homogeneous
Mn-Slov(1)	1.12 ± 0.04	Granules/Pellets	Homogeneous
Mn-Slov(2)	0.97 ± 0.04	Granules/Pellets	Homogeneous
FeMn-Slov	0.91 ± 0.04	Granules/Pellets	Homogeneous
CaMn-Slov	1.11 ± 0.04	Granules/Pellets	Homogeneous
Khol	0.90 ± 0.04	Granules/Pellets	Homogeneous
Fe-Khol	0.96 ± 0.04	Granules/Pellets	Homogeneous

Table 1. Material bulk density, form and homogeneity.

Material	Fe content (mas%)	Mn content (mas%)
4A	0.19 ± 0.01	0.00 ± 0.01
Mn-4A	0.03 ± 0.00	0.57 ± 0.02
13X	0.34 ± 0.01	0.01 ± 0.01
Fe-13X	2.92 ± 0.11	0.02 ± 0.00
Ukr	0.53 ± 0.02	0.01 ± 0.01
Fe-Ukr(1)	1.37 ± 0.05	0.02 ± 0.01
Fe-Ukr(2)	1.67 ± 0.06	0.01 ± 0.01
Fe-Ukr(3)	1.70 ± 0.06	0.05 ± 0.01
Slov	0.45 ± 0.02	0.01 ± 0.01
Fe-Slov	8.75 ± 0.33	0.05 ± 0.01
Mn-Slov(1)	0.47 ± 0.02	4.58 ± 0.17
Mn-Slov(2)	0.43 ± 0.02	0.33 ± 0.01
FeMn-Slov	19.22 ± 0.73	2.80 ± 0.10
CaMn-Slov	0.35 ± 0.01	3.68 ± 0.13
Khol	0.33 ± 0.01	0.03 ± 0.01
Fe-Khol	1.43 ± 0.05	0.06 ± 0.01

Table 2. Fe and Mn content of materials obtained using FAAS.

(19.22 ± 0.73 mas%). Materials with highest Mn content are Mn-Slov(1) (4.58 ± 0.17 mas%), CaMn-Slov (3.68 ± 0.13 mas%) and FeMn-Slov (2.80 ± 0.10 mas%).

6.3. Optical microscopy

All raw and modified materials were studied using optical microscopy. Optical micrographs were obtained at different magnifications: x7.1, x20 and x80; and x115 for some materials. Optical micrographs with magnification of x80 for all studied materials are summarized in **Figure 1**.

Optical micrographs (**Figure 1**) indicate that obtained materials FeMn-Slov, Fe-Khol, Fe-13X, Fe-Ukr(1), Fe-Ukr(2), Fe-Ukr(3) and Fe-Slov are modified with an iron compound. Furthermore, also in x80 magnification materials look homogeneous, except Fe-Ukr(1), Fe-Ukr(2), Fe-Ukr(3) and Fe-Slov, where iron compound covers only parts of the materials' surface. Optical micrographs (**Figure 1**) also indicate that obtained materials Mn-4A, Mn-Slov(1), Mn-Slov(2), FeMn-Slov and CaMn-Slov are modified with manganese compounds.

6.4. Scanning electron microscopy

All raw and modified materials, except for nonhomogeneous Fe-Ukr(1), Fe-Ukr(2), Fe-Ukr(3) and Fe-Slov are studied with scanning electron microscopy (SEM). SEM micrographs are summarized in **Figure 2**.

SEM micrographs (**Figure 2**) indicate that obtained materials FeMn-Slov, Fe-Khol and Fe-13X are modified with an amorphous compound, which is also further proved using EDX (for more details, also see source [17]). SEM micrographs (**Figure 2**) indicate that obtained materials Mn-4A, Mn-Slov(1), Mn-Slov(2), FeMn-Slov and CaMn-Slov are modified with manganese compounds. In case of Mn-4A and Mn-Slov(2), manganese compound is amorphous, while for Mn-Slov(1), FeMn-Slov and CaMn-Slov a new crystalline phase ($Mn_8O_{10}Cl_3$) is obtained (more details can be found in source [17]).

6.5. Energy-dispersive X-ray spectroscopy

All raw and modified materials, except nonhomogeneous Fe-Ukr(1), Fe-Ukr(2), Fe-Ukr(3) and Fe-Slov were studied with energy-dispersive X-ray spectroscopy (EDX). EDX results are summarized in **Table 3**. Elements with probability ≥95% are shown as an average of 6 repeated measurements at different locations.

Analysing amorphous iron compounds with EDX, it was deduced that it consists of 65.28 ± 3.91 mas% Fe and 34.72 ± 2.08 mas% O. This result is in agreement with elemental content of FeOOH (62.85 mas% Fe, 36.01 mas% O and 1.14 mas% H).

Analysing manganese crystals with EDX, it was deduced that it consists of 54.58 ± 3.27 mas % Mn, 30.27 ± 1.82 mas% O and 15.15 ± 0.91 mas% Cl. This result is in agreement with elemental content of $Mn_8O_{10}Cl_3$ (62.26 mas% Mn, 22.67 mas% O, 15.07 mas% Cl). Elevated oxygen content can be explained with signal from zeolite oxygen and/or with other manganese oxide presence.

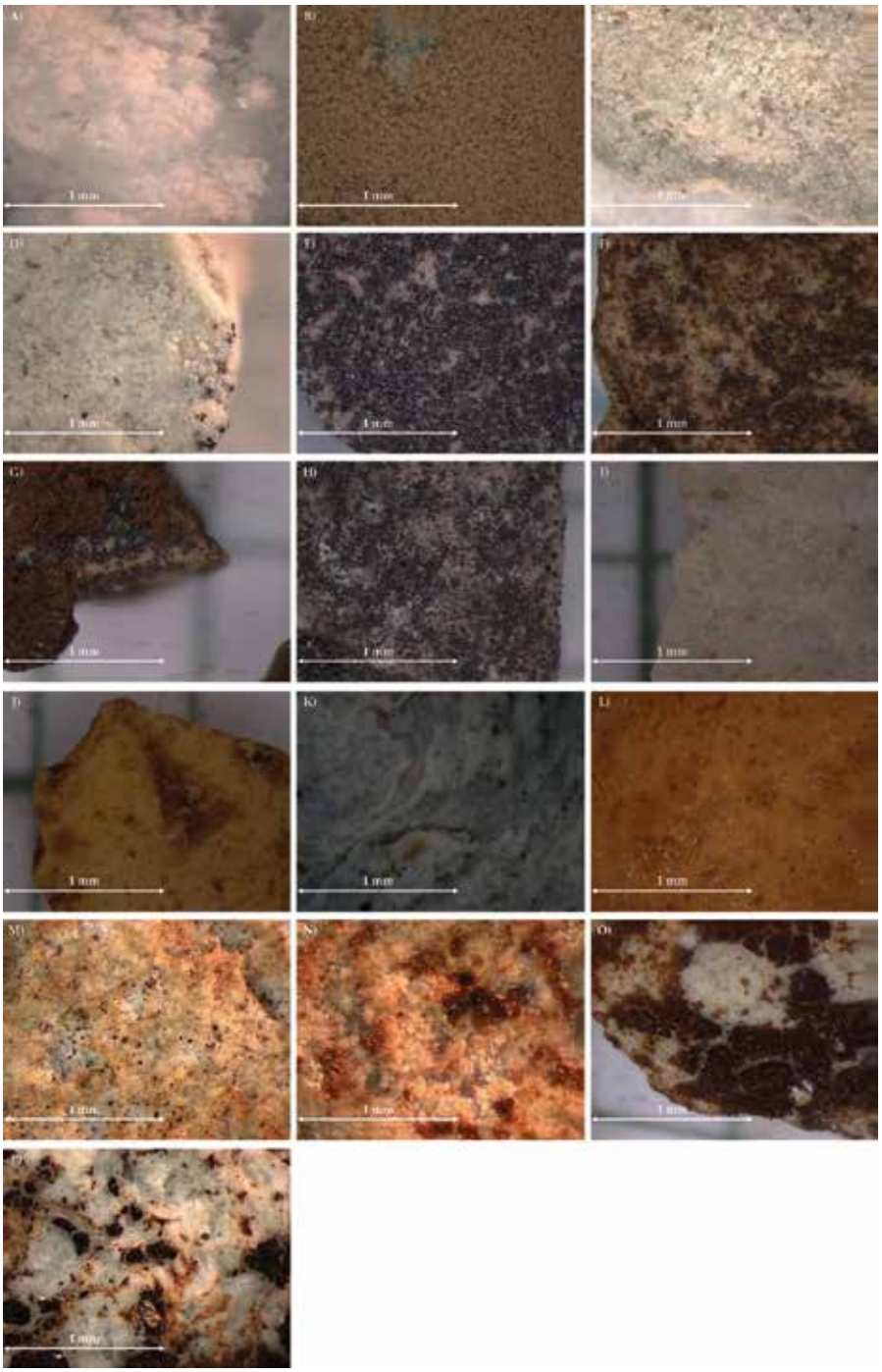

Figure 1. Optical micrographs with x80 magnification of all studied materials: (A) 4A; (B) Mn-4A; (C) Ukr; (D) Slov; (E) Mn-Slov(1); (F) Mn-Slov(2); (G) FeMn-Slov; (H) CaMn-Slov; (I) Khol; (J) Fe-Khol; (K) 13X; (L) Fe-13X; (M) Fe-Ukr(1); (N) Fe-Ukr(2); (O) Fe-Ukr(3); (P) Fe-Slov.

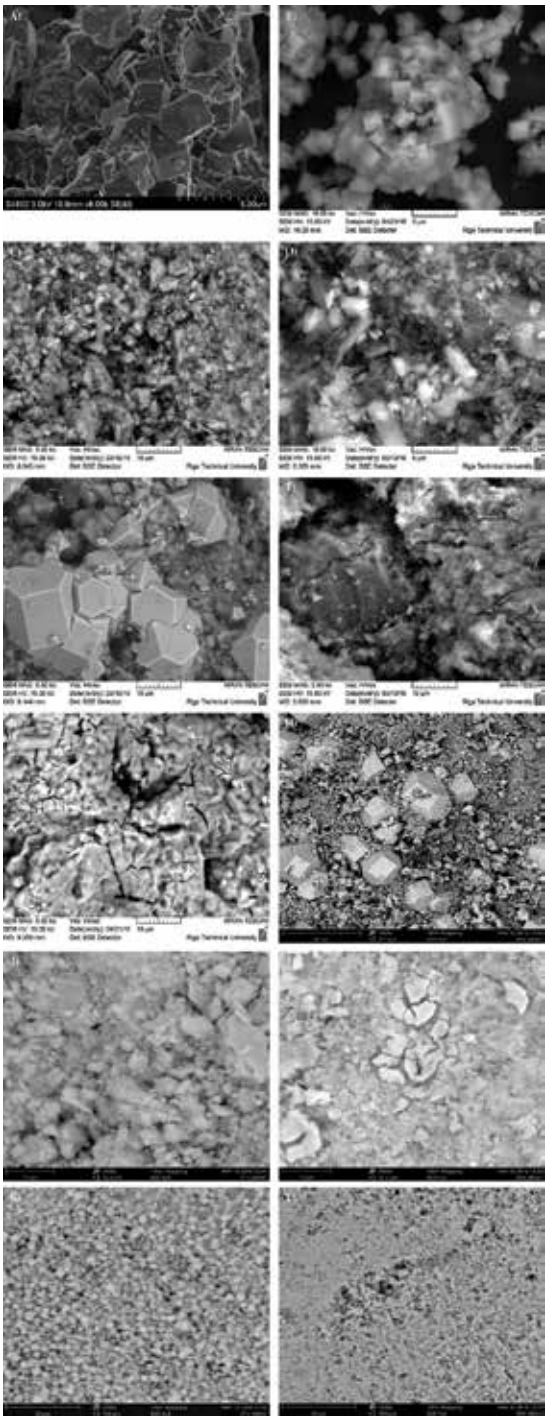

Figure 2. SEM micrographs of studied materials: (A) 4A; (B) Mn-4A; (C) Ukr; (D) Slov; (E) Mn-Slov(1); (F) Mn-Slov(2); (G) FeMn-Slov; (H) CaMn-Slov; (I) Khol; (J) Fe-Khol; (K) 13X; (L) Fe-13X.

Material	Elemental content [mas%]							
	Al	Si	O	Fe	Mn	Cl	Na	Ca
4A	14.76 ± 0.91	15.71 ± 0.95	55.59 ± 1.89	—	—	—	13.94 ± 0.53	—
Mn-4A	19.90 ± 1.22	20.62 ± 1.26	46.55 ± 2.85	—	1.74 ± 0.11	—	11.19 ± 0.68	—
Ukr	6.43 ± 0.39	35.94 ± 2.20	52.10 ± 3.19	2.80 ± 0.17	—	—	—	2.74 ± 0.17
Slov	5.27 ± 0.32	31.70 ± 1.94	59.94 ± 3.67	1.50 ± 0.09	—	—	—	1.58 ± 0.10
Mn-Slov(1)	3.86 ± 0.24	31.66 ± 1.94	47.33 ± 2.90	0.71 ± 0.04	8.40 ± 0.51	5.97 ± 0.37	0.24 ± 0.01	1.83 ± 0.11
Mn-Slov(2)	4.05 ± 0.25	22.51 ± 1.38	59.66 ± 3.65	1.37 ± 0.08	10.64 ± 0.65	—	—	1.76 ± 0.11
FeMn-Slov	3.16 ± 0.17	19.38 ± 1.05	43.28 ± 2.34	6.31 ± 0.34	11.10 ± 0.60	6.15 ± 1.04	9.24 ± 0.50	1.38 ± 0.07
CaMn-Slov	3.48 ± 0.22	24.69 ± 1.51	48.37 ± 3.06	1.80 ± 0.11	7.86 ± 0.48	7.41 ± 0.45	—	6.40 ± 0.39
Khol	8.96 ± 0.55	36.15 ± 2.21	51.25 ± 3.14	2.50 ± 0.15	—	—	0.42 ± 0.03	0.73 ± 0.04
Fe-Khol	5.20 ± 0.31	17.43 ± 1.05	64.08 ± 3.80	7.38 ± 0.57	—	1.53 ± 0.09	4.28 ± 0.26	0.10 ± 0.01
13X	14.56 ± 0.89	22.97 ± 1.41	52.15 ± 3.19	1.95 ± 0.12	—	—	7.95 ± 0.48	0.41 ± 0.03
Fe-13X	16.67 ± 1.02	23.59 ± 1.44	51.00 ± 3.12	5.62 ± 0.34	—	—	2.91 ± 0.18	0.20 ± 0.01

Table 3. EDX results (elements with probability ≥95%).

6.6. As(V) sorption experiments

Experimental data is compared with sorption models: Langmuir, Freundlich, Dubinin–Radushkevich, Temkin and Redlich–Peterson isotherm linearized forms comparing obtained determination coefficients (R^2). As(V) sorption experimental results and determination coefficients of fit with the sorption models are reported in **Table 4**.

As(V) sorption on raw zeolites is most precisely characterized by Freundlich's sorption model in all cases. As(V) sorption on iron oxohydroxides indicates that for these materials physisorption is dominant [3]. As(V) on Fe(III)-modified clinoptilolite and synthetic zeolites is most precisely characterized by Langmuir model [17, 20], which is also consistent with experimental data in this work, except for Fe-Ukr(2). Inconsistency in case of Fe-Ukr(2) can be explained by material's inhomogeneity, leaving large areas of zeolite unmodified.

As(V) sorption on Mn-modified zeolites is most precisely characterized with Freundlich model in cases of Mn-Slov(1), FeMn-Slov and CaMn-Slov and with Redlich–Peterson model in cases of Mn-4A and Mn-Slov(2).

Obtained As(V) equilibrium sorption capacities and Langmuir monolayer coverage (where applicable) are systematized in **Table 5**. Improvement shows how much material's equilibrium sorption capacity (at the highest studied As(V) solution concentration of 300 mg As(V)/L) increased after modification. Each sorption experiment was performed 3 times and obtained results represent average with standard deviation.

As(V) sorption isotherms for each respective material group (raw and modified, from top to bottom: Slov, Ukr, Khol, A and X) are shown in **Figure 3**.

Material	Determination coefficient R^2				
	Langmuir	Freundlich	Dubinin–Radushkevich	Temkin	Redlich–Peterson
4A	0.0586	**0.8401**	0.2180	0.7655	0.3729
Mn-4A	0.9911	0.9935	0.5360	0.9629	**0.9990**
Ukr	0.3874	**0.9724**	0.4559	0.7704	0.7768
Fe-Ukr(1)	**0.9853**	0.8693	0.6305	0.8840	0.9342
Fe-Ukr(2)	0.9062	**0.9872**	0.6655	0.8849	0.9635
Fe-Ukr(3)	**0.9990**	0.9342	0.8974	0.9452	0.9875
Slov	0.7607	**0.9801**	0.4944	0.8226	0.9314
Fe-Slov	**0.9936**	0.9299	0.8849	0.9404	0.8459
Mn-Slov(1)	0.9896	**0.9932**	0.6416	0.8834	0.7678
Mn-Slov(2)	0.9625	0.9838	0.4748	0.9015	**0.9938**
FeMn-Slov	0.9704	**0.9722**	0.7660	0.9174	0.3561
CaMn-Slov	0.5771	**0.9750**	0.5346	0.6840	0.8770
KHol	0.6213	**0.9379**	0.3429	0.7111	0.8379
Fe-KHol	**0.9968**	0.8968	0.9726	0.9599	0.8998
13X	0.5236	**0.9610**	0.5364	0.7113	0.6179
Fe-13X	0.7705	**0.9720**	0.4454	0.8207	0.9271

Table 4. As(V) sorption data and comparison with sorption models. Values marked in bold signify a respective model with the highest fit.

6.7. As(V) equilibrium sorption capacity correlation with Fe and Mn content

A correlation analysis was performed using obtained sorption data and Fe and Mn content of materials. The analysis was performed using Microsoft Excel Data Analysis toolpack (USA; International). Three different As(V) equilibrium concentrations were chosen – at initial As(V) solution concentration of 300, 100 and 5 mg/L. Correlation coefficients are summarized in **Table 6**. Correlation analysis was performed using all studied materials, as well as separate material groups (where applicable).

Correlation between material's As(V) equilibrium sorption capacity q_e and Fe content is strong (correlation strength ≥0.67 by absolute value) for all groups and for all materials altogether at all studied concentrations.

Correlation between material's As(V) equilibrium sorption capacity q_e and Mn content is strong (correlation strength ≥0.67 by absolute value) only for Ukrainian natural zeolites at initial As(V) solution's concentration of 5 and 100 mg/L. Medium correlation (correlation strength between 0.33 and 0.67 by absolute value) is observed for Ukrainian and Slovakian natural zeolites at initial As(V) solution's concentrations of 300 mg/L. For studied materials altogether at all concentrations and for Slovakian zeolite group at initial As(V) solution's concentration of 5 and 100 mg/L correlation is weak (correlation strength <0.33 by absolute value).

Material	Equilibrium sorption capacity $q_{e,300}$ [mg/g]	Equilibrium sorption capacity $q_{e,100}$ [mg/g]	Equilibrium sorption capacity $q_{e,5}$ [mg/g]	Langmuir monolayer coverage q_m [mg/g]	Improvement [times]	Water remediation [%]
4A	0.15 ± 0.01	0.06 ± 0.00	0.01 ± 0.00	—	—	4.2
Mn-4A	0.39 ± 0.02	0.30 ± 0.02	0.13 ± 0.01	0.40	2.6	43.0
Ukr	0.43 ± 0.02	0.14 ± 0.01	0.02 ± 0.00	—	—	6.6
Fe-Ukr(1)	1.08 ± 0.06	0.96 ± 0.07	0.17 ± 0.02	1.19	2.5	57.2
Fe-Ukr(2)	0.87 ± 0.05	0.40 ± 0.03	0.05 ± 0.01	—	2.0	17.4
Fe-Ukr(3)	0.92 ± 0.05	0.83 ± 0.04	0.24 ± 0.01	0.93	2.1	80.2
Slov	0.36 ± 0.02	0.14 ± 0.01	0.02 ± 0.00	—	—	8.2
Fe-Slov	4.74 ± 0.29	4.08 ± 0.29	0.29 ± 0.03	4.92	13.2	>98.0
Mn-Slov(1)	4.92 ± 0.30	2.21 ± 0.13	0.12 ± 0.01	10.50	13.7	41.2
Mn-Slov(2)	0.66 ± 0.04	0.41 ± 0.02	0.13 ± 0.01	0.71	1.8	44.3
FeMn-Slov	6.96 ± 0.49	3.79 ± 0.27	0.30 ± 0.02	6.82	19.3	>98.0
CaMn-Slov	1.32 ± 0.10	0.51 ± 0.04	0.06 ± 0.00	—	3.7	21.3
KHol	0.24 ± 0.02	0.10 ± 0.01	0.02 ± 0.00	—	—	7.9
Fe-KHol	1.25 ± 0.06	1.18 ± 0.06	0.30 ± 0.02	1.28	5.2	>98.0
13X	0.30 ± 0.02	0.12 ± 0.01	0.01 ± 0.00	—	—	3.2
Fe-13X	1.05 ± 0.05	0.42 ± 0.02	0.08 ± 0.00	—	3.5	26.0

Table 5. As(V) equilibrium sorption capacities.

7. Conclusion

Natural and synthetic zeolites were modified and tailored for As(V) sorption using novel methods. Based on optical microscopy, SEM, EDX and FAAS results, it was proved that zeolites were modified with amorphous Fe(III) oxohydroxide, amorphous Mn(IV) oxide and crystalline mixed oxidation state manganese oxide-chloride $Mn_8O_{10}Cl_3$. FeOOH, and $Mn_8O_{10}Cl_3$-modification improves As(V) sorption capacities of these aluminosilicates. Granulated material with the highest As(V) sorption capacity is $Mn_8O_{10}Cl_3$-FeOOH-modified Slovakian clinoptilolite natural zeolite (6.96 ± 0.49 mg/g). These materials are effective and potential As(V) sorbents, able to remove >98% As(V) in water environments. Sorption capacity of granulated materials (per unit volume) was improved up to 26.5 times. As(V) sorption on FeOOH-modified zeolites follows Langmuir model most precisely, while sorption on unmodified zeolites is described by Freundlich isotherm. In case of $Mn_8O_{10}Cl_3$-modified and MnO_2-modified zeolites, Freundlich and Redlich–Peterson models show the most precise fit, respectively. There is a strong and positive correlation between As(V) sorption capacity and Fe content among all zeolites. Among studied materials, Mn content showed a strong positive correlation only among Ukrainian clinoptilolite natural zeolites.

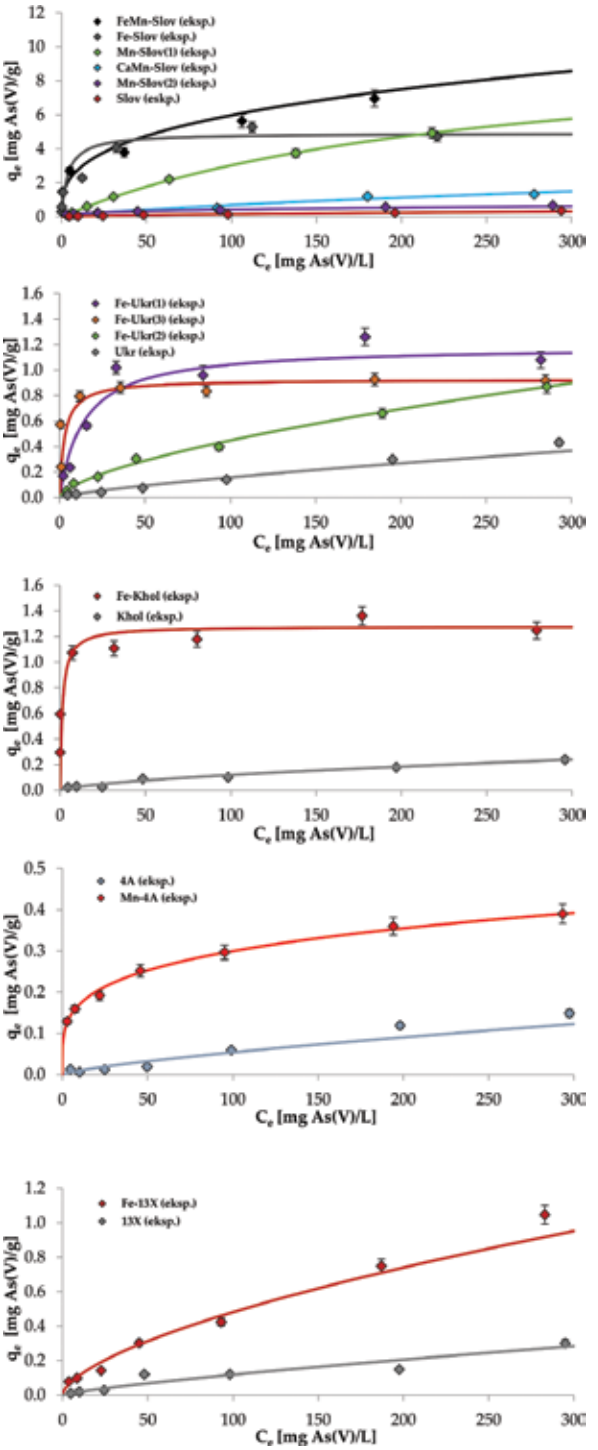

Figure 3. As(V) sorption experimental data and constructed isotherms.

As(V) equilibrium sorption capacity	Correlation with Fe content	Correlation with Mn content
All studied materials		
$q_{e,300}$	0.76	0.20
$q_{e,100}$	0.84	0.17
$q_{e,5}$	0.71	0.05
Ukrainian zeolites		
$q_{e,300}$	0.83	0.50
$q_{e,100}$	0.68	0.70
$q_{e,5}$	0.67	0.94
Slovakian zeolites		
$q_{e,300}$	0.80	0.40
$q_{e,100}$	0.80	0.09
$q_{e,5}$	0.86	−0.07

Table 6. As(V) equilibrium sorption capacities, Fe and Mn content correlation.

Acknowledgements

The author is thankful for an opportunity to perform this work in the laboratory of Department of Environmental Science of Latvian University. This would not be possible without Prof. Maris Klavins, to whom the author is deeply grateful. Acknowledgement also goes to the author's colleagues and teachers who have supported him during this work, Juris Burlakovs, Kristine Rugele and Ruta Ozola.

Author details

Andrey E. Krauklis[1,2,3]*

*Address all correspondence to: andrejs.krauklis@ntnu.no

1 Department of Mechanical and Industrial Engineering, Norwegian University of Science and Technology, Trondheim, Norway

2 Department of Environmental Science, University of Latvia, Riga, LV, Latvia

3 Institute of General Chemical Engineering, Riga Technical University, Riga, LV, Latvia

References

[1] Mukherjee A, Bhattacharya P, Savage K, Foster A, Bundschuh J. Distribution of geogenic arsenic in hydrologic systems: Controls and challenges. Journal of Contaminant Hydrology. 2008;**99**:1-7

[2] Kemper K, Minnatullah K. The World Bank and the Water and Sanitation Programs of South and East Asia, Technical Report No. 31303. 2005

[3] Glocheux Y, Albadarin AB, Mangwandi C, Stewart E, Walker GM. Production of porous aluminium and iron sulphated oxyhydroxides using industrial grade coagulants for optimised arsenic removal from groundwater. Journal of Industrial and Engineering Chemistry. 2014;**25**:56-66

[4] Ma J, Sengupta MK, Yuan D, Dasgupta PK. Speciation and detection of arsenic in aqueous samples: A review of recent progress in non-atomic spectrometric methods. Analytica Chimica Acta. 2014;**831**:1-23

[5] World Health Organization (http://www.who.int/en/)

[6] CAA. Art.1 Res. MS y AS No. 494. Ley 18284, Dec. Reglamentario 2126, Anexo I y II, Marzocchi, Buenos Aires, Argentina. 1994

[7] A textbook of modern toxicology, 3rd edn., ed by Hodgson E. John Wiley and Sons, Hoboken, New Jersey. 2004

[8] Ravenscroft P (http://www.geog.cam.ac.uk/research/projects/arsenic/symposium/S1.2_P_Ravenscroft.pdf)

[9] Bhattacharya P, Claesson M, Bundschuh J, Sracek O, Fagerberg J, Jacks G, Martin RA, Storniolo AR, Thir JM. Distribution and mobility of arsenic in the Río Dulce alluvial aquifers in Santiago del Estero Province, Argentina. Sci Total Environ. 2006;**358**:97-120

[10] Ansone-Bertina L, Klavins M. Sorption of V and VI group metalloids (as, Sb, Te) on modified peat sorbents. Open Chem. 2016;**14**:46-59

[11] Dupont L, Jolly G, Aplincourt M. Arsenic adsorption on lignocellulosic substrate loaded with ferric ion. Environmental Chemistry Letters. 2007;**5**:125-129

[12] Figueiredo H, Quintelas C. Tailored zeolites for the removal of metal oxyanions: Overcoming intrinsic limitations of zeolites. Journal of Hazardous Materials. 2014;**274**:287-299

[13] Zhang F-S, Itoh H. Iron oxide-loaded slag for arsenic removal from aqueous system. Chemosphere. 2005;**60**:319-325

[14] Faure G. Principles and Applications of Inorganic Geochemistry, 2nd Ed., Prentice-Hall. 1998

[15] Bogdanov B, Georgiev D, Angelova K, Yaneva K. International Science Conference. Bulgaria: Stara Zagora; 2009

[16] Hrenovi J, Büyükgüngör H, Orhan Y. Food Technology and Biotechnology. 2003;**41**(2): 157-165

[17] Krauklis A, Ozola R, Burlakovs J, Rugele K, Kirillov K, Trubaca-Boginska A, Rubenis K, Stepanova V, Klavins M. FeOOH and $Mn_8O_{10}Cl_3$ modified zeolites for as(V) removal in aqueous medium. Journal of Chemical Technology and Biotechnology. 2017 Special Issue

[18] Cheung O. Narrow-Pore Zeolites and Zeolite-Like Adsorbents for CO_2 Separation, PhD Thesis, Stockholm University. 2014

[19] Yang RT. Adsorbents: Fundamentals and Applications. Hoboken, New Jersey, USA: John Wiley & Sons, Inc.; 2003

[20] Payne KB, Abdel-Fattah TM. Journal of Environmental Science and Health. 2005;**A40** (4):723-749

[21] Katsoyiannis IA, Zouboulis AI. Removal of arsenic from contaminated water sources by sorption onto iron-oxide-coated polymeric materials. Water Research. 2002;**36**:5141-5155

[22] Sun X, Doner HE. An investigation of arsenate and arsenite bonding structures on goethite by FTIR. Soil Science. 1996;**161**:865-872

[23] Sherman DM, Randall SR. Surface complexation of arsenic(V) to iron(III) (hydr)oxides: Structural mechanism from ab initio molecular geometries and EXAFS spectroscopy. Geochimica et Cosmochimica Acta. 2003;**67**:4223-4230

[24] Мищенко КП, Равдель АА. Краткий справочник физико-химических величин, 7ое Изд., Л.: Химия. 1974 (in Russian)

[25] Bundschuh J, Bhattacharya P, Sracek O, Mellano MF, Ramírez AE, del Storniolo AR, Martin RA, Cortés J, Litter MI, Jean JS. Arsenic removal from groundwater of the Chaco-Pampean plain (Argentina) using natural geological materials as adsorbents. Journal of Environmental Science and Health, Part A. 2011;**46**:1297-1310

[26] PubChem Substance and Compound database (https://pubchem.ncbi.nlm.nih.gov PubChem)

[27] Camacho LM, Parra RR, Deng S. Arsenic removal from groundwater by MnO2-modified natural clinoptilolite zeolite: Effects of pH and initial feed concentration. Journal of Hazardous Materials. 2011;**189**:286-293

[28] Manning BA, Fendorf SE, Bostick B, Suarez DL. Environmental Science and Technology. 2002;**36**(5):976-981

[29] Kemmitt RDW, Peacock RD. The Chemistry of Manganese, Technetium and Rhenium: Pergamon Texts in Inorganic Chemistry. Volume I3. Pergamon Press. 1973

[30] Zhang L, Zeng Y, Cheng Z. Journal of Molecular Liquids. 2016;**214**:175-191

[31] Foo KY, Hameed BH. Chemical Engineering Journal. 2010;**156**(1):2-10

[32] Allen SJ, McKay G, Porter JF. Journal of Colloid and Interface Science. 2004;**280**(2):322-333

[33] Dada AO, Olalekan AP, Olatunya AM. Dada O. IOSR Journal of Applied Chemistry. 2012;**3**(1):38-45

[34] F-C W, Liu B-L, K-T W, Tseng R-L. Chemical Engineering Journal. 2010;**162**(1):21-27

[35] http://www.vskpro-zeo.sk/en/zeolite/natural/ Slovakian natural zeolite (acc. 12.04.2016)

[36] http://www.dpzzz.com/ru/info/1/5.html Ukrainian natural zeolite (acc. 27.02.2016)

[37] http://www.zeolite.spb.ru/nat_zeo.htm Russian natural zeolite (acc. 17.05.2016)

[38] Grace Davison – Materials & Packaging Technologies. SYLOSIV Molecular Sieve Powder Brochure (2008)

[39] Ozola R, Krauklis A, Leitietis M, Burlakovs J, Vircava I, Ansone-Bertina L, Bhatnagar A, Klavins M. FeOOH-modified clay sorbents for arsenic removal from aqueous solutions. Environmental. Technology and Innovation. 2016

[40] Jankēvica M, Ansone L, Kļaviņš M. Material Science and Applied Chemistry. 2013;**29**:101-108

[41] Wang S, Gao B, Li Y, Mosa A, Zimmerman AR, Ma LQ, Harris WG, Migliaccio KW. Bioresource Technology. 2015;**181**:13-17

[42] Mahadik KR. Concise Inorganic Pharmaceutical Chemistry. Pragati Books Pvt. Ltd; 2008

[43] http://www.leica-microsystems.com Leica Microscopes (acc. 27.05.2016)

[44] The United States Pharmacopeial Convention. Bulk Density and Tapped Density of Powders, Stage 6 Harmonization. 2011

[45] FMP Group (Australia) Pty. Ltd. Standart Test Method, Bulk Density/Volume Tapped. 2009

[46] World Health Organization. Bulk density and tapped density of powders, Document QAS/11.450 FINAL. 2012

Chapter 7

Zeolite Mixed Matrix Membranes (Zeolite-MMMs) for Sustainable Engineering

Mahboobeh Maghami and Amira Abdelrasoul

Additional information is available at the end of the chapter

http://dx.doi.org/10.5772/intechopen.73824

Abstract

Mixed matrix membranes (MMMs) could provide a solution to the permeability and selectivity trade-off in polymeric membranes and bridge the gap with inorganic membranes. MMM could offer the physicochemical stability of a ceramic material while ensuring the desired morphology with higher permeability, selectivity, hydrophilicity, fouling resistance, as well as greater thermal, mechanical, and chemical strength over a wider temperature and pH range. Zeolites are fascinating and versatile materials, vital for a wide range of industries due to their unique structure, greater mechanical strength, and chemical properties. This chapter focused on zeolite-MMM and characterized various zeolite-reinforced polymeric membrane types and applications. Several key rules in the synthesis procedures have been comprehensively discussed for the optimum interfacial morphology between the zeolites and polymers. Furthermore, the influence of the zeolite filler incorporation has been discussed and explored for a range of applications. This chapter provided a broad overview of the MMM's challenges and future improvement investigative directions.

Keywords: mixed matrix membrane, filler, zeolites, hydrophilicity, interfacial, morphology

1. Introduction

Both polymeric and ceramic membranes have been the center of interest for their tremendous contribution in water treatment industry. Despite their advantages, these synthetic membranes have limitations in terms of performance and durability. Over the years, researchers have been trying to combine the effective features of both, polymeric and ceramic, materials in one new material called mixed matrix membrane (MMM) or hybrid membrane. The sole purpose of

IntechOpen

© 2018 The Author(s). Licensee IntechOpen. This chapter is distributed under the terms of the Creative Commons Attribution License (http://creativecommons.org/licenses/by/3.0), which permits unrestricted use, distribution, and reproduction in any medium, provided the original work is properly cited.

developing new materials has been to associate the advantageous characteristics of the two types of membranes boosting the overall process efficacy. Conventionally, objectives such as enhancement in permeability or selectivity, reduction in fouling and removal of specific contaminants have been attained either by combining two or more processes or by developing an integrated filtration process. However, material advancement in membrane technology and nanotechnology has made it possible to fine tune the process efficiency and have successfully paved the way for the synthesis of MMMs for different applications. Apart from the water purification applications, the advent of MMMs has revolutionized other areas also where separation or purification is of great significance. Some of these potential applications reported in literature include water purification, medical industry, catalytic, and gas separation. Nevertheless, MMMs have not yet crossed the lab-scale barrier because the MMM technology is still in a developmental phase and only a few lab-scale developments have been reported so far.

2. Types of MMMs

MMMs can be defined as incorporation of dispersed nanomaterials such as zeolite, carbon molecular sieve, and carbon nanotubes incorporated in a continuous polymer phase. **Figure 1** presented a schematic of an ideal MMM structure including the dispersed phase and the polymer matrix [1].

MMM could offer the physicochemical stability of a ceramic material and the membrane forming ease of polymeric materials while promising the desired morphology with higher permeability, selectivity, higher hydrophilicity, high fouling resistance, high thermal, mechanical, and chemical strength over a wider temperature and pH range [2–7]. These types of MMMs are named as inorganic filler-based MMMs, organic filler-based MMMs, biofiller-based MMMs, and hybrid filler-based

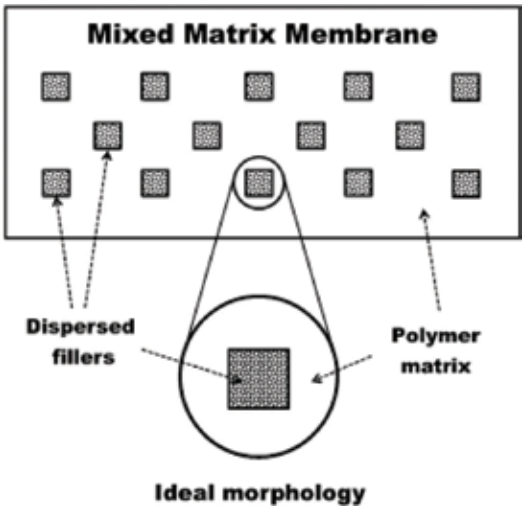

Figure 1. Schematic diagram of an ideal MMM structure [1].

MMMs, depending on the type of the dispersed fillers in the polymer matrix, as presented in **Figure 1** [1]. This chapter will focus on inorganic filler-based MMM, especially zeolite-MMM.

2.1. Inorganic filler-based MMMs

The field of inorganic filler-based membrane is a promising type of membrane, which has been explored extensively over the recent years. In the polymeric matrix, the inorganic fillers attach themselves to support materials by covalent bonds, van der Waals forces, or hydrogen bonds. These inorganic fillers are prepared through processes such as sol gel, inert gas condensation, pulsed laser ablation, spark discharge generation, ion sputtering, spray pyrolysis, photothermal synthesis, thermal plasma synthesis, flame synthesis, low-temperature reactive synthesis, flame spray pyrolysis, mechanical alloying/milling, mechano-chemical synthesis, and electrodeposition. Currently, different types of inorganic fillers have been added to the polymeric phases. Some of these fillers are zeolite [8], silica [9], TiO_2 [10], carbon nanotubes [11], and silver [12]. There are two methods to incorporate inorganic fillers into membrane structure by blending with the solution or by attaching the fillers to the surface through different techniques [4]. Inorganic-based filler MMMs have been employed in water industry for the adsorptive removal of pollutants, disinfection and/or microbial control, catalytic degradation, and desalination [13]. They also have potentials to provide both high gas superior selectivity and the desirable mechanical and economical properties. Researchers believe that a suitable combination of polymers and inorganic fillers should offer superior permeability and selectivity compared to simple materials. In this review, zeolite-MMM will be comprehensively studied, as a promising membrane for several applications.

2.1.1. Zeolite-MMMs

Zeolites are microporous crystalline aluminosilicate materials with uniform pore and channel size, thus they are used in various fields such as catalysts in the petrochemical industry, ion-exchangers, and absorbents for softening and purification of water [14–16]. Incorporation of zeolites into a polymer matrix has attracted great attention in membrane technology, due to several excellent advantages such as permeability improvement of the selective component, in addition to the enhancement of the thermal stability and the mechanical strength of a polymeric membrane, [17] and its molecular sieving property, thermal resistance and chemical stability [18–20]. On the other hand, zeolites are expensive. Limitation in both polymeric and zeolite offers the need to synthesize the novel polymer–zeolite MMM. The interaction of zeolites in the membrane matrix and its shape-selective catalytic properties could improve permeability and selectivity separations [21]. There have been numerous attempts to incorporate zeolite particles in polymer matrices for gas separation due to its superior separation and size exclusion and in water purification applications [22, 23].

Rezakazemi et al. [24] studied the gas transport properties of zeolite-reinforced polydimethylsiloxane (PDMS) MMM. They evaluated the feasibility of this zeolite-MMM for hydrogen purification and natural gas sweetening, and also the permeation rates of CH_4, H_2, C_3H_8, and CO_2 were assessed. The filler was dispersed homogenously in the matrix without any voids at the zeolite–polymer interface. It was confirmed that the homogenous incorporation of filler in the matrix resulted in higher gas permeability for the MMM, as compared with the polymeric membranes.

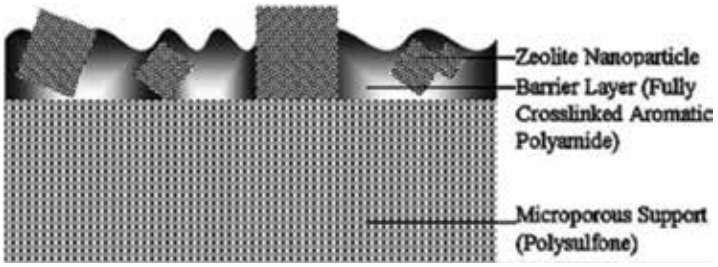

Figure 2. Schematic cross-section of zeolite nanocomposite membrane (zeolite-MMM) [26].

Ciobanu et al. [25] reported that zeolite-polyurethane membranes demonstrated improved properties. The good interaction between the polymer and the zeolite at the interface was confirmed and the membrane swelling was reduced. Consequently, the water flux through membrane increased with increasing zeolite concentration.

Hoek [26] studied the formation of mixed matrix reverse osmosis membranes by the interfacial polymerization of thin film nanocomposite polysulfone supports impregnated with zeolites. **Figure 2** represents the cross-section image of zeolite nanocomposite reverse osmosis membrane, which is utilized for water purification through desalination process. It was found that increasing the zeolite nanofillers concentrations resulted in smoother, more hydrophilic, and more negatively charged MMM. As a consequence, the MMM membrane demonstrated high flux and a slight improvement in salt rejection compared to TFC membrane without zeolite nano-particles due to changes of membrane morphology.

3. Interfacial morphology of zeolite-MMMs

To obtain the optimum interfacial morphology between the zeolites and polymer, several key roles should be considered. The first one is to promote the adhesion between polymer matrix and molecular sieve phases by modifying the zeolite surface with silane coupling agents [27–29]. The second one is to introduce low molecular weight materials to fill the voids between polymer and molecular sieve phases [30, 31]. The third one is to apply high processing temperatures close to glass transition temperature (Tg) of polymeric materials to maintain the polymer chain flexibility during the membrane formation [32]. The fourth one is to prime the surface of zeolites by polymer [33].

The polymer matrix plays an important role for permeability and the inorganic filler has a controlling factor for the selectivity of the separation process. As a result, interfacial compatibility between the two phases has profound impact on the separation performance for such membranes. The addition of inorganic fillers has key impacts on the interfacial void formation, aggregation, pore blockage of the morphology, and the transport phenomenon. Consequently, the impregnation of zeolites has a significant influence on the overall performance of the newly developed MMMs. The formation of these interfacial voids is attributed to two main phenomena, the interaction between the polymer phase and the filler and the stress exerted during preparation [1, 32]. The presence of interfacial voids creates additional

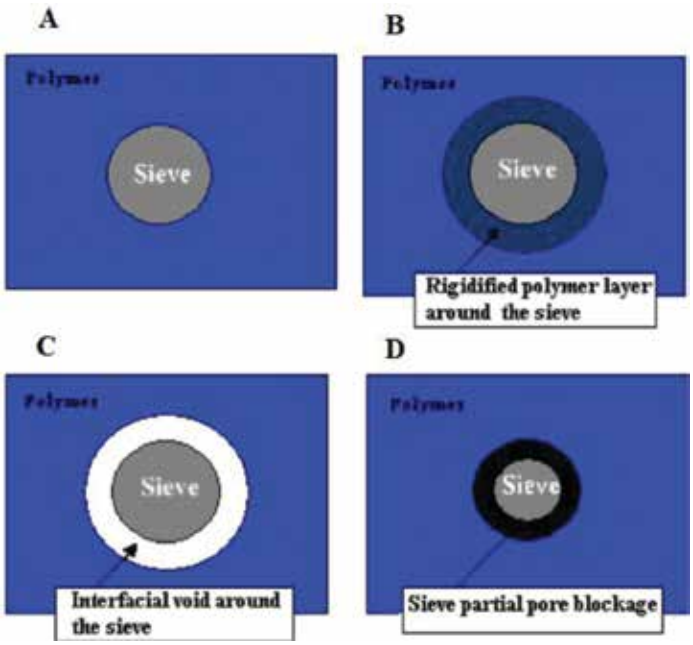

Figure 3. Illustration of various structures at the polymer/zeolite interface region [36].

channels that allow the solvent to pass through the membrane [34]. However, mechanical strength and rejection rate are also concerned by the channel density [35].

Figure 3 represents various structures at the polymer/zeolite interface region [36]. **Figure 3a** demonstrates a homogenous blend of polymer and sieve, indicating an ideal interphase morphology. **Figure 3b** shows polymer chains rigidification due to the shrinkage stresses generated during solvent removal. **Figure 3c** confirmed poor compatibility between zeolite and polymer matrix morphology, due to the formation of voids at the interfacial region. **Figure 3d** indicates sealing surface pores of zeolites by the rigidified polymer chains. Overall, the interaction between polymer and zeolite is related to chemical nature of the polymer and sieve surfaces, and the stress encountered during material preparation, which are the critical factors to form the interphase.

These features are a challenge and should be controlled or avoided for the synthesis of the targeted zeolite-MMM for several applications. The formation of relatively nonselective defects at the interface between the zeolite particles and the polymer medium will result in MMMs, which fail to demonstrate their performance [37]. Therefore, despite the good properties of the polymer-zeolite membranes MMMs, they still face some challenges to overcome.

4. Interfacial modification of zeolite-MMMs

Several strategies have been offered to improve the polymer–zeolite interaction; hence to avoid nonselective voids. These methods are included incorporation of a plasticizer into

the polymer solution that can decrease the polymer glass transition temperature (Tg) [32]. Consequently, polymer chain flexibility maintains during membrane preparation either by annealing the membranes above glass transition temperature of polymer [38, 39] or external surface of zeolites can be modified by coupling agents. The surface-initiated polymerization is a most frequent technique to improve the polymer–filler adhesion in polymer-zeolite MMMs [40]. Furthermore, adding the low molecular-weight (LMWAs) to the membrane formulation can act as a compatibilizer or a third component to prepare glassy polymer/ LMWAs blend membranes [31, 41], priming method can be also used to reduce the stress at the polymer-particle interface, and to minimize agglomeration of the particles. Consequently, the interfacial interaction between the two components will be improved through coating the surface of the filler particles with a dilute polymer dope [31], to minimize the zeolite-solvent/non-solvent interaction, especially for the use of modified zeolite in asymmetric membranes [42]. Therefore, the obtained hydrophobic surface can suppress the zeolite particles from acting as nucleating agents. As a result, it will minimize the voids induced by the unfavorable interaction between polymer and zeolite particles.

4.1. Interfacial modification with silane agents

Silane coupling agents were commonly proposed to modify the zeolite surface in order to improve the compatibility of the inorganic filler with the polymeric matrix [43, 44]. It is known from literatures related to the silanation of zeolites that silane coupling agents have two types of reactive groups. First, the hydroxyl groups of zeolites, which could make hydrogen bonds with the amino silane agent [43]. Second, the organo functional group, such as amino and epoxy, which could be used to bond polymer chains to the zeolite. Therefore, improving adhesion between the zeolite and the bulk polymer phase in the membrane was achieved [42]. **Figure 4** shows a schematic silanation of zeolite surface with 3-aminopropyldimethylethoxysilane (APDMES) coupling agent [42].

Koros [45] indicated that the glass transition temperature of MMMs is influenced by silane modification. In other words, the Tg of the zeolite-MMMs increased with the increasing of silane concentration on the surface of the zeolite particles. As a result, the silane modification of zeolite affects the mechanical properties of continuous phase due to the formation of the hydrogen bonding between the zeolite particles and polymer matrix and the movement reduction of the polymer chains [29, 41].

Leo [46] investigates the effects of silane-grafting on the separation performance of MMM for gas permeation. The 3-aminopropyltrimethoxysilane (APMS) was added to modify SAPO-34 zeolite before the impregnation into the asymmetric polysulfone (PSf) MMMs through dry–wet phase inversion method. Both PSf/modified SAPO-34 membranes showed great enhancement in terms of selectivity and permeability, compared to the original PSf membrane. The increment of CO_2 selectivity and permeability was correlated to the diminishing of the interfacial voids, when SAPO-34 zeolite was modified using APMS in ethanol.

Pechar et al. [47] studied the use of 3-aminopropyltrimethoxysilane (APTMS) influence to modify ZSM-2 zeolite to synthesize polyimide MMMs. Although micrographs showed the absence of voids, however, the modified ZSM-2-MMMs performance for CO_2 selectivity and

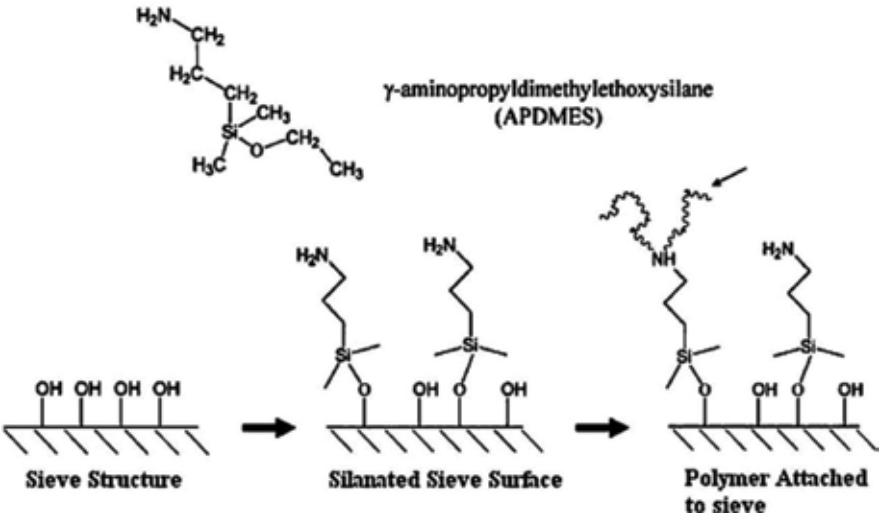

Figure 4. Schematic of the envisioned coupling reaction [42].

permeability was dropped relatively, similarly, to the performance of pure polymeric membrane, due to the pore blockage of the ZSM-2 zeolite [48].

In order to overcome this problem, other researchers such as Li et al [28] modified zeolite 3A, 4A, and 5A using 3-aminopropylmethyldiethoxysilane (APMDES) in toluene solvent. Hence, rigidification of polymer chain and partial pore blockage reduced through this modification process. As a result, they showed high improvement for both of the selectivity and permeability of CO_2 than those MMMs containing zeolite without the modification and without major blockage the zeolite pores. Therefore, in some cases, surface modification by the silane coupling agents was recommended to enhance interfacial adhesion but hardly improve permselectivity.

4.2. Addition of low molecular weight materials (LMWMs)

Adding low molecular weight additives (LMWAs) to the membrane formulation acts as a compatibilizer or a third component to improve the compatibility between zeolite and polymer matrix. The low molecular weight materials induce a hydrogen bond with hydroxyl and carbonyl moiety. In addition, the formation of hydrogen bond confirms its solubility in the solvent used to make the polymer dope solution. It should be noted that LMWMs should be solid at room temperature, in order to prevent their evaporation during membrane fabrication, and consequently losing their ability of forming interfacial voids [31]. Once hydrogen bonds are formed between polymer chains and LMWMs, the free volume of polymers decreases, which results in a decrease in their gas permeability whereas increase in their gas permselectivity.

Yilmaz [49] reported mixed matrix membranes for the use in gas separation by blending polycarbonates (PC) with an additive p-nitroaniline (pNA) and incorporating zeolite 4A particles as filler. The permeability of all gases was measured using differential scanning calorimetry (DSC) analysis through PC/(pNA)/zeolite 4A membranes, which were lower than those through pure

PC membrane. The incorporation of pNA was essential, since pNA acts as a facilitator for provision of better interaction between rigid, glassy polymer PC and zeolite 4A particles. Therefore, the incorporation of a molecular-weight additive with functional groups into zeolite-MMMs can be used as a tool to improve the structure and performance properties of the membranes.

One of the examples of LMWMs is 2,4,6-triaminopyrimidine (TAP) that contained three primary amine groups, which are able to form hydrogen bonds with both hydroxyl and carbonyl groups [31]. Furthermore, it had been reported that the carbonyl groups of polyimides (PI) could interact with amine groups of urethanes through the hydrogen bond formation.

Park [31] used TAP to obtain the interfacial void-free PI membranes filled with zeolites. TAP enhanced the contact of zeolite particles with polyimide chains presumably by forming the hydrogen bonding. As a consequence, the void-free PI/zeolite 13X/TAP membrane showed the higher gas permeability for He, N_2, O_2, CO_2, and CH_4 with little expense of selectivity compared to the PI/TAP membrane having the same PI/TAP ratio, while the PI/zeolite 4A/TAP membrane showed the lower permeability but higher permselectivity. The difference between both membranes was influenced by the pore size of zeolites. In addition, the molecular sieving effect of zeolites seemed to take place when the kinetic diameter of gas penetrants approached the pore size of zeolites.

4.3. Annealing

One of the largest challenges in designing zeolite-MMMs is the poor contact between polymer and zeolite defects. Many efforts made to overcome to this problem associated with the zeolite-MMMs through the annealing of zeolite-MMMs above the glass transition temperature (Tg) [32]. In other words, Tg is considered as a qualitative estimation to compare the polymer chain rigidity of mixed matrix membranes at different zeolite types with simple polymer membrane and it also leads to better contact between zeolite and polymer chain [50]. Annealing process at temperature above the Tg results in the formation of stronger bond between polymer matrix and zeolite. Despite advantages of annealing in relaxing the stress imposed to the hollow fiber membrane, it results in higher packing density of polymer chains. Therefore, there are drawbacks associated with annealing. In addition, it did not lead to significant improvement in the morphology of the membranes. Annealing at high Tg formed sieve-in-a-cage morphology, which will be difficult to create a good contact between the polymer and the sieve [32]. In order to overcome to this disadvantage of annealing, incorporation of a plasticizer into the polymer solution can decrease the polymer Tg and thus maintain polymer chain mobility and flexibility during membrane fabrication [51]. Therefore, to develop membrane fabrication technology, a quench method after annealing membranes above Tg can be effective in gas separation process by forming frozen polymer chains quickly [52]. Therefore, it will have a higher free volume in the polymer matrix and subsequently higher gas permeability without the loss of selectivity.

4.4. Priming method

The dilute polymers are the same as the bulk polymers used for the preparation of MMMs. Coating the surface of the filler particles with a dilute polymer dope is known as the priming

method [45]. The agglomeration is considered as responsible for defects between polymer matrix and zeolite particle phases [53]. Since more agglomeration occurs in the polymer matrix when smaller particles are used, especially at high particle loadings, and large zeolite particles are used to form practical mixed matrix membranes. Therefore, zeolite particles were primed by increasing amount of polymer. It should be considered that polymer effectively coats the zeolite particles before adding remaining bulk polymer and mixing with the priming polymer [54]. The purpose of priming is to reduce stress at the polymer-particle interface, increase the compatibility between zeolite and polymer in MMMs, and to minimize agglomeration of zeolite particles [55, 56].

5. Applications of zeolite-MMM

The advent of zeolite-MMMs enhances the separation or purification performance of the membranes significantly. The review represents various applications of zeolite-reinforced polymeric membranes. Some of these potential applications reported in literature include water purification, gas separation, medical, catalytic, and biomedical applications.

5.1. Zeolite-MMM for water purification

Water treatment is increasingly important to remove water pollutants and solve water problems. Drinking water may compose of hazardous substances such as toxins and endocrine disrupting compound. Therefore, it would be urgent to invent more sustainable and reliable treatment process to remove water contaminations and to regulate the quality of drinking water. The development of cost-effective membranes is in a great need to effectively replace the conventional water treatment technologies to produce water that meet or exceed stringent standards.

Recent studies have demonstrated that the zeolite-MMMs were applied to design reverse osmosis membrane to enhance the membrane properties such as permeability, selectivity, stability, surface area, or catalytic activity in water purification and separation processes [57, 58]. Nevertheless, there are only few studies performed on zeolite-MMMs for water treatment, it is determined that the size of zeolite was designed to match the expected polyimide active film thickness, thereby providing a preferential flow path through the nanochannels of zeolites [26, 59].

For example, thin film nanocomposite (TFN) reverse osmosis (RO) membranes have been used by incorporating zeolite particles into the PA rejection layer. It has shown that the incorporation of zeolite in a PA layer could improve its water permeability without significant loss of salt rejection under high pressure during RO process [60]. Main reason for that is nanochannels of zeolites with great sub-nanometer pores in zeolite nanoparticles that behave as preferential flow channels for water molecules. The zeolite-PA-based TFN membranes are considered as superior separation performance for RO applications due to their enhanced water permeability of active layer [61].

Tanga [61] provided an additional study to confirm that thin film nanocomposite membranes can significantly improve FO water flux significant with a relatively low zeolite loading due to both the surface and intrinsic separation properties of TFN membranes. Compared with TFC membrane, the TFN membrane is potentially more favorable during the application of treating feed solutions with relative higher salinity water under AL-FS orientation.

Sridhar [62] studied reactive separation of lactic acid (LA) using a microporous hydrophobic H-beta zeolite/polyvinylidene fluoride (PVDF) mixed matrix membrane from aqueous streams. Experiments were conducted using a stirred cell assembly consisting of two bell-shaped glass pipe reducers containing aqueous LA separated by the membrane from an organic solution of tri-noctylamine (TOA) carrier in alcoholic medium. The interfacial concentrations of species adjacent to the membrane in aqueous and organic chambers are influenced by mass transfer coefficients, the concentration of TOA in organic phase and the zeolite loading, and forward extraction rates. Overall, the mass transfer rates were improved with the zeolite addition, due to the kinetics of complex formation and diffusion. The continuous separation of LA by a membrane contactor could enhance the fermentation yield of the acid, which is inhibited by LA through deactivating of the lactate dehydrogenase enzyme of Lactobacillus bulgaricus microorganism used in the production of LA.

5.2. Zeolite-MMM for gas separation

Membrane technologies, such as pervaporation and gas separation, are recognized as highly promising approaches to reduce the energy consumption of industrial processes. Compared with polymeric membranes that show *Robeson upper bound* between selectivity and permeability, MMM are attracting research attention, due to their high permeability and selectivity.

It is known that the permeability of a gas through an MMM depends on several factors such as intrinsic properties of the filler and polymer, the filler loading, and the filler–polymer matrix interface, and the filler loading [58]. For designing a mixed matrix system for separating a certain gas pair, the molecular sieving phase must provide precise size and shape discrimination ability to distinguish the molecules. Moreover, zeolites with three-dimensional networks are generally preferred for gas separation since they offer less restricted diffusion paths. As a result, the attractive polymer matrix materials are generally glassy with relatively lower permeability and much higher selectivities. Indeed, addition of zeolites or another highly selective media would only improve the already industrially acceptable properties, if defects can be eliminated.

Pechar et al. [63] used silanated zeolite L filler modified with 3-aminopropyltriethoxysilane (APTES) and a glassy polyimide as polymer matrix for fabricating MMMs for gas separations. Both CO_2 selectivity and permeability of the modified MMM dropped relatively to the neat membrane, due to the blocked zeolite pores by APTES.

Furthermore, metal–organic frameworks (MOFs), as porous fillers possessing molecular sieving properties, have been combined with polymers to give MMM with substantial enhanced separation performance of CO_2/CH_4 for natural gas sweetening or CO_2/N_2 in flue [64]. MOF-74 series recently have demonstrated superior CO_2 adsorption capacities, due to the presence of open metal sites. This finding positions the materials as a very promising candidate for CO_2 capture from flue gas. **Figure 5** represents MIL-101/PSF membranes at different MOF loadings. It was found that the CO_2 permeability increases from about 5 to over 35 barrer from pure PSF to 24 wt % MIL-101/PSF. The increase for CO_2 also raises the ideal selectivity for CO_2/N_2 and CO_2/CH_4 from about 20 to 25 [65].

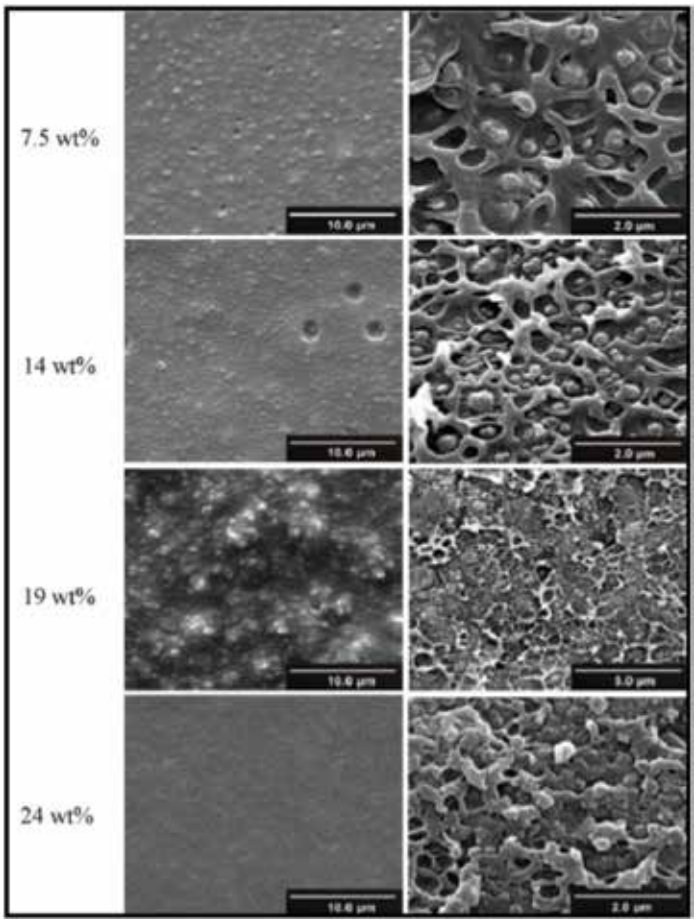

Figure 5. SEM image of a MIL-101/PSF MMMs shows a homogenous distribution of MOF particles in the polymer matrix at different load [65].

5.3. Zeolite-MMM for catalysis

Recently, many reports demonstrated catalytic activity of polymer–zeolite MMM, because the interaction of materials in the membrane matrix and the shape-selective catalytic properties of zeolites can improve permselective separations. Membrane also functions as a separator in gas phase between different gaseous molecules. Thus, membrane should be permeable enough to give efficient separation. For liquid phase separation, metal organic complexes and inorganic filler such as zeolite have been used [66]. It is well presented mostly that polydimethylsiloxane (PDMS) is incorporated as a polymer matrix because of high permeability, affinity for reagents, thermal, mechanical, and chemical stability [67].

Langhendries and Baron [68] studied the catalytic activity of zeolite-filled poly(dimethylsiloxane) polymer membranes. The incorporation of zeolite-encaged iron-phthalocyanine partial oxidation catalysts into a dense hydrophobic polymer membrane results in a substantial

improvement in catalyst performance. Both mathematical model and kinetics determined exact concentrations in polymer and catalyst, and subsequently, the resulting catalyst activity and selectivity. Their results also indicate that hydrophobic poly-(dimethylsiloxane) is an attractive polymer for the incorporation of the hydrophilic zeolite-encaged iron-phthalocyanine catalyst. As a result, diffusion through composite catalytic membranes can be predicted using the mass transfer coefficients of pure zeolite and pure polymer material, and a tortuosity factor based on the zeolite loading as a catalyst.

Another study, Jia and Peinemann [69] investigated the incorporation of polydimethylsiloxane (PDMS) into a polymer matrix and silicalite-1, a hydrophobic zeolite in order to study the permeation of various gases. In their study, only a couple of very high zeolite loadings were investigated, and they indicated that zeolite played the role of a molecular sieve in the membrane by facilitating the permeation of smaller molecules while it prevents the permeation of larger ones.

5.4. Zeolite-MMM for biomedical application

Combination of polymer materials with zeolite particles has been attracted attention not only due to enhanced mechanical and thermal properties, but also because of antibacterial properties. Polymer hosting can provide the enhanced antibacterial activity. There are three methods such as, production of reactive oxygen species (ROS) MMM, mixed matrix membrane direct damage to cell membrane; uptake of ions from mixed matrix membrane followed by DNA replication; and disruption of adenosine triphosphate (ATP) production [70].

Siddiq [71] studied the antibacterial effects of polysulfone/polyimide (PSf/PI) mixed matrix membranes fabricated by incorporation of modified zeolite (MZ) particles through solution casting method. The antibacterial property of fabricated zeolite-MMMs against Gram-negative bacteria (*Klebsiella pneumonia*, *Salmonella typhi*) and gram positive bacteria (*Staphylococcus aureus*, *Bacillus subtilis*) were also investigated. The MMM showed good antibacterial activity and a highest activity by PSf/PI/MZ mixed matrix membrane. Therefore, the combination effect of polysulfone/polyimide and modified zeolite sufficiently increased the antibacterial effect of mixed matrix membranes.

6. Challenges and future prospects

Recently, novel zeolite-MMMs have attracted great attention in membrane technology, due to the excellent advantages such as improvement in the permeability, selectivity, thermal stability, mechanical strength of a polymeric membrane. Furthermore, the recent developments demonstrated that gas separation as well as water treatment has significantly benefited from membrane technology so far and advancements in these areas are still in progress in order of their wider use can become a reality. However, the comprehensive understanding of organic–inorganic interfaces is in a great need. Zeolite-MMMs performance suffers from defects caused by poor contact at the molecular sieve/polymer interface, the complexity of the synthesis process, high cost, identification of compatible inorganic particles, agglomeration,

inorganic particle concentration, phase separation, control of morphology and structural defects. Moreover, some zeolite-MMMs for water purification application is considered a potential hazard to humans and environmental, which also needs to more study to determine the hazardous character of these nanoparticles and mechanism of nanoparticles embedded membrane fouling in industrially water purification in the future.

One of most difficulties associated with membrane technology is fouling for a long time. Although, several strategies such as incorporation of antifouling nanoparticles, and surface modification have been used to overcome this problem, intensive investigations are needed to stop regeneration of microbial colonies on membrane surface and to reduce the leaching of filler. The next generation MMM should be developed with producing nano-size fillers without aggregation to improve their separation properties for membrane industry especially MMMs. There are several reasons to produce nano-size fillers, especially zeolite fillers such as more polymer/particle interfacial area and enhanced polymer–filler interface contact by smaller particles. The potential of incorporating fillers such as zeolite particles has not been attained up to the expectation of zeolite-MMMs performance, due to the smaller sizes, homogeneous distribution, agglomeration, price, availability, compatibility with polymer interface, their relation with water chemistry, better interfacial contact, and stability.

Despite many novel MMMs and fillers are being investigated so far but their performances are restricted due to limited synthesis processes. Previously process fails to demonstrate their performance due to the formation of relatively nonselective defects at the interface between the zeolite particles and the polymer medium on laboratory scale. Therefore, other major issue related to MMM is the interface defects that can lead to isolating zeolite fillers from the transport processes. Therefore, new techniques to achieve a perfect interface between inorganic fillers and polymers in membranes without compromising performance and scaling up these novel membranes under industrially relevant conditions is greatly needed [72].

In addition, many of these novel MMMs reported so far have been only tested on a laboratory scale and need further research to use commercially in industry. It is required to produce novel materials that can have high selectivity as well as nano-sized fillers with incredibly small sizes. There are limitations on developing novel materials due to high prices or expensive synthesis processes. The molecular dynamic simulations (MD) of mixed matrix materials could be effective approach to predict diffusive performance of MMM, especially zeolite-MMMs, and to provide experimental guidelines for tuning the membrane permeability at the molecular level without high costs. Although there are previously predicted models for predicting the processes contributing to membrane separations, however, studies in MMMs showed inadequate suitable models. Therefore, MD will be essential and effective to predict the morphology and intrinsic properties of these fillers and its interaction of the polymeric matrix.

Last but not least factor, is changing and membrane morphology could change properties of membranes, and subsequently will influence the membrane performance. Therefore, improving membrane performance in real conditions such as high temperature, high pressure, and with incorporating of a plasticizer into the polymer solution would be possible and essential in order to provide better thermally and chemically zeolite-MMMs at different operating conditions.

Although there is development success of the synthesis and the application of MMMs impregnated with zeolites for gas, water separation, and other applications, however, the mechanisms behind these phenomena require intensive investigations for more advanced MMM technology.

7. Conclusion

Mixed matrix membranes with zeolite fillers has attracted a lot of attention in membrane technology research due to its excellent advantages, such as high permeability and improved selectivity. Zeolite-MMMs could be considered an ideal candidate for purification industry since it combines the properties of polymeric matric and zeolite inorganic fillers. Application and fabrication techniques of zeolite reinforced polymeric membranes have been comprehensively reviewed in this article with the aim of optimizing interfacial interaction between the zeolite and the polymeric matrix. Compatibility between zeolite and polymer matrix can be improved with a number of methods, such as: by applying high processing temperature during membrane formation, the silane modification, and priming on the particle's surface, annealing that can relax the stress imposed to hollow fiber and result in higher packing density of polymer chains, and the introduction of a LMWA agent between the polymer matrix and inorganic particles.

There have been numerous attempts to incorporate zeolite particles in polymer matrices in water purification applications and for gas separation due to its superior separation properties and size exclusion. Applications of zeolite-MMMs were re-evaluated for a variety of industrial processes, including water purification, medical industry, catalytic, and gas separation. However, despite its advantages, there are still issues and difficulties associated with zeolite-MMMs that have restricted their wider applications.

It can be concluded that the advancements in the application and fabrication of zeolite-MMM needs further intensive investigations. Future research should be conducted with the aim of developing new techniques that provide better understanding of zeolite incorporation into polymer structures. New materials should also be considered as a way of reducing the fouling concerns. Additional study is necessary for an improved understanding of the basic transport mechanism occurring through the MMMs. The next generation MMMs must be developed with nano-size fillers and without aggregation so as to improve their separation properties severely needed in the membrane industry. Some results indicate that the nanosize zeolite particles incorporated in MMMs offer better performance in comparison with micron size particles. New additives and modification agents should be produced to improve adhesion between polymer and inorganic fillers. In conclusion, despite of all the identified problems, MMM technology with zeolites could be considered a strong candidate for modern purification industry due to the remarkable properties of polymeric and inorganic zeolite materials.

Acknowledgements

The authors would like to acknowledge the Department of Chemical and Biological Engineering at the University of Saskatchewan for the support provided.

Author details

Mahboobeh Maghami and Amira Abdelrasoul*

*Address all correspondence to: amira.abdelrasoul@usask.ca

Department of Chemical and Biological Engineering, University of Saskatchewan, Saskatoon, Saskatchewan, Canada

References

[1] Aroon MA, Ismail AF, Matsuura T, Montazer-Rahmati MM. Performance studies of mixed matrix membranes for gas separation: A review. Separation and Purification Technology. 2010;**75**:229

[2] Mahajan R, Koros W, Thundyil M. Mixed matrix membranes: Important and challenging! Membrane Technology. 1999;**19**:6

[3] Ahn J, Chung W-J, Pinnau I, Guiver MD. Polysulfone/silica nanoparticle mixed-matrix membranes for gas separation. Journal of Membrane Science. 2008;**314**:123

[4] Celik E, Park H, Choi H, Choi H. Carbon nanotube blended polyethersulfone membranes for fouling control in water treatment. Water Research. 2011;**45**:274

[5] Peng F, Hu C, Jiang Z. Novel ploy (vinyl alcohol)/carbon nanotube hybrid membranes for pervaporation separation of benzene/cyclohexane mixtures. Journal of Membrane Science. 2007;**297**:236

[6] Peng F, Pan F, Sun H, Lu L, Jiang Z. Novel nanocomposite pervaporation membranes composed of poly (vinyl alcohol) and chitosan-wrapped carbon nanotube. Journal of Membrane Science. 2007;**300**:13

[7] Kim J, Van der Bruggen B. The use of nanoparticles in polymeric and ceramic membrane structures: Review of manufacturing procedures and performance improvement for water treatment. Environmental Pollution. 2010;**158**:2335

[8] Genné I, Kuypers S, Leysen R. Effect of the addition of ZrO_2 to polysulfone based UF membranes. Journal of Membrane Science. 1996;**113**:343

[9] Ng LY, Leo CP, Mohammad AW. Optimizing the incorporation of silica nanoparticles in polysulfone/poly(vinyl alcohol) membranes with response surface methodology. Journal of Applied Polymer Science. 2011;**121**:1804

[10] Yang Y, Zhang H, Wang P, Zheng Q, Li J. The influence of nano-sized TiO_2 fillers on the morphologies and properties of PSf UF membrane. Journal of Membrane Science. 2007;**288**:231

[11] Ge L, Zhu Z, Li F, Liu S, Wang L, Tang X, Rudolph V. Modification of $NaYF_4$:Yb,Er@SiO_2 nanoparticles with gold Nanocrystals for tunable green-to-red Upconversion emissions. Journal of Physical Chemistry C. 2011;**115**:6661

[12] Haider MS, Shao GN, Imran SM, Park SS, Abbas N, Tahir MS, Hussain M, Bae W, Kim HT. Aminated polyethersulfone-silver nanoparticles (AgNPs-APES) composite membranes with controlled silver ion release for antibacterial and water treatment applications. Materials Science and Engineering. 2016;**62**:732

[13] Brame J, Li Q, Alvarez PJ. Nanotechnology-enabled water treatment and reuse: Emerging opportunities and challenges for developing countries. Trends in Food Science and Technology. 2011;**22**:618

[14] Urtiaga A, Casado C, Ortiz I. Pervaporative dehydration of industrial solvents using a zeolite NaA commercial membrane. Separation and Purification Technology. 2003;**32**:207

[15] Ciobanu G, Carja G, Cioban O. Use of SAPO-5 zeolite–filled polyurethane membranes in wastewater treatment. Desalination. 2008;**222**:197

[16] Han R, Zhang S, Liu C, Wang Y, Jian X. Effect of NaA zeolite particle addition on poly(phthalazinone ether sulfone ketone) composite ultrafiltration (UF) membrane performance. Journal of Membrane Science. 2009;**345**:5

[17] Hilal N, Khayet M, Wright CJ. Membrane Modification: Technology and Applications. Boca Raton, FL: CRC Press; 2012

[18] Sano T, Yanagishita H, Kiyozumi Y, Mizukami F, Haraya K. Separation of ethanol/water mixture by silicalite membrane on pervaporation. Journal of Membrane Science. 1994;**95**:221

[19] Liu Q, Noble DR, Falconer JL, Funke HH. Organics/water separation by pervaporation with a zeolite membrane. Journal of Membrane Science. 1996;**117**:163

[20] Sano T, Ejiri S, Yamada K, Kawakami Y, Yanagishita H. Separation of acetic acid-water mixtures by pervaporation through silicalite membrane. Journal of Membrane Science. 1997;**123**:225

[21] Qiao X, Chung TS, Rajagopalan R. Zeolite filled P84 co-polyimide membranes for dehydration of isopropanol through pervaporation process. Chemical Engineering Science. 2006;**61**:6816

[22] Dorosti F, Moghadam F. Fabrication and characterization of polysulfone/polyimide–zeolite mixed matrix membrane for gas separation. Chemical Engineering Journal. 2011;**171**:1469

[23] Hoek EMV, Ghosh AK, Huang X, Liong M, Zink JI. Physical–chemical properties, separation performance, and fouling resistance of mixed-matrix ultrafiltration membranes. Desalination. 2011;**283**:89

[24] Rezakazemi M, Shahidi K, Mohammadi T. Hydrogen separation and purification using crosslinkable PDMS/zeolite a nanoparticles mixed matrix membranes. International Journal of Hydrogen Energy. 2012;**37**:14576

[25] Ciobanu G, Carja G, Ciobanu O. Structure of mixed matrix membranes made with SAPO-5 zeolite in polyurethane matrix. Microporous and Mesoporous Materials. 2008;**115**:61

[26] Jeong BH, Hoek EM, Yan Y, Subramani A, Huang X, Hurwitz G, Jawor A. Interfacial polymerization of thin film nanocomposites: A new concept for reverse osmosis membranes. Journal of Membrane Science. 2007;**294**:1

[27] Clarizia G, Algieri C, Regina A, Drioli E. Zeolite-based composite PEEK-WC membranes: Gas transport and surface properties. Microporous and Mesoporous Materials. 2008;**115**:67

[28] Li Y, Guan HM, Chung T-S, Kulprathipanja S. Effects of novel silane modification of zeolite surface on polymer chain rigidification and partial pore blockage in polyethersulfone (PES)–zeolite A mixed matrix membranes. Journal of Membrane Science. 2006;**275**:17

[29] Ismail AF, Kusworo TD, Mustafa A. Enhanced gas permeation performance of polyethersulfone mixed matrix hollow fiber membranes using novel Dynasylan Ameo silane agent. Journal of Membrane Science. 2008;**319**:306

[30] Duval JM, Kemperman AJB, Folkers B, Mulder MHV, Desgrandchamps G, Smolders CA. Preparation of zeolite filled glassy polymer membranes. Journal of Applied Polymer Science. 1994;**54**:409

[31] Yong HH, Park HC, Kang YS, Won J, Kim WN. Zeolite-filled polyimide membrane containing 2,4,6-triaminopyrimidine. Journal of Membrane Science. 2001;**188**:151

[32] Mahajan R, Burns R, Schaeffer M, Koros WJ. Challenges in forming successful mixed matrix membranes with rigid polymeric materials. Journal of Applied Polymer Science. 2002;**86**:881

[33] Şen D, Kalıpçılar H, Yilmaz L. Development of polycarbonate based zeolite 4A filled mixed matrix gas separation membranes. Journal of Membrane Science. 2007;**303**:194

[34] Alpatova A, Meshref M, McPhedran KN, Gamal El-Din M. Composite polyvinylidene fluoride (PVDF) membrane impregnated with Fe_2O_3 nanoparticles and multiwalled carbon nanotubes for catalytic degradation of organic contaminants. Journal of Membrane Science. 2015;**490**:227

[35] Chung T-S, Jiang LY, Li Y, Kulprathipanja S. Mixed matrix membranes (MMMs) comprising organic polymers with dispersed inorganic fillers for gas separation. Progress in Polymer Science. 2007;**32**:483

[36] Moore TT, Koros WJ. Non-ideal effects in organic–inorganic materials for gas separation membranes. Journal of Molecular Structure. 2005;**739**:87

[37] Merkel TC, He Z, Pinnau I, Freeman BD, Meakin P, Hill AJ. Effect of nanoparticles on gas sorption and transport in poly (1-trimethylsilyl-1-propyne). Macromolecules. 2003;**36**:6844

[38] Ismail AF, Rahim RA, Rahman WAWA. Characterization of polyethersulfone/Matrimid® 5218 miscible blend mixed matrix membranes for O_2/N_2 gas separation. Separation and Purification Technology. 2008;**63**:200

[39] Li Y, Chung TS, Huang Z, Kulprathipanja S. Dual-layer polyethersulfone (PES)/BTDA-TDI/MDI co-polyimide (P84) hollow fiber membranes with a submicron PES–zeolite beta mixed matrix dense-selective layer for gas separation. Journal of Membrane Science. 2006;**277**:28

[40] Hu CC, Liu TC, Lee KR, Ruaan RC, Lai JY. Zeolite-filled PMMA composite membranes: influence of coupling agent addition on gas separation. Desalination. 2006;**193**:14

[41] Karatay E, Kalıpçılar H, Yılmaz L. Preparation and performance assessment of binary and ternary PES-SAPO 34-HMA based gas separation membranes. Journal of Membrane Science. 2010;**364**:75

[42] Husain S, Koros WJ. Mixed matrix hollow fiber membranes made with modified HSSZ-13 zeolite in polyetherimide polymer matrix for gas separation. Journal of Membrane Science. 2007;**288**:195

[43] Xu L, Rungta M, Koros WJ. Matrimid® derived carbon molecular sieve hollow fiber membranes for ethylene/ethane separation. Journal of Membrane Science. 2011;**380**:138

[44] Khan AL, Cano-Odena A, Gutie' rrez B, Minguillo' n C, Vankelecom IFJ. Hydrogen separation and purification using polysulfone acrylate–zeolite mixed matrix membranes. Journal of Membrane Science. 2010;**350**:340

[45] Vu DQ, Koros WJ, Miller SJ. Mixed matrix membranes using carbon molecular sieves: I. Preparation and experimental results. Journal of Membrane Science. 2003;**211**:311

[46] Junaidi MUM, Khoo CP, Leo CP, Ahmad A. The effects of solvents on the modification of SAPO-34 zeolite using 3-aminopropyl trimethoxy silane for the preparation of asymmetric polysulfone mixed matrix membrane in the application of CO_2 separation. Microporous and Mesoporous Materials. 2014;**192**:52

[47] Pechar TW, Tsapatsis M, Marand E, Davis R. Preparation and characterization of a glassy fluorinated polyimide zeolite-mixed matrix membrane. Desalination. 2002;**146**:3

[48] Pechar TW, Kim S, Vaughan B, Marand E, Tsapatsis M, Jeong HK, Cornelius CJ. Fabrication and characterization of polyimide–zeolite L mixed matrix membranes for gas separations. Journal of Membrane Science. 2006;**277**:195

[49] Şen D, Kalıpçılar H, Yılmaz L. Gas separation performance of polycarbonate membranes modified with multifunctional low molecular-weight additives. Separation Science and Technology. 2006;**41**:1813

[50] Li Y, Chung TS, Cao C, Kulprathipanja S. The effects of polymer chain rigidification, zeolite pore size and pore blockage on polyethersulfone (PES)-zeolite A mixed matrix membranes. Journal of Membrane Science. 2005;**260**:45

[51] Kulprathipanja S, Charoenphol J. U.S. Mixed Matrix Membrane for Separation of Gases, Patent 6,726,744, 2004

[52] Dolveck JY, Dai GH, Moser P, Pineri M, Aldebert P, Escoubes M, Avrillon R, Mileo JC. Materials Science Forum. 1992 1549, 105

[53] Li Y, Krantz WB, Chung TS. A novel primer to prevent nanoparticle agglomeration in mixed matrix membranes. AIChE Journal. 2007;**53**:2470

[54] Hillock AMW, Mille SJ, Koros WJ. Crosslinked mixed matrix membranes for the purification of natural gas: Effects of sieve surface modification. Journal of Membrane Science. 2008;**314**(1-2):193

[55] Chen XY, Ghaffari, Nik O, Rodrigue D, Kaliaguine S. Polymer. 2012;**3**:3269

[56] Ward JK, Koros WJ. Crosslinkable mixed matrix membranes with surface modified molecular sieves for natural gas purification: I. Preparation and experimental results. Journal of Membrane Science. 2011;**377**:75

[57] Tin PS, Chung TS, Jiang LY, Kulprathipanja S. Carbon–zeolite composite membranes for gas separation. Carbon. 2005;**43**:2025

[58] Zimmerman CM, Singh A, Koros WJ. Tailoring mixed matrix composite membranes for gas separations. Journal of Membrane Science. 1997;**137**:145

[59] Lind ML, Ghosh AK, Jawor A, Huang X, Hou W, Yang Y, Hoek EMV. Influence of zeolite crystal size on zeolite-polyamide thin film Nanocomposite membranes. Langmuir. 2009;**25** 10139

[60] Kim SH, Kwak SY, Sohn BH, Park TH. Design of TiO_2 nanoparticle self-assembled aromatic polyamide thin-film-composite (TFC) membrane as an approach to solve biofouling problem. Journal of Membrane Science. 2003;**211**:157

[61] Maa N, Weia J, Liao R, Tanga CY. Zeolite-polyamide thin film nanocomposite membranes: Towards enhanced performance for forward osmosis. Journal of Membrane Science. 2012;**405**:149

[62] Madhumala MS, Sankarshan D, Sridhar S. Selective extraction of lactic acid from aqueous media through a hydrophobic H-Beta zeolite/PVDF mixed matrix membrane contactor. Industrial and Engineering Chemistry Research. 2014;**53** 17770

[63] Pechar T, Kim W, Vaughan S, Marand B, Baranauskas E, Riffle V, Jeong HK. Preparation and characterization of a poly(imide siloxane) and zeolite L mixed matrix membrane. Journal of Membrane Science. 2006;**277**:210

[64] Dechnik J, Sumby CJ, Janiak C. Enhancing mixed-matrix membrane performance with metal–organic framework additives. Crystal Growth & Design. 2017;**17**:4467

[65] Harold B, Jeazet T, Koschine T, Staudt C, Raetzke K, Janiak C. Correlation of gas permeability in a metal-organic framework MIL-101(Cr)–Polysulfone mixed-matrix membrane with free volume measurements by positron annihilation lifetime spectroscopy (PALS). Membranes. 2013;**3**:331

[66] Wales MD, Joos LB, Traylor WA, Pfromm P, Rezac M. Composite catalytic tubular membranes for selective hydrogenation in three phase systems. Catalysis Today. 2015. DOI: 10.1016/j.msec.2016.02.025

[67] Gu Y, Emin C, Remigy JC, Favier I, Gomez M, Noble RD, Lahitte JF. Hybrid catalytic membranes: Tunable and versatile materials for fine chemistry application. Materials Today Proceedings. 2016;**3**:419

[68] Langhendries G, Baron GV. Mass transfer in composite polymer-zeolite catalytic membranes. Journal of Membrane Science. 1998;**141**:265

[69] Jia M, Peinemann KV. Molecular sieving effect of zeolite filled silicone rubber membranes. Journal of Membrane Science. 1991;**57**:289

[70] Marambio-Jones C, Hoek EM. A review of the antibacterial effects of silver nanomaterials and potential implications for human health and the environment. Journal of Nanoparticle Research. 2010;**12**:1531

[71] Muntha ST, Siddiq M, Kausar A, Khan K. Mixed matrix membranes of polysulfone/polyimide reinforced with modified zeolite based filler: Preparation, properties and application. Chinese Journal of Polymer Science. 2018;**36**:65

[72] Wind JD, Paul DR, Koros WJ. Natural gas permeation in polyimide membranes. Journal of Membrane Science. 2004;**228**:227

Chapter 8

Characterizations and Industrial Applications for Cement and Concrete Incorporated Natural Zeolite

Iván Ayoseth Chulines Domínguez,
Youness Abdellaoui, Mohamed Abatal and
Cristóbal Patiño-Carachure

Additional information is available at the end of the chapter

http://dx.doi.org/10.5772/intechopen.74953

Abstract

Zeolites have been widely used in various industries, leading to a high commercial value; this is mainly due to the wide diversity of naturally occurring species and the ability to synthesize new types. In the cement and concrete industry, natural zeolite is a popular natural pozzolanic material in some regions of the world owing to their economic, environmental, and technical advantages, among others, used pozzolanic materials. Many works have reported the use of natural zeolite as substituent material for cement in mortar and concrete. Generally, the use of natural zeolite can overcome environmental and economic problems associated with the use of high quantity of cement; furthermore, it is shown a strength enhancement and durability improvement properties of cement and concrete composites. In this context, this chapter strives to review the application of natural zeolite as pozzolan in cement and concrete composites, its characteristic, its proper incorporation, and each of the influencing parameters. In addition, the elaboration methods, textural and mechanical characterization, and applications of these composites will be treated.

Keywords: cement substitution, concrete, hydration, pozzolanic material, natural zeolite

1. Introduction

The number of zeolites is constantly increasing; currently, the commission of structures of the International Zeolite Association (IZA) recognizes 232 unique structures that have been approved and have been assigned three letters of code [1]. The chemistry of zeolite has been

IntechOpen

© 2018 The Author(s). Licensee IntechOpen. This chapter is distributed under the terms of the Creative Commons Attribution License (http://creativecommons.org/licenses/by/3.0), which permits unrestricted use, distribution, and reproduction in any medium, provided the original work is properly cited.

a subject of significant interest due to the ion exchange properties of zeolite, crystallinity, thermal stability, and well-defined molecular size closed structures [2]. The code ASTM-618 (American Society for Testing Materials) defines pozzolans as siliceous or aluminum-siliceous materials, which by themselves have little to no cementing value, but when they are finely divided and in the presence of water and calcium hydroxide (Cal), they react chemically at room temperature to form cementitious agents [3].

Concrete made from Portland cement is the most widely used construction material today, mainly due to its cost-benefit ratio, in terms of compressive strength. Its manufacture involves the release of approximately 900 kg of carbon dioxide per 1000 kg of produced cements. Likewise, this amount of cement demands the use of 1693 kg of water and 4798 MJ in energy resources [4]. This is the importance of reducing the environmental impact that the manufacture of the same produces. The use of mineral additions in the production of concrete is a technologically possible alternative. However, its use requires high standards of assurance and quality assurance, similar to those of cement [5].

The extent of the benefits provided by the use of blended cements increases with increasing content of additives in blended Portland cements. However, the content of additives in blended Portland cements, especially for natural pozzolans, is limited by some factors, such as an increase in water requirement and a decrease in the rate of strength development of the cementitious systems. It has been found that the blended cements containing high volume (55% by weight) of natural pozzolans (volcanic tuff) possess lower 28-day compressive strength when compared to the reference Portland cement, although they show similar strength values at 91 days of age [6, 7]. Therefore, the production of high-volume natural pozzolan blended cements, which are able to compete against ordinary Portland cement, requires natural pozzolans exhibiting significantly high-strength activity.

In this chapter, we intend to review the literature available on these topics, addressing structural, mineralogical, and morphological properties, in the case of zeolites, and manufacturing processes, characterization, evaluation, and application, in the case of cement. As well each of the parameters influences the formation of cementing pastes, such as hydration, porosity, transport properties, durability, and carbonation, among others.

2. Properties of natural zeolite

2.1. Pozzolanic activity surface area

Pozzolans are materials with an amorphous and aluminous siliceous or siliceous content, which react with calcium hydroxide in the presence of water to form cementitious hydration products [8]. Among the most common natural pozzolanic materials, such as fly ash and silica fume, is zeolite, which is used in some regions of the world, due to its lower cost and accessibility [9, 10]. Zeolites generally show pozzolanic activity due to their structural characteristics, and their use as additions in cements provides additional technical advantages to construction materials [11].

The pozzolanic properties of natural zeolites are determined by their high sorption ability, ion exchange potential, and specific structure. Their action involves various steps, including

cation exchange; dissolution and/or breakdown of the zeolitic structure; possible formation of transient gel phases; and precipitation of hydrated calcium silicates and aluminates [12].

There are different methods of work for the evaluation of pozzolanic activity. In general, these methods are classified as indirect or direct, depending on the parameter to be studied [13]. Direct methods monitor the presence of $Ca(OH)_2$ and its subsequent reduction in abundance over time, as the pozzolanic reaction proceeds, using analytical methods such as X-ray diffraction (XRD), thermogravimetric analysis (TGA), or assessment chemistry.

The Frattini test is a commonly used direct method involving chemical titration to determine the concentrations of Ca^{2+} and OH^- dissolved in a solution containing Portland cement and the test pozzolan. This method has been used to measure the pozzolanic activity of metakaolin [14], catalytic cracking residues [15], fly ash [16], and zeolites [17].

The saturated lime method is a simplified version of the Frattini test, in which pozzolan is mixed with a saturated solution of lime (slaked lime, $Ca(OH)_2$) instead of Portland cement and water. The amount of lime set by the pozzolan is determined by measuring the residual dissolved calcium [18].

Indirect test methods measure a physical property of a test sample, which indicates the degree of pozzolanic activity. This may involve the measurement of properties such as compressive strength, electrical conductivity, or heat evolution by conduction calorimetry. The results of an indirect pozzolanic activity test are often corroborated by direct tests to confirm that pozzolanic reactions are occurring [19–22].

2.2. Ion exchange

Zeolites naturally occur from volcanic origin and belong to the family of hydrated aluminosilicates. Their microporous structures can accommodate a wide variety of cations, which compensate the negative charge created by the substitution of Si by Al. Therefore, natural zeolites appear as cation exchangers in many applications, thanks to this property. Some of the main applications of zeolites in this area include the selective treatment of wastewater, extraction of ammonia, odor control, extraction of heavy metals from nuclear, mining and industrial wastes, soil conditioning for agricultural use, and even as an additive for animal feedstock [23].

Among all identified zeolites, clinoptilolite is the most abundant natural zeolite. In the structure of the zeolite, there are three relatively independent components: the aluminosilicate system, the interchangeable cations, and the zeolitic water. The simplified empirical formula of zeolites is:

$$M^{n^+}_{y/n}\, Al_2\, Si_{1-x}\, O_2 . y\, H_2O \tag{1}$$

where x can vary from 0 to 0.5 and M^{n+} represents Alkali and alkaline earth metals. The structure of aluminosilicates is the most conserved and stable component and defines the type of structure water molecules that can be presented in voids of large cavities and joined between ion systems and ions interchangeable through aqueous bridges. Water can also serve as a bridge between interchangeable cations.

The channels of the natural zeolites are predominantly occupied by Na^+, K^+, Ca^{2+}, and H_2O, as well as traces of Mg^{2+}, Ti^{4+}, Pd^{2+}, K^+, and Ba^{2+}. Among them, Na^+, K^+, Ca^{2+}, and Mg^{2+} can be

exchanged with NH_4^+ ions. The type and density of interchangeable cations influence the stability of the cavities and the thermal behavior of a zeolite [24–27].

2.3. Expansion at elevated temperatures

Concrete is more durable against elevated temperature and fire effects than many other construction materials. Although ordinary concrete is considered to have a satisfactory fire resistance, it can lose 40–60% of its original strength upon exposure to 500°C [28]. Bilim [29] reported mortars containing zeolite show generally better performance to high temperatures about 900°C.

Negative thermal expansion (NTE) is an unusual phenomenon in which materials shrink in volume when heated (or expand when cooled). It has only been observed in a small number of solids, including some metallic oxides, cyanide metal, polymers, and zeolites [30]. It is important to understand how zeolites behave as a function of temperature. In recent years, research has been carried out on NTE in purely siliceous zeolitic structures [31, 32] and with a little less attention [31, 33] to aluminum-containing zeolites, in which it is known that structures and properties are particularly sensitive to extra-structural charge balancing cations and host molecules in the pores.

Water is an important guest molecule in the pore system of natural and synthetic zeolites. Adsorbent and catalytic properties of zeolites are also strongly affected by their water content. Cations seek the most energy-stable positions, and these positions play an important role in the catalytic activity.

This subject was investigated by Ilić and Wettstein [34], who examined three distinct temperature ranges for volumetric thermal expansion. Associates with the dehydration of coordinated water molecules and with transverse vibrations of bridging oxygen atoms result in the reduction in the bonding angle.

2.4. Desorption of water at low humidities

As already mentioned, zeolite is a porous solid with a large capacity to house water molecules and can be used as a pozzolanic aggregate. The efficiency of porous aggregates as an internal curing agent in concrete depends on its water absorption and desorption characteristics. The desorption behavior of zeolite and other porous aggregates depends on the structure of their pores and mainly on the porosity size distribution. In general, a thick pore structure will lead to better desorption behavior [35–37].

Ghourchian et al. [38] were conducted a study of the performance of the porous aggregates and concluded that the water desorption of the zeolites is closely related to their microstructure. For a proper desorption, a thick-pored structure is needed with a high proportion of well-interconnected pores. While, in the case of zeolites, despite having a high-water adsorption capacity, they have a fine pore structure, which leads to retaining the water absorbed.

2.5. Re-adsorption of water at high humidities

Zeolites are selective adsorbents for the removal of carbon dioxide, water vapor, and other impurities from the mixtures. The impurities adversely affect the capacity of the adsorbents used for the separation or purification. Water is a strongly adsorbed component in zeolite [39].

Due to the nature of the cation exchange, natural zeolites show a high performance in the adsorption of cations in aqueous solution such as ammonium and heavy metals. However, zeolites show varied ion selectivity and competitive adsorption for multicomponent system [27]. In addition, these materials are not good adsorbents for the adsorption of anionic and organic ions. Surface modification with cationic surfactant can change the surface charge of the natural zeolite, making them applicable for adsorption of anions and organics. Most zeolites when heated give off water continuously rather than in separate stages at certain temperatures. The dehydrated zeolite can then reabsorb the original amount of water when exposed to water vapor. Recent investigation has shown that some zeolites such as phillipsite and gismondite lose and gain water in a stepwise manner. All-silica zeolites are chemically and hydrothermally more stable than aluminum containing ones and are therefore preferred for membrane application, including for dehydration, even though these types of membranes are hydrophobic [40].

The adsorption characteristics of any zeolite depend on the detailed chemical/structural composition of the adsorbent. The Si/Al ratio, the type of cation, the number, and the location are particularly influential in the adsorption. These properties can be modified by various chemical treatments to improve the separation efficiency of the natural raw zeolite. Acid/base treatment and impregnation with surfactant by ion exchange are commonly used to change the hydrophilic/hydrophobic properties for the adsorption of various ions or organic [27].

3. Effects of natural zeolite on the properties of cement and concrete composites

3.1. Mechanical properties

In general, the higher the cement replacement by natural zeolite has the lower the compressive strength. However, the percentages of reduction in resistance generally decrease with increasing age in cement. This behavior may be related to the pozzolanic activity of the natural zeolite. In terms of compressive strength, it appears that natural zeolite performs better in mixed cement compounds with lower water-cementitious material (w/cm) ratio [41].

In term of compressive strength, it seems that natural zeolite performs better in blended cement composites with lower w/cm ratios. Ahmadi and Shekarchi [42] showed that the concretes containing natural zeolite with a w/cm ratio of 0.40 displayed higher compressive strength than the control mixture at the ages of 3, 7, 28, and 90 days, whereas contrary results were obtained for the concretes with a w/cm ratio of 0.5 in the present study. Markiv et al. [43] showed, recently, that the substitution of cement by zeolite resulted in some reduction in strength until 90 days of hardening, but after 180 days, compressive strength of concretes containing zeolite exceeds the strength of concrete without zeolite.

Uzal and Turanlı [44] reported the similar compressive strength of mortar with 55% zeolite in the binder to that of 100% Portland cement mortar, but this could only be achieved using superplasticizers. Karakurt and Topçu [45] found 30% replacement of Portland cement by zeolite in their blended cement mortars as optimum; the compressive strength was similar to the reference mortar. Valipour et al. [46] observed a fast decrease in the compressive strength

of concrete with the increasing amount of zeolite (10–30% of the mass of Portland cement) in the mix, even with an increasing superplasticizer dosage.

3.2. Alkali-silica reaction

It is generally recognized that the addition of pozzolan reduces the calcium hydroxide content in cement paste and improves the permeability of concrete [47]. The most important concerns in the design of durable concrete are the alkali-silica reaction (ASR) and sulfate attack.

ASR causes the premature deterioration in concrete. Alkali hydroxides present in the concrete pore solution react with amorphous or poorly crystalline silica phases in aggregates, forming a gel that imbibes water and expands [48]. The expansive pressure generated by the hydrated alkali silicate has been widely believed to induce cracking and deterioration of concrete. However, this notion may not be necessarily correct. Concrete is a porous material, and the hydrated alkali silicate is rheologically a fluid material that can slowly diffuse into the pores and preexisting cracks to lose its expansive pressure. The diffused alkali silicate has been proposed to generate an expansive pressure by reacting with Ca^{2+} ions [49].

3.3. Transport properties

The transport properties of concrete with the addition of zeolite have been studied by Ahmadi and Shekarchi [42] and Najimi et al. [41], who found a significant reduction in the penetration of water and chlorides, in the concrete with natural zeolite. On the other hand, Valipour et al. [50] reported that water sorptivity and gas permeability increase with the increase of zeolite in the mixture. Similar results were obtained for the oxygen permeability of Ahmadi and Shekarchi [42] but only for the dose of zeolite greater than 10%.

The liquid water transport parameters increase with the increasing addition of zeolite in the mixed binder. This is due to the pore distribution, that is, the volume of capillary pores, which is the most important factor, in the capacity of a porous medium to transport water in liquid form. In studies conducted by Vejmelková et al. [51], it was found that, for lower zeolitic contents, up to 20%, the values of water absorption coefficient and apparent moisture diffusivity were still acceptable. However, for high levels of cement replacement, the acceleration of water transport is so high that it could present a concrete durability risk.

Ahmadi et al. [52] reported that natural zeolitic addition in concrete results in better water absorption, water penetration, and electrical resistivity, and the ternary mixtures containing natural zeolite with silica fume or fly ash perform best in water permeability and chloride penetration tests.

3.4. Durability properties

3.4.1. Sulfate and acid attack resistance

The durability of a concrete is a determining feature for its use, and this is due to the different corrosive environments to which it is exposed, including marine construction or hydraulic engineering. One of the important factors of this characteristic of concrete is the type of cement.

It has been shown that the use of pozzolanic additives for cements increases their resistance to corrosion, due to the high impermeability, the decrease in the content of $Ca(OH)_2$, and the reduction in the presence of capillary pores in the matrix. In fact, it hinders the penetration of aggressive media [53]. Concrete can be attacked by acids both internally and externally. The existence of different kinds of acid in the environment around the concrete causes a great reduction in the pH of the concrete, and the reaction between the acids and the hydrated and unhydrated cement finally leads to the deterioration of the concrete. The primary effect of any type of acid attack on concrete is the dissolution of the cement paste matrix [54].

Małolepszy and Grabowska [55] carried out a study dedicated to studying the sulfate resistance of a cementing paste with zeolitic addition. They confirmed the beneficial effect of the zeolitic additive for cement mortars because those containing zeolite did not show visible damage in the surface in an aggressive solution of sulfate, while in the mortar that did not possess it, I present surface microcracks pronounced. Exfoliation of corners and colors changes (yellow and gray incursions on the walls of the samples).

3.4.2. Drying shrinkage

The contraction is a phenomenon in which the concrete reduces its volume with time. The internal and external drying of the concrete is the main factor that causes the contraction. Internal drying, also known as self-desiccation, is caused by the consumption of water in the hydrating cement paste and the resulting creation of interfacial menisci between the pore fluid and the vapor in progressively smaller pores [56]. The creation of meniscus leads to the accumulation of capillary pressure that puts the solids under compression and causes a macroscopic contraction, called autogenous contraction [56, 57]. External drying takes place due to the evaporation of water from the surface of the concrete to the ambient air or due to the migration of water to adjacent members. The evaporation of moisture from the surface of the fresh concrete can cause cracking of the plastic shrinkage [58], and a greater moisture loss of the hardened concrete can cause shrinkage by drying [59].

Generally, the durability properties of concrete improved by partial replacement of cement with natural zeolite. However, the concrete that contains 15% of natural zeolite achieves a suitable drying shrinkage. The latter does not have a satisfactory performance in the acid environment [41].

3.4.3. Freeze and thaw resistance

The pores can have an effect on the properties of the material in different ways. The compressive strength is primarily related to the total porosity, the size of pores and their distribution, the size and form of the biggest pores, and the relation between the pores. Shrinking is the function of energy exchange on the surface of pore walls. Durability depends on freeze-thaw resistance and is controlled by the volume of air entrained in the pores and spaces between the pores [60].

Water absorption and freeze-thaw resistance of hardened cement paste depend on the size of pores and capillaries, their type and distribution, and the closing of the pores. Closed and small

pores are not filled with water completely. Pores that are not filled up with water are called reserve pores. In freezing conditions, some water from fully filled pores may move to these reserve pores and thus create a space for ice expansion. The distance between filled and unfilled pores must be small, so that the freezing water would move from filled to unfilled pores [60].

Capillary pores in hardened cement paste are formed through the evaporation of excessive water used in producing the cement paste. Usually, the cement paste is made using more water, and it is necessary for chemical reactions that occur during the setting of concrete. According to A. K. Kallipi, capillary pores are open and easily fill with water. The destructive effect during freezing depends on the amount of water in hardened cement paste. Presumably, the bigger amount and size of the pores reduce the freeze-thaw resistance of concrete. Furthermore, it is important to mention that the concrete prepared with saturated and dry recycled aggregates exhibits poorer freeze-thaw resistance, whereas better results obtained from the concrete made with the semi-saturated aggregates [61].

3.4.4. Carbonation

When a cementitious paste begins to harden with an air cure, and after the first minute of hydration, it is subjected to the action of carbon dioxide ions (CO_{3-}^{2}) contained in the air, which reacts with Ca^{2+} ions of the portlandite, ettringite, and the silica gel of calcium in the form of Ca-carbonates ($CaCO_3$). This carbonation of the hydrate products is provided in the following schemes [62]:

$$Ca(OH)_2 + CO_2 \rightarrow CaCO_3 + H_2O, \tag{2}$$

$$3CaO \cdot 2SiO_2 \cdot 3H_2O + 3CO_2 \rightarrow 3CaCO_3 + 2SiO_2 + 3H_2O, \tag{3}$$

$$\begin{aligned} &3CaO \cdot Al_2O_3 \cdot 3CaSO_4 \cdot 32H_2O + 3CO_2 \rightarrow 3CaCO_3 + 3(CaSO_4 \cdot 2H_2O) \\ &+ Al_2O \cdot x\,H_2O + (26 - x)\,H_2O \end{aligned} \tag{4}$$

The air-curing conditions normally increase carbonation and cause incomplete hydration, self-neutralization, and drying shrinkage. These effects are most probably caused by decreasing the capacity for retaining sufficient water during the hydration and pozzolanic reactions. The depth of the carbonate layer formed depends on the contact time with CO_2 and its concentration in the surrounding environment as well as the diffusion coefficient of the hardened cement paste [63–65]. As the air-curing conditions are more important for long-term reactions than for short-term ones, the C2S phase, which usually reacts after 21 days, is the most readily affected cement phase. The volume changes, which accompany the carbonation processes, lead to the filling of empty pore volumes with Ca carbonates and densify the structure of the hardened cement paste. Groves et al. [66], the microstructure of hardened pastes of C_3S and a smoke mixture of C_3S/silica by TEM, before and after partial carbonation in a pure CO_2 atmosphere, concluded that calcium carbonate forms mainly in the outer product regions such as microcrystalline vaterite or calcite, which leads to a substantial level of carbonation of pulp in a day with a little additional carbonation in the coming days. The depth of penetration of $CaCO_3$ in the cement matrix depends on the time of contact of carbon dioxide and its concentration in the medium and on the coefficient of diffusion [67].

Lilkov et al. [62] have studied the early hydration of the cement, mixed with additives of natural zeolite (clinoptilolite), and they concluded that the process of carbonation on the surface of the cement paste takes place directly between the calcium ions of the solution and the carbon dioxide of the air without the formation of portlandite and ettringite. The depth of the carbonate layer formed depends on the contact time with the CO_2 and the rate of diffusion through the formed layer, where the crystallite size of the calcite is reduced overtime days.

3.4.5. Corrosion of steel reinforcement

The main causes of reinforcing steel corrosion are reacted with various aggressive agents, such as atmospheric carbon dioxide and chloride ions, and chemical attack throughout the service life of the concrete [68]. In ordinary Portland cement, these harmful effects can be reduced by substitute pozzolans [69]. Under a corrosive environment, concrete properties can be improved by using pozzolans such as zeolite and diatomite [68].

Steel rebars are protected against corrosion by both chemical and physical mechanisms. The chemical protection is provided by the concrete high pH (12–13), which promotes the formation of a passive film on the steel surface. On the other hand, concrete acts as a physical barrier, hindering the access of aggressive agents. However, oxygen, water, chlorides, and/or carbon dioxide can be transported through concrete, reaching the rebars and inducing the corrosion attack. The chloride ions, when above a threshold value, provoke a local breakdown of the passive film and pitting corrosion. Carbon dioxide and its hydrolysis products react with the alkaline species present in concrete, leading to pH values as low as 9 [70].

Ahmadi and Shekarchi [42] found a positive effect of zeolite in cement mortar on the resistance to alkali-silica reaction. Janotka and Krajči [71] reported an improvement of sulfate corrosion resistance of zeolite-containing concrete. Similar effects of zeolite on alkali-silica reaction and sulfate resistance were observed by Karakurt and Topçu [45]. On the other hand, Najimi et al. [41] reported a significant strength reduction of zeolitic concrete after exposure to sulfuric-acid environment, that is, ~20% after 356 days when compared with ~5% for reference Portland-cement concrete.

3.4.6. Chloride-induced corrosion

Besides eco-friendly, concrete should be sustainable and durable due to its use in infrastructure applications, which are mostly in aggressive environments, such as harsh marine environments with highly possible chloride-induced corrosion. Valipour et al. [72] reported that natural zeolite from a durability point of view in harsh marine environments could be a good option for replacement of cement even comparing with metakaolin and silica fume, which would be beneficial even from environmentally friendly point of view. Because concrete containing 20% replacement level in splash exposure showed chloride diffusion resistance even better than metakaolin with 5% replacement level and silica fume with 5 and 7.5% replacement level.

Several studies have indicated that lowering the w/b ratio and adding different types of pozzolanic materials to the mix can improve the compressive strength, durability, and permeability of concrete. Lowering the w/b ratio reduces the porosity, which thereby reduces chloride

ingress during the exposure period by as much as 25% [46]. Moreover, pozzolanic materials are being used widely as mineral admixtures to enhance the mechanical properties of concrete and thereby improve the concrete's microstructure. These admixtures, either natural or artificial, reduce the $Ca(OH)_2$ content produced during the cement hydration process and instead form C—S—H gel through the secondary reactions. This process retards the hydration process, significantly reducing the porosity and permeability of the concrete [73–75].

Valipour et al. [76] found that the partial replacement of cement by 10 and 20% natural zeolite drives a higher compressive strength at 28 days, while 30% zeolitic replacement decrease the compressive strength when compared with conventional concrete. Moreover, the use of natural zeolite to improve the durability of concrete in aggressive environments, such as the Persian Gulf, results in a concrete with appreciably low chloride permeability.

3.4.7. Heat of hydration

Nowadays, there is a discussion concerning the role of natural zeolitic effects on the blended cement hydration during the time. During the early stage of hydration, the effects of zeolite are related to the critical role played by their structure and the large surface area of the particles determining the cation ability in the pore solution and the collateral effect on stimulation of Portland cement hydration due to the low reaction degree of the zeolite [77]. The later stage is the proper pozzolanic reaction between the CH liberated during the hydration of cement and the soluble SiO_2 and Al_2O_3 present in bulk zeolite occur after 2 weeks producing compounds with cementing properties [78, 79]. Some zeolites are thermally activated [80]. Özen et al. [10], Cornejo et al. [81], and García de Lomas et al. [82] studied the early-age hydration heat of Portland cement blended with a spent zeolite catalyst in an amount of up to 35% of the mass of cement, but the composition of the applied catalysts was significantly different from the natural zeolite. Caputo et al. [83] analyzed the hydration heat development in natural zeolite samples mixed with portlandite in a 1:1 ratio.

Furthermore, Tydlitát et al. [84] concluded that natural zeolite did not react during the early age, but it causes the acceleration of cement phase's hydration. Hence, the early effects of zeolitic addition depend on their physical and chemical characteristics, and it also depends on the Portland cement composition.

4. Application of natural zeolite as pozzolan in cement and concrete composites

4.1. Characteristic

Supplementary cementitious materials (SCMs) are natural or by-product materials, which react with $Ca(OH)_2$, (CH), and form hydraulic compounds, such as hydrated calcium silicate hydrate (C—S—H) and calcium aluminate hydrate (C—A—H) [1]. Natural zeolite belongs to the group of natural SCM, whose pozzolanic activity depends on several factors (chemical and mineralogical composition, particle size distribution, specific surface area, cation-exchange capacity, Si/Al ratio of the zeolite framework, etc.) [77]. Each of these factors provides unique characteristics to each cement mix.

In the previous studies concerning the use of zeolites in concrete production, one of the most frequent topics was their pozzolanic activity as a fundamental condition for their utilization as supplementary cementitious materials (SCMs). Perraki et al. [77] reported a good pozzolanic reactivity of zeolite, 0.555 g of $Ca(OH)_2$ per 1 g of zeolite according to the Chapelle test. Ahmadi and Shekarchi [42] found out that the pozzolanic activity of zeolite was lower than silica fume but higher than fly ash.

Many studies have promoted the use of the zeolite-bearing tuffs as SCMs due to their positive influence on the long-term compressive strength and durability. Nevertheless, the variability in tuff's mineralogical and physical properties results in limited understanding of pozzolanic activity of natural zeolites.

When zeolite is added to the cement, at a level of around 10%, some characteristics are modified, such as, an increase in compressive strength [43, 85], a decrease in pore size [86, 87], and an increase in corrosion resistance to the acid solution [55, 88].

4.2. Proper incorporation

Many authors have talked about the appropriate amount of zeolite that must be incorporated into the cement, so that it improves its properties or it can maintain them. Najimi et al. [41] found out that incorporation of 15% natural zeolite in the blended binder improved compressive strength of concrete, but for concrete with 30% zeolitic content, they observed a 25% strength decrease even with adding a superplasticizer, which was not used in the reference mix; they concluded that concretes incorporating zeolite are characterized by the reduction in the heat of hydration and consequently of thermal cracking; and they also improved durability properties such as chloride ion penetration, corrosion rate, drying shrinkage, and water penetration. Ahmadi and Shekarchi [42] also reported that the incorporation of natural zeolite as a mineral admixture in concrete enhanced its durability properties. However, various types, structures, and purities of natural zeolites influence concrete strength and durability in different ways and can lead in some cases to contradictory results in experimental studies and observed an increase in compressive strength for up to 20% of natural zeolite used as Portland cement replacement, but this was achieved with an increasing amount of superplasticizer in the mixes containing zeolites. Uzal and Turanli [44] reported the similar compressive strength of mortar with 55% zeolite in the binder to that of 100% Portland cement mortar, but once again, this could only be achieved using superplasticizers; they describe that a lime reactivity of the clinoptilolite zeolite is comparable to silica fume, higher than fly ash and a non-zeolitic natural pozzolan. Therefore, calcium hydroxide as a cement hydration product combines with natural zeolite consisting of reactive SiO_2 and Al_2O_3 to form calcium hydrosilicates. Karakurt and Topçu [88] found 30% replacement of Portland cement by zeolite in their blended cement mortars as optimum; the compressive strength was similar to the reference mortar. Valipour et al. [50] observed a fast decrease in the compressive strength of concrete with the increasing amount of zeolite (10–30% of the mass of Portland cement) in the mix, even with an increasing superplasticizer dosage. Investigations of mechanical properties of concretes show that the substitution of cement by zeolite resulted in some reduction in strength until 90 days of hardening, but after 180 days, compressive strength of concretes containing zeolite exceeds the strength of concrete without zeolite. Introduction of zeolite and chemical admixtures in concrete permits the modifications of the phase composition of

cement hydration products with the formation of an extra amount of calcium hydrosilicates, hydrogelenite, and ettringite [43].

4.3. Influencing parameters

Najimi et al. [41] concluded that concretes incorporating zeolite are characterized by the reduction of the heat of hydration and consequently of thermal cracking and improved durability properties such as chloride ion penetration, corrosion rate, drying shrinkage, and water penetration. Sabet et al. [89] and Ahmadi and Shekarchi [42] also reported that the incorporation of natural zeolite as a mineral admixture in concrete enhanced its durability properties. However, various types, structures, and purities of natural zeolites influence concrete strength and durability in different ways and can lead in some cases to contradictory results in experimental studies.

Uzal and Turanli [44] reported that the type of major cation was found to be one of the probable factors governing the pozzolanic activity of clinoptilolite zeolites by affecting their degree of solubility in alkaline conditions. Experimentally demonstrated that pastes of blended cements containing a large amount of clinoptilolite tuff contain less amount of pores >50 nm when compared with Portland cement paste, which is beneficial in terms of mechanical strength and impermeability of the pastes.

4.4. Elaboration methods

The methods of preparation of cement mixtures with zeolite vary according to the type of study and parameter that is intended to know, and this is due to the constant search to improve their properties. However, there are regulations that help to delimit the use and management of pozzolans, this, if it is intended that the study has a commercial impact, or that meets the standards established for the development of mortars (**Table 1**).

Several authors have investigated how to improve the mechanical properties of cement with zeolite, and its resistance to compression is specific. Valipour et al. [50] and Chan [90] were agreed that, to improve this characteristic, cement mixtures should not exceed 45% of zeolitic addition. While if what is desired is to avoid the carbonation process of the cement, the additions should

Name	Scope
ASTM C-618	Standard specification for coal fly ash and raw or calcined natural pozzolan for use in concrete
ASTM C-191	Standard test methods for time of setting of hydraulic cement by the Vicat needle
ASTM C-33	Standard specification for concrete aggregates
ASTM C-311	Standard test methods for sampling and testing fly ash or natural pozzolans for use in Portland-cement concrete
ASTM C-1202	Standard test method for electrical indication of concrete's ability to resist chloride ion penetration
ASTM C-876	Standard test method for corrosion potentials of uncoated reinforcing steel in concrete
ASTM C150	Standard specification for Portland cement

Table 1. Standard specifications by ASTM.

not exceed 30% [62, 91, 92] because this process is more evident in the early hydration phase, but it reduces with the passage of time. It is necessary to consider that the hydration of the cement is perhaps the most important aspect because it will derive almost all the processes addressed in this article, besides being a determining factor in the cementing process of the mixture. Several researchers [84, 93, 94] concluded that the addition of zeolite to the cement paste greatly increases the early stage of hydration, and therefore, it is not recommended to exceed 40% of pozzolanic addition in the mixture. In this way, operational parameters that contribute to the development of a composite mix with the best features and operational performance can be established.

It is not enough to establish limits in the substitution of cement with pozzolans because the structure of the zeolite also plays a very important role in the interaction with the mixture; as already mentioned, there is a great variety of zeolites, each with its respective family and structure [95], and the treatment that each one must receive before its incorporation into the cementing pastes can be very different. First, it must be understood that the Si/Al ratio will define the homogeneity of the mixture and the setting process [96] with a higher percentage of alumina in their structure that will tend to have a weaker and slower setting, while those that have a very large pore diameter will facilitate the carbonation of the mixtures. There are many ways to incorporate zeolite to cement pastes, but they have in common the amorphization of the same, whether, by mechanical, chemical, or thermal methods, the main objective is to generate a correct balance between the Portland cement and the percentage of Si/Al content in the zeolite.

The dealumination is one of the most widespread methods for the control of the percentage Si/Al present in the zeolite and encompasses the aforementioned methods. In 1968, McDaniel and Maher prepared the ultra-stable Y zeolite by combining procedures for the exchange of sodium ions with ammonium and hydrothermal treatments at elevated temperatures ($T \geq 600°C$). Under the conditions of "deep bed," these treatments caused the removal of structural Al with the consequent decrease of the cell parameter. On the contrary, when the hydrothermal treatment was carried out in a "shallow bed," the protonated form of the zeolite was obtained without causing dealumination. It has been possible to dealuminate up to 98% Y zeolite by hydrothermal treatments without an appreciable loss of crystallinity.

In 1968, Kerr developed a method to dealuminate Y zeolites at low temperature (around 100°C) by using a hydrolyzing and complexing agent of aluminum such as EDTA [97] with this method; however, you cannot dealuminate above 70% without drastic losses of crystallinity.

Subsequently, the use of $SiCl_4$ at high temperatures was reported to dealuminate Y-type zeolites in a single step, quickly and with percentages of Al removal that could reach values above 90% [98].

Finally, Skeels and Breck reported a procedure in which ammonium hexafluorosilicate is used as a deadening agent, under mild conditions at low temperatures. It is a quick and simple method, but the superior level of dealumination, as with EDTA, is limited to 70% to avoid crystalline collapse.

4.5. Textural and mechanical characterization

The textural characterization of the zeolite-cement compound consists of measuring the pore size present in the element; the analysis of this porosity has as an objective to measure the surface of the pores and the volume of the same. It should be mentioned that the compound

may have microporosity or mesoporosity; as the study by Franus et al. [99], there are several ways to calculate the volume, distribution, and surface area of the pores among which are the general isotherm equation based on the combination of a modified Kelvin equation and a statistic thickness of the adsorbed film and the multilayer adsorption theory [100].

The mechanical characterization performed on cement pastes with zeolitic content does not differ from the typical mechanical compression tests (performed to see the maximum load before causing a fracture), which are carried out by means of a universal machine. However, both the size of the specimens and the laboratory conditions (temperature, pressure, and percentage of aggregates) depend on the author and the results that he intends to obtain. There is a lot of research on the mechanical state of the test tubes [41, 51, 99, 101], and it is important to mention that in most of them, the state of operation is evaluated after having been subjected to adverse media, such as chloride attack or exposure to acid media.

4.6. Special applications of these composites

At present, due to the many investigations that exist on cement with zeolitic addition, we can find large areas of opportunity for its application. However, its use as a cement for construction is the most researched application [9, 41, 93, 96], and this is obvious when the main function of this compound is to work as an alternative to ordinary cement (usually the Portland type) in the cement industry building. Although there are other applications of the same scope and not so obvious, which have not been given the same attention, among them we can find its use for the stabilization of sandy soils prior to the construction of roads [102, 103], agent for the reduction in pollutants and environmental conditions [76, 104], and its application in cementing operations carried out on the high seas and oil platforms [46, 105].

5. Concluding remarks

The partial replacement of cement is a fact that every day becomes more important; it is an activity that is already carried out and that although there are few cement producers that commercialize with these compounds, it is a great step for the reduction in emissions of CO_2. Many authors have contributed and are still investigating the properties that this mixture provides us in order to improve them and to be able to develop a mixed cement paste that is capable of equalizing the effectiveness of Portland cement, which although it is close to it, in the case of zeolite as a pozzolan, it has not yet been achieved that this represents 50% of the mixture. Fortunately, with the growing research and development of new methods for the synthesis and management of these minerals, achieving a balance between the costs of production and the effectiveness of the product can be a reality. It should be mentioned that the use of zeolite as a pozzolan is not a whim, and although it competes with other pozzolans that can deliver a better mechanical performance such as silica fume and volcanic ash, the possible production savings due to availability and improvement from other areas such as resistance to carbonation, transport properties, hydration of the mixture, and absorption of contaminants are concepts that are worth investigating and investing for their development and improvement.

Author details

Iván Ayoseth Chulines Domínguez[1], Youness Abdellaoui[2], Mohamed Abatal[1]* and Cristóbal Patiño-Carachure[1]

*Address all correspondence to: mabatal@pampano.unacar.mx

1 Facultad de Ingeniería, Universidad Autónoma del Carmen, Ciudad del Carmen, Campeche, Mexico

2 Universidad Autónoma de Yucatán Facultad de Ingeniería, Mérida, Yucatán, Mexico

References

[1] Gebbink BK. Zeolites in Catalysis Series Editors. 2nd ed. Croydon: Royal Society of Chemistry, Croydon. 2017. DOI: 10.1039

[2] Doula M, Ioannou A, Dimirkou A. Copper adsorption and Si, Al, Ca, Mg, and Na release from Clinoptilolite. Journal of Colloid and Interface Science. 2002;**245**:237-250. DOI: 10.1006/jcis.2001.7961

[3] Miranda I, Burgos D, Castro S. Technical study of impact of hydraulic concrete mixer for the replacement part of cement by zeolite. Iberoamerican Journal of Project Management. 2014;**5**:1-10

[4] Villa C, Pecina ET, Torres R, Gómez L. Geopolymer synthesis using alkaline activation of natural zeolite. Construction and Building Materials. 2010;**24**:2084-2090. DOI: 10.1016/j.conbuildmat.2010.04.052

[5] Ortiz LR, Gutiérrez AE, Lara ÁVG. Behavior of the resistence test to compression of cement P 35 for different additions of zeolite. 2016;**5**:13-29 http://revistas.unica.cu/uciencia

[6] Turanli L, Uzal B, Bektas F. Effect of material characteristics on the properties of blended cements containing high volumes of natural pozzolans. Cement and Concrete Research. 2004;**34**:2277-2282. DOI: 10.1016/j.cemconres.2004.04.011

[7] Uzal B, Turanli L. Studies on blended cements containing a high volume of natural pozzolans. Cement and Concrete Research. 2003;**33**:1777-1781. DOI: 10.1016/S0008-8846(03)00173-X

[8] Walker R, Pavía S. Physical properties and reactivity of pozzolans, and their influence on the properties of lime-pozzolan pastes. Materials and Structures. 2011;**44**:1139-1150. DOI: 10.1617/s11527-010-9689-2

[9] Feng N-Q, Peng G-F. Applications of natural zeolite to construction and building materials in China. Construction and Building Materials. 2005;**19**:579-584. DOI: 10.1016/j.conbuildmat.2005.01.013

[10] Özen S, Göncüoɔlu MC, Liguori B, De Gennaro B, Cappelletti P, Gatta GD, Iucolano F, Colella C. A comprehensive evaluation of sedimentary zeolites from Turkey as pozzolanic addition of cement- and lime-based binders. Construction and Building Materials. 2016;**105**:46-61. DOI: 10.1016/j.conbuildmat.2015.12.055

[11] Vigil De La Villa R, Fernández R, Rodríguez O, García R, Villar-Cociña E, Frías M. Evolution of the pozzolanic activity of a thermally treated zeolite. Journal of Materials Science. 2013;**48**:3213-3224. DOI: 10.1007/s10853-012-7101-z

[12] Lilkov V, Petrov O, Petkova V, Petrova N, Tzvetanova Y. Study of the pozzolanic activity and hydration products of cement pastes with addition of natural zeolites. Clay Minerals. 2011;**46**:241-250. DOI: 10.1180/claymin.2011.046.2.241

[13] Moisés Frías E, Villar-Cociña E, De Rojas MIS, Valencia-Morales E. The effect that different pozzolanic activity methods has on the kinetic constants of the pozzolanic reaction in sugar cane straw-clay ash/lime systems: Application of a kinetic-diffusive model. Cement and Concrete Research. 2005;**35**:2137-2142. DOI: 10.1016/j.cemconres.2005.07.005

[14] Liu Y, Lei S, Lin M, Li Y, Ye Z, Fan Y. Assessment of pozzolanic activity of calcined coal-series kaolin. Applied Clay Science. 2017;**143**:159-167. DOI: 10.1016/j.clay.2017.03.038

[15] Costa C, Ribeiro MS, Brito N. Effect of waste oil-cracking catalyst incorporation on durability of mortars. Materials Sciences and Applications. 2014;**5**:905-914. DOI: 10.4236/msa.2014.513092

[16] Rahhal V, Talero R. Influence of two different fly ashes on the hydration of Portland cements. Journal of Thermal Analysis and Calorimetry. 2004;**78**:191-205. DOI: 10.1023/B:JTAN.0000042167.46181.17

[17] Cornejo MH, Elsen J, Baykara H, Paredes C. Hydration process of zeolite-rich tuffs and siltstone-blended cement pastes at low W/B ratio, under wet curing condition. European Journal of Environmental and Civil Engineering. 2014;**18**:629-651. DOI: 10.1080/19648189.2014.897005

[18] Donatello S, Tyrer M, Cheeseman CR. Comparison of test methods to assess pozzolanic activity. Cement and Concrete Composites. 2010;**32**:121-127. DOI: 10.1016/j.cemconcomp.2009.10.008

[19] Agarwal SK. Pozzolanic activity of various siliceous materials. Cement and Concrete Research. 2006;**36**:1735-1739. DOI: 10.1016/j.cemconres.2004.06.025

[20] Pan SC, Tseng DH, Lee CC, Lee C. Influence of the fineness of sewage sludge ash on the mortar properties. Cement and Concrete Research. 2003;**33**:1749-1754. DOI: 10.1016/S0008-8846(03)00165-0

[21] Shi C, Wu Y, Riefler C, Wang H. Characteristics and pozzolanic reactivity of glass powders. Cement and Concrete Research. 2005;**35**:987-993. DOI: 10.1016/j.cemconres.2004.05.015

[22] Tseng YS, Huang CL, Hsu KC. The pozzolanic activity of a calcined waste FCC catalyst and its effect on the compressive strength of cementitious materials. Cement and Concrete Research. 2005;**35**:782-787. DOI: 10.1016/j.cemconres.2004.04.026

[23] Misaelides P. Application of natural zeolites in environmental remediation: A short review. Microporous and Mesoporous Materials. 2011;**144**:15-18. DOI: 10.1016/j.micromeso.2011.03.024

[24] Ates A, Hardacre C. The effect of various treatment conditions on natural zeolites: Ion exchange, acidic, thermal and steam treatments. Journal of Colloid and Interface Science. 2012;**372**:130-140. DOI: 10.1016/j.jcis.2012.01.017

[25] Leyva-Ramos R, Monsivais-Rocha JE, Aragon-Piña A, Berber-Mendoza MS, Guerrero-Coronado RM, Alonso-Davila P, Mendoza-Barron J. Removal of ammonium from aqueous solution by ion exchange on natural and modified chabazite. Journal of Environmental Management. 2010;**91**:2662-2668. DOI: 10.1016/j.jenvman.2010.07.035

[26] Gómez-Hortigüela L, Pinar AB, Pérez-Pariente J, Sani T, Chebude Y, Díaz I. Ion-exchange in natural zeolite stilbite and significance in defluoridation ability. Microporous and Mesoporous Materials. 2014;**193**:93-102. DOI: 10.1016/j.micromeso.2014.03.014

[27] Wang S, Peng Y. Natural zeolites as effective adsorbents in water and wastewater treatment. Chemical Engineering Journal. 2010;**156**:11-24. DOI: 10.1016/j.cej.2009.10.029

[28] Beycıoglu A, Aruntaş HY, Gencel O, Hagg Lobland HE, Şamandar A, Brostow W. Effect of elevated temperatures on properties of blended cements with clinoptilolite. Medziagotyra. 2016;**22**:548-552. DOI: 10.5755/j01.ms.22.4.13354

[29] Bilim C. The effect of sodium carbonate on elevated temperature resistance of cement mortars containing natural zeolite. Turkish Journal of Engineering. 2018;**2**:12-16

[30] Carey T, Corma A, Rey F, Tang CC, Hriljac JA, Anderson PA. The effect of extra framework species on the intrinsic negative thermal expansion property of zeolites with the LTA topology. Chemical Communications. 2012;**48**:5829. DOI: 10.1039/c2cc30582h

[31] Attfield MP, Feygenson M, Neuefeind JC, Proffen TE, Lucas TCA, Hriljac JA. Reprobing the mechanism of negative thermal expansion in siliceous faujasite. RSC Advances. 2016;**6**:19903-19909. DOI: 10.1039/C5RA23827G

[32] Leardini L, Quartieri S, Vezzalini G, Arletti R. Thermal behaviour of siliceous faujasite: Further structural interpretation of negative thermal expansion. Microporous and Mesoporous Materials. 2015;**202**:226-233. DOI: 10.1016/j.micromeso.2014.10.006

[33] Krokidas PG, Skouras ED, Nikolakis V, Burganos VN. Lattice dynamics simulation of thermal contraction of faujasites. The Journal of Physical Chemistry C. 2010;**114**:22441-22448. DOI: 10.1021/jp1073736

[34] Ilić B, Wettstein SG. A review of adsorbate and temperature-induced zeolite framework flexibility. Microporous and Mesoporous Materials. 2017;**239**:221-234. DOI: 10.1016/j.micromeso.2016.10.005

[35] Lura P, Bentz DP, Lange DA, Kovler K, Bentur A. Pumice aggregates for internal water curing. In: Proceedings of International RILEM Symposium on Concrete Science and Engineering: A Tribute to Arnon Bentur. 2004. pp. 22-24. DOI:10.1617/2912143586.013

[36] Bentz DP, Weiss WJ. Internal Curing: A 2010 State-of-the-Art Review. In: National Institute of Standards and Technology (NIST) Report 7765. 2011. p. 82

[37] Kovler K, Jensen OM, Chapter 1—Introduction, Internal Curing of Concrete, RILEM TC 196-ICC: State-of-the-Art Report. 2007. pp. 1-3. DOI: http://dx.doi.org/10.1016/B978-0-08-057116-4.50007-9

[38] Ghourchian S, Wyrzykowski M, Lura P, Shekarchi M, Ahmadi B. An investigation on the use of zeolite aggregates for internal curing of concrete. Construction and Building Materials. 2013;**40**:135-144. DOI: 10.1016/j.conbuildmat.2012.10.009

[39] Wang Y, LeVan MD. Adsorption equilibrium of binary mixtures of carbon dioxide and water vapor on zeolites 5A and 13X. Journal of Chemical & Engineering Data. 2010;**55**:3189-3195. DOI: 10.1021/je100053g

[40] Mishra M, Jain SK. Properties and applications of zeolites: A review. Proceedings of the National Academy of Sciences, India, Section B: Biological Sciences. 2011;**81**:250-259

[41] Najimi M, Sobhani J, Ahmadi B, Shekarchi M. An experimental study on durability properties of concrete containing zeolite as a highly reactive natural pozzolan. Construction and Building Materials. 2012;**35**:1023-1033. DOI: 10.1016/j.conbuildmat.2012.04.038

[42] Ahmadi B, Shekarchi M. Use of natural zeolite as a supplementary cementitious material. Cement and Concrete Composites. 2010;**32**:134-141. DOI: 10.1016/j.cemconcomp.2009.10.006

[43] Markiv T, Sobol K, Franus M, Franus W. Mechanical and durability properties of concretes incorporating natural zeolite. Archives of Civil and Mechanical Engineering. 2016;**16**:554-562. DOI: 10.1016/j.acme.2016.03.013

[44] Uzal B, Turanli L. Blended cements containing high volume of natural zeolites: Properties, hydration and paste microstructure. Cement and Concrete Composites. 2012;**34**:101-109. DOI: 10.1016/j.cemconcomp.2011.08.009

[45] Karakurt C, Topçu IB. Effect of blended cements produced with natural zeolite and industrial by-products on alkali-silica reaction and sulfate resistance of concrete. Construction and Building Materials. 2011;**25**:1789-1795. DOI: 10.1016/j.conbuildmat.2010.11.087

[46] Valipour M, Pargar F, Shekarchi M, Khani S, Moradian M. In situ study of chloride ingress in concretes containing natural zeolite, metakaolin and silica fume exposed to various exposure conditions in a harsh marine environment. Construction and Building Materials. 2013;**46**:63-70. DOI: 10.1016/j.conbuildmat.2013.03.026

[47] Chindaprasirt P, Kanchanda P, Sathonsaowaphak A, Cao HT. Sulfate resistance of blended cements containing fly ash and rice husk ash. Construction and Building Materials. 2007;**21**:1356-1361. DOI: 10.1016/j.conbuildmat.2005.10.005

[48] Maas AJ, Ideker JH, Juenger MCG. Alkali silica reactivity of agglomerated silica fume. Cement and Concrete Research. 2007;**37**:166-174. DOI: 10.1016/j.cemconres.2006.10.011

[49] Ichikawa T. Alkali-silica reaction, pessimum effects and pozzolanic effect. Cement and Concrete Research. 2009;**39**:716-726. DOI: 10.1016/j.cemconres.2009.06.004

[50] Valipour M, Pargar F, Shekarchi M, Khani S. Comparing a natural pozzolan, zeolite, to metakaolin and silica fume in terms of their effect on the durability characteristics of concrete: A laboratory study. Construction and Building Materials. 2013;**41**:879-888. DOI: 10.1016/j.conbuildmat.2012.11.054

[51] Vejmelková E, Koňáková D, Kulovaná T, Keppert M, Žumár J, Rovnaníková P, Keršner Z, Sedlmajer M, Černý R. Engineering properties of concrete containing natural zeolite

as supplementary cementitious material: Strength, toughness, durability, and hygrothermal performance. Cement and Concrete Composites. 2015;**55**:259-267. DOI: 10.1016/j.cemconcomp.2014.09.013

[52] Ahmadi B, Sobhani J, Shekarchi M, Najimi M. Transport properties of ternary concrete mixtures containing natural zeolite with silica fume or fly ash. Magazine of Concrete Research. 2014;**66**:150-158. DOI: 10.1680/macr.13.00224

[53] Bukowska M, Pacewska B, Wilińska I. Influence of spent catalyst used for catalytic cracking in a fluidized bed on sulphate corrosion of cement mortars: I. Na_2SO_4 medium. Cement and Concrete Research. 2004;**34**:759-767. DOI: 10.1016/j.cemconres.2003.08.007

[54] Mohseni E, Tang W, Cui H. Chloride diffusion and acid resistance of concrete containing zeolite and tuff as partial replacements of cement and sand. Materials. 2017;**10**:1-15. DOI: 10.3390/ma10040372

[55] Małolepszy J, Grabowska E. Sulphate attack resistance of cement with zeolite additive. Procedia Engineering. 2015;**108**:170-176. DOI: 10.1016/j.proeng.2015.06.133

[56] Lura P, Jensen OM, Van Breugel K. Autogenous shrinkage in high-performance cement paste: An evaluation of basic mechanisms Modeling of autogenous relative humidity change and autogenous. Cement and Concrete Research. 2003;**33**:223-232

[57] Mounanga P, Bouasker M, Pertue A, Perronnet A, Khelidj A. Early-age autogenous cracking of cementitious matrices: Physico-chemical analysis and micro/macro investigations. Materials and Structures. 2011;**44**:749-772. DOI: 10.1617/s11527-010-9663-z

[58] Lura P, Pease B. Influence of shrinkage-reducing admixtures on development of plastic shrinkage cracks. ACI Materials Journal. 2007;**104**:187-194. DOI: 10.14359/18582

[59] Leemann A, Lura P, Loser R. Shrinkage and creep of SCC—The influence of paste volume and binder composition. Construction and Building Materials. 2011;**25**:2283-2289. DOI: 10.1016/j.conbuildmat.2010.11.019

[60] Girskas G, Skripkiūnas G. The effect of synthetic zeolite on hardened cement paste microstructure and freeze-thaw durability of concrete. Construction and Building Materials. 2017;**142**:117-127. DOI: 10.1016/j.conbuildmat.2017.03.056

[61] Poon CS, Shui ZH, Lam L, Fok H, Kou SC. Influence of moisture states of natural and recycled aggregates on the slump and compressive strength of concrete. Cement and Concrete Research. 2004;**34**:31-36. DOI: 10.1016/S0008-8846(03)00186-8

[62] Lilkov V, Petrov O, Kovacheva D, Rostovsky I, Tzvetanova Y, Petkova V, Petrova N. Carbonation process in cement with mineral additions of natural zeolite and silica fume—Early hydration period (minutes) up to 24 hours. Construction and Building Materials. 2016;**124**:838-845. DOI: 10.1016/j.conbuildmat.2016.07.117

[63] Wang X-Y, Lee H-S. A model predicting carbonation depth of concrete containing silica fume. Materials and Structures. 2009;**42**:691-704. DOI: 10.1617/s11527-008-9413-7

[64] Ukrainczyk N, Ukrainczyk M, Sipusic J, Matusinovic T. XRD and TGA investigation of hardened cement paste, 11. In: Conference on Materials, Processes, Friction And Wear MATRIB'06, Vela Luka. 2006. pp. 22-24

[65] Villain G, Thiery M, Platret G. Measurement methods of carbonation profiles in concrete: Thermogravimetry, chemical analysis and gammadensimetry. Cement and Concrete Research. 2007;**37**:1182-1192. DOI: 10.1016/j.cemconres.2007.04.015

[66] Rodway DI, Groves GW, Richardson IG. The carbonation of hardened cement pastes. Advances in Cement Research. 1990;**3**:117-125. DOI: 10.1680/adcr.1990.3.11.117

[67] Chen JJ, Thomas JJ, Jennings HM. Decalcification shrinkage of cement paste. Cement and Concrete Research. 2006;**36**:801-809. DOI: 10.1016/j.cemconres.2005.11.003

[68] Gerengi H, Kocak Y, Jazdzewska A, Kurtay M, Durgun H. Electrochemical investigations on the corrosion behaviour of reinforcing steel in diatomite- and zeolite-containing concrete exposed to sulphuric acid. Construction and Building Materials. 2013;**49**: 471-477. DOI: 10.1016/j.conbuildmat.2013.08.033

[69] Tae SH. Corrosion inhibition of steel in concrete with natural inorganic minerals in corrosive environments due to chloride attack. Construction and Building Materials. 2012;**35**:270-280. DOI: 10.1016/j.conbuildmat.2012.04.001

[70] Morozov Y, Castela AS, Dias APS, Montemor MF. Chloride-induced corrosion behavior of reinforcing steel in spent fluid cracking catalyst modified mortars. Cement and Concrete Research. 2013;**47**:1-7. DOI: 10.1016/j.cemconres.2013.01.011

[71] Janotka I, Krajči L. Sulphate resistance and passivation ability of the mortar made from pozzolan cement with zeolite. Journal of Thermal Analysis and Calorimetry. 2008;**94**: 7-14. DOI: 10.1007/s10973-008-9180-2

[72] Valipour M, Shekarchi M, Arezoumandi M. Chlorine diffusion resistivity of sustainable green concrete in harsh marine environments. Journal of Cleaner Production. 2017;**142**:4092-4100. DOI: 10.1016/j.jclepro.2016.10.015

[73] Rodríguez-Camacho RE, Uribe-Afif R. Importance of using the natural pozzolans on concrete durability. Cement and Concrete Research. 2002;**32**:1851-1858. DOI: 10.1016/S0008-8846(01)00714-1

[74] Design D. Durability-Based Design in the Persian Gulf. Concrete International. 2007;**29**:50-55

[75] Bai J, Wild S, Sabir BB. Chloride ingress and strength loss in concrete with different PC-PFA-MK binder compositions exposed to synthetic seawater. Cement and Concrete Research. 2003;**33**:353-362. DOI: 10.1016/S0008-8846(02)00961-4

[76] Valipour M, Yekkalar M, Shekarchi M, Panahi S. Environmental assessment of green concrete containing natural zeolite on the global warming index in marine environments. Journal of Cleaner Production. 2014;**65**:418-423. DOI: 10.1016/j.jclepro.2013.07.055

[77] Perraki T, Kakali G, Kontoleon F. The effect of natural zeolites on the early hydration of Portland cement. Microporous and Mesoporous Materials. 2003;**61**:205-212. DOI: 10.1016/S1387-1811(03)00369-X

[78] Perraki T, Kontori E, Tsivilis S, Kakali G. The effect of zeolite on the properties and hydration of blended cements. Cement and Concrete Composites. 2010;**32**:128-133. DOI: 10.1016/j.cemconcomp.2009.10.004

[79] Snellings R, Mertens G, Cizer Ö, Elsen J. Early age hydration and pozzolanic reaction in natural zeolite blended cements: Reaction kinetics and products by in situ synchrotron X-ray powder. Cement and Concrete Research. 2010;**40**:1704-1713. DOI: 10.1016/j.cemconres.2010.08.012

[80] Perraki T, Kakali G, Kontori E. Characterization and pozzolanic activity of thermally treated zeolite. Journal of Thermal Analysis and Calorimetry. 2005;**82**:109-113. DOI: 10.1007/s10973-005-0849-5

[81] Cornejo MH, Elsen J, Paredes C, Baykara H. Thermomechanical treatment of two Ecuadorian zeolite-rich tuffs and their potential usage as supplementary cementitious materials. Journal of Thermal Analysis and Calorimetry. 2014;**115**:309-321. DOI: 10.1007/s10973-013-3345-3

[82] García De Lomas M, Sánchez De Rojas MI, Frías M. Pozzolanic reaction of a spent fluid catalytic cracking catalyst in FCC-cement mortars. Journal of Thermal Analysis and Calorimetry. 2007;**90**:443-447. DOI: 10.1007/s10973-006-7921-7

[83] Caputo D, Liguori B, Colella C. Some advances in understanding the pozzolanic activity of zeolites: The effect of zeolite structure. Cement and Concrete Composites. 2008;**30**: 455-462. DOI: 10.1016/j.cemconcomp.2007.08.004

[84] Tydlitát V, Zákoutský J, Černý R. Early-stage hydration heat development in blended cements containing natural zeolite studied by isothermal calorimetry. Thermochimica Acta. 2014;**582**:53-58. DOI: 10.1016/j.tca.2014.03.003

[85] Chen JJ, Li LG, Ng PL, Kwan AKH. Effects of superfine zeolite on strength, flowability and cohesiveness of cementitious paste. Cement and Concrete Composites. 2017;**83**: 101-110. DOI: 10.1016/j.cemconcomp.2017.06.010

[86] Lovra E. The "Modern City": Urban Tissue Typology (Limitations of Caniggian and Conzenian Practice and the New Typology). Conference Proceedings International Conference. 2016;**4**:807-814. DOI: 10.14415/konferencijaGFS

[87] Gervais C, Ouki SK. Performance study of cementitious systems containing zeolite and silica fume: Effects of four metal nitrates on the setting time, strength and leaching characteristics. Journal of Hazardous Materials. 2002;**93**:187-200. DOI: 10.1016/S0304-3894(02)00005-5

[88] Karakurt C, Topu LB. Effect of blended cements with natural zeolite and industrial by-products on rebar corrosion and high temperature resistance of concrete. Construction and Building Materials. 2012;**35**:906-911. DOI: 10.1016/j.conbuildmat.2012.04.045

[89] Sabet FA, Libre NA, Shekarchi M. Mechanical and durability properties of self consolidating high performance concrete incorporating natural zeolite, silica fume and fly ash. Construction and Building Materials. 2013;**44**:175-184. DOI: 10.1016/j.conbuildmat.2013.02.069

[90] Chan SYN, Ji X. Comparative study of the initial surface absorption and chloride diffusion of high performance zeolite, silica fume and PFA concretes. Cement and Concrete Composites. 1999;**21**:293-300. DOI: 10.1016/S0958-9465(99)00010-4

[91] Bilim C. Properties of cement mortars containing clinoptilolite as a supplementary cementitious material. Construction and Building Materials. 2011;**25**:3175-3180. DOI: 10.1016/j.conbuildmat.2011.02.006

[92] Kontori E, Perraki T, Tsivilis S, Kakali G. Zeolite blended cements: Evaluation of their hydration rate by means of thermal analysis. Journal of Thermal Analysis and Calorimetry. 2009;**96**:993-998. DOI: 10.1007/s10973-009-0056-x

[93] Rahhal VF, Pavlík Z, Tironi A, Castellano CC, Trezza MA, Černý R, Irassar EF. Effect of cement composition on the early hydration of blended cements with natural zeolite. Journal of Thermal Analysis and Calorimetry. 2017;**128**:721-733. DOI: 10.1007/s10973-016-6007-4

[94] Radeka M, Milovic T, Malesev M, Radonjanin V, Laban M. Hydration process and compressive strength of cement pastes containing natural zeolite. Gradjevinski Materijali I Konstrukcije. 2016;**59**:29-45. DOI: 10.5937/grmk1602029R

[95] Wright PA, Lozinska M. Structural Chemistry and Properties of Zeolites, 3rd ed. Valencia: Editorial Universitat Politècnica de València; 2011

[96] Poon C, Lam L, Kou S, Lin Z. A study on the hydration rate of natural zeolite blended cement pastes. Construction and Building Materials. 1999;**13**:427-432. DOI: 10.1016/S0950-0618(99)00048-3

[97] Kerr GT. Chemistry of crystalline aluminosilicates. V. Preparation of aluminum-deficient faujasites. The Journal of Physical Chemistry. 1968;**72**:2594-2596. DOI: 10.1021/j100853a058

[98] Beyer HK, Belenykaja I. A New Method for the Dealumination of Faujasite-Type Zeolites. Amsterdam: Elsevier Scientific Publishing Company; 1980. DOI: 10.1016/S0167-2991(08)64880-6

[99] Franus W, Wdowin M, Franus M. Synthesis and characterization of zeolites prepared from industrial fly ash. Environmental Monitoring and Assessment. 2014;**186**:5721-5729. DOI: 10.1007/s10661-014-3815-5

[100] Wdowin M, Tarkowski R, Franus W. Supplementary studies of textural and mineralogical changes in reservoir and Caprocks from selected potential sites suitable for underground CO_2 storage. Arabian Journal for Science and Engineering. 2014;**39**:295-309. DOI: 10.1007/s13369-013-0862-0

[101] Rovnaníková P, Schmid P, Keršner Z. Effect of cement replacement by zeolite on the basic mechanical fracture properties of concrete: A parametric study. Advanced Materials Research. 2014;**969**:140-143. DOI: 10.4028/www.scientific.net/AMR.969.140

[102] Mola-Abasi H, Kordtabar B, Kordnaeij A. Parameters controlling strength of zeolite–cement–sand mixture. International Journal of Geotechnical Engineering. 2017;**11**:72-79. DOI: 10.1080/19386362.2016.1186412

[103] Mola-Abasi H, Shooshpasha I. Influence of zeolite and cement additions on mechanical behavior of sandy soil. Journal of Rock Mechanics and Geotechnical Engineering. 2016;**8**:746-752. DOI: 10.1016/j.jrmge.2016.01.008

[104] Sedlmajer M, Zach J, Hroudová J, Rovnaníková P. Possibilities of Utilization Zeolite in Concrete. 2015;**9**:525-528

[105] Gjørv OE. Vennesland, diffusion of chloride ions from seawater into concrete. Cement and Concrete Research. 1979;**9**:229-238. DOI: 10.1016/0008-8846(79)90029-2

Chapter 9

Potential Desalination of Coal Seam Gas Coproduced Water Using Zeolite

Xiaoyu Wang and Anh V. Nguyen

Additional information is available at the end of the chapter

http://dx.doi.org/10.5772/intechopen.73613

Abstract

Natural clinoptilolite type zeolite was examined for its potential to treat coal seam gas (CSG) water and remove sodium ions to lower sodium adsorption ratio and reduce pH. The effectiveness of unmodified and modified natural zeolite is due to their regular composition and open porous structure, high exchange capacity, mechanical strength and stability, and consistency in particle size. The effects of acid modification in bringing about changes to the physicochemical properties of clinoptilolite underpin the effectiveness of this material for treatment of CSG saline water. The sodium adsorption capacity of acid-modified zeolite increases up to three times greater than that of the unmodified zeolite. The atomic percentage and binding energies of the chemical elements comprising zeolite are changed significantly following the acid modification. The Si/Al atomic ratio increases with increasing sulfuric acid concentration. Dealumination is the main reason for the increase in the surface charge and cation exchange capacity of clinoptilolite after acid modification. It is due to the increased defects in the crystal structure/lattice, which result in increasing numbers of charge vacancies. Sodium-rich synthetic zeolites 4A and Na—Y after acid modification are also examined by following the dissolution of the first-order fast kinetics and recrystallization processes which can be homogeneous or heterogeneous.

Keywords: CSG, acid treatment, SAR, clinoptilolite, surface potential, XPS

1. Introduction

Zeolite is a cost-effective material that has been investigated for its potential use as adsorbents because of its large volumes of internal space [1–3]. It belongs to the group of natural silicate minerals which have high sorption capacity and selectivity resulting from high porosity and sieving properties. The capability of zeolite to exchange cations is one of their most useful

IntechOpen

© 2018 The Author(s). Licensee IntechOpen. This chapter is distributed under the terms of the Creative Commons Attribution License (http://creativecommons.org/licenses/by/3.0), which permits unrestricted use, distribution, and reproduction in any medium, provided the original work is properly cited.

properties as it has been used to remove heavy metals, such as Cd^{2+}, Cu^{2+}, Ni^{2+}, and Pb^{2+}. Of the natural zeolites, clinoptilolite is regarded as the most useful adsorbent. It is also the most researched of all zeolites. Clinoptilolite has a cage-like structure with pores and channels running through the crystal. The cage consisting of SiO_4 and AlO_4 tetrahedral joined by shared oxygen atoms carries a net negative charge which is balanced by the presence of exchangeable cations—especially calcium, sodium, magnesium, potassium, and iron. These ions can be readily replaced by other cations that can easily interact with the negative zeolite framework, such as heavy metals [4–6] and ammonium ions [7, 8]. Due to its very high cationic exchange capacity, clinoptilolite is a potential adsorbent for removing cations from an aqueous solution, for example, in desalination, drinking water purification [9–14] and processing coal seam gas (CSG) coproduced water [15].

CSG can be considered as conventional natural gas that is adsorbed into coal seams in deep underground [16]. The CSG extraction discharges a large amount of water (several megaliters per day). For example, 12.5 giga litres of CSG water was produced and discharged by CSG industry in Queensland, Australia, in 2007 [17]. However, high salt content of the CSG water can potentially harm the environment. Therefore, it cannot be released directly to land or other water resources. Sodium concentration must be reduced to less than 200 ppm for irrigation. Management of CSG water is an environmental challenge. Desalination but with cost-effective technologies is in demand to allow the CSG water usage for beneficial purposes, including irrigation use [18].

Current CSG water management and treatment technologies include infiltration ponds, shallow or deep aquifer injection, reverse osmosis, ion exchange, and subsurface drip irrigation [16]. Unfortunately, these treatments are either rather time-consuming or very expensive. For example, using reinjection to clean up an aquifer with dissolved volatile organic compounds over an area of 3 km^2 needs around 50 years [18]. In addition, reverse osmosis (RO) is effective in removing dissolved salts but produces a significant amount of brines that also need to be addressed and dealt with high capital costs than most other strategies. The additional effort and costs and high capital costs make it difficult for RO to be a cost-effective management option in a large geographical area where raw water is spread over. Hence, a better way of CSG water treatment is urgently needed.

Sodium adsorption ratio (SAR) is an important parameter to analyses the effective removal of sodium when dealing with CSG water managed irrigation [16]. Being calculated as the ratio of Na^+ to Ca^{2+} and Mg^{2+} in the soil, SAR describes the tendency for Na^+ to be adsorbed at soil ion-exchange sites at the expense of other ions (in this case calcium and magnesium ions). Soils with an excess of Na^+, compared to of Ca^{2+} and Mg^{2+}, remain in a dispersed condition, almost impermeable to rain or irrigation water. In general, the higher the SAR, the less suitable the water is for irrigation. Irrigation using water with high SAR may require soil amendments to prevent long-term damage to the soil.

To increase adsorption capacity, natural zeolites can be modified by sole or combined treatments such as chemical attacks (alkali, acids, and salts of alkaline metals) and heating. Different methods are used to prepare zeolites with specific properties for different applications. For example, acid treatment has been shown to improve the adsorption ability and enlarge the pore system of different synthetic zeolites [19–21]. Acid treatment can

dealuminate the zeolite structure by applying protons to attack and weaken Al—O bonds, thereby causing skeletal vacancies and defects. They can enlarge the pore mouth of the zeolite and increase the surface area and adsorption ability. Acid treatment is a simple and economical option for increasing the adsorption capacity of natural zeolites that improve the viability of zeolite on CSG water treatment.

In this regard, the applicability of the water treatment method for CSG water using natural zeolite (to reduce the Na^+ content less than 200 ppm, sodium adsorption ratio (SAR) value between 12 and 25, and pH value is about 7) and improved treatments to increase the adsorption ability of the natural zeolite by acid modification is reviewed in this chapter.

2. The effect of zeolite modification by acids on sodium adsorption ratio of coal seam gas water

2.1. Characterization of zeolite before and after acid treatment

The chemical composition of the zeolite (Zeolite Australia Pty Ltd) is shown in **Table 1**. Zeolite treatment was carried out with different acids (H_2SO_4, HCl, and HAc) at various concentrations (0.001, 0.1, 1, and 2 M) in order to increase the adsorption capacity of the sample. The acid treatment included mixing the natural zeolite sample with acid solutions (1:1 weight ratio) and drying of the washed treated zeolite overnight at 80°C. The adsorption experiments were carried out at 10, 20, and 30% solid ratios (w/w) separately for 6 h using an orbital shaker at 200 rpm at room temperature. Primary exchangeable cations and effective cation exchange capacity (CEC) for the natural zeolite sample are Na^+, Mg^{2+}, Ca^{2+}, and K^+. The total CEC for natural zeolite was about 119 meq/100 g, as for cations released from zeolite sample during NH^{4+} exchange [22]. The CEC of 0.1 M H_2SO_4 acid-modified zeolite was about 300 meq/100 g based on the adsorption calculation.

The analysis by X-ray diffraction (XRD) showed that the main compositions were clinoptilolite and quartz and 0.1 M H_2SO_4 acid modification did not change the phases of the zeolite sample. With increasing concentration of H_2SO_4 from 0 to 2 M, the BET surface area of zeolite samples increased from 9.8 to 15.7 m^2/g. The change was attributed to removing fine particles that can clog the zeolite pores and slow the exchange rates [23–26]. In addition, SEM images showed that the modified zeolite surface contained more cracks and small openings compared to the natural zeolite. These details prove the structural changes on the zeolite surfaces after the acid treatment (**Figure 1**).

Compound	SiO_2	TiO_2	AlO_3	Fe_2O_3	MnO	MgO	CaO	Na_2O	K_2O	P_2O_5	LOI	SO_3	Total
Zeolite (%)	68.3	0.2	13.0	1.4	0.1	0.8	2.1	0.6	4.1	0.1	8.8	0.5	100

Table 1. Chemical composition of zeolite [15].

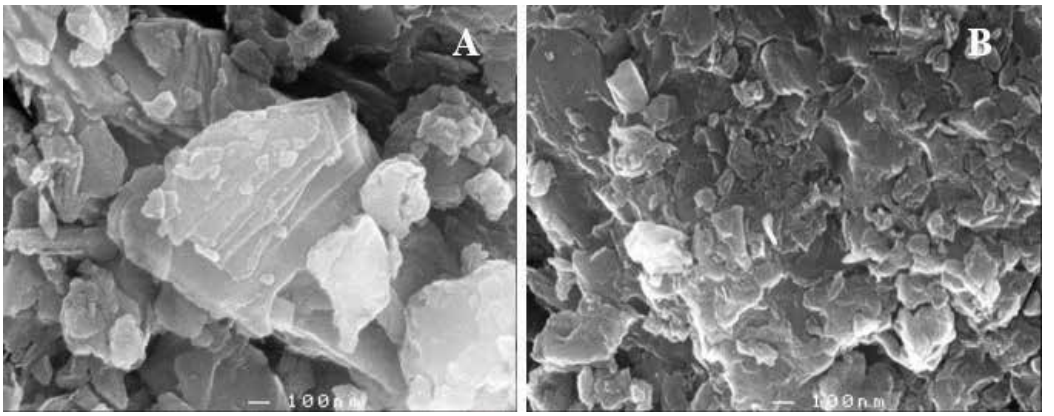

Figure 1. SEM images of (A) natural zeolite and (B) modified zeolite with 0.1 M H_2SO_4 [15].

The DTA/TG tests showed that the natural and acid-modified zeolite samples had the same trend of weight loss. This indicates that both natural and acid-modified zeolite samples have just physically lost moisture content [27]. DTG analysis (**Figure 2**) also showed the surface water desorption decreased with increasing acid concentration at 200°C. Interestingly, for the zeolite modified by 2 M H_2SO_4 solution, the surface water desorption at around 100°C was much reduced. At a higher temperature (350°C), there was no such an evidence of loss of hydrated water occurred with natural and 0.1 M H_2SO_4 acid-modified zeolites. This suggests that acid with high concentration can destroy the pore structure of the zeolite. Particle size analysis showed that the particle size was less than 200 μm, with a mean of about 50 μm.

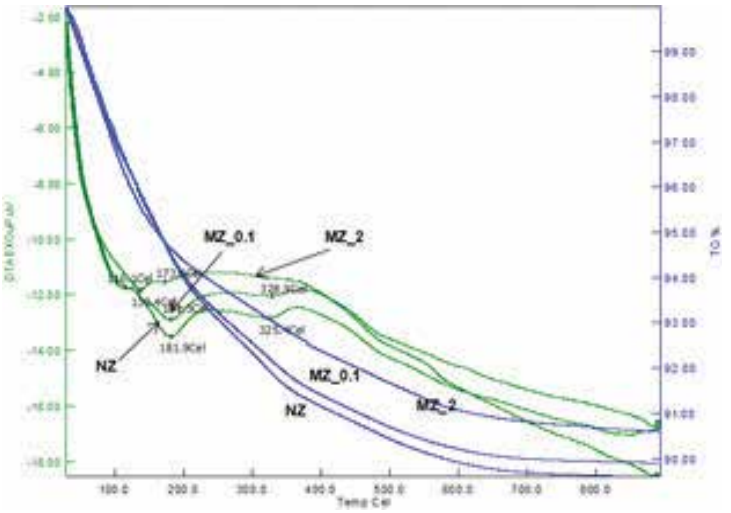

Figure 2. DTA/TG results of the natural and modified zeolite samples with 0.1 M H_2SO_4 (NZ, natural zeolite; MZ_0.1, modified zeolite 0.1 M; MZ_2, modified zeolite 2 M) [15].

The surface potential analysis by electrophoresis (with −38 μm size fractions) was carried out for natural and modified zeolite samples (**Figure 3**). Substitutions of Al^{3+} ions for Si^{4+} in the clinoptilolite lattice and the broken Si—O—Si bonds at the particle surface during the grinding process were the reasons for the surface charge negative [24, 25, 28]. With the pH value changing, H^+ could easily become exchangeable cations. These results agree with the literature data [6, 24]. For each pH value tested, the zeta potential of acid-modified zeolite was always around 9 mV more negative than natural zeolite. It indicates that acid modification weakens the Si—O bond. When there is a cation exchange environment exists, ion exchange can occur easily in acid-modified zeolite surface than natural zeolite.

2.2. CSG water treatment using untreated and acid-treated zeolite

As per the chemical analysis of the CSG water, its pH value is 8.4, SAR 94, concentration Na^+ 563 ppm, Mg^{2+} less than 1 ppm, and Ca^{2+} 2 ppm. SAR is defined as follows:

$$\mathrm{SAR} = \frac{[\mathrm{Na}^+](\mathrm{meq})}{\sqrt{\frac{[\mathrm{Ca}^{2+}](\mathrm{meq}) + [\mathrm{Mg}^{2+}](\mathrm{meq})}{2}}} \tag{1}$$

where $[Na^+]$, $[Ca^{2+}]$, and $[Mg^{2+}]$ are the concentrations in solution and meq is the milliequivalent weight.

The results for Na^+ removal using natural zeolite as a function of solid concentration (weight of zeolite per weight of solution) are shown in **Figure 4A**. A slight decrease in the Na^+ concentration was seen with increasing the solid ratio, while the Mg^{2+} and Ca^{2+} concentrations increased correspondingly. This is the direct result of the ion exchange of sodium with calcium and magnesium which are exchanged and entered the bulk

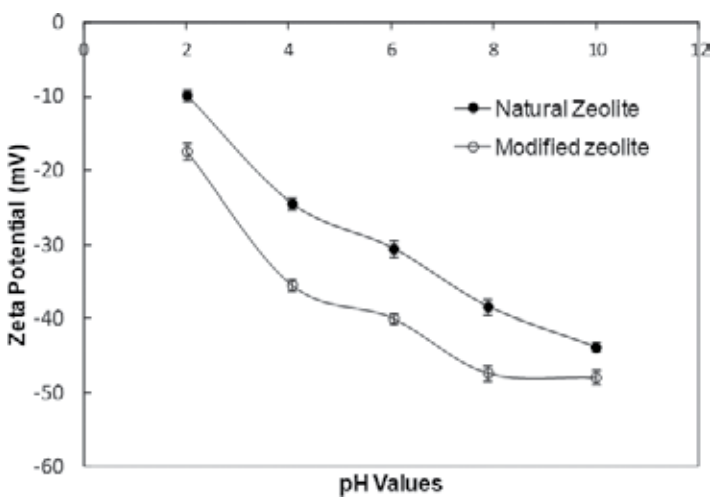

Figure 3. Zeta potential profiles of natural and 0.1 M H_2SO_4 modified zeolite samples [15].

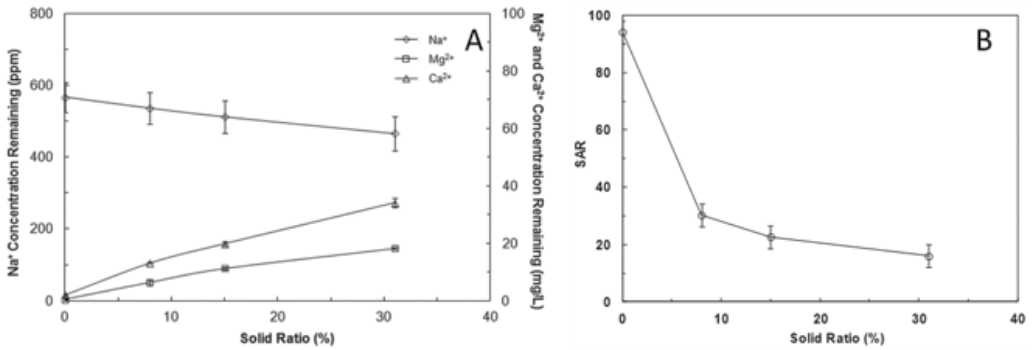

Figure 4. (A) Ion concentrations in CSG water after treatment with natural zeolite. (B) SAR values of CSG water after treatment with natural zeolite [15].

aqueous phase. Because of the decrease in sodium concentration and increase in calcium and magnesium concentrations, the value of SAR decreases with the solid ratio as shown in **Figure 4B**, which is expected. While the SAR value is in the acceptable range between 12 and 25, Na^+ concentration remains high, making the treated water unacceptable for practical purposes.

Figure 5 (left panel) shows the effect of acid modification of zeolite particles on the adsorption of Na^+ ions. The tests were conducted with different concentrations of H_2SO_4 to establish the most suitable acid concentration. The adsorption tests were carried out using an orbital shaker at 200 rpm at the solid ratio of 30% for 6 h. The Na^+ concentration of the CSG water after treatment with the modified zeolite decreases with the increasing acid concentration: The Na^+ adsorption capacity of zeolite can be significantly improved by acid modification. The SAR values with the modified zeolite were slightly higher than natural zeolite due to the release of Mg^{2+} and Ca^{2+} ions during the washing and acid modification process and sequentially lessening Mg^{2+} and

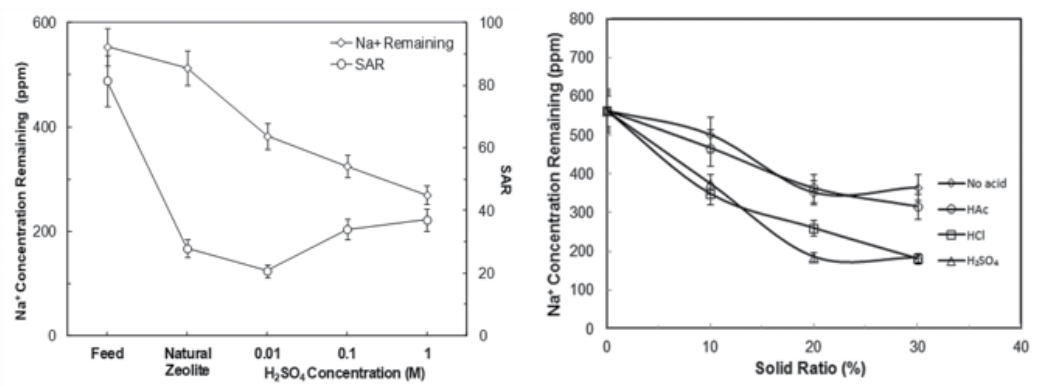

Figure 5. Left: Na^+ concentration and SAR in CSG water after treatment with 30% solid ratio zeolite (natural and modified by H_2SO_4) [15]. Right: Na^+ removal by the modified zeolite as a function of acid type and solid concentration at room temperature [15].

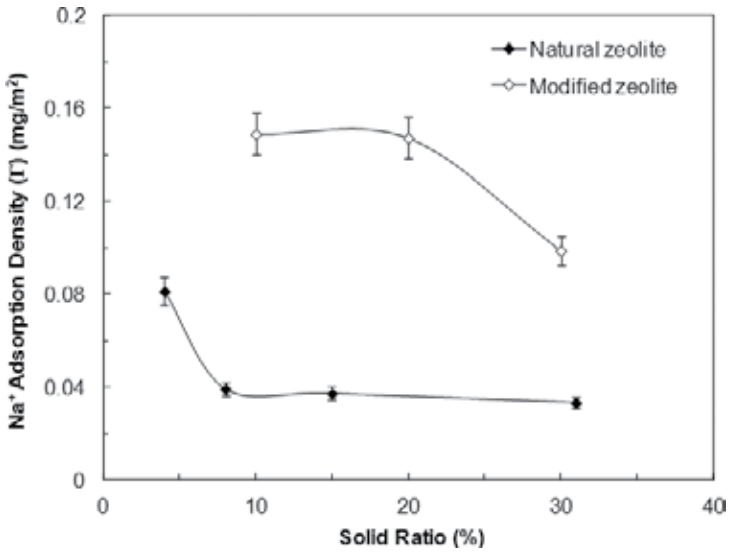

Figure 6. Na^+ adsorption density by zeolite samples versus solid ratio [15].

Ca^{2+} ions exchanged during the adsorption process. These results suggested that 0.1 M acid concentration was optimal for the modification process.

Based on the optimum acid concentration, systematic adsorption tests were carried out with zeolite sample modified at 0.1 M with different acids (**Figure 5**, right). The Na^+ removal by the modified zeolite was considerably increased. For example, the modified zeolite reduced Na^+ concentrations to approximately 180 ppm at 30% solid ratio that is acceptable for irrigation. However, zeolite modified by HAc did not change the Na^+ adsorption significantly. There was no significant difference on the SAR values for the samples due to how much Mg^{2+} and Ca^{2+} ions released from the zeolite, which could be affected by ions releasing in modification and washing process before adsorption tests.

Figure 6 shows an increase in adsorption capacity of Na^+ by the acid-modified zeolite as compared with the natural zeolite. The adsorption density (Γ) of Na^+ in the batch tests was calculated by the following formula:

$$\Gamma = \frac{(C_i - C_r) \times V}{mA} \tag{2}$$

where C_i and C_r represent the initial and residual concentrations in Na^+ (mg/L), m is the amount of zeolite used (g), V is the volume of the solution (L), A is the BET surface area (m^2/g), and Γ is the adsorption density (mg/m^2). The results in **Figure 6** evidently indicate that the modification process increased the sodium adsorption capacity of zeolite up to four times. The modified zeolite had a larger surface area than the natural zeolite. The DTA/TG, XRD, and particle size distribution results for both samples also indicated that there was no structural difference between two samples.

3. X-ray photoelectron spectroscopy (XPS) investigation of sulfuric acid modification of natural zeolite

XPS analysis of the zeolite structural composition of zeolite samples shows the presence of the O_{1s}, C_{1s}, Na_{1s}, Ca_{2p}, Si_{2p}, Al_{2p}, and K_{2p} photoelectron lines [29]. The variations of the atomic concentrations are significant as shown in **Figure 7**. With increasing sulfuric acid concentration from 0 to 5 M, the atomic proportions of each element change differently. When the acid concentration increases from 0 to 1 M and beyond, the atomic % of Na decreases from 0.6% to 0. Changes in the atomic % of Ca and Mg follow a similar trend, i.e., after treating by 1 M acid, their atomic proportion is either near zero or cannot be detected. That suggests most of the cations which are not part of the main structure and can be easily removed by acid modification. However, K cannot be totally removed after acid treatment, i.e., although the change in its atomic percentage fluctuates, the overall trend is decreasing. The proportion of Al decreases with increasing the acid concentration from 0 to 2 M and then slightly increases by 5 M acid treatment. This may due to the significant decrease in the atomic proportion of the other cations, especially at high acid concentrations. The atomic percentage of O increases from 52% (unmodified) to 60.9% after treating with 0.1 M acid and then does not change much with higher acid concentrations as Si. The atomic proportions of Al, O, and Si do not change significantly as they are the building elements of zeolite structure.

These XPS results support the sodium adsorption ratio studies. **Figure 7** shows a significant decrease in the atomic % of Ca and Mg after 0.01 M acid modification. This data agrees with the hypothesis that Ca and Mg are removed from the zeolite surface after the modification (0–1 M acid). **Figure 8** shows the trend of Si/Al ratio on the zeolite surface and [Si_{2p}-Al_{2p}] BE separation. With increasing the acid concentration, the Si/Al ratio increases from 2.99 to 4.92. However, the [Si_{2p}-Al_{2p}] BE separation increases to 29 eV when acid concentration increases from 0.01 to 0.1 M. It remains unchanged up to 2 M and finally decreases to 28.5 eV after 5 M acid modification. The increase in Si/Al atomic ratio also indicates the dealumination process occurred within the zeolite structure on the surface. Na, Mg, and Ca ions can be released into

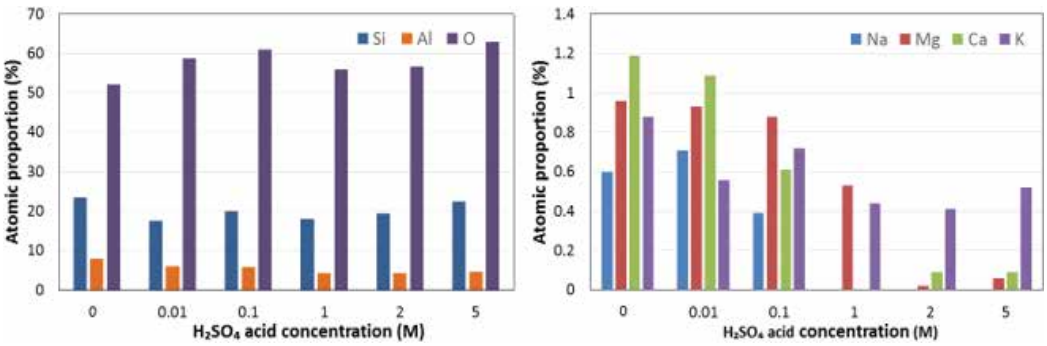

Figure 7. Effect of acid concentration on elemental atomic proportions revealed by XPS [29].

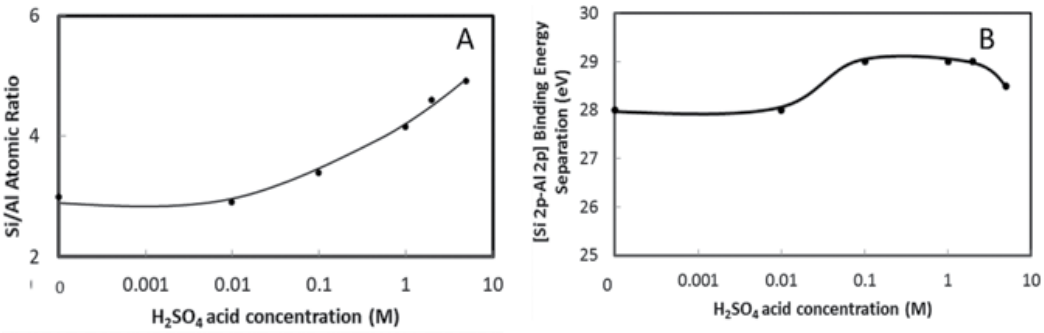

Figure 8. The effect of increasing acid concentration on Si/Al ratio (A) and [Si_{2p}-Al_{2p}] binding energy separations (B) (trend line included to illustrate the relationship) [29].

the acid solutions during the modification process. K ions as an exception (unaffected by the acid modification) remain in zeolite structure at relatively constant levels. **Figure 9** shows high-resolution scan results for Si, Al, and O which cannot be easily detected in the survey scan.

High-resolution scans for Si_{2p}, Al_{2p}, O_{1s}, K_{2p}, and Ca_{2p} of natural and sulfuric acid modification show different extents of BE increase for each element. For the building elements of zeolite, such as Si, Al, and O, the BE shifts are greater than K^+ and Ca^{2+}. The small increase in K_{2p} BE can be observed by analyzing $K_{2p3/2}$ peaks. Because of Ca removal, the progressive shifting patterns show the relative covalency-ionicity of the chemical bonds within the zeolite structure [30]. For natural zeolite studied here, the easy removal of Na from the zeolite surface after acid modification may be due to the high ionicity of the Na—O bond. Likewise, Ca—O and Mg—O ionic bonds are similarly strong, and the atomic proportion can also reduce significantly.

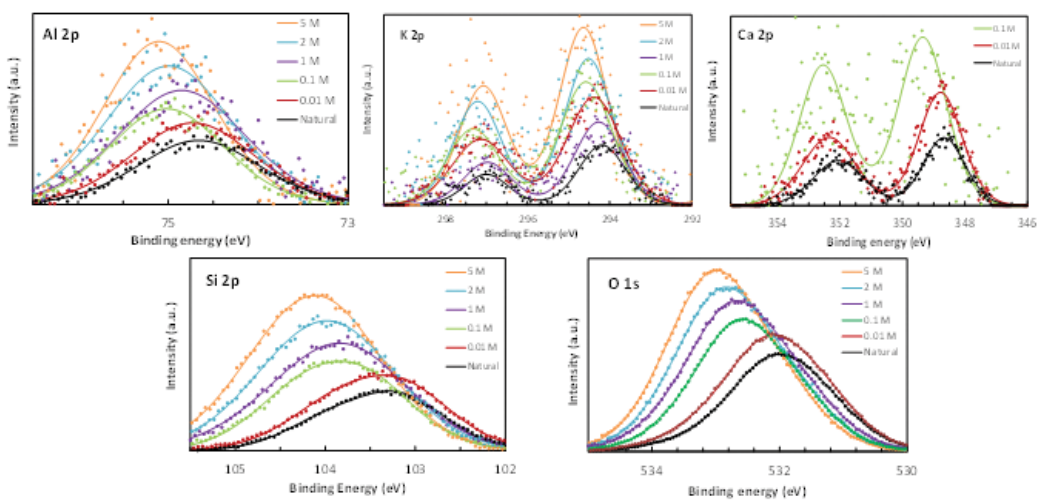

Figure 9. XPS high-resolution spectra of natural and acid-modified zeolite for Si_{2p}, Al_{2p}, O_{1s}, K_{2p}, and Ca_{2p} [29].

4. Characterization of electrokinetic properties of clinoptilolite before and after activation by sulfuric acid for treating CSG water

The change in pH of zeolite suspensions versus time can be an important parameter for the surface dissociation as well as the environmental and industrial applications. **Figure 10** shows a rapid increase in the pH value of the suspensions from pH = 5.6 of DI water (before adding natural zeolite) to 8.02 within the first 2 min. The increase in pH is due to the rapid adsorption of H^+ from solution. After the first 2 min, a very slow pH decrease to 7.13 is observed for 2 h. It shows the adsorption of H^+ in water onto the negative surface charge of zeolite. Therefore, the H^+ acts as a potential determining ion (PDI) in the electrical double layer to provide electroneutrality for the first 2 min. Besides, the H exchange with some of the cations in the lattice of zeolite structure is also the reason for the consumption of H^+ in the suspension [31]. Zeolite tends to neutralize the aqueous medium acting the H^+ desorption from the solution onto the surface of particles.

In the acidic medium, the initial pH of water was changed to 2 by 0.1 M HCl addition and then zeolite particles into the solution. The suspension pH increased to 2.4 in first 2 min and attained the equilibrium of pH 2.9 for 120 min. Al^{3+} from the octahedral sheets moves into the acid solution. They were conducive to ion exchange. Indeed, if the pH was adjusted to a lower value, dealumination process occurred throughout the measurements.

In basic medium, the initial pH of water was changed to 11.5 by 0.1 M NaOH, and then the zeolite particles were added into the solution. The suspension pH decreased to 11.27 in 2 min and equilibrated to pH = 10.5 in 120 min. The decrease in the pH value may be due to (i) the adsorption of OH^- in the suspension onto the positive charge sites, which were presented on

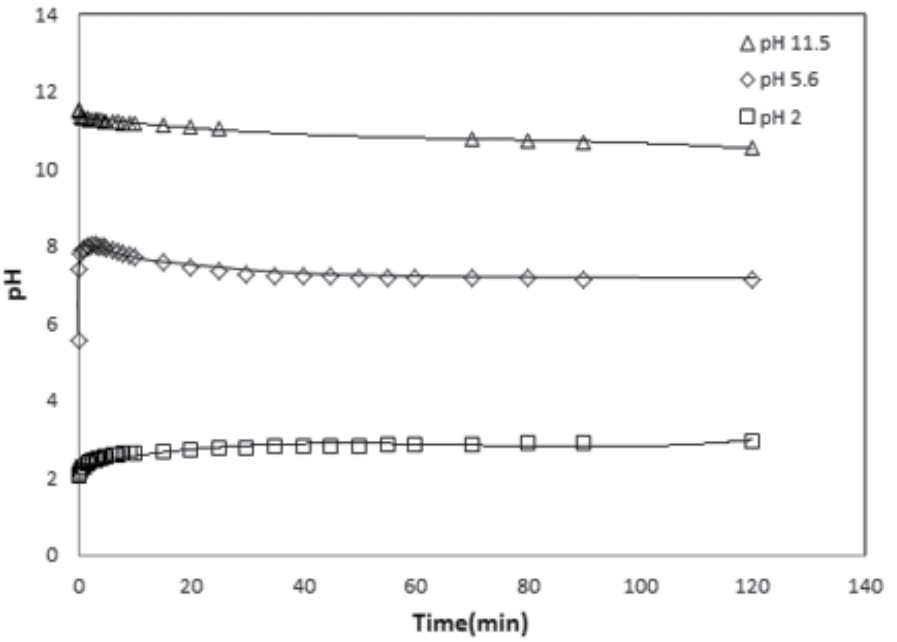

Figure 10. Transient pH profiles of suspensions of natural zeolite sample [32].

the surface of zeolite particles and exposed to water after grinding as a result of the chemical bonds breaking, and/or (ii) the desorption or transfer of the H^+ ions from —SiOH groups inside the lattice to free OH^- of H_2O into the suspension.

Since the cation exchange capacity (CEC) of zeolite mainly results from the permanently negative surface charge, surface (zeta) potential of acid-activated zeolite is an interesting parameter to be examined. As shown in **Figure 11**, the zeta potential of natural and acid-modified zeolite became more negative with the pH value increasing from 2 to 10. However, the value of zeta potential is more negative with increasing the acid concentration. In the first place, zeta potential became more negative after being modified by sulfuric acid with the concentration up to 0.1 M. With the acid concentration increased further, generally the zeta potential became less negative. The change in zeta potential versus pH was not significant at 5 M of sulfuric acid. In the neutral pH environment (pH 7), the most negative charge can be detected on the surface of zeolite modified by 0.1 M sulfuric acid.

Investigation of electrical double layer (EDL) of zeolite structure via zeta potential measurements demonstrated that H^+ plays an important role as a counterion in EDL; it adsorbs onto the inner Helmholtz plane (IHP) of the Stern layer on zeolite surface as a charge reversal. Meanwhile, OH^- was adsorbed by the outer Helmholtz plane (OHP), between the Stern layer and diffuse layer. Dealumination occurred during the acid activation process of natural zeolite [31]. It is assumed as the main reason for increasing surface charge and cation exchange capacity of zeolite surface due to the increasing of defects in zeolite crystal structure and lattice. It leads to the increase in charge vacancies. Thus, it can be assumed that the H^+ adsorption in IHP increased due to more zeolite crystal defects appeared after dealumination.

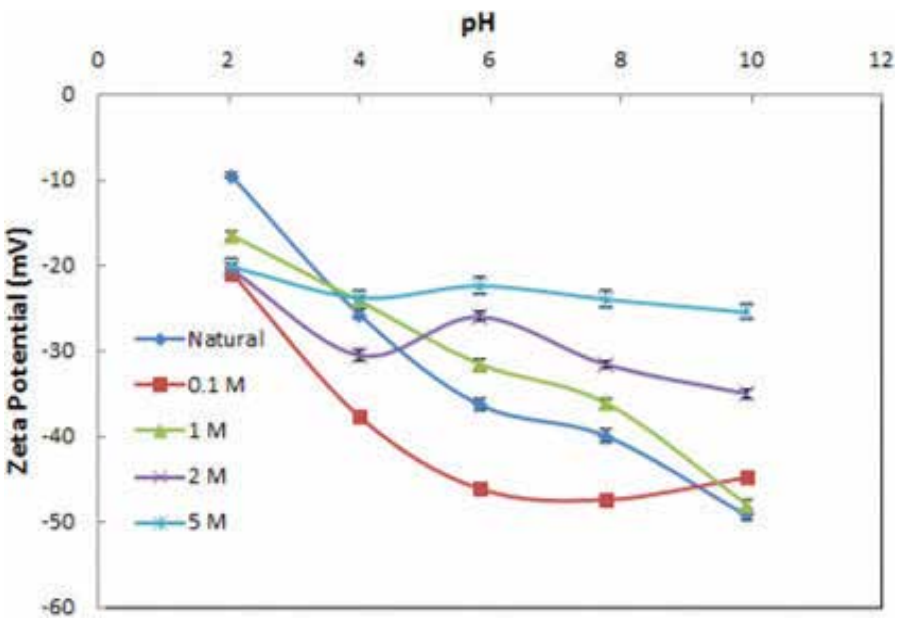

Figure 11. Surface (zeta) potential of natural and acid-modified zeolites vs. pH [32].

5. Effect of sulfuric acid modification on surface and particle properties of 4A and Na—Y synthetic zeolites

4A and Na—Y are sodium-rich synthetic zeolites, which are well-known crystalline microporous materials and widely used as solid acid catalysts and molecular sieves. Both of them have three-dimensional structures which are composed of $[SiO_4]^{4-}$ and $[AlO_4]^{5-}$ tetrahedra. All of the tetrahedra are interconnected with shared corners to form channels of molecular dimensions. Each AlO_4 tetrahedron bears a net charge which is neutralized by the additional positive charge from the non-framework Na^+ which is located within the channel. Because of the purity of crystalline products and the uniformity of particle sizes, synthetic zeolites are used commercially more often than natural zeolites [33]. Application of the acid modification to synthetic zeolites could provide a useful reference for understanding into improving their adsorption or ion-exchange properties, given that the effects of sulfuric acid modification of zeolite 4A and Na—Y are unknown.

5.1. Stability and resistance of 4A and Na—Y zeolites against H_2SO_4 modification

After 3-day acid modification, 4A zeolite particles were observed to become totally settled in 0 and 0.1 M H_2SO_4 solutions and partly settled in 0.2 and 0.3 M H_2SO_4 solutions. However, they completely dissolved to form a gel in the 0.5 and 1 M H_2SO_4 solutions. Low concentrations of sulfuric acid, such as 0.2 and 0.3 M, cannot dissolve the zeolite particles completely but are strong enough to break bigger 4A particles into smaller ones.

After mixing Na—Y powder with various concentrations of H_2SO_4 solutions, cloudy white suspensions were generated. Substantial settling occurred for the first day and continued to a lesser extent over the subsequent 2 days. **Table 2** describes the appearance of the suspensions after 3-day settlement.

The Na—Y powder can also be dissolved in sulfuric acid to a certain extent. The dissolution of small Na—Y particles is limited with a low concentration of sulfuric acid (0.1 M). Some of

H_2SO_4 (M)	0	0.1	0.5	1	2	3	5
Observation	* Layered; *Upper liquid clear; *Small volume sediment; *Clear interface.	* Layered; *Upper liquid slightly muddy; *Sediment volume expansion; *Misty interface.	* Layered; *Upper liquid clear; *Sediment volume expansion; *Clear interface.	* Layered; *Upper liquid clear; *Sediment volume expansion; *Clear interface.	* Layered; *Upper liquid clear; *Sediment volume expansion; *Clear interface.	* Layered; *Upper liquid clear; *Sediment volume expansion; *Clear interface.	* Layered; *Upper liquid slightly muddy; *Sediment volume expansion; *Misty interface.

Table 2. Behavior of the Na—Y suspensions after 3-day standing [34].

the Na—Y fine particles were observed to remain in a suspending state and swell significantly and then formed a diffuse solid-liquid interface. The small Na—Y particles dissolved fully at higher acid concentrations (0.5, 1, 2, and 3 M). A significant amount of acid was consumed in this process, leaving less amount of acid that was insufficient to cause the larger particles to swell to a state of suspension. That can be the reason for observing a clear solid-liquid interface. With the acid concentration increased to 5 M, not only the fine Na—Y particles were dissolved, but also a proportion of the larger particles underwent a partial dissolution, which led to swelling and suspension in solutions as being observed. Thus, the solid-liquid interface developed a diffuse appearance, like that seen at the 0.1 M acid concentrations.

As increasing the acid concentration to 0.5 M, the 4A molecular sieve could be completely dissolved and formed a gel. It was hard to observe the particle dissolution as occurred in Na—Y system. It indicates Na—Y has a strong acid resistance and is consequently more stable than 4A, possibly attributable to the higher Si/Al ratio in the structure.

5.2. Impact of H_2SO_4 concentration on solid mass in Na—Y zeolite suspensions

Figure 12 shows the experimental data of solid mass of the Na—Y samples left/gained over time in the suspensions after standing for 6, 24, 48, and 70 h after treatment with sulfuric acid. The data can be well fitted by the following equation of the first-order kinetics:

$$y = a + b\exp(-kx) \tag{3}$$

where y is the solid mass (obtained by filtration) of the collected Na—Y sample (grams), x is the acid concentration used in the treatment process (mole/L), and a, b, and k are the fitting parameters, with grams and L/mol as their units, respectively.

As per **Figure 12A**, the residual mass of Na—Y particles was rapidly decreased with increasing acid concentration from 0 to 0.5 M. The dissolution kinetics was fast. For concentrations higher than 0.5 M, the residual mass of Na—Y particles inclined to constant values.

Figure 12A shows that less than 6 h is required for dissolution of the acid-soluble component to reach completion. It was concluded that the acid-soluble component of Na—Y was

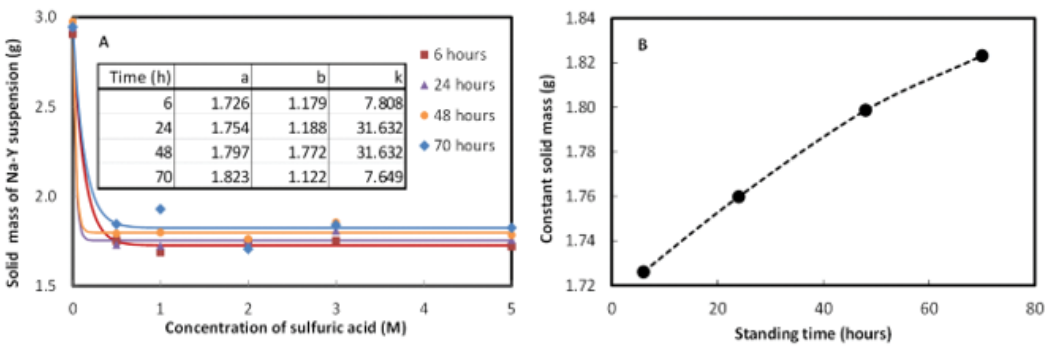

Figure 12. (A) Effect of H_2SO_4 concentration on mass of solid of Na—Y zeolite suspension and (B) its constant values versus standing time [34].

dissolved by sulfuric acid, after that specific component has been totally dissolved, and the residual mass did not change with increasing acid concentration. It was difficult to identify the precise nature of this dissolution by the mass loss or XRD analysis. However, it likely represented Na and Al losses based on the known structure of Na—Y. The final solid mass of the acid-treated sample increased with increasing standing time (**Figure 12B**). Therefore, it was argued that with the standing time increasing, the dissolved component partly recrystallized, leading to the mass increase. Combining with the XPS analysis shows that it is the Al content that has been reduced significantly after acid modification, as discussed in a later section. Also, the components of Na—Y which were dissolved in sulfuric acid included both Al and non-Al contents. The non-Al content was recrystallized.

XRD analysis showed the crystal structure collapsed after acid modification [34]. Comparing the untreated Na—Y to that exposed to water only, the crystal phases did not change after contacting Milli-Q water. However, the XRD results for the acid treatments showed a significant energy intensity reduction of all the crystal peaks at 0.1 M, indicating most of the crystal phases were destroyed at 0.1 M. The XRD results for 0.5–5 M acid treatments showed the same line shapes which indicated that the crystal peaks were no longer present and a transformation to noncrystalline SiO_2 took place. Therefore, the crystal structure was totally changed into a noncrystalline one after treating with sulfuric acid of >0.1 M.

5.3. XPS analysis of the effect of acid treatment on Na—Y zeolite

The results of XPS survey scans showed two different significant changes in atomic proportions of the Na—Y zeolite elements [34]: Na and Al decreased from 7.98% to 0 as the acid concentration increases from 0 to 0.5 M, but O and Si increased until the acid concentration reaches 0.5 M as well and then remained almost constant to 5 M. Sulfuric acid modifications on Na—Y zeolite could totally remove Na and Al from the surface, such that the main structural elements remaining were only Si and O. Together with the XRD results, the XPS data confirmed that Na and Al have been removed not only on the particle surface but also from the internal structure.

Figure 13 shows the detailed results of XPS high-resolution scans for the Si_{2p}, O_{1s}, and Al_{2p} regions of unmodified and modified Na—Y. The BE of Si_{2p} initially decreased by 0.10 eV after washing by Milli-Q water and then increased after 0.1 and 0.5 M sulfuric acid modification. The BE of O 1s increased with increasing acid concentration, but no BE shift in Al_{2p} was observed up to 0.1 M acid modification. No Al component was detected after being modified by 0.5 M and higher concentrations of acid. The change in O1s BE energy is explained by the interactions between the two known O bonds in the structure of Na—Y [35] (i.e., bridging oxygen

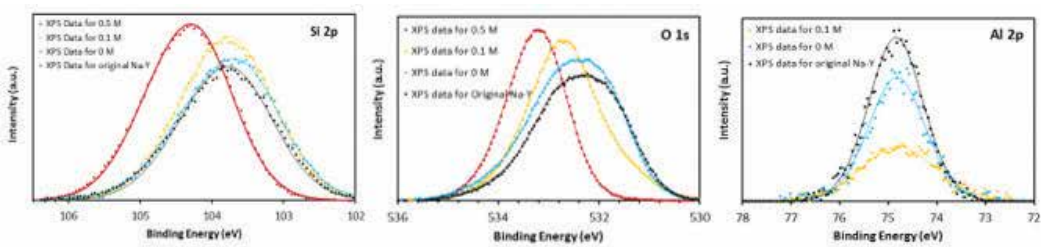

Figure 13. XPS high-resolution spectra of original and sulfuric acid-treated Na—Y for Si_{2p}, O_{1s}, and Al_{2p} [34].

incorporated in structures such as Si—O—Si and non-bridging oxygen (NBO) comprising structures such as Si—O—M (where M represents other elements such as Na, Al, etc.) and H from water [34]. There are two possible reasons for the increase in BE of Si (and O): (1) the placement of Na and Al by H and (2) partly or full destruction of the surface structure dissolved in acid solution and recrystallized into amorphous SiO_2. The presence of the recrystallized amorphous SiO_2 was detected by XRD. Similar to the case of interaction with H, the BE of both Si and O can readily increase because the electronegativity of Si is higher than Al and Na. The deconvolution of XPS high-resolution spectra of O1s [33] also demonstrates that the NBO of the Na—Y surface can be lost. It supports the argument that the surface structure of Na—Y has been dissolved and re-formed into a Si—O—Si structure after being modified by 0.5 M sulfuric acid.

Analyzing the BE shifts with the Si/Al ratio determined from survey scans, we can see after sulfuric acid modification that the BE of O and Si increases with increasing Si/Al ratio, and even at a high Si/Al ratio (Si/Al = 8.18), the BE shifts are still significant [34]. However, the BE of Al is almost unchanged in comparison with that of Si and O, no matter what acid concentration has been used or how much Al has been removed from the Na—Y structure. It may indicate that the Al—O bond is too strongly ionic in order to be affected by Na removal from the structure and H replacement.

5.4. The effect of acid treatment on the particle size of Na—Y

Figure 14 shows the effect of acid treatment on the change in Na—Y zeolite particle size. The particle size of the original Na—Y was distributed around two peaks, i.e., 4.5 μm (fine particle peak, volume in 4.21%) and 1124.7 μm (coarse particle peak, volume in 1.49%). After being washed with Milli-Q water, the fine particle peak did not change but its volume % reduced to 3.38%, while the coarse particle peak changed to 447.7 μm, and its volume decreased to 1.14%. The big particles of original Na—Y powder were formed by aggregation of smaller particles via the van der Waals force and electrostatic attractions. The large particle size fraction of the Milli-Q water-washed sample has a wider range of particle size distribution than the original Na—Y. However, it converges on the lower particle size region. The total number of particles increased because of the lager particle separation; thus, the relative volume % of the fine particles decreased. The newly created small particles did not affect the size distribution of original fine particles due to the small proportion of larger particles.

After 0.1 M acid modification, no particles larger than 1000 μm remained in solutions, and the volume % of coarse particles increased to 1.61%. The particles might be further separated, and the Na—Y structure partly dissolved in 0.1 M acid due to the dealumination process. Another type of stable silicon aluminum oxide with a particle size distributed at 399.1 μm was formed by the partly de-aluminized Na—Y.

There was no significant change of fine particle distribution after 0.5 M sulfuric acid modification. However, the peak position of coarse particle distribution has shifted to a smaller particle size region. Combined analysis of XRD and XPS revealed neither the Na—Y crystal phases nor Al was present in this sample [34]. It agrees with the experimental results showing that the structure of Na—Y was totally de-aluminized with increasing concentration of sulfuric acid to a certain level. However, the remaining Si-O structures still remained, with a size distribution peaked at 251.8 μm.

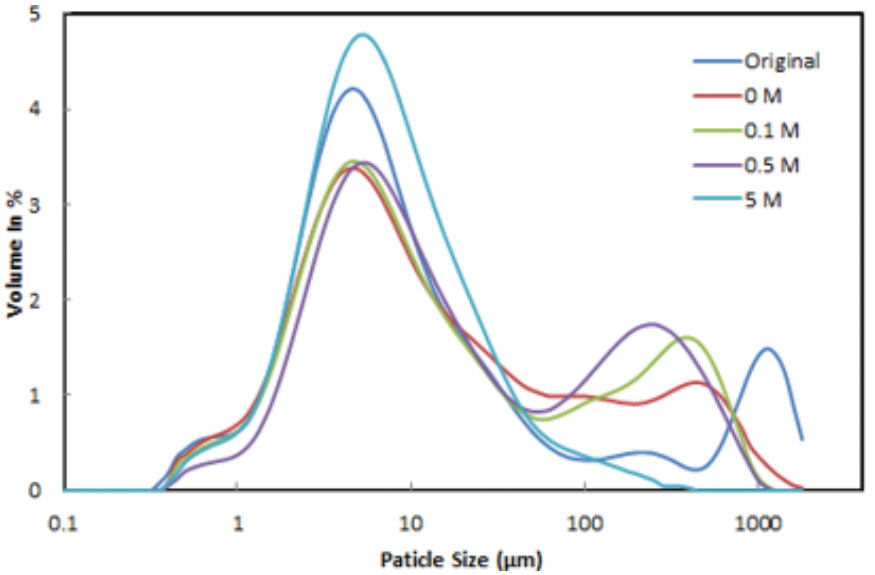

Figure 14. Particle size distribution of original and acid-treated Na—Y [34].

Comparing with 0.5 M acid modification, the volume % of fine particles increased greatly after treating with 5 M acid. The distribution of the coarse particles disappeared, but the fine particle size distribution remained the same. Thus, coarse particles dissolved to fine particles by 5 M acid modification, and the newly generated fine particles displayed a similar size distribution as the original fine particles. As per both XRD and XPS analyses for the 5 M acid-modified sample, there were no crystal phases, and Al was present in the sample, and the Si atomic ratio was slightly lower than for the case of the 0.5 M modification. Therefore, after the 5 M acid modification, not only was the Na—Y structure but also the remaining Si—O structure was fully destroyed by dealumination. It is the reason for the disappearance of the coarse particles. The dissolved Si and O recrystallized and formed an amorphous SiO_2 with a particle size distribution peaked at 5.0 μm.

As there was a constant peak of fine particle size at 4.5–5.0 μm in each sample, this particle size did not characterize the particles of the crystal phase of original Na—Y. On the contrary, the coarse particles with changing size from 1124.7 to 399.1 μm when the acid concentration increased from 0 to 0.1 M could be considered as the characteristic peak of the silica-alumina structure in Na—Y crystal phase. Even if there was a coarse particle peak at 251.8 μm detected for the 0.5 M acid-modified sample, these particles would not be considered as representative of the Na—Y crystal phase.

6. Conclusions

The major objective of this chapter is to investigate the potential use of natural and acid-activated zeolites (clinoptilolite) for CSG water treatment. Both natural and synthetic zeolites

have been studied in unchanged and acid-activated forms in regard to surface composition, surface binding energy, and surface charge properties. The CSG water treatment study by applying the natural and acid-activated zeolites has been completed. The possibility of reducing the sodium concentration and SAR of CSG water using natural zeolite has been demonstrated.

Natural zeolite containing mainly clinoptilolite can be modified and activated by different concentrations of sulfuric acid. The XPS analysis of the natural zeolite and acid-modified zeolite shows significant changes in the surface properties of natural zeolite because of acid modification. Increasing acid concentration from 0 to 5 M can increase the Si/Al ratio on the zeolite surface from 2.99 up to 4.92. Cations within the zeolite atomic structure exchange with hydrogen ion, weakening the zeolite surface structure. The structural bonds become relatively covalent after acid modification and can be indicated by the BE increase of each main element. High-resolution spectral analysis also shows that the covalent nature of the remaining bonds within the structure can be increased by the ionic bond breakage inside the modified zeolite. The surface properties of clinoptilolite-type natural zeolite can be affected by sulfuric treatment which causes zeolite surface charge more pH-independent by increasing the acid concentration. Based on the results obtained from these studies, dealumination can be the main reason for the increase in surface charge of the zeolite. The hydrogen ions adsorb onto the negatively charged surface sites, reducing the surface potential and charge density. The adsorbed hydrogen ions can be very useful for neutralizing bicarbonate ions in CSG water, thereby reducing its pH.

Examining the dissolution and recrystallization of the zeolite particles, particle size measurement, XRD, and XPS have successfully been applied for investigating the changes in structure and properties of Na-rich synthetic 4A and Na—Y zeolites by modifying with H_2SO_4 at room temperature. The XRD analysis shows the acid modification can cause structural damage, where sodium cations can be removed and dealumination occurs as dissolution progress takes place, thereby the main tetrahedral structure is affected. The Si/Al atomic ratio increases from 2.94 at 0 M to 8.18 at 0.1 M, and a significant binding energy (BE) shift of Si and O can be observed even at a high Si/Al ratio. A relatively low acid concentration (lower than 0.3 M) can be used in the modification of 4A zeolite (low Si/Al ratio) because higher acid concentrations dissolve and can destroy it completely. Na—Y zeolite (high Si/Al ratio) has stronger acid resistivity than 4A zeolite and can be treated with H_2SO_4 up to 5 M. For both 4A and Na—Y zeolites, the acid modification produces dissolution (of both Si and Al) of the first-order fast kinetics and then recrystallization comes about. Gel generation after the acid dissolution can be homogenous or heterogeneous. The constant mass of solid, which left in solution after a long time formed by the recrystallization, increases with time. However, neither Al nor Na participates in the recrystallization process, only the dissolved Si gradually recrystallizes with the standing time goes on once the solubility of Na—Y achieves a threshold value. The Al and Na sites of Na—Y zeolite structure can be completely removed when the acid concentration reaches 0.5 M, which is observed as the threshold value for the Na—Y zeolite. The peak particle size of the size distribution which can characterize the change of the Na—Y crystal phase before and after acid modification is found to vary from 1124.7 to 399.4 μm.

Acknowledgements

The authors gratefully acknowledge the facilities and the scientific and the technical assistance of the Australian Microscopy & Microanalysis Research facility at the Center for Microscopy and Microanalysis, The University of Queensland. We thank Professor Duong D. Do, Dr. Marc A. Hampton, and Dr. Chris A. Plackowski from The University of Queensland; Prof. Kunping Wang from Chongqing University, China; and Dr. Orhan Ozdemir from Istanbul University, Turkey, for providing useful feedback on this manuscript.

Conflict of interest

There is no conflict of interest.

Author details

Xiaoyu Wang* and Anh V. Nguyen

*Address all correspondence to: xiaoyu.wang@uq.edu.au

School of Chemical Engineering, The University of Queensland, Brisbane, QLD, Australia

References

[1] Taffarel SR, Rubio J. Adsorption of sodium dodecyl benzene sulfonate from aqueous solution using a modified natural zeolite with CTAB. Minerals Engineering. 2010;**23**:771-779. DOI: 10.1016/j.mineng.2010.05.018

[2] Ozdemir O, Armagan B, Turan M, Çelik MS. Comparison of the adsorption characteristics of azo-reactive dyes on mezoporous minerals. Dyes and Pigments. 2004;**62**:49-60. DOI: 10.1016/j.dyepig.2003.11.007

[3] Armagan B, Turan M, Celik MS. Equilibrium studies on the adsorption of reactive azo dyes into zeolite. Desalination. 2004;**170**:33-39. DOI: 10.1016/j.desal.2004.02.091

[4] Mamba BB, Nyembe DW, Mulaba-Bafubiandi AF. Removal of copper and cobalt from aqueous solutions using natural clinoptilolite. Water SA. 2009;**35**:307-314. DOI: 10.4314/wsa.v35i3.76768

[5] Sprynskyy M, Buszewski B, Terzyk AP, Namiesnik J. Study of the selection mechanism of heavy metal (Pb^{2+}, Cu^{2+}, Ni^{2+}, and Cd^{2+}) adsorption on clinoptilolite. Journal of Colloid and Interface Science. 2006;**304**:21-28. DOI: 10.1016/j.jcis.2006.07.068

[6] Bektas N, Kara S. Removal of lead from aqueous solutions by natural clinoptilolite: Equilibrium and kinetic studies. Separation and Purification Technology. 2004;**39**:189-200. DOI: 10.1016/j.seppur.2003.12.001

[7] Xie B, Dai X, Xu Y. Enhancement of activated sludge performance on ammonium removal by clinoptilolite. Toxicological & Environmental Chemistry. 2006;**88**:197-206. DOI: 10.1080/02772240500443944

[8] Karadag D, Tok S, Akgul E, Turan M, Ozturk M, Demir A. Ammonium removal from sanitary landfill leachate using natural Gördes clinoptilolite. Journal of Hazardous Materials. 2008;**153**:60-66. DOI: 10.1016/j.jhazmat.2007.08.019

[9] Dimirkou A, Doula MK. Use of clinoptilolite and an Fe-overexchanged clinoptilolite in Zn^{2+} and Mn^{2+} removal from drinking water. Desalination. 2008;**224**:280-292. DOI: 10.1016/j.desal.2007.08.014

[10] Dimirkou A. Uptake of Zn^{2+} ions by a fully iron-exchanged clinoptilolite. Case study of heavily contaminated drinking water samples. Water Research. 2007;**41**:2763-2773. DOI: 10.1016/j.watres.2007.02.045

[11] Doula MK. Simultaneous removal of cu, Mn and Zn from drinking water with the use of clinoptilolite and its Fe-modified form. Water Research. 2009;**43**:3659-3672. DOI: 10.1016/j.watres.2009.05.037

[12] Doula MK. Removal of Mn^{2+} ions from drinking water by using clinoptilolite and a clinoptilolite-Fe oxide system. Water Research. 2006;**40**:3167-3176. DOI: 10.1016/j.watres.2006.07.013

[13] El-Hady HMA, Grünwald A, Vlčková K, Zeithammerová J. Clinoptilolite in drinking water treatment for ammonia removal. Acta Polytechnica. 2001;**1**:41-45. DOI: ctn.cvut.cz/ap/

[14] Zhao H, Vance GF, Ganjegunte GK, Urynowicz MA. Use of zeolites for treating natural gas co-produced waters in Wyoming, USA. Desalination. 2008;**228**:263-276. DOI: 10.1016/j.desal.2007.08.014

[15] Wang X, Ozdemir O, Hampton MA, Nguyen AV, Do DD. The effect of zeolite treatment by acids on sodium adsorption ratio of coal seam gas water. Water Research. 2012;**46**:5247-5254. DOI: 10.1016/j.watres.2012.07.006

[16] Johnston CR. Soil Chemical and Physical Changes Resulting from Irrigation with Coalbed Natural Gas Co-Produced Water: Effects of Soil Amendments and Water Treatments. Laramie: Department of Renewable Resources, University of Wyoming; 2007. p. 68

[17] A. Queensland Government. Management of Water Produced from Coal Seam Gas Production. In: D.o.I.a. Planning; 2009

[18] Nghiem LD, Ren T, Aziz N, Porter I, Regmi G. Treatment of coal seam gas produced water for beneficial use in Australia: A review of best practices. Desalination and Water Treatment. 2011;**32**:316-323. DOI: 10.5004/dwt.2011.2716

[19] Isherwood WF, Ziagos J, Nichols E, Rice D, Krauter P. Enhancing Aquifer Cleanup with Reinjection. Prevention, Detection and Remediation Conference. Dublin, Ohio; 1992. pp. 103-109

[20] Panneerselvam P, Thinakaran N, Thiruvenkataravi KV, Palanichamy M, Sivanesan S. Phosphoric acid modified-Y zeolites: A novel, efficient and versatile ion exchanger. Journal of Hazardous Materials. 2008;**159**:427-434. DOI: 10.1016/j.jhazmat.2008.02.033

[21] Liu XM, Yan ZF. Studies of the Nitrogen Adsorption of Citric-Modified USY Zeolites. Singapore: World Scientific Publ Co Pte Ltd; 2000

[22] Cooper S. Escott Zeolite Major Elements. Zeolite Australia Pty Ltd

[23] Harland CE. Ion Exchange Theory and Practice. Cambridge: The Royal Society of Chemistry; 1994

[24] Athanasiadis K, Helmreich B. Influence of chemical conditioning on the ion exchange capacity and on kinetic of zinc uptake by clinoptilolite. Water Research. 2005;**39**:1527-1532. DOI: 10.1016/j.watres.2005.01.024

[25] Breck DW. Zeolite Molecular Sieves. Wiley; 1984. pp. 669-717. DOI: 661.183.6/978-08987 46488

[26] Inglezakis VJ, Diamandis NA, Loizidou MD, Grigoropoulou HP. Effect of pore clogging on kinetics of lead uptake by clinoptilolite. Journal of Colloid and Interface Science. 1999;**215**:54-57. DOI: 10.1006/jcis.1999.6247

[27] Zholobenko V, Garforth A, Dwyer J. TGA-DTA study on calcination of zeolitic catalysts. Thermochimica Acta. 1997;**294**:39-44. DOI: 10.1016/s0040-6031(96)03140-1

[28] Grim M. Clay Mineralogy. New York: Mc Graw-Hill Inc.; 1968

[29] Wang X, Plackowski CA, Nguyen AV. X-ray photoelectron spectroscopic investigation into the surface effects of sulfuric acid treated natural zeolite. Powder Technology. 2016;**295**:27-34. DOI: 10.1016/j.powtec.2016.03.025

[30] Barr TL, Chen LM, Mohsenian M, Lishka MA. XPS valence band study of zeolites and related systems. 1. General chemistry and structure. Journal of the American Chemical Society. 1988;**110**:7962-7975. DOI: 10.1021/ja00232a003

[31] Ersoy B, Çelik MS. Electrokinetic properties of clinoptilolite with mono- and multivalent electrolytes. Microporous and Mesoporous Materials. 2002;**55**:305-312. DOI: 10.1016/S1387-1811(02)00433-X

[32] Wang X, Nguyen AV. Characterisation of electrokinetic properties of clinoptilolite before and after activation by sulfuric acid for treating CSG water. Microporous and Mesoporous Materials. 2016;**220**:175-182. DOI: 10.1016/j.micromeso.2015.09.003

[33] Yilmaz B, Müller U. Catalytic applications of zeolites in chemical industry. Topics in Catalysis. 2009;**52**:888-895. DOI: 10.1007/s11244-009-9226-0

[34] Wang X, Wang K, Plackowski CA, Nguyen AV. Sulfuric acid dissolution of 4A and Na—Y synthetic zeolites and effects on Na—Y surface and particle properties. Applied Surface Science. 2016;**367**:281-290. DOI: 10.1016/j.apsusc.2016.01.103

[35] Barr TL. The nature of the relative bonding chemistry in zeolites: An XPS study. Zeolites. 1990;**10**:760-765. DOI: 10.1016/0144-2449(90)90058-y

Edited by M.Nageeb Rashed and P.N. Palanisamy

Zeolites are hydrated aluminosilicate minerals of the family of microporous solids. According to the US Geological Survey, there are about 40 naturally occurring zeolites, forming in sedimentary and volcanic rocks. The most commonly mined forms include clinoptilolite, chabazite and mordenite. There are over 200 synthetic zeolites. For their abundance, natural and synthetic zeolites are widely used in the industry, agriculture, water treatment, wastewater treatment and as dietary supplements to treat diarrhea, autism, cancer and other.

This book *Zeolites and Their Applications* deals with several aspects of zeolite morphology, synthesis and applications. The book is divided into three sections and structured into nine chapters. The first section includes the introductory chapter, the second section explains mineralogy, morphology and synthesis of zeolites and the third section focuses on the different applications of both natural and synthetic zeolites.

So, in this book, the readers will obtain updated information on mineralogy, morphology, synthesis and application of zeolites. Scientists from different scientific fields reported in this book their findings.

Published in London, UK
© 2018 IntechOpen
© Lyocsa / iStock

IntechOpen

ISBN 978-1-83881-505-9
9 781838 815059